Exploring the relationship between metabotype and the inflammatory phenotype of the osteoarthritis synovial fibroblast

HUSSEIN FARAH

A thesis submitted to the University of Birmingham for the degree of

DOCTOR OF PHILOSOPHY

Institute of Inflammation and Ageing

College of Medical and Dental Sciences

University of Birmingham

September 2022

Supervisors

Prof. Simon W. Jones

Prof. Claudio Mauro

Dr. Stephen Young

Abstract

Osteoarthritis (OA) is a painful joint condition and a leading cause of disability worldwide. Unfortunately, there is currently no cure for the disease, and there are limited treatment options available. Importantly, despite historically being seen as a “wear and tear” disease of the cartilage there is now increasing evidence that inflammation of the synovial joint lining (synovitis) plays a key role in the disease pathology. Synovitis is pronounced in obese OA patients, with elevated levels of pro-inflammatory cytokines in the synovial fluid

The aim of this study was therefore to characterise the metabolic profile of synovial joint fluid and synovial fibroblasts under both basal and inflammatory conditions in a cohort of obese and normal-weight OA patients. Furthermore, we sought to ascertain whether modulation of a metabolic pathway in OA synovial fibroblasts could alter their inflammatory activity.

1H NMR Metabolomics analysis of synovial fluid and synovial fibroblast conditioned media showed altered metabolism in obese OA patients compared to normal weight patients with increased enrichment of glycolytic metabolites. This was confirmed in vitro using metabolic flux analysis of isolated synovial fibroblasts. Obese OA synovial fibroblasts exhibited increased basal lactate secretion and glycolysis, compared to normal weight fibroblasts and could further increase oxidative phosphorylation upon inflammatory challenge.

Furthermore, metabolomic analysis of OA synovial fluid revealed enrichment of glutamine-glutamate metabolism in obese OA patients. Modulation of glutamine-glutamate metabolism through inhibition of glutaminase 1 (GLS1) reduced the

expression and secretion of inflammatory cytokine IL6. Therefore, the synovial joint inflammation observed in obese OA patients is potentially underpinned by therapeutically targetable metabolic pathways. These differences in OA pathology suggest that lean and obese OA patients might benefit from different treatment strategies

Acknowledgments

All praise and thanks is due to Allāh, the Extremely Merciful and the Bestower of Mercy. May the prayers and peace from Allāh be upon our Prophet Muhammed, his family, and his companions.

To proceed: I would like to start by thanking my supervisors Prof. Simon W. Jones, Prof. Claudio Mauro, and Dr. Stephen Young for all their support, advice, and encouragement throughout this project. I would especially like to thank Simon for the immense patience, perseverance, and guidance throughout these past few years. You believed in me and without your constant help and support, I don't believe I could have done this at all. I am also very grateful for the time that he put in to read all of my lengthy thesis chapters through multiple iterations! A special thank you also to my second supervisor Claudio, you have been brilliant, providing me with helpful advice and guidance in the very challenging world of metabolism. I would like to thank Steve, for all the thought-provoking and practical advice, and for getting me to do old-school experiments like boiling my TNFα!

I would like to thank all the members of the Jones group, past and present including Sue, Dominika, and Tom, all of whom helped teach me what I know. A big thank you to legends Jon and Michelangelo (who have been like extra supervisors) for giving the best advice in life and science. Throughout my PhD I shared a lab with some great people including the most enthusiastic scientist I have ever met Mr. Joshua Price, Josh it's been excellent. I would also like to thank everyone from lab 1 and lab 3 including Lord Group and Mauro Group.

My next thanks goes to my parents, who are the reason I even decided to do a PhD in the first place. A special thank you to my brothers and sisters Mohammed, Mahad, Hafsa and Zainab!

I would like to thank all the people who volunteered to take part in this study as without them there would not be a thesis to present. I thank Prof. Ed Davis and all the research nurses at the Royal Orthopaedic Hospital and Russell Hall Hospital for their help running this study. Finally, I would like to thank the Medical Research Council (MRC) Versus Arthritis Centre for Musculoskeletal Ageing Research who have funded this PhD.

Table of Contents

Abstract 2

Acknowledgments 4

Table of Figures 13

List of Tables 22

List of Abbreviations 25

CHAPTER 1. GENERAL INTRODUCTION 29

1.1 Osteoarthritis 30

1.2 Osteoarthritis Pathology 32

1.3 Synovial Inflammation 37

1.4 Obesity and Osteoarthritis 46

1.6 Fibroblasts metabolism and inflammation 48

1.7 Thesis Hypothesis 61

1.8 Thesis Aims 62

Chapter 2. MATERIALS AND METHODS 63

Materials 64

Methods 71

2.1 Ethical approval and subject recruitment 71

2.2 Primary synovial fibroblast isolation and culture 71

2.3 Confirmation of the maintenance of synovial fibroblast phenotype during in vitro culture 72

2.4 Isolation of RNA from primary human OA synovial fibroblasts 72

2.5 Isolation of total protein from primary human OA synovial fibroblasts 73

2.6 Reverse transcription Polymerase Chain Reaction 74

2.7 siRNA Transfection 75

2.8 SDS polyacrylamide gel electrophoresis and immunoblotting 75

2.9 Mitotracker Green Staining 76

2.10 Fluorescence Glucose Uptake 77

2.11 ROS production assay 77

2.12 MTS Assay 78

2.13 ELISA 79

2.14 Cellular proliferation assays 80

2.14 Annexin V-PI apoptosis flow assay 80

2.15 Lactate Assay 81

2.16 Seahorse metabolic analysis of OA synovial fibroblasts 82

2.17 NMR Spectroscopy 82

2.18 RNA Sequencing Analysis 83

2.19 Bioinformatic Pathway Analysis 84

2.20 Data handling and statistical analysis 86

Chapter 3 88

Metabolomics Analysis of Osteoarthritic Synovial Fluid and Synovial Fibroblast Secretomes using ^{1}H NMR Spectroscopy 88

3.1 Introduction 89

3.1.1 Metabolomics 89

3.1.2 Metabolomics in Inflammation and Obesity 93

3.1.2.1 Metabolomics in Cardiovascular Disease 93

3.1.2.2 Metabolomics in Neurological Disease 94

3.1.2.3 Metabolomics in Metabolic Disorders 95

3.1.3 Multivariate Analysis using Soft Independent Modelling by Class Analogy (SIMCA) 99

3.2 Hypothesis 103

3.3 Methods 104

3.3.1 Patient Characteristics and Anthropometric Data 104

3.4 Results 107

3.4.1 Univariate Metabolite Analysis from OA synovial fluid and OA Synovial Fibroblast Conditioned Media 107

3.4.2 Linear Regression Analysis of Significantly Altered Metabolites in OA Synovial Fluid 120

3.4.3 Metabolomic multivariate analysis of obese OA synovial fluid compared to normal weight OA synovial fluid 134

3.4.4 Metabolic Pathway Analysis of OA synovial fluid and synovial fibroblast conditioned media from obese patients compared to normal weight patients .. 147

3.4.4.1 OA Synovial Fluid 147

3.4.4.2 OA Synovial Fibroblast Secretomes 150

3.5 Discussion 156

3.5.1 The impact of obesity on the metabolome of synovial joint fluid and synovial joint tissue in hip osteoarthritis patients 156

3.5.1.1 Metabolomics of biological fluids in OA patients and animal models ... 156

3.5.1.2 Preclinical animal model data 156

3.5.1.3 Clinical patient data 159

3.5.1.4 Metabolomics of OA synovial fibroblast conditioned media 160

3.5.1.5 Formate Metabolism 161

3.5.1.6 Galactose Metabolism 161

3.5.1.7 Caffeine Metabolism 162

3.5.1.8 N-Acetylglycine 163

3.5.1.9 Imidazole 164

3.5.1.10 Phenylalanine 164

3.5.2 Metabolomics Studies in OA 166

3.5.3 Pathway analysis 168

3.5.3.1 Aminoacyl-tRNA Biosynthesis 168

3.5.3.2 Glutamine-Glutamate Metabolism 170

3.5.3.3 Glycine, serine and threonine metabolism 173

3.5.3 Limitations 174

3.5.4 Summary 177

Chapter 4 178

Modulating Glutamine Metabolism to Control Inflammatory Phenotype of the OA synovial fibroblast 178

4.1 Introduction 179

4.2 Hypothesis 183

4.4 Results 184

4.5 Discussion 205

4.5.1 Limitations 206

4.5.2 Future Studies 207

Chapter 5 208

Integration of the Synovial Fibroblast Transcriptome and Metabolome Provides Unique Insights to Pathways Associated with Obesity and Osteoarthritis 208

5.1 Introduction 209

5.1.2 Biomechanical loading of joint 214

5.1.3 The use of integrative Multi-Omics in Inflammatory Joint Diseases 217

5.2 Hypothesis 220

5.3 Methods 221

5.3.1 Patient Characteristics and Anthropometric Data 221

5.4 Results 222

5.4.1 Heatmaps of metabolic pathways identified within metabolomics data of OA synovial fibroblast 227

5.4.2 Ingenuity Pathway Analysis (IPA) of obese and normal weight OA synovial fibroblast from different joints 233

5.4.3 Joint Pathway Analysis 249

5.5 Discussion 258

5.5.1 Shared metabolic gene expression across loadbearing and obesity 258

5.5.2 Heatmaps of metabolomic pathways highlight differentially expressed genes in obesity 260

5.5.3 IPA analysis of the transcriptome of OA synovial fibroblast highlights distinctively altered metabolic pathways in the context of obesity 263

5.5.4 Joint pathway analysis of hip OA synovial fibroblasts 266

5.5.5 Limitations 267

5.5.6 Future Directions 270

Chapter 6 271

Metabolic Flux Analysis of OA synovial fibroblasts 271

6.1 Introduction 272

6.1.1. Glycolysis 273

6.1.2 Mitochondrial Respiration 277

6.2 Hypothesis 280

6.3 Methods 281

6.3.3 Seahorse metabolic analysis explained 281

6.4 Results 283

6.4.1 Patient characteristics 283

6.4.2 Comparative analysis of metabolic flux in OA synovial fibroblasts isolated from lean and obese patients 285

6.4.3 Comparative analysis of metabolic flux in OA synovial fibroblasts isolated from loadbearing and non-loadbearing joints 288

6.4.4 Obese hip OA synovial fibroblasts show altered metabolic phenotype ... 296

6.5 Discussion ... 308

6.5.1 Limitations ... 312

6.5.2 Future Studies ... 313

Chapter 7. General Discussion ... 315

7.1 Discussion of main findings ... 316

7.2 Future directions ... 320

7.2.1 Rationale for the therapeutic targeting of metabolism in stromal synovial fibroblast pathotypes in inflammatory joint disease ... 320

7.2.2 Metabolism and Inflammation are Intricately Connected in Synovial Fibroblasts and Present Potential Targetable Pathways to Modulate Inflammation ... 322

7.2.3 Pre-clinical animal models ... 327

7.2.4 Precision and Personalised Medicine: Treating Obese Osteoarthritis Patients ... 328

Chapter 8. References ... 333

Table of Figures

Figure 1.1: Osteoarthritis is driven by different factors which can be classified into different phenotypes..... 32

Figure 1.2: Schematic diagram showing the cell types and mechanisms from which fibroblast may be derived from. 50

Figure 1.3: Schematic diagram showing the metabolic pathways altered in fibroblasts in different disease pathologies (Farah *et al.*, 2020). 54

Figure 3.1: Boxplot of significantly increased metabolites in obese OA synovial fluid (n = 5) compared to normal weight (n = 6) OA synovial fluid..... 108

. 108

Figure 3.2: Boxplot of metabolites in OA synovial fibroblast conditioned media unstimulated and stimulated (10ng/ml TNFα for 24hrs) from obese (OB) (n = 6) and normal weight (NW) (n = 5) patients which were identified to be altered in OA synovial fluid1..... 115

Figure 3.3: Boxplot of significantly increased metabolites in OA synovial fibroblast conditioned media unstimulated and stimulated (10ng/ml TNFα for 24hrs) from normal weight (NW) patients (n= 5)..... 116

Figure 3.4: Boxplot of significantly increased metabolites in OA synovial fibroblast conditioned media unstimulated and stimulated (10ng/ml TNFα for 24hrs) from obese (OB) patients (n= 6)[1]..... 118

Figure 3.5: Regression analysis of the relationship between the synovial fluid concentration of 1,3-Dimethylurate and (A). BMI, (B) W:H (C) WC and (D) HC. (n = 15 patients). 123

Figure 3.6: Regression analysis of the relationship between the synovial fluid concentration of Glucose and (A). BMI, (B) W:H (C) WC and (D) HC. (n = 15 patients). 124
Figure 3.7: Regression analysis of the relationship between the synovial fluid concentration of Glycine and (A). BMI, (B) W:H (C) WC and (D) HC. (n = 15 patients). 125
Figure 3.8: Regression analysis of the relationship between the synovial fluid concentration of Lactate and (A). BMI, (B) W:H (C) WC and (D) HC. (n = 15 patients). 126
Figure 3.10: Regression analysis of the relationship between the synovial fluid concentration of N-Nitrosodimethylamine and (A). BMI, (B) W:H (C) WC and (D) HC. (n = 15 patients). 127
Figure 3.11: Regression analysis of the relationship between the synovial fluid concentration of Pyruvate and (A). BMI, (B) W:H (C) WC and (D) HC. (n = 15 patients). 128
Figure 3.12: Regression analysis of the relationship between the synovial fluid concentration of Succinate and (A). BMI, (B) W:H (C) WC and (D) HC. (n = 15 patients). 129
Figure 3.13: Regression analysis of the relationship between the synovial fluid concentration of Tyrosine and (A). BMI, (B) W:H (C) WC and (D) HC. (n = 15 patients). 130
Figure 3.14: Regression analysis of the relationship between the synovial fluid concentration of Glutamine and (A). BMI, (B) W:H (C) WC and (D) HC. (n = 15 patients). 131

Figure 3.15: Regression analysis of the relationship between the synovial fluid concentration of Glutamate and (A). BMI, (B) W:H (C) WC and (D) HC. (n = 15 patients). 132
Figure 3.16: Regression analysis of the relationship between the synovial fluid concentration of Glutamine:Glutamate and (A). BMI, (B) W:H (C) WC and (D) HC. (n = 15 patients). 133
Figure 3.17: Scores plot of 1D 1H NMR spectra of normal weight (NW) and obese (OB) OA synovial fluid subjected to PCA-X plot 135
Figure 3.18: Summary of fit of 1D 1H NMR spectra of normal weight and obese OA synovial fluid subjected to PCA-X plot. 137
Figure 3.19: Scores plot of 1D 1H NMR spectra of normal weight (NW) and obese (OB) OA synovial fluid subjected to OPLS-DA plot. 139
Figure 3.20: Summary of fit of 1D 1H NMR spectra of normal weight and obese OA synovial fluid subjected to subjected to OPLS-DA plot. 140
Figure 3.21: VIP scores for metabolites derived from 1H NMR spectra of normal weight and obese OA synovial fluid subjected to OPLS-DA plot. 141
Figure 3.22: Scores plot of 1H NMR spectra of normal weight and obese OA synovial fluid subjected to OPLS-DA plot with a VIP cut-off of ≥ 1. 143
Figure 3.23: Summary of fit of 1H NMR spectra of normal weight and obese OA synovial fluid subjected to OPLS-DA plot with a VIP cut-off of ≥ 1. 144
Figure 3.24: VIP scores for metabolites derived from 1H NMR spectra of normal weight and obese OA synovial fluid subjected to OPLS-DA plot with a VIP cut-off of ≥ 1. 146

Figure 3.25: Pathway analysis of the most altered metabolic pathways in obese OA synovial fluid (n = 5) compared to normal weight OA synovial fluid (n = 6) patients. 148
Figure 3.26: Pathway analysis of OA synovial fibroblast conditioned media with the most altered metabolic pathways in normal weight TNFα stimulated synovial fibroblasts secretomes compared to unstimulated synovial fibroblasts (n = 5)..... 151
Figure 3.26: Pathway analysis of OA synovial fibroblast conditioned media with the most altered metabolic pathways in obese TNFα stimulated synovial fibroblasts secretomes compared to unstimulated synovial fibroblasts (n = 6). 154
Figure 4.1: Glutamine receptors expression is not altered in obese and normal weight OA synovial fibroblasts 185
Figure 4.2: OA synovial fibroblasts express primary glutamine transporter expression in obese and normal weight patients 186
Figure 4.3: OA synovial fibroblasts express key glutamine enzyme GLS..... 187
Figure 4.4: Inhibition of GLS1 attenuates IL6 inflammatory response in OA synovial fibroblasts 189
Figure 4.5: Inhibition of GLS1 in OA synovial fibroblasts alters cellular morphology 191
Figure 4.6: 1-day inhibition of GLS1 in OA synovial fibroblasts alters fibroblast morphology 192
Figure 4.7: 2-day inhibition of GLS1 in OA synovial fibroblasts alters fibroblast morphology 193
Figure 4.8: 4-day inhibition of GLS1 in OA synovial fibroblasts alters fibroblast morphology 194

Figure 4.9: Synovial fibroblast proliferation increases with glutamine treatment and decreases with GLS1 inhibition 195
Figure 4.10: Unstained cells displayed in gating strategy used for annexin V:Pi staining as measure of apoptosis in fibroblasts 197
Figure 4.11: Gating strategy used for Annexin V:Pi staining as measure of apoptosis in fibroblasts 198
Figure 4.12: Short term GLS1 inhibition does not increase apoptosis 199
Figure 4.13: Short term GLS1 inhibition does not increase cell death 200
Figure 4.14: Short term GLS1 inhibition does not alter cell proliferation 201
Figure 4.15: Short term GLS1 inhibition attenuates IL6 mediated inflammation in dose-dependent manner 202
Figure 4.16: Short term GLS1 inhibition increases NAD(P)H-dependent oxidoreductase activity in dose-dependent manner but does not increase ROS generation 203
Figure 4.17: Glutamine supplementation and GLS1 inhibition increases glucose uptake but not mitochondrial mass 204
Figure 5.1: Venn Diagram of differentially expressed genes in obesity and loadbearing OA synovial fibroblasts 223
Figure 5.2: Venn diagram of differentially expressed genes (DEGs) in OA synovial fibroblasts from different joints 226
Figure 5.3: Differential Gene Expression of Glycolysis/Gluconeogenesis KEGG pathway 229
Figure 5.4: Differential Gene Expression of Aminoacyl-tRNA Biosynthesis KEGG pathway 230

Figure 5.5: Differential Gene Expression of Serine, Glycine and Threonine metabolism KEGG pathway 231
Figure 5.6: Differential Gene Expression of Alanine, Aspartate and Glutamate metabolism KEGG pathway 232
Figure 5.7: Canonical Pathway Analysis of loadbearing (n = 18) compared to non-loadbearing (n =6) OA synovial fibroblast. 234
Figure 5.8: Salvage Pathway of Pyrimidine Ribonucleotides highlighted in canonical pathway analysis of loadbearing compared to non-loadbearing OA synovial fibroblast 236
Figure 5.9: Salvage Pathway of Pyrimidine Deoxyribonucleotides highlighted in canonical pathway analysis of loadbearing compared to non-loadbearing OA synovial fibroblast..... 237
Figure 5.10: Canonical pathway analysis of obese (n = 12) compared to normal weight (n = 11) OA synovial fibroblast..... 238
Figure 5.11: NADH repair pathway highlighted in metabolic pathway analysis of obese synovial fibroblast compared to normal weight synovial fibroblast..... 240
Figure 5.13: Salvage pathway of pyrimidine deoxyribonucleotides pathway highlighted in canonical pathway analysis of obese synovial fibroblasts compared to normal weight synovial fibroblast 241
Figure 5.14: Percentage upregulated and downregulated DEGs within metabolic canonical pathway analysis of obese (n = 3) compared to normal weight (n = 3) hip OA synovial fibroblast..... 242
Figure 5.15: Metabolic canonical pathway activity of obese (n = 3) compared to normal weight hip (n = 3) OA synovial fibroblast 243

Figure 5.16: Metabolic canonical pathway analysis of obese (n = 3) knee OA synovial fibroblast compared to normal weight (n = 3) knee OA synovial fibroblast 244
Figure 5.17: Branched chain α ketoacid dehydrogenase complex highlighted in metabolic canonical pathway of obese compared to normal weight knee OA synovial fibroblast..... 245
Figure 5.18: Percentage upregulated and downregulated DEGs within metabolic canonical pathway analysis of obese (n = 3) compared to normal weight (n = 3) foot OA synovial fibroblast..... 246
Figure 5.19: Metabolic canonical pathway analysis of obese (n = 3) compared to normal weight (n = 3) foot OA synovial fibroblast 247
Figure 5.20: Metabolic canonical pathway analysis of obese (n = 3) compared to normal weight (n = 3) hand OA synovial fibroblast 248
Figure 5.21: Joint pathway analysis using transcriptomics and metabolomics data from obese OA synovial fibroblast compared to normal weight OA synovial fibroblast 251
Figure 5.22: Phosphonate and phosphinate metabolism highlighted in multi-omics pathway analysis of obese compared to normal OA synovial fibroblast. 253
Figure 5.23: Histidine metabolism highlighted in multi-omics pathway analysis of obese compared to normal weight hip OA synovial fibroblast. 254
Figure 5.24: Phoshotidylinositol signalling system highlighted in multi-omics pathway analysis of obese compared to normal weight hip OA synovial fibroblast. 255
Figure 5.25: Inositol phosphate metabolism highlighted in multi-omics pathway analysis of obese compared to normal weight hip OA synovial fibroblast. 256

Figure 5.26: Glycolysis highlighted in multi-omics pathway analysis of obese compared to normal weight hip OA synovial fibroblast. 257
Figure 6.1: Diagram of metabolic changes observed in synovial fibroblasts in inflammatory joint diseases. 276
Figure 6.2: Glycolysis stress test of OA synovial fibroblasts from normal weight and obese patients either basal or following TNFα stimulation. 286
Figure 6.3: Mitochondrial stress test of OA synovial fibroblasts from normal weight and obese patients either basal or following TNFα stimulation. 287
Figure 6.4: Glycolysis stress test of OA synovial fibroblasts from loadbearing and non-loadbearing joints either basal or following TNFα stimulation. 289
Figure 6.5: Mitochondrial stress test of OA synovial fibroblasts from loadbearing and non-loadbearing joints either basal or following TNFα stimulation. 290
Figure 6.6: Metabolic rates of OA synovial fibroblasts from different joints either basal or following TNFα stimulation. 292
Figure 6.7: Glycolysis stress test of OA synovial fibroblasts from hip, knee, and hand joints either basal or following TNFα stimulation. 294
Figure 6.8: Mitochondrial stress test of OA synovial fibroblasts from hip, knee, and hand joints either basal or following TNFα stimulation. 295
Figure 6.9: Lactate secretion is greater in obese OA synovial fibroblasts and is induced during the inflammatory response. 297
Figure 6.10: Gene expression of transporter proteins in hip OA synovial fibroblasts from normal weight and obese patients either basal or following TNFα stimulation. 299

Figure 6.11: Protein expression of MCT1 lactate transporter in hip OA synovial fibroblast from normal weight and obese patients either basal or following TNFα stimulation. 300
Figure 6.12: Glucose uptake of hip OA synovial fibroblasts from normal weight and obese patients either basal or following TNFα stimulation. 302
Figure 6.13. Obese and normal-weight OA synovial fibroblasts exhibit differential glycolytic metabolism. 304
Figure 6.14. Obese and normal-weight OA synovial fibroblasts exhibit differential mitochondrial respiration. 306
Figure 6.15: Mitochondrial mass of obese hip OA synovial fibroblasts either basal or following TNFα stimulation. 307
Figure 7.1: Altered metabolic pathways in synovial fibroblast can be targeted through multiple therapeutics to ameliorate inflammatory phenotype (adapted from Farah *et al.*, 2020) 325
Figure 7.2: Personalised medicine (PM) can be derived from the amalgamation of three patient characteristics which include clinical features, environmental factors, and molecular characterisation 331

List of Tables

Table 1.1: Common markers used to identify fibroblasts..... 51

Table 1.2: Dysregulated metabolic pathways in stromal fibroblasts (Farah *et al.*, 2020). 58

Table 2.1 Cell culture general reagents..... 64

Table 2.2 Cell culture plasticware 65

Table 2.3 Recombinant proteins, stains, and inhibitors..... 66

Table 2.4 Assay kits and Reagents..... 66

Table 2.5 Seahorse Metabolic Flux Assay 67

Table 2.6 Western blotting reagents..... 68

Table 2.7 Western blotting antibodies 68

Table 2.8 siRNA knockdown reagents 69

Table 2.9 RT-qPCR Primers 70

Table 3.1: Advantages and Disadvantages of using NMR Spectroscopy compared to Mass Spectroscopy..... 92

Table 3.2: Terminology of Cross-Validated (CV) ANOVA explained..... 102

Table 3.3: Patient characteristics from OA synovial fluid from obese (n = 5) and normal weight (n = 6) patients..... 104

Table 3.4: Patient Characteristics from OA synovial fibroblast conditioned media from obese (n = 6) and normal weight (n = 5) patients..... 105

Table 3.5: Kellgren and Lawrence system for classification of osteoarthritis (KELLGREN and LAWRENCE, 1957)..... 106

Table 3.6: Full list of detected metabolite concentrations from normal weight (NW) (n = 5) and obese (OB) (n = 6) OA synovial fluid..... 109

Table 3.7: Top 20 detected metabolite concentrations from normal weight (NW) Basal and normal weight TNFα (10ng/ml for 24hrs) synovial fibroblast conditioned media. Statistical analysis using one tailed paired Student T test. 118
Table 3.8: Top 20 detected metabolite concentrations from obese (OB) Basal and obese TNFα (10ng/ml for 24hrs) synovial fibroblast conditioned media. Statistical analysis using one tailed paired Student T test. 119
Table 3.9: Regression analysis of synovial fluid metabolite concentrations with parameters of OA patient adiposity/body composition (n = 15 patients)[1]. 122
Table 3.11: Cross Validation Analysis of Variance (CV-ANOVA) performed on OPLS-DA model of normal weight and obese OA synovial fluid with a VIP cut-off of ≥ 1 . 145
Table 3.12: Metabolomics pathway analysis of normal weight and obese OA synovial fluid using KEGG metabolomics library on MetaboAnalyst 5.0. 149
Table 3.13: Metabolomics pathway analysis of normal weight basal synovial fibroblast conditioned media compared to normal weight TNFα (10ng/ml for 24hrs) synovial fibroblast conditioned media. 152
Table 3.14: Metabolomics pathway analysis of obese basal synovial fibroblast conditioned media compared to obese TNFα (10ng/ml for 24hrs) synovial fibroblast conditioned media. 155
Table 5.1 Patient Characteristics Data 221
Table 5.2: Shared differentially expressed genes in obesity (OB) and loadbearing (LB) comparison 224
Table 5.3: Multi-omics pathway analysis of obese OA synovial fibroblasts compared to normal weight OA synovial fibroblasts 252
Table 6.1: Definition and calculations of terms used within the Glycolysis stress test 281

Table 6.2: Definition and calculations of terms used within the Mitochondrial stress test 282
Table 6.3: Patient Characteristics 284
Table 6.4: Expression of glucose transporters from OA synovial fibroblasts in normal weight compared to obese OA patients..... 301
Table 7.1: Considerations prior to development of potential metabolic therapeutic treatments 324

List of Abbreviations

µM	Micromolar
ACL	Anterior cruciate ligament
ADAMTS	a disintegrin and metalloproteinase with thrombospondin motifs
ADP	Adenosine diphosphate
ATP	Adenosine triphosphate
BCAA	Branched Chain Amino Acid
BMI	Body mass index
CAD	Coronary artery diseases
CCL2	C-C Motif Chemokine Ligand 2
CCL8	C-C Motif Chemokine Ligand 8
circRNAs	Circular RNAs
CNS	Central nervous system
COL	Collagen
CRP	C reactive protein
CVD	Cardiovascular diseases
CXCL1	C-X-C motif chemokine 1
DEGs	Differentially expressed genes
DMM	Destabilization of the medial meniscus
DMOADs	Disease-modifying OA drugs
DMRs	Differentially methylated regions
DMSO	Dimethyl sulfone

DNA	Deoxyribonucleic acid
DSS	Sodium trimethylsilylpropanesulfonate
ECM	Extracellular Matrix
FBS	Foetal bovine serum
FcεRI	c epsilon RI
GABA	Gamma-aminobutyric acid
GC	Gas chromatography
GO	Gene ontology
GSEA	Gene set enrichment analysis
GSIS	Glucose-stimulated insulin secretion
HD	Huntington's disease
HDL-C	High-density lipoprotein cholesterol
HFD	High fat diet
HOX	Homeobox genes
HRMAS	High-resolution magnetic angle spinning
ICRS	International Cartilage Regeneration & Joint Preservation Society
IHD	Ischemic heart disease
IL1	Interleukin-1
IL6	Interleukin 6
KEGG	Kyoto Encyclopaedia of Genes and Genomes
Kg	Kilogram
LC	Liquid chromatography
lincRNAs	Long intergenic non-coding RNAs
lnc	Long-non coding

MMP	Matrix metalloproteinases
mRNA	Messenger RNA
MS	Mass spectrometry
MS	Multiple sclerosis
mTOR	Mechanistic target of rapamycin
mTORC1	Mammalian target of rapamycin complex 1
NF-κB	Nuclear factor kappa B
nM	Nanomolar
NMR	Nuclear magnetic resonance
NTC	Non targeting control
OA	Osteoarthritis
OARSI	Osteoarthritis Research Society International
^{o}C	Degrees Celsius
OPG	Osteoprotegerin
OPLS	Orthogonal Partial Least Squares
OXPHOS	Oxidative phosphorylation
PBS	Phosphate-buffered saline
PCA	Principal component analysis
PCR	Polymerase chain reaction
PD	Parkinson’s disease
PLS	Partial Least Squares Projections to Latent Structures
PPAR	Peroxisome proliferator-activated receptors
PTOA	Post traumatic osteoarthritis
PVDF	Polyvinylidene difluoride
RA	Rheumatoid Arthritis

RANKL	Receptor activator of nuclear factor kappa-B ligand
RIPA	Radioimmunoprecipitation assay buffer
RNA	Ribonucleic acid
RNAseq	RNA sequencing
ROS	reactive oxygen species
SASP	senescence-associated secretory phenotype
scRNA-seq	Single cell RNA sequencing
SDS	Sodium dodecyl sulphate
SDS PAGE	SDS polyacrylamide gel electrophoresis
SIMCA	Soft Independent Modelling by Class Analogy
siRNA	Small interfering RNA
T2D	type 2 diabetes
TBS-T	Tris buffered saline with Tween 20
TC	Tibial compression
TLR	Toll- like receptor
TMB	Tetramethylbenzidine
TMS	Tetramethylsilane
TNF	Tumour necrosis factor
tRNA	Transfer RNA
VFF	human vocal folds

CHAPTER 1. GENERAL

INTRODUCTION

1.1 Osteoarthritis

Osteoarthritis (OA) is a progressive degenerative joint disease that is known to affect specific joints including knee, hips, spine and hand. OA is typified by changes to multiple tissues within the joint including the characteristic degradation of articular cartilage, subchondral bone remodelling, and synovial inflammation, which ultimately leads to loss of joint function and severe pain. As one of the leading causes of pain and disability worldwide, OA has had a significant detrimental impact to quality of life in those dealing with this condition (Kawano *et al.*, 2015). OA is the most common joint disease worldwide and is estimated to affect 18% of women and 10% of men over the age of 60 (Glyn-Jones *et al.*, 2015). Around 8.5 million people in the U.K have OA with an estimated one third of people aged 45 and over have sought treatment for OA based on Global Burden of Disease Study 2019 (Institute for Health Metrics and (IHME), 2019). It is projected that by 2025, the prevalence of knee OA will increase by 40% as a result of an ageing population (Kawano *et al.*, 2015). People with OA have a low perception of their quality of life in areas such as functional capacity and pain (Kawano *et al.*, 2015). Likewise, the economic impact of arthritis joint disease in the UK is substantial, with treatment of OA and rheumatoid arthritis (RA) costing the economy £10.2 billion, which is projected to increase to over £118 billion over the next decade (York Health Economics, 2017).

Although OA is a major burden in patients, there are unfortunately no approved therapeutic drugs which can alter the disease course. Therefore, the National Institute for Health and Care Excellence (NICE) guidelines have recommended therapeutics aimed at providing symptomatic pain relief through prescriptions of non-steroidal anti-inflammatory drugs (NSAIDs) (NICE, 2020). Due to the heterogeneity

of OA, locating the source of the pain in the OA joint is particularly difficult and therefore NSAIDs are mostly ineffective, particularly for patients with advanced disease (Creamer, 2000). Alternative treatments such as intra-articular injections of glucocorticoids are listed in NICE guidelines as a secondary treatment option, however this line of treatment has so far been unsuccessful in altering disease course in patients suffering with OA (NICE, 2020). Therefore, exploring a new line of treatment may provide the insights required to generate disease-modifying OA drugs (DMOADs).

Without DMOADs, severe cases of OA are treated using total joint replacement surgery. Although total joint replacement surgeries are generally successful, a significant proportion of patients who undergo joint replacement surgeries have complications related to long-term pain. A systematic review found 7% to 23% of patients who underwent hip replacement surgery reported unfavourable long-term pain outcomes and this figure was 10% to 34% following knee replacement surgery (Beswick *et al.*, 2012). Likewise, 9.7% of patients who underwent total hip arthroplasty and 10.5% of patients who underwent total knee arthroplasty reported being unsatisfied with the surgery outcome, which alongside the brief lifespan of joint implants (10-14 years) is not a sustainable system of healthcare for OA patients (Heath *et al.*, 2021).

1.2 Osteoarthritis Pathology

Previously thought to be a “wear and tear” disease, recent research has classified OA as a multi-factorial whole joint disease whose progression is affected by a number of factors. OA is a highly heterogeneous disease state and consists of several different phenotypes as a result of different driving factors (figure 1.1) (Mobasheri *et al.*, 2019). As a result of these phenotypic changes, a number of cellular components at the joint are affected by OA including articular chondrocytes, synovial fibroblast, osteoclasts, myoblast, adipocytes, synovial macrophages and lymphocytes.

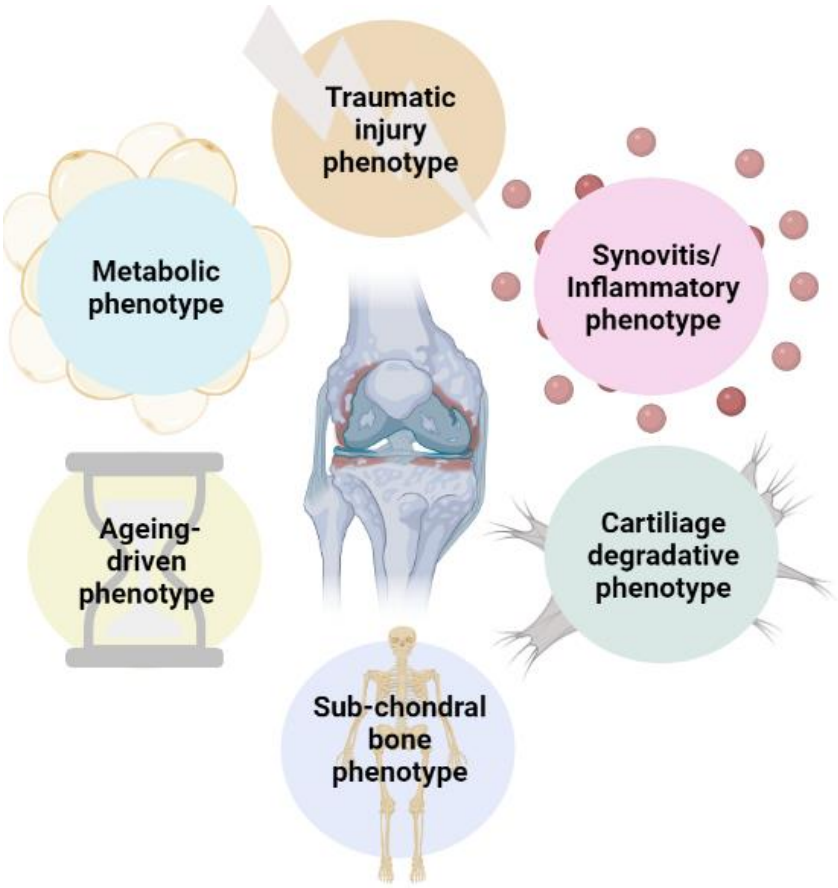

Figure 1.1: Osteoarthritis is driven by different factors which can be classified into different phenotypes

Ageing is major risk factor for developing OA, with the majority of OA patients being over the age of 65 (Chen *et al.*, 2017). Ageing has a large impact on joint tissues including the cartilage, synovium, subchondral bone and muscle. Ageing articular chondrocytes display elevated levels of oxidative stress, which promotes cellular senescence (Chen *et al.*, 2017). Likewise, chondrocytes show decreased repair response to damage, which is partly a result of altered receptor expression patterns. For example, chondrocytes derived from aged and OA cartilage express more ALK1-ALK5 receptor, which results in a downregulation of the TGF-β pathway and a switch from anabolic matrix synthesis to increased catabolic matrix metalloproteinase (MMP) expression (Davidson *et al.*, 2009). During ageing, there is accumulation of epigenetic changes, such as DNA methylation, which is believed to contribute to age-associated pathologies (Salameh, Bejaoui and El Hajj, 2020). Recent research has also shown that DNA methylation of cartilage from OA knee and hip joint is used to maintain cartilage integrity in adulthood (Den Hollander *et al.*, 2014). Genome-wide sequencing of OA chondrocytes show a 50% increase in differentially hydroxymethylated regions in OA chondrocytes implicated in OA pathology including *MMP3, LRP5, GDF5,* and *COL11A1* (Taylor *et al.*, 2015). Another aspect of ageing is the presence and accumulation of senescent cells. Senescent cells are cells which exist in a permanent state of growth arrest, however these cells remain metabolically active and are known to secrete bioactive molecules such as chemokines, cytokines, proteases and growth factors collectively termed senescence associated secretory phenotype (SASP) (Coryell, Diekman and Loeser, 2020). Like other organs, joint tissues are also affected by the presence of senescent cells (Diekman *et al.*, 2018; Manuel J Del Rey *et al.*, 2019). Joint injury can accelerate senescence in chondrocytes and contribute to joint degradation (Jeon *et al.*, 2017). Alongside

chondrocytes, other resident cells of joint tissue such as osteocytes and synovial fibroblasts can become senescent and contribute to the inflammation at the joint through SASP (Farr *et al.*, 2016; Manuel J. Del Rey *et al.*, 2019).

Another phenotype observed in OA is as a result of traumatic injury, with knee injuries a key secondary cause of OA observed amongst younger adults. Recent findings show 51% of women who sustained anterior cruciate ligament injury (ACL) (mean age 31) had OA radiographical changes in the joint after 12 years and 41% of men (mean age 36) had OA after 14 years (Roos, 2005). Deconditioning of the musculoskeletal system alongside damage to bone, cartilage and ligaments is observed after joint injury in young adults, which results in increased joint loading and altered biomechanical dynamics of the joint thereby increasing the risk of developing knee OA.

Another driver of OA pathology is inflammation. Inflammation observed in the OA joint is classified as chronic low grade localised inflammation. Localised inflammation is understood to begin in early stages of the disease and is strongly correlated with tibiofemoral cartilage breakdown (Ayral *et al.*, 2005; Felson, 2006). IL-1β and TNF-α are the central cytokines associated with the inflammatory milieu observed in OA, with both elevated in the synovial fluid and synovial membrane of OA patients. Additionally, IL-1 receptor type 1 (IL-1R1) and TNF receptor 1 (p55) are both highly expressed in OA synovial fibroblast compared to non-OA controls (Kapoor *et al.*, 2011). IL-1β and TNF-α is also produced by a number of neighbouring mesenchymal stromal cells, such as chondrocytes, osteoblast and synovial macrophages, implicating both of these cytokines as the principal drivers of OA. When applied to a rabbit knee joint, IL-1β and TNF-α work in a synergistic fashion, causing more articular cartilage damage than when injected alone (Henderson and Pettipher,

1989). However, attributing IL-1β as simply a pro or anti-inflammatory cytokine is inappropriate as one study confirms IL-1β-/- and ICE-/- (IL-1β converting enzyme) knockout mice resulted in accelerated development of OA lesions, suggesting IL-1β has a more nuanced role in the inflammatory response and cartilage homeostasis (Clements *et al.*, 2003). IL-1β and TNF-α are responsible for inducing the expression and production of other pro-inflammatory cytokines through various signalling pathways.

IL-6 is amongst the most abundant cytokines present in OA sera and synovium compared to healthy serum (Sohn *et al.*, 2012). The role of IL6 in OA is multifaceted and nuanced. Early research shows ablation of IL6 using monoclonal antibody 15A7, which neutralizes the murine IL-6 receptor alpha chain, in collagen-induced arthritis (CIA) in DBA/1J mice and the inflammatory polyarthritis of TNF-α transgenic mice resulted in opposite effects (Alonzi *et al.*, 1998). However, the severity of inflammatory arthritis in the TNF-α transgenic mouse model , (Alonzi *et al.*, 1998) is not significantly reduced when these mice are crossed with transgenic TIL-$6^{-/-}$ mice, suggesting IL6 does not play a pathogenic role in the onset and development TNF-α–dependent arthritis (Alonzi *et al.*, 1998).

On the other hand, IL-$6^{-/-}$ DBA/1J mice were completely protected from CIA induced arthritis, alongside a reduced antibody response to type II collagen, the absence of inflammatory cells and tissue damage in knee joints (Alonzi *et al.*, 1998). This may be due to a differentiated involvement of the immune system in the two murine models. As previous research has shown, TNF-α transgenic mice bearing a RAG null mutation develop arthritis even in the absence of functional lymphocytes (Douni *et al.*, 1995). Furthermore, it has previously been shown the majority of TNF-α

activity in this model is mediated through its ability to induce and synergize with IL-1β (Probert *et al.*, 1995).

In a zymosan induced arthritis (ZIA) murine model, IL-$6^{-/-}$ mice showed increased depletion of cartilage proteoglycan levels in the early phase of arthritis compared to wild type mice whereas joint inflammation was similar suggesting IL6 does not play a role in the onset of inflammation in the ZIA murine model (Van de Loo *et al.*, 1997). However, at later time points of arthritis, joint inflammation was lower in the IL-$6^{-/-}$ mice compared to wild type control suggesting IL6 is involved in the chronic phase of inflammation (Van de Loo *et al.*, 1997).

This highlights the dichotomic role IL-6 plays in the inflammatory response, acting as a defensive mechanism in the acute phase and a pro-inflammatory factor in the chronic phase. In acute response, inducible IL- 6 reduces the production of pro-inflammatory cytokines while not affecting the levels of circulating anti-inflammatory cytokines, shifting away from the inflammatory response (Xing *et al.*, 1998). IL-6 is partially responsible from the switch to chronic inflammation from acute inflammation, assisting in leucocyte recruitment and infiltration to the synovial joint. In murine models, IL-6 and soluble IL-6 receptor (sIL-6Ra), stimulates stromal cells to express IL-8 and MCP-1 as well as adhesion proteins (Romano *et al.*, 1997).

1.3 Synovial Inflammation

Although inflammation during OA progression is present in many joint tissues such as the cartilage and subchondral bone, a major site for inflammation observed in OA is at the synovial membrane. The synovial membrane (synovium) is a specialized connective membrane, which is present at diarthrodial joints. The synovium provides a barrier between the synovial fluid and cavity from neighbouring tissues and is responsible for the maintenance of synovial fluid volume as well as its production of lubricant and hyaluronic acid (Mathiessen and Conaghan, 2017). It is two to three cell layers thick and contains two synoviocyte populations: synovial fibroblasts and resident synovial macrophages. Biopsies obtained from OA knee joints have shown three main differences in synovium taken from early-stage OA to advanced OA; namely synovial lining hyperplasia, inflammatory cell infiltration and stromal vascularisation (Prieto-Potin *et al.*, 2015). Myers et al, 1990 have shown, amongst 29 people with knee pain and arthroscopic evidence of OA but no or minimal radiographic changes in OA, over 50% have histologically observed synovitis with increased mononuclear cell infiltration and synoviocyte proliferation suggesting synovial membrane inflammation is amongst the early pathophysiological changes in OA (Myers *et al.*, 1990). The infiltration of inflammatory immune cells such as activated B and T cells as well as high levels of pro-inflammatory cytokines has been observed in both early and late OA patients (Benito *et al.*, 2005). Furthermore, IL-1 and TNF are elevated in both early and late OA synovial membranes, however there are particularly higher levels of both pro-inflammatory cytokine in moderate and severe OA as a result of increased percentage of synoviocytes (Benito *et al.*, 2005).

Inflammation at the synovial membrane results in the recruitment of immune cells to the inflammatory site through the increased production of chemokines. However, the role immune cells have in OA pathology and their respective subsets has not been well characterised. A systematic review on this subject by de Lange-Brokaar et al, 2012 attempted to collate the information already present in the literature on the presence of immune cell infiltration at synovial tissue. However, the study has only established that synovial tissue inflammation is common in OA patients and has not been able to provide precise and conclusive characterisation of immune cell populations present in OA synovial tissue based on the literature (de Lange-Brokaar *et al.*, 2012). Previous studies have reported that macrophages and T cells are amongst the most abundant immune cell type present in OA synovial tissue and although the percentage population of inflammatory cells is lower in OA patients compared to those with rheumatoid arthritis, they are higher than those observed in healthy controls (Lindblad and Hedfors, 1987; Revell *et al.*, 1988; Ponchel *et al.*, 2015). Early research examining leukocyte populations in peripheral blood could not distinguish statistical differences between RA and OA patients and therefore postulated whether abnormalities in T cell populations and its sub-sets may provide insight into the pathogenesis of OA thereby setting up an environment of chronic inflammation at the synovial joint (Leheita *et al.*, 2005). Conversely, OA serum and synovial fluid had lower levels of the soluble form of the leukocyte surface antigen CD4 (sCD4) compared to RA. However, OA levels were higher compared to age-matched healthy controls (Symons *et al.*, 1991). Later research found that though the percentage population of $CD4^+$ and $CD8^+$ T cells in the peripheral blood of OA patients compared to healthy controls did not differ, the percentage of T cells in the synovial fluid was significantly higher compared to peripheral blood with greater

expression of HLA class II, signifying increased activation of T cell population (Haynes, Hume and Smith, 2002; Hussein *et al.*, 2008). This same study also reported a similar percentage of $CD4^+$ and $CD8^+$ T lymphocytes at the OA synovial fluid as that of RA (Hussein *et al.*, 2008). Immunohistochemistry of the synovium from OA patients compared to normal controls revealed $CD4^+$ and $CD8^+$ T lymphocytes represent a large percentage of leukocytes present and that a greater proportion of the lymphocytes where $CD4^+$ compared to $CD8^+$ (Haynes, Hume and Smith, 2002). Likewise, $CD8^+$ T cells where predominantly located at the periphery of the OA synovium whereas $CD4^+$ T cells where predominantly located at the sub lining layer of the OA synovium when compared to normal subjects (Ishii *et al.*, 2002). Though a conclusive characterisation of the immune cell populations present in OA patients has yet to be conducted, several studies have highlighted the increased presence of T lymphocytes at the synovium. Their function and impact in OA pathogenesis has not yet been established and further research is required to provide insight and clarity into the impact of the adaptive immune system in OA.

The infiltration of inflammatory cells to the OA joint also includes the presence of the first responders to injury and insult, neutrophils. Neutrophils have been shown to make up 8% of the immune cells present in knee synovium in OA patients and 26.1% of immune cells in OA synovial fluid (Hsueh *et al.*, 2021). Neutrophils are known to express several classes of proteases including matrix metalloproteinases MMPs 8-9, cysteine proteases (caspases and calpain) and serine proteases such as neutrophil elastase (NE). NE is primarily found in azurophilic granules of polymorphonuclear leukocytes, is released following cell degranulation and is involved in a number of roles including cellular extravasation (Pham, 2006). NE itself has been shown to directly degrade proteoglycans and is a potent activator of a key

collagenase in OA pathology, MMP13 (Mcdonnell *et al.*, 1993; Wilkinson *et al.*, 2022). NE has been detected in synovial fluid and, interestingly, is absent in samples without synovitis but is present in those with synovitis (Wilkinson *et al.*, 2022). In non-OA cartilage, NE inhibitor, alpha-1 antitrypsin expression (*SERPINA1*) is highly expressed and its expression is markedly downregulated in OA cartilage (Wilkinson *et al.*, 2022). Likewise, systemic administration of human plasma alpha-1 antitrypsin has been shown to reduce arthritis scores and joint destruction in a pre-clinical murine collagen-induced arthritis model (Grimstein *et al.*, 2011). Furthermore, in a KBxN serum-transfer and NE arthritis model, alpha-1 antitrypsin treatment reversed cartilage destruction and reduced synovitis scores (Kaneva *et al.*, 2021). *In vitro*, NE has been shown to reduce chondrocyte proliferation, induce apoptosis and prevent cell migration (Wang *et al.*, 2021). Finally, synovial fluid derived elastase is a strong predictor of knee OA progression, suggesting NE could be used to identify patients at risk of rapid OA disease progression (Hsueh *et al.*, 2021). Neutrophils also secrete other serine proteases like cathepsin G which has been shown to degrade ECM components *in vitro* and *in vivo* (Mcdonnell *et al.*, 2009). Likewise, neutrophils contribute to the cytokines and chemokines found in OA synovial fluid including interleukin (IL)-1β, IL-6, IL-21, IL-22, IL-23, tumour necrosis factor (TNF)-α, and transforming growth factor (TGF)-β (Hsueh *et al.*, 2021). This wide array of cytokine secretion which includes classically pro- and anti-inflammatory activities suggest the low-grade inflammation observed in synovitis is complex and nuanced which reflects the catabolic-anabolic dynamic processes in chondrocytes within the cartilage.

Another class of immune cells intricately involved in maintaining normal joint tissue and in OA pathology are macrophages. Macrophages are the second population of resident cells present within the synovium and make up 53% of the immune cells in

synovium and 37% of those within the synovial fluid (Hsueh *et al.*, 2021). Macrophages within the joint primarily come from both bone-marrow derived monocyte lineage and monocyte independent lineage with distinctive transcriptomic profiles (Culemann *et al.*, 2019). These macrophages were identified using the marker CX3CR1. CX3CR1-expressing macrophages form an internal immunological barrier similar to a thin protective membrane which physically separates the synovium from the synovial fluid (Culemann *et al.*, 2019). In a pre-clinical arthritic murine model, this barrier underwent active remodelling which loosened the interactions between these macrophages and the fibroblasts (Culemann *et al.*, 2019). In OA, macrophages are thought to be activated by the sensing of cytokines and cartilage fragments which are recognised as damage-associated molecular patterns (DAMPs) (Chen *et al.*, 2020). Upon activation of pattern recognition receptors (PRRs), different intra-cellular signalling pathways are activated including NF-κB pathway, which results in further production of inflammatory cytokines and chemokines (Amos *et al.*, 2006; Chen *et al.*, 2020). Likewise, cartilage fragments also increase the expression of catabolic enzyme *MMP-9* alongside *TNF-α* and *IL-6* in bone marrow–derived macrophages (Hamasaki *et al.*, 2021). Additionally, co-culture systems with activated macrophages and OA chondrocytes resulted in significantly higher levels of MMP-1, MMP-3, MMP-9, MMP-13, IL-1β, TNF-α, IL-6, IL-8, and IFN-γ in OA chondrocytes suggesting proinflammatory macrophages may intensify the abnormal matrix degradation and cytokine secretion already observed in OA chondrocytes (Samavedi *et al.*, 2017).

Synovial macrophage M1 polarisation has also been shown to exacerbate OA progression, promote cartilage degeneration and osteophyte formation in a collagenase-induced murine OA model through R-spondin-2 (Zhang *et al.*, 2018). On

the other hand, M2 macrophages immunomodulated by squid type II collagen (SCII) inhibited chondrocyte apoptosis and hypertrophy suggesting macrophages are involved in chondrogenesis with varying roles depending on their different polarized phenotypes (Zhang, Cai and Bai, 2020).

Macrophages are known to secrete several of the aforementioned cytokines and chemokines involved in OA pathology and macrophage associated TGF-β has been reported to be a strong predictor of OA progression in a cohort of knee OA patients (Hsueh *et al.*, 2021). TGF-β is responsible for stimulating bone formation and the production of proteoglycan, type II collagen and chondrogenesis (Zhang, Cai and Bai, 2020). Furthermore, SPECT-CT (single-photon emission computed tomography) of OA knees using etarfolatide, identified 76% of patients have evidence of recruitment of activated macrophages and this was associated with symptoms of OA including knee pain, joint space narrowing, and osteophytes (Kraus *et al.*, 2016). Additionally, levels of the macrophage marker CD14 in the synovial fluid (SF) is positively associated with the severity of joint space narrowing and osteophytes and SF CD14 and plasma derived CD14 are positively associated with self-reported pain severity (Daghestani, Pieper and Kraus, 2015). Furthermore, SF CD14 and SF CD163 are positively associated with osteophyte progression providing further evidence to support the central role of macrophage in OA pathological changes (Daghestani, Pieper and Kraus, 2015). The association between pain perception and $CD14^+$ macrophages is possibly due to increased nerve growth factor (NGF) levels which is produced by $CD14^+$ macrophages upon stimulation with pro-inflammatory cytokines (Takano *et al.*, 2017).

In summary, immune cells at the synovial joint are known to contribute to the maintenance of tissue homeostasis through regulation of resident and infiltrating

cells at the joint and in OA and other arthritic conditions are known to contribute to the pathological changes whether through secretion of inflammatory factors or through the secretion of degradative and catabolic enzymes.

Cartilage degradation

Articular cartilage is a highly specialised and hydrated connective tissue present at diarthrodial joints which is devoid of neurones, blood and lymphatic vessels (Sophia Fox, Bedi and Rodeo, 2009). The primary function of articular cartilage is to provide a smooth lubricated surface which permits articulation (Sophia Fox, Bedi and Rodeo, 2009). It is approximately 2-4mm in width and is primarily composed of ECM components that are synthesised by quiescent chondrocytes. Chondrocytes produce and secrete collagen proteins (II, IV, IX and XI) and proteoglycans (aggrecans) which are primary components of ECM. However, during the development of OA these chondrocytes become activated resulting in a phenotypic shift towards fibrillation and degradation of ECM through upregulation of cartilage degrading enzymes such as the aforementioned matrix metalloproteinases (MMPs) and A Disintegrin and Metalloproteinase with Thrombospondin motifs (ADAMTS) (Akkiraju and Nohe, 2015). This degradation of the articular cartilage by chondrocytes results in reduced joint space width, a key symptom of arthritis. As previously mentioned, inflammatory cytokines released by resident and infiltrating immune cells stimulate the production of these degradative MMPs such as MMP2, 3 and 9. Pro-inflammatory cytokines IL1β and TNFα secreted by macrophages, synovial fibroblast and chondrocytes are capable of activating MMP-1, 3, 9 and 13 (Mehana, Khafaga and El-Blehi, 2019). MMP 1 and 13 have a predominant role in OA as these are the rate-limiting enzymes in collagen degradation (Mehana, Khafaga and El-Blehi, 2019). MMP1 is predominantly secreted by synovial cells however MMP13 is

primarily released by chondrocytes (Mehana, Khafaga and El-Blehi, 2019). Furthermore, MMP13 is capable of breaking down aggrecan, a major component of cartilage, alongside collagen proteins. Knockout of endogenous MMP13 in a *Col2CreER;*Mmp13$^{fx/fx}$ murine model which underwent meniscal-ligamentous injury (MLI), found reduced cartilage degeneration at 8, 12 and 16 weeks post-surgery compared to Cre-negative mice (Wang *et al.*, 2013). Furthermore, there was reduced chondrocyte apoptosis compared to control mice and a small molecule inhibitor of MMP13, CL82198, reduced MLI-induced OA progression, increased type II collagen and proteoglycan levels as well as inhibiting chondrocyte apoptosis providing further evidence MMP13 is critical for OA progression and pharmacological inhibition may provide a means of decelerating OA progression (Wang *et al.*, 2013).

Another degradative enzyme critical for OA cartilage degradation is ADAMTS-5. ADAMTS-5 has received particular attention for its role in aggrecan degradation which is thought to proceed irreversible collagen loss. siRNA knockdown MMP13 and ADAMTS5 have both been shown to reduce cartilage degradation in rodent models, however these enzymes also have homeostatic roles in processes such as wound healing, muscle regeneration, angiogenesis and cell migration and therefore in addition to off-target effects, MMP inhibitors can have on-target effects at sites outside of the joint (McClurg, Tinson and Troeberg, 2021). Another possible means of targeting these degradative enzymes is through endogenous inhibitors, such as tissue inhibitors of metalloproteinases (TIMPs). TIMP3 is the most effective TIMP inhibitor of both MMPs and ADAMTS and is reduced within OA cartilage suggesting promoting TIMP3 expression in OA cartilage early in disease course may ameliorate OA progression (Morris, Cs-Szabo and Cole, 2010). Another alternative approach is to promote cartilage repair through autologous mesenchymal stem cell therapies or

through the use of anabolic growth factors such as FGF18, which are capable of increasing chondrocyte proliferation and proteoglycan production *in vitro* (McClurg, Tinson and Troeberg, 2021). Attempts have been made to promote anabolic repair pathways using methods such as platelet-rich plasma (PRP) therapy, which works by platelet activation releasing cytoplasmic components which include TGF-β1, platelet-derived growth factor (PDGF), insulin-like growth factor (IGF), and FGF2 which have been shown to promote aggrecan and collagen synthesis, while reducing expression and activity of catabolic metalloproteases (Everts *et al.*, 2020). However, clinical trials of PRP therapies have produced mixed results, with some studies showing reduced Western Ontario and McMaster Universities Osteoarthritis Index (WOMAC) scores compared to hyaluronan for up to 6 months whereas others have shown PRP to be no more effective than hyaluronan at improving several patient-reported outcome measures at 2, 6, and 12 months (Cerza *et al.*, 2012; Filardo *et al.*, 2012). This can possibly be due to differences in PRP preparation such as double filtration compared to centrifugation with the former more likely to exclude leukocytes. Standardisation of PRP preparation across RCTs may provide a clearer picture on their use as a disease modifying OA drug (DMOAD).

In summary, cartilage degradation is a major symptom of OA and alongside pathological changes in joint tissues such as bone and synovium, is a major target of new therapies. Promoting anabolic repair pathways and ameliorating catabolic changes in chondrocytes remains the principal means of altering OA disease course.

1.4 Obesity and Osteoarthritis

Obesity is a well-recognised global epidemic, with the number of obese people worldwide doubling over the past 30 years and is currently predicted at 200 million men and 300 million women by World Health Organisation (WHO) (World Health Organisation, 2016). The Health Survey for England 2019 estimates that 28% of adults (≤16) in England are obese and 36.2% are overweight and obesity increased across age groups up to 75 years old (NHS Digital, 2019).In a survey conducted by Sports England in November 2020, 62.8% of adults (≤18) in England were overweight or obese (Sports England, 2020). This obesity epidemic also affects those with musculoskeletal conditions. Data collected and analysed from the Netherlands Working Conditions Survey (n = 44,793) found workers (15–64 years age group) with a high body mass index (BMI) had increased 12 month prevalence of self-reported musculoskeletal symptoms based on Dutch Musculoskeletal Questionnaire (Hildebrandt *et al.*, 2010; Viester *et al.*, 2013). Odd ratio (OR) adjusted for age and gender found significant association between these musculoskeletal symptoms in overweight workers (BMI 25.0-29.9 kg/m^2) (OR 1.13, 95% CI: 1.08-1.19) and obese workers (BMI ≥ 30 kg/m^2) (OR 1.28, 95% CI: 1.19-1.39) (Viester *et al.*, 2013).

Obesity has major implications for the musculoskeletal system, including the risk of developing OA. Indeed, OA patients that have a BMI greater than 30 kg/m^2 have a significantly increased risk of developing knee OA compared to those of normal weight (Coggon *et al.*, 2001). A systematic review and meta-analysis of risk factors for OA found pooled OR for developing OA was 2.63 (95% CI 2.28-3.05) for obese subjects compared to normal-weight controls (Blagojevic *et al.*, 2010). Obese adults

who have knee OA report reduced quality of life, affecting daily living activities which impacts leisure, social life, sleep quality and results in losses in labour relations (Sutbeyaz *et al.*, 2007).

Recent meta-analyses by Jiang et al, 2011 and 2012 reported a positive correlation between BMI and the risk of developing both knee and hip OA (clinical and radiographical) (Jiang *et al.*, 2011, 2012). They found a 5-unit increase in BMI was associated with a 35% increased risk of knee OA (RR: 1.35; 95% CI: 1.21-1.51) and an 11% increased risk of hip OA (RR: 1.11; 95% CI: 1.07-1.16) (Jiang *et al.*, 2011). Notably, the relationship between BMI and development of knee OA was greater in women compared to men however this significance was abolished with hip OA (Jiang *et al.*, 2011). A case control study found that those who became overweight earlier on in adulthood were at an increased risk of developing knee and hip OA providing further evidence of increased risk in developing obesity associated OA in patients whose BMI is greater than 30 kg/m^2 (Bliddal, Leeds and Christensen, 2014). The pathophysiology of obesity associated OA is likely due to a number of factors including structural damage and increased weight loading on joints, decreased muscle strength and altered biomechanics of the joint (King, March and Anandacoomarasamy, 2013). Another major aspect of obesity associated OA is the alterations in metabolic state of cellular components of the joint. Obesity has been well described in the literature as perpetuating a chronic low grade inflammatory state which is thought to contribute to synovial inflammation observed in OA. This is particularly observed in obese patients with increased risk of developing OA in non-weight bearing joints such as the hand (Oliveria *et al.*, 1999). Obese OA patients also exhibit elevated levels of pro-inflammatory cytokine TNF-α, IL6 and IL8 in the synovial fluid compared to normal weight OA patients (Pearson *et al.*, 2017). In

particular synovial fibroblasts from obese OA patients were found to secrete higher amounts of IL-6 compared to normal weight OA synovial fibroblast indicating obese OA synovial fibroblast are imprinted with a more inflammatory phenotype compared to normal weight OA synovial fibroblast (Pearson *et al.*, 2017).

1.6 Fibroblasts metabolism and inflammation

Introduction to fibroblast biology

Fibroblast are spindle-shaped mesenchymal stromal cells found in a wide variety of parenchymal tissues and are responsible for maintaining the structural architecture of these tissues through maintenance of the ECM (Farah *et al.*, 2020). Fibroblasts are chemotactic and therefore migrate in response to chemical signals such as chemokines, cytokines, and growth factors to participate in wound healing and tissue repair and remodelling. Dysregulation of these processes is associated with several disease pathologies such as fibrosis, cancer, and inflammation.

Research on fibroblasts is made particularly difficult due to their heterogeneity and therefore identifying fibroblasts is a challenge. There are several mesenchymal markers which are used to identify fibroblasts (table 1.1) however none are unique to fibroblasts and therefore another means of distinguishing fibroblasts is using epithelial, endothelial and leukocyte markers as negative/exclusion markers. Primary fibroblasts originate from the primary mesenchyme during gastrulation (LeBleu and Neilson, 2020). After the development of the mesoderm into the true mesenchyme, mature fibroblast develop alongside connective tissue, bone, cartilage and blood and

lymphatic circulatory systems (LeBleu and Neilson, 2020). Mesenchyme derived fibroblast from post-embryonic resident fibroblast in tissues maintain quiescent phenotype until they are stimulated in injury, cancer or other inflammatory conditions (LeBleu and Neilson, 2020). The mesoderm also contributes to several cell types such as mesenchymal stem cells, epithelial and endothelial cells, adipocytes and fibrocytes. These cells with common embryonic lineages can become fibroblasts upon de-differentiation (figure 1.2). Epithelial cells undergo epithelial-to-mesenchymal transition (EMT) in cancer and adipocytes will lose their lipid storage, migrate to wounds, and become fibroblasts in wound healing (figure 1.2). Fibroblast plasticity is highest in embryonic and early development and lowest during ageing (LeBleu and Neilson, 2020).

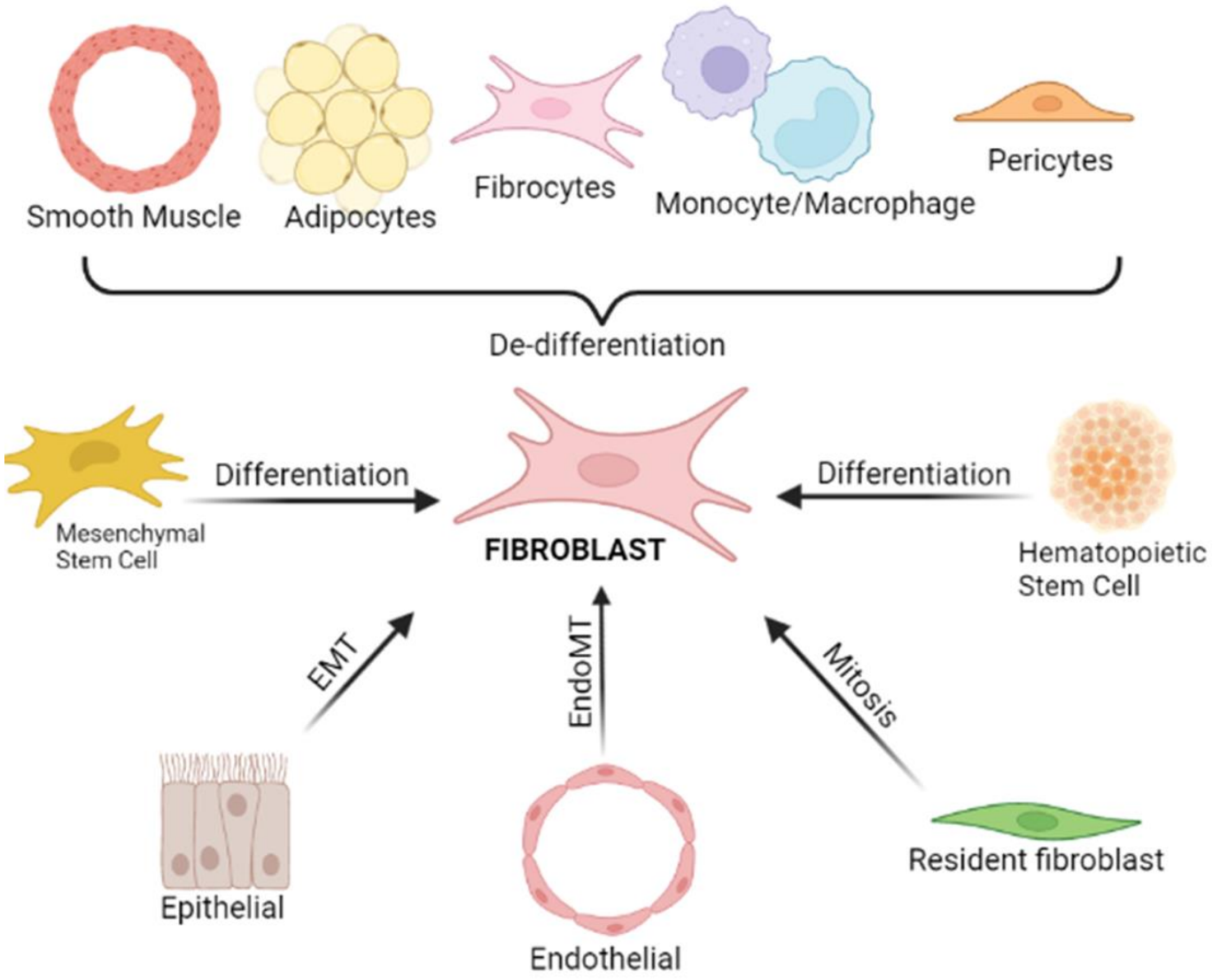

Figure 1.2: Schematic diagram showing the cell types and mechanisms from which fibroblast may be derived from.

Table 1.1: Common markers used to identify fibroblasts

Mesenchymal markers	Cell location
Podoplanin (PDPN)	Cell Surface
Thy-1	Cell Surface
FAPα	Cell Surface
Vimentin	Intracellular
PDGFRα	Cell Surface
alpha-Smooth Muscle Actin (SMA)	Intracellular
1B10	Cell Surface
TE-7	Cell Surface
Aminopeptidase N/CD13	Cell Surface
DLK1	Cell Surface
DPPIV/CD26	Cell Surface
FSP1 (S100A4)	Cell Surface
Integrin beta 1/CD29	Cell Surface
MAS516	Cell Surface

Collagen	Secreted
Elastin	Secreted
Fibronectin	Secreted
Laminin	Secreted

Fibroblast metabolism in inflammation and fibrosis

In inflammatory microenvironments, fibroblasts adopt a more active, invasive and inflammatory phenotype (Farah *et al.*, 2020) . As a results, fibroblasts have been identified as central contributors to disease pathology in several chronic inflammatory diseases such as fibrosis and inflammatory joint diseases (Farah *et al.*, 2020). In tumorous environment, fibroblasts undergo a switch to an activated state and are labelled cancer associated fibroblasts (CAFs). CAFs promote tumour growth and invasion through remodelling of the ECM through production of type I and II collagen as well as fibronectin (Clarke *et al.*, 2016; Erdogan *et al.*, 2017). CAFs also promote angiogenesis and secrete pro-inflammatory cytokines and chemokines thereby contributing to the inflammatory microenvironment (Farah *et al.*, 2020).

This switch in cellular phenotype is accompanied by concomitant changes in the metabolic state of the cell to provide energy and generate biosynthetic materials to fuel and sustain these adoptive phenotypic states. As a results of the Warburg effect, CAFs upregulate glycolytic enzymes such as hexokinase 2 (HK2) and phosphofructokinase (PFKL) (Avagliano *et al.*, 2018). This increased glycolytic flux

means increased glucose is required and so therefore alongside other metabolites lactate is used to generate this glucose and is imported using monocarboxylate transporters such as MCT4 (Whitaker-Menezes *et al.*, 2011). In fact, MCTs are key therapeutic targets for disrupting CAF cancer metabolic symbiosis with genetic ablation of MCT4 expression overcoming adaptive resistance of cancer drug therapies (Pisarsky *et al.*, 2016). On the other hand, CAFs metabolic reprogramming results in the downregulation of TCA cycle metabolites, with reduced levels of isocitrate dehydrogenase 3a (IDH3α) observed in transforming growth factor beta 1 (TGFβ1)-induced differentiation of CAFs (Zhang *et al.*, 2015). Alongside this, knockdown of IDH3α in fibroblasts increases glucose uptake and lactate production with concomitant reduction in oxygen consumption alternatively overexpression of IDH3α results in the opposite effect (Zhang *et al.*, 2015). Another key aspect of CAFs metabolism is the secretion of glutamine and ketone bodies which are thought to be internalised by cancer cells which cannot generate further glutamine internally and so therefore are dependent on exogenous glutamine (Farah *et al.*, 2020).

Metabolic Process	Normal Fibroblast	Cancer Associated Fibroblast	RA Synovial Fibroblast	Fibrotic Myofibroblast
				
Aerobic Glycolysis	+	+++	+++	++
OXPHOS	+	++	++	+
Pentose Phosphate Pathway	+		++	
Glutamine Metabolism	+	+++	++	++

Figure 1.3: Schematic diagram showing the metabolic pathways altered in fibroblasts in different disease pathologies (Farah *et al.*, 2020).

Another example of the intricate relationship between fibroblasts phenotype and its metabolism is in fibrosis. Fibroblast-mediated ECM remodelling is essential for normal tissue structural integrity however trauma and inflammation negatively affect ECM homeostasis (Farah *et al.*, 2020). In chronically inflamed tissues, cytokines such as TNFα, IFNy and TGF-β regulate the expression of ECM proteins through changes in fibroblast phenotype (Sorokin, 2010). Genome wide transcriptomic data of human skin fibrosis post radiation therapy compared to age-matched healthy controls displayed reduced oxidative phosphorylation, fatty acid oxidation and TCA cycle activity alongside increased glycolytic processes (Zhao *et al.*, 2019; Farah *et al.*, 2020). Induction of peroxisome proliferator-activated receptor (PPAR) signalling using caffeic acid in primary dermal fibroblasts reduced production of profibrotic proteins and blocking glycolysis using hexokinase inhibitor 2-deoxy-D-glucose (2DG) downregulated ECM protein levels (Zhao *et al.*, 2019; Farah *et al.*, 2020). Renal fibrosis has been identified as a cause of chronic kidney disease. Activated fibroblasts are the key culprit in renal interstitial fibrosis, producing large amount of ECM components (Fujigaki *et al.*, 2005; Farah *et al.*, 2020). Recent research have shown activated renal interstitial fibroblast stimulated with TGF-β increased aerobic glycolysis and expression of glycolytic enzymes HK1/2 and pyruvate kinase M2 (PKM2) as well as reduced mitochondrial respiration (Farah *et al.*, 2020). Likewise, analysis of a unilateral ureteral obstruction mouse model of renal interstitial fibrosis, showed increased expression of increased glycolytic enzymes HK and PKM2 and overexpression of PKM2 induced renal interstitial fibrosis (Yin et al., 2018; Farah et al., 2020).

In pulmonary fibrosis, lung fibroblasts undergo a major transformation and exhibit increased proliferation and an activated phenotype. These fibroblasts have been

termed myofibroblasts and are often characterised by presence of increased alpha smooth muscle actin (α-SMA) (table 1.1). Myofibroblasts also display altered metabolic state with a shift towards increased aerobic glycolysis such as the increased expression of glycolytic enzyme 6-Phosphofructo-2-Kinase/Fructose-2,6-Biphosphatase 3 (PFKFB3) (table 1.2) (Xie *et al.*, 2015; Farah *et al.*, 2020). Blocking PFKFB3 using metabolic inhibitor 3PO, attenuates the differentiation of lung fibroblasts and reduces their pro-fibrotic phenotype in patients with idiopathic pulmonary fibrosis (Xie *et al.*, 2015; Farah *et al.*, 2020). Likewise, myofibroblasts exhibit significantly augmented glutaminolysis alongside increased expression of glutaminase 1 (GLS1) (table 1.2). siRNA knockdown of GLS1 and pharmacological using small molecule inhibitors BPTES and CB-839, reduced expression of collagens I and III but did not affect fibronectin, elastin, or α-SMA expression (Ge *et al.*, 2018). Glutaminolysis enhanced collagen translation and stability through mTOR complex 1 (mTORC1) activation and collagen proline hydroxylation (Ge *et al.*, 2018). This suggests glutamine metabolism is intricately involved in regulating the pro-fibrotic phenotype of lung myofibroblasts. Finally excessive collagen deposition in lung fibrosis has been linked to altered serine, glycine synthesis. TGF-β stimulation which promotes excessive collagen production also induces the expression of de novo serine synthesis enzymes phosphoglycerate dehydrogenase (PHGDH), phosphoserine aminotransferase 1 (PSAT1) and phosphoserine phosphatase (PSPH), alongside the expression of the de novo glycine synthesis enzyme serine hydroxy methyltransferase 2 (SHMT2) in primary lung fibroblasts (Nigdelioglu *et al.*, 2016).

Synovial fibroblasts are one of the two resident cell types found at the synovial membrane (synovium) in synovial joints. These cells are responsible for maintaining

cartilage integrity and the lubrication of the synovial joint by secreting ECM components into the synovial fluid (Farah *et al.*, 2020). In inflammatory joint conditions like rheumatoid arthritis (RA), synovial fibroblasts adopt an inflammatory and invasive phenotype becoming hyperplastic and proliferating rapidly to create formation of pannus-like structures as they lose contact inhibition (Farah *et al.*, 2020), RA synovial fibroblasts increase the expression of degradative enzymes such as matrix metalloproteases (MMPs) and aggrecanases including ADAMTS4/5 which promotes cartilage degradation (Farah *et al.*, 2020). In OA, a lower grade of chronic inflammation has been observed in OA synovial fibroblasts compared to non-OA controls with an increase in pro-inflammatory stimuli such as IL6 and CXCL8 (Nanus *et al.*, 2020).

	Metabolic pathways			
	Aerobic glycolysis	**Oxidative phosphorylation**	**Pentose phosphate pathway**	**Glutamine metabolism**
CAFs	Upregulation of HK2 and PFKL	IDH3α is reduced in CAFs resulting in increased glycolysis and decreased oxidative phosphorylation		Inhibiting glutamine synthetase in stroma and glutaminase in cancer cells reduces tumour weight, nodules and metastasis
Activated Synovial Fibroblasts	High levels of PGK1 present in blood and synovial tissue of RA patients and silencing of PGK1 in RA synovial fibroblasts reduced the secretion of IL-1β and IFN-γ	Hypoxia in RA synovial fibroblasts results in reduced oxidative phosphorylation and increased glycolysis	GC/TOF-MS-based metabolomic profiling of RA synovial fibroblasts shows upregulation of the pentose phosphate pathway	RA synovial fibroblasts show increased expression of GLS1
Myofibroblasts	Myofibroblasts show increased expression of the glycolytic enzyme PFKFB3 and inhibiting glycolysis using the PFKFB3 inhibitor 3PO reduced the differentiation of lung fibroblasts into activated myofibroblasts	Dermal fibrotic skin and lung fibroblasts stimulated with TGF-β results in a switch from mitochondrial respiration to aerobic glycolysis		Lung myofibroblasts show significantly augmented glutaminolysis, which is mediated by elevated Gls1 and inhibition of glutaminolysis using glutaminase 1 inhibitor (BPTES), reduced the expression of ECM components
Senescent fibroblasts	Senescent fibroblasts show increased expression of glycolytic enzymes PDK2, PDK3, PDK4	Metabolomic profiling of intracellular senescent fibroblasts metabolome shows reduced TCA cycle metabolites such as citrate, indicative of a decline in mitochondrial metabolisms	GC/TOF-MS-based metabolomic profiling of senescent fibroblasts conditioned media show reduced TCA activity and shift energy production towards glycolysis, gluconeogenesis, and the pentose phosphate pathway	Metabolomics analysis shows glutamate levels increase in senescent fibroblasts

Table 1.2: Dysregulated metabolic pathways in stromal fibroblasts (Farah *et al.*, 2020).

Like in other inflammatory microenvironments, synovial fibroblast metabolism is altered relying on increased aerobic glycolysis to maintain their active phenotype (Farah *et al.*, 2020). In RA, high levels of glycolytic enzyme phosphoglycerate kinase 1 (PGK1) where observed in blood and synovial tissue of RA patients and inhibiting PGK1 using siRNA knockdown in RA synovial fibroblasts reduced the secretion of pro-inflammatory cytokines IL-1β and TNFα (Zhao *et al.*, 2016). Likewise, blocking PFKFB3 using 3PO reduced fructose-2,6-bisphosphate and lactate levels as well as reducing the secretion of pro-inflammatory cytokines in RA synovial fibroblasts (M Biniecka *et al.*, 2016). RA synovial fibroblasts are also reliant on glutamine metabolism and exhibit increased expression of GLS1 (table 1.2) (Takahashi *et al.*, 2017). Blocking glutamine metabolism using GLS1 inhibitor compound 968 (5-(3 bromo-4-(dimethylamino) phenyl)-2,2-dimethyl-2,3,5,6-tetrahydrobenzo[a] phenanthridin-4(1H)-one) reduced RA synovial fibroblasts proliferation (Takahashi *et al.*, 2017).

Although there has been much research establishing the link between the RA synovial fibroblast inflammatory phenotype and its metabolism there has been very little investigation on the role metabolism plays in the inflammatory phenotype of OA synovial fibroblasts. Furthermore, recent research by our group has shown that obesity affects OA synovial fibroblast phenotype, increasing their rate of proliferation and exacerbating the inflammatory phenotype of these cells (Nanus *et al.*, 2020). OA synovial fibroblasts from obese patients show increased expression of inflammatory cytokines and chemokines such as IL6, IL-1β, CXCL8, CXCL5 and CCL2 alongside an altered transcriptome which exhibits upregulation of inflammatory pathways such as cytokine-cytokine interactions, toll-like receptor signalling and chemokine signalling pathways (Nanus *et al.*, 2020).

Therefore, investigating the metabolic phenotype (metabotype) of these obese OA synovial fibroblasts might yield insights into which metabolic pathways are required to maintain this inflammatory phenotype observed in these synovial fibroblasts and whether modulating these metabolic pathways through metabolic inhibitors might ameliorate their inflammatory profile.

1.7 Thesis Hypothesis

Given the relationship between the metabolic and inflammatory state of the cell, obese OA synovial fibroblast are more metabolically active compared to normal weight OA synovial fibroblast and therefore release more pro-inflammatory cytokines resulting in a more inflammatory microenvironment at the synovial membrane of obese OA patients.

1.8 Thesis Aims

The aim of this thesis is to determine the relationship between cellular metabolic phenotype (metabotype) and inflammatory phenotype of synovial fibroblasts from patients with OA.

This thesis will use primary human OA synovial fibroblasts from patients with different BMIs ranging from normal weight to obese to determine whether:

1. OA synovial fibroblasts from obese patients exhibit distinct metabotypes compared to normal weight controls
2. Changes in OA synovial fibroblast metabotype from obese patients drives changes in inflammatory phenotypes compared to normal weight controls
3. Does modulating altered metabotype of OA synovial fibroblasts from obese patients ameliorate inflammation observed within the OA synovial joint

CHAPTER 2. MATERIALS AND METHODS

Materials

Table 2.1 Cell culture general reagents

Reagent or Resource	Source	Identifier
RPMI-1640 Medium With L-glutamine and sodium bicarbonate, liquid, sterile-filtered, suitable for cell culture	Sigma Aldrich	R8758
RPMI-1640 Medium With sodium Bicarbonate and without L-glutamine and liquid, sterile-filtered, suitable for cell culture	Sigma Aldrich	R0883
Gibco™ Fetal Bovine Serum, qualified, heat inactivated, E.U.-approved, South America Origin	Gibco (ThermoFisher)	11550356
Penicillin-Streptomycin (10,000 U/mL)	Gibco (ThermoFisher)	15140122
L-Glutamine (200 mM)	ThermoFisher	25030024
MEM Non-Essential Amino Acids Solution (100X)	Gibco (ThermoFisher)	11140050
Sodium Pyruvate (100 mM)	Gibco (ThermoFisher)	11360070
Phosphate buffered saline (PBS) tablets 1 tablet per 500ml distilled water	Gibco (ThermoFisher)	18912014

Trypsin-EDTA solution (10x)	Sigma Aldrich	T4174
Cell Dissociation Solution Non-enzymatic 1x phosphate buffered saline without calcium and magnesium	Sigma Aldrich	C5914

Table 2.2 Cell culture plasticware

Reagent or Resource	Source	Identifier
Corning Multiple Well Cell Culture Plates (12-well, 24-well, 48-well, 96-well)	Corning	BC011, BC012, BC014, BC015
Corning TC Flask 75cm2 canted neck vented cap (100)	Corning	BC301
TC Dishes 100mm (20-sleeve)	Corning	BC153

Table 2.3 Recombinant proteins, stains, and inhibitors

Reagent or Resource	Source	Identifier
Recombinant Tumour Necrosis Factor-α	Sigma Aldrich	T6674
MitoTracker™ Green FM	Invitrogen (ThermoFisher)	M7514
6-NBDG (6-(N-(7-Nitrobenz-2-oxa-1,3-diazol-4-yl)amino)-6-Deoxyglucose)	Invitrogen (ThermoFisher)	N23106
Bis-2-(5-phenylacetamido-1,3,4-thiadiazol-2-yl)ethyl sulfide (BPTES)	Sigma Aldrich	SML0601
Dimethyl sulfoxide	Sigma Aldrich	D2650

Table 2.4 Assay kits and Reagents

Reagent or Resource	Source	Identifier
DCFDA / H2DCFDA - Cellular ROS Assay Kit	Abcam	ab113851
BrdU Cell Proliferation ELISA Kit (colorimetric)	Abcam	ab126556
iTaq™ Universal SYBR® Green One-Step Kit	Bio-Rad	#1725151
Lactate Assay Kit	Sigma Aldrich	MAK064
Bradford assay	Bio-Rad	#5000002

Pierce™ BCA Protein Assay	ThermoFisher	23225
Human IL-6 DuoSet ELISA	R & D Systems	DY206
Seahorse XFe96 FluxPak mini	Agilent	102601-100
TRIzol™ Reagent	Invitrogen (ThermoFisher)	15596018
Chloroform	Sigma Aldrich	366927
2-Propanol	Sigma Aldrich	I9516
GlycoBlue™ Coprecipitant	Invitrogen (ThermoFisher)	AM9516
Nuclease-free water	Promega	P1193

Table 2.5 Seahorse Metabolic Flux Assay

Reagent or Resource	Source	Identifier
Seahorse XF RPMI medium, pH 7.4, 500 mL	Agilent	103576-100
D-(+)-Glucose	Sigma-Aldrich	G7021
2-Deoxy-D-Glucose	Sigma-Aldrich	D8375
Oligomycin	Sigma-Aldrich	O4876
Carbonyl cyanide 4-(trifluoromethoxy)phenylhydrazone (FCCP)	Sigma-Aldrich	C2920
2-Deoxy-D-glucose	Sigma-Aldrich	D8375
Rotenone	Sigma-Aldrich	R8875
Antimycin A	Sigma-Aldrich	A8674

Table 2.6 Western blotting reagents

Reagent or Resource	Source	Identifier
Protease Inhibitor Cocktail	Sigma-Aldrich	P8340
Phosphatase Inhibitor Cocktail 3	Sigma-Aldrich	P0044
Amersham ECL Prime	GE Healthcare	RPN2232
Immun-Blot® PVDF Membrane	Bio-Rad	1620177

Table 2.7 Western blotting antibodies

Reagent or Resource	Source	Identifier	Dilution
HRP-linked anti-rabbit IgG secondary antibody	GE Healthcare	NA931	1:2000
HRP-linked anti-mouse IgG secondary antibody	GE Healthcare	NA934	1:10,000
monoclonal anti-GLS1 Primary antibody	Abcam	ab156876	1:1000
Anti-MCT1 primary antibody	Abcam	ab85021	1:1000
monoclonal anti-beta-actin antibody	Sigma-Aldrich	SAB1305546	1:5000

Table 2.8 siRNA knockdown reagents

Reagent or Resource	Source	Identifier
siGENOME non-targeting siRNA Pool #1, 5 nmol	Dharmacon	D-001206-13-05
siGENOME Human GLS (2744) siRNA - Set of 4, 5 nmol	Dharmacon	MQ-004548-01-0005
Opti-MEM™ Reduced Serum Medium	ThermoFisher Scientific	11058021
Lipofectamine 3000	Invitrogen	L3000001

Table 2.9 RT-qPCR Primers

Gene Symbol	Forward Sequence (5'-3')	Reverse Sequence (5'-3')	Melting Temperature (Tm)	G-C content (GC%)
18s	GTAACCCGTTGAACCCCCATT	CCATCCAATCGGTAGTAGCG	F: 60.55 R: 57.93	F: 52.38 R: 55.00
IL6	GCGCAGCTTTAAGGAGTTCCT	CCATGCTACATTTGCCGAAGA	F: 60.95 R: 58.98	F: 52.38 R: 47.62
MCT1/SLC16A1	GAAATCTGGAGGATAGCGTTACACT	CAAAATGCAGGTCAAATCCAAA	F: 60.45 R: 56.31	F: 44 R: 36
MCT2/SLC16A7	TGCTGGCTGTTATGTACGCAGG	GCCAACACCATTCCAAGACAGC	F: 63.18 R: 62.54	F: 54 R: 54
MCT4/SLC16A3	CAGTTCGAGGTGCTCATGG	ATGTAGACGTGGGTCGCATC	F: 64.7 R: 65.0	F: 57 R: 55
GLUT3/SLC2A3	TTCGTCTCTAGCCTGCACTG	ACACAACTTCTCCGGGTGAC	F: 59.47 R: 59.89	F: 55 R:55

Methods

2.1 Ethical approval and subject recruitment

Ethical approval was granted by the UK National Research Ethics Committee (NRES16/SS/0172) to collect OA joint tissue from consenting patients following elective total joint replacement. Patients were recruited to the study at the Royal Orthopaedic Hospital, Birmingham (United Kingdom) or at Russell's Hall Hospital, Dudley (United Kingdom). Synovial joint tissue was collected peri-operatively and used to isolate primary synovial fibroblasts. Patients were classified as either normal-weight (18-25) or obese (>30) based on their BMI.

2.2 Primary synovial fibroblast isolation and culture

For the isolation of synovial fibroblasts, synovial tissue was dissected using a scalpel into $1mm^3$ pieces, placed into a tissue culture flask and incubated at 37^oC, 5% CO_2 in complete fibroblast growth media RPMI-1640 media (Sigma-Aldrich, R8758) supplemented with 10% foetal calf serum (Sigma-Aldrich, F7524), 1% non-essential amino acids (Sigma-Aldrich, M7145), 1% sodium orthopyruvate (Sigma-Aldrich, S8636), 2mM L-glutamine (ThermoFisher Scientific, 25030024), 1% penicillin and streptomycin (100U/ml penicillin and 100µg/ml streptomycin) (Sigma-Aldrich, P4333). Fibroblasts were characterised by FACS analysis by confirmation of GP38+ CD31-,CD235a- and CD45- cell surface expression markers (data not shown).

Growth media was replaced every 3-4 days, and cells passaged upon reaching 70% confluency. Passaged fibroblasts from P2 to P4 were harvested at 70-80% confluence for downstream experiments. Fibroblast conditioned media was collected after 24 hours of conditioning.

2.3 Confirmation of the maintenance of synovial fibroblast phenotype during in vitro culture

One area of research that required establishment was whether OA synovial fibroblasts maintained their phenotype in vitro following cell culture. Previous research by others have shown synovial fibroblasts maintain their phenotype up to 5 passages and our research has shown synovial fibroblast from obese patients with hip OA are imprinted with a greater inflammatory phenotype (Neumann *et al.*, 2010; Pearson *et al.*, 2017). This was further confirmed by research conducted within this group by showing cultured OA synovial fibroblast (passage 2-5) are positive for fibroblast markers podoplanin ($GP38^+$) and negative for endothelial cell marker ($CD31^-$), red blood cell marker ($CD235a^-$) and leukocyte, monocyte and macrophage haematopoietic marker ($CD45^-$) (Supplementary figure S2) (Farah *et al.*, 2022).

2.4 Isolation of RNA from primary human OA synovial fibroblasts

To isolate RNA from OA synovial fibroblasts, cells were seeded and incubated (37^oC, 5% CO_2) in 48 well tissue culture plates at 40,000 cells/well. At the

appropriate timepoint, cells were lysed using 1ml of TRIzol® reagent (Life technologies, Paisley, UK) per well. Plates containing cell lysates were then either frozen at -80^{o}C, or RNA was extracted immediately by following the manufacturer's protocol. In brief, TRIzol reagent was transferred to 1.5ml microcentrifuge tube and chloroform added (200µl) and then centrifuged at 12,000xG for 30 minutes at 4^{o}C to cause phase separation. The top aqueous phase (containing RNA) was suspended in isopropanol and GlycoBlue™ co-precipitant dye (Thermo Fischer Scientific, Loughborough, UK) before being centrifuged at 10,000xG for 10 minutes at 4^{o}C. RNA samples are then washed with 75% ethanol and centrifuged at 8000xG for 5 minutes at 4^{o}C before being dried (vacuum desiccator) and suspended in 20µl of Nuclease free H_2O. RNA concentrations were quantified using a Nanodrop 2000 spectrophotometer (Life technologies, Paisley, UK).

2.5 Isolation of total protein from primary human OA synovial fibroblasts

OA synovial fibroblasts grown in 12 well plates (120,000 cells/well) were lysed with 100µl of RIPA buffer 4^{o}C (Thermo Fisher Scientific, MA, USA), containing phosphatase inhibitor cocktail 3 (1:100) (Sigma-Aldrich, Dorset, UK) and protease inhibitor cocktail (1:100) (Sigma-Aldrich, Dorset, UK). Following lysis, cells lysates were collected from well and transferred to a 1.5ml microcentrifuge tube. Total protein was quantified using a BCA assay (Thermo Fisher Scientific, MA, USA) in a clear 96-well plate as described by the manufacture's protocol. Samples were measured in duplicate and optical density was measured at 550nm using BioTek

EL808 spectrophotometer (Biotek, Swindon, UK). Following measurement of absorbance, a standard curve was generated, and protein concentrations were calculated (µg/µl).

2.6 Reverse transcription Polymerase Chain Reaction

Forward and reverse primers were designed using Primer Express (Primer Express Software v3.0.1 License Thermo Fisher Scientific, UK) for RT-qPCR using SYBR Green detection (Bio-Rad, Hertfordshire, UK) and are detailed in Table 2. RNA isolated from OA synovial fibroblasts from different cohorts were diluted to 5ng/µl in nuclease free water (Thermo Fischer Scientific, Loughborough, UK). Quantitative real time PCR was performed on a Bio-Rad CFX384 Touch™ Real-Time PCR Detection System (Bio-Rad, Hertfordshire, UK) using a one-step SYBR Green kit (Bio-Rad, Hertfordshire, UK), with each well containing SYBR Green Master Mix (2.5µl), 1.5nM of forward and reverse primers (0.1µl), Taq reverse transcriptase (0.06µl), 5ng/µl of template RNA (1µl) and RNase free water (1.24µl). A one-step amplification protocol was used with 40 cycles; reverse transcription at 55^{o}C for 10 minutes, enzyme activation at 95^{o}C for 5 minutes, denaturation at 95^{o}C for 10 seconds and data collection at 60^{o}C for 30 seconds. Ribosomal 18s was used as an internal housekeeping control. Relative gene expression was calculated using the ΔCt method. Each sample was run in duplicate with four biological replicates per group and data was analysed using Prism9 software (GraphPad, CA, USA).

2.7 siRNA Transfection

OA synovial fibroblasts were seeded overnight in 48-well plates at a concentration of 40,000 cells per well. Cells were cultured in RPMI-1640 (Sigma-Aldrich, R8758) in 1% FCS (Sigma-Aldrich, Dorset, UK, F7524), sodium orthopyruvate (1%) (Sigma-Aldrich, S8636), non-essential amino acids (1%) (Sigma-Aldrich, Dorset, UK, M7145). Cells were then transfected with either a non-targeting control (NTC) siRNA (Dharmacon, D-001206-13) or a GLS1 siRNA (Dharmacon, MQ-004548-01-0005) at concentrations of either 5 nM or 100 nM. Following 24 hours, the supernatants were collected for cytokine analysis by enzyme-linked immunosorbent assay (ELISA) (IL-6 DuoSet kit, R&D Systems, DY206), and cells were lysed with TRIzol reagent (Life technologies, Paisley, UK, 15596026) for RNA extraction.

2.8 SDS polyacrylamide gel electrophoresis and immunoblotting

Protein lysates were diluted to the desired concentration in loading buffer containing 2-mercaptoethanol (Sigma-Aldrich, Dorset, UK), 4x Laemmli Sample (Bio-Rad, Hertfordshire, UK) and ddH2O. Samples were then loaded into a 5% SDS-polyacrylamide stacking gel and separated using 10-12% SDS-PAGE with respect to protein of interest, cast in Novex 1.0 mm Cassettes (Life technologies, Paisley, UK). SDS PAGE was performed using the Invitrogen Novex mini-cell (Thermo Fisher Scientific, MA, USA), containing 1X running buffer using ultrapure 10X tris/glycine/SDS (Geneflow, Staffordshire, UK) and ddH20, and run at 150 V and 50 mA using Novex x-cell sure lock (Thermo Fisher Scientific, USA) through a Omnipac CS-300 V power supply (Cleaver Scientific, Rugby, UK). Following SDS PAGE,

proteins were transferred onto methanol-activated PVDF membrane (Bio-Rad, Hertfordshire, UK) using a Trans Turboblot™ transfer system (Bio-Rad, Hertfordshire, UK). This membrane was then rinsed using ddH2O and washed using 1X tris buffered saline with 0.1% Tween®20 (Sigma-Aldrich, Dorset, UK) (TBS-T) for 15 minutes, on a shaker at room temperature. Following this, membranes were blocked using TBS-T with 5% bovine serum albumin (BSA) for 1 hour on a shaker at room temperature. Membranes were then immunoprobed with the primary antibody of interest overnight on a shaker at 4^{o}C. The next day, the membranes were washed with 1X TBS-T (three times for 15 minutes) and subsequently immune probed with the corresponding secondary antibody in TBS-T for 2 hours on a shaker at room temperature. This antibody was removed, and the membranes were washed with 1X TBS-T (three times for 15 minutes) before the addition of Amersham ECL Western Blotting Detection Reagent (GE Healthcare, Buckinghamshire, UK). Proteins were visualised using the ChemiDoc™ MP System (Bio-Rad, Hertfordshire, UK) and protein expression was quantified using image J software.

2.9 Mitotracker Green Staining

Mitochondrial mass was measured using Mitotracker Green staining (Invitrogen). Synovial fibroblasts (15,000 cells/well) were plated into 96 well black flat bottom microplates (Scientific Laboratory Supplies, Nottingham, UK) and left to adhere for 24 hours in a cell culture incubator (37°C and 5% CO2). Following adherence, synovial fibroblasts were stimulated with TNFα (10ng/ml) for 24 hours. Cells were then washed twice with PBS and stained with green fluorescent Mito Tracker dye (Invitrogen) for 45 minutes. Following staining the cells were washed twice with PBS

and measured using Synergy 2 plate reader (Biotek, Swindon, UK) at excitation/emission maxima of 490/516nm.

2.10 Fluorescence Glucose Uptake

Glucose uptake was measured using a fluorescent glucose analog 6-NBDG (6-(N-(7-Nitrobenz-2-oxa-1, 3-diazol-4-yl) amino)-6-Deoxyglucose) (Thermo Fischer Scientific, Loughborough, UK). OA synovial fibroblasts (30,000 cells/well) were plated into 96 well black flat bottom microplates (Scientific Laboratory Supplies, Nottingham, UK) and left to adhere for 24 hours in a cell culture incubator (37°C and 5% CO2). Following adherence, cells were stimulated with TNFα (10ng/ml) for 24 hours, and then washed twice with PBS and incubated in glucose-free RPMI-1640 media (Sigma-Aldrich, Dorset, UK) for one hour (Thermo Fischer Scientific, Loughborough, UK). The cells were then treated with glucose analog 6NBDG (200µM) and left for 30 minutes. Following this incubation period, RPMI-1640 media was removed, and cells were washed twice with PBS and measured using Synergy 2 plate reader (Biotek, Swindon, UK) at excitation/emission maxima of 465/540 nm.

2.11 ROS production assay

Reactive oxygen species production was measured using the cell-permeable reagent 2′,7′-dichlorofluorescein (DCFDA) (catalog no. ab113851; Abcam, Cambridge, MA). OA synovial fibroblast (30,000 cells/well) were plated into 96 well

black flat bottom microplates (Scientific Laboratory Supplies, Nottingham, UK) and left to adhere for 24 hours in a cell culture incubator (37°C and 5% CO2). Following adherence, cells were incubated in low glutamine RPMI-1640 media (2mM) or high glutamine RPMI-1640 media (20mM) alongside TNFα (10ng/ml) stimulation for 24 hours or with BPTES (20µM) for 1 hour. Following this, cells were washed using a commercial buffer provided and stained in the dark (37°C and 5% CO2) for 45 minutes with diluted DFCDA solution according to the manufacturer's instructions. Finally, fluorescence was measured using Synergy 2 plate reader (Biotek, Swindon, UK) at excitation/emission maxima of 465/540 nm.

2.12 MTS Assay

As a measure of the number of viable cells, quantification of NAD(P)H-dependant oxidoreductase activity was conducted using MTS [3-(4,5-dimethylthiazol-2-yl)- 5-(3-carboxymethonyphenol)-2-(4-sulfophenyl)-2H-tetrazolium, inner salt] Cell Titer 96 AQueous One Solution Reagent (Promega, USA). Cells were treated with MTS to monitor NADH and NADPH activity, which are reducing agents that reduce MTS into soluble formazan dye as previously described (Dunigan, Waters and Owen, 1995). Absorbance of this dye was measured at 490nm using BioTek EL808 microtiter plate reader (BioTek, Swindon, UK).

2.13 ELISA

Quantification of IL-6 production was determined using a commercially available ELISA (IL-6 DuoSet kit, R&D Systems, DY206). Cell supernatants were diluted 1:200 with assay buffer. First, the capture antibody was diluted in PBS (pH7.2) as specified by the manufacturer and pipetted into nunc-Immuno ELISA plate (Thermo Fisher Scientific, MA, USA) overnight at RT. Following this, the wells were washed three times with 300µl wash buffer (PBS pH 7.2, containing 0.05% Tween®20) and were then blocked with reagent diluent (1% BSA in PBS) for an hour. Plates were then aspirated and washed three times with 300µl wash buffer. Following this the protein standards were pipetted into the well in duplicate (100µl) following manufacturer instructions and samples were also pipetted into wells in duplicate and incubated for 2 hours at RT. Next, the wells were aspirated and washed three times and the detection antibody was diluted in PBS (pH7.2) as specified by the manufacturer and pipetted into the wells and incubated for 2 hours at RT. Plates were then aspirated and washed three times with 300µl wash buffer. Following this, 100 µL of the working dilution of Streptavidin-HRP was added to each well and incubated in the dark for 20 minutes at RT. Plates were then aspirated and washed three times with 300µl wash buffer. Then, 100 µL of Substrate Solution was added to each well and incubated in the dark for 20 minutes at RT. Finally, reactions were stopped by the addition of stop solution (2N H_2SO_4) and optical density immediately measured at 450 nm using a BioTek EL808 microtiter plate reader (BioTek, Swindon, UK). Optical imperfections in the plate were limited by correcting with absorbance measured at 570 nm. The average absorbance for each standard was used to generate a standard curve using GraphPad Prism 9 statistical package. Samples

were quantified using standard curve from 600-9.38 pg/ml. The lower limit of detection for this assay is 9.38pg/ml, all samples were above this concentration.

2.14 Cellular proliferation assays

Proliferation rates of synovial fibroblasts was conducted using Bromodeoxyuridine (BrdU) cell proliferation ELISA colorimetric kit (Abcam, ab126556, Cambridge, UK following the manufacturer's instructions). Synovial fibroblasts were seeded at 20,000 cells/well in 96 well plate. Then 20µL BrdU label was added to each well and incubated for 24 hours. Following this, the synovial fibroblasts were fixed using 200 µL/well fixing solution for 30 minutes. After fixing the cells, the fixing solution was aspirated, and cell were incubated with a pre-diluted anti-BrdU monoclonal antibody. This was subsequently washed and aspirated and before the addition of secondary peroxidase goat anti-mouse IgG conjugated to HRP for 30 minutes and given TMB substrate. Absorbance was measured at 450/540 nm BioTek EL808 microtiter plate reader (BioTek, Swindon, UK).

2.14 Annexin V-PI apoptosis flow assay

Fibroblast apoptosis was quantified using Annexin-V and Propidium Iodide (PI) staining. BJ human dermal fibroblast cell line (foreskin) were treated with varying concentration of GLS1 inhibitor BPTES (5-5000nM) for one hour alongside a 0.5% DMSO vehicle control. Following treatment, fibroblasts were harvested using cell

dissociation solution non-enzymatic (1x) (Sigma-Aldrich, Dorset, UK) and washed with 1x PBS solution. Cells were then centrifuged at 300xG for 10 minutes before being resuspended on ice in 100µL Annexin V binding buffer (0.01M HEPES, 0.14M NaCl, 2.5mM CaCl2). Cells were incubated in the dark with 2µl Annexin V-FITC antibody for 10 minutes. Propidium iodide (0.001 mg/ml) (PI) stain was added immediately prior to the running of the cells on BD FACSVia™ Flow Cytometry System (BD Biosciences, UK). Gating strategy is described in figure 4.1 and 4.2, flow cytometry data was compensated through use of unstained, single stained and dual stained conditions. The condition chosen for the purpose of generating a compensation matrix was 1:1 heat killed and live, unstimulated cells. Data was analysed using BD Accuri C6+. Live and dead cells were counted prior to the experiment using Invitrogen Trypan blue staining (0.4%) (Thermo Fisher Scientific, MA, USA) and quantified using Countess™ Automated Cell Counter.

2.15 Lactate Assay

The lactate concentration in cultured OA synovial fibroblasts was quantified using a commercially available lactate assay (MAK064-1KT Sigma-Aldrich, UK). In brief, culture supernatants were centrifuged at 12,000g for 10 minutes in 10kDa molecular weight cut-off spin columns (Abcam, UK) to remove proteins including lactate dehydrogenase (LDH). Absorbance was measured at 570nm (A570) on a microplate and lactate concentration was obtained from the standard curve.

2.16 Seahorse metabolic analysis of OA synovial fibroblasts

The Seahorse XFe96 Analyzer (Agilent, California, USA) was used to measure oxidative phosphorylation and glycolysis through the oxygen consumption rate (OCR) and extracellular acidification rate (ECAR) respectively in cultured OA synovial fibroblasts. Synovial fibroblasts were seeded at 30,000 cells/well 24 hours prior to the assay. Cells were washed with Seahorse XF RPMI-1640 medium (Agilent, California, USA) and the microplate was warmed for 60 minutes in a CO^2-free incubator before a mitochondrial and glycolytic stress test was initiated. The seahorse assay was conducted according to standard protocol with the injection of 10mM Glucose, 2µM Oligomycin (ATP-synthase inhibitor), 5µM cyanide-4-(trifluoromethoxy) phenylhydrazone/FCCP (oxidative phosphorylation uncoupler), 50mM 2-Deoxy-D-glucose/2-DG (non-metabolisable glucose analog), 3µM Rotenone (complex I inhibitor) and 3µM Antimycin A (complex III inhibitor). OCR and ECAR were measured five times at baseline and four times after each drug was added, with the average taken for multiple measurements.

2.17 NMR Spectroscopy

Synovial fluids were treated with Hyaluronidase (1000 units/mL) for 15 min at 37^{o}C in order to decrease viscosity of samples. For the NMR analysis of synovial fibroblasts, conditioned media were collected from cells seeded at 40,000 cells per well following 24 hours either unstimulated or stimulated with TNFα at a concentration of 10 ng/mL. Samples were prepared for NMR analyses by centrifuging at 15,000xG for 5 min at

4ºC before being placed into 3 kDa Molecular weight cut-off (MWCO) filters (Pall Nanosep). Samples were then centrifuged at 10,000xG for 15 min at 4ºC. The filtrate was mixed 1:3 with NMR buffer (provided by Dr. Stephen Young) (containing 400 mM phosphate, 1.6 mM DFTMP, 40% D2O, 0.4% azide, DSS (2 mM) at pH 7.0) and an aliquot (50 µL) added to a 1.7 mm OD NMR tube and capped. NMR spectra were acquired using a 600 MHz 4-channel Bruker AVANCE III spectrometer equipped with a Samplejet refrigerated autosampler (Bruker BioSpin, Billerica, MA, USA). For each sample, one-dimensional (1D) 1H-NMR NOSEY spectra were acquired. NMR spectra were automatically phased, and baseline corrected, and the chemical shifts were internally referenced to DSS at 0.00 ppm using Metabolab (Ludwig and Günther, 2011). Spectral regions containing only noise and the residual water peak were excluded. Metabolites were identified and labelled using the metabolite discovery software Chenomx (Chenomx, Edmonton, AB, Canada), using the in-house library of metabolite spectra. Multivariate analysis was undertaken using SIMCA 16 (Umetrics).

2.18 RNA Sequencing Analysis

Total RNA was extracted from synovial fibroblasts isolated from hand, hip, knee and foot OA samples from n = 6 patients each using RNeasy Mini Kit (Qiagen) and DNase treated (Qiagen DNase kit). RNA integrity was assayed using Agilent Bioanalyser. Library preparation and RNA-sequencing was performed by Genomics Facility at University of Birmingham using QuantSeq 3’ kit (Lexogen) and sequenced on Illumina's NextSeq 500. The sequenced reads were mapped to the hg38

reference human genome using Star Aligner and differential gene expression analysis and log2 fold changes were computed using DESeq2. RNA Sequencing sample preparation and primary data analysis was performed by Dr. Susanne Wijesinghe (unpublished data, S. Wijesinghe et al, 2022)

2.19 Bioinformatic Pathway Analysis

Differentially expressed genes (DEGs) from hand, hip, knee and foot OA synovial fibroblasts from normal weight and obese patients were analysed using Ingenuity Pathway Analysis (IPA) (www.ingenuity.com) (Qiagen, Germantown, MD, USA) software. Core functional analysis was performed to identify the canonical pathways most significantly associated with the DEGs within each analysis. The significance of the association of a given canonical pathway with the genes within a given subset was measured in two ways. Firstly, by the ratio of the number of differentially expressed genes in the dataset that mapped to the canonical pathway divided by the total number of genes that map to the canonical pathway. Secondly, Fisher's exact test was used to calculate a p- value of the association between the genes and the network/canonical pathway. Canonical pathways were filtered to only include metabolic pathways when analysing the data. The right tailed Fisher’s Exact tests indicates the probability of association of transcripts from the dataset canonical pathway by random chance alone resulting in a p value of overlap. This was set at a score cut-off of -log p value of 1.3 and canonical pathways were filtered to only include those pathways associated with metabolism. Using z-score, those pathways which are orange indicate predicted pathway activation, those which are blue indicate predicted pathway inhibition and those which remain grey are those which

no prediction can be made due to insufficient evidence within IPA's knowledge base for confident activity predictions across the datasets.

Multi-omics analysis was conducted using MetaboAnalyst 5.0 (www.metaboanalyst.ca) (Pang et al., 2021). For the data analysis, transcriptomics data utilised for this analysis was RNASeq data from obese hip OA synovial fibroblast (n = 3 patients) compared to normal weight hip OA synovial fibroblast (n = 3 patients). The metabolomics data was obtained from obese hip OA synovial fibroblast conditioned media (n = 5 patients) compared to normal weight hip OA synovial fibroblast conditioned media (n = 4 patients). Patient samples were not matched for this analysis. An exclusion criterion was placed on both the transcriptomic data and metabolomics data of differentially expression genes or compounds with a log2 fold change of equal to or greater than 0.48 or equal to or less than -0.48. Metabolic pathways were mapped using KEGG global metabolic map (map01100) with enrichment analysis using Fisher's exact test. Tight integration was conducted on the datasets, pooling all the genes and metabolites into a single query and performing enrichment analysis on this combined dataset. Topological analysis was conducted on the datasets which focused on degree centrality (measures the number of links/edges that connect to a node (compound or DEGs)). A raw p value for each metabolic pathway with a group of functionally associated metabolites and genes were calculated. False discovery rate (FDR) (0.05) was used to control for false positives (Shen et al., 2021). A pathway impact score was calculated as the sum of the importance measures of identified metabolites divided by the total sum of the importance measure of all identified/unidentified metabolites within a pathway (Shen et al., 2021). The importance of a given pathway relative to

the global metabolic network was estimated by its pathway impact score, with an impact score >0.1 considered to be important pathways (Shen et al., 2021).

2.20 Data handling and statistical analysis

Data were analysed using GraphPad Prism 9 software (GraphPad Software, San Diego, CA, USA) or SPSS Version 27 (Armonk, NY: IBM Corp). Statistical test and corrections are indicated within figure legend or footnotes. * $p<0.05$; ** $p<0.01$; *** $p<0.001$; **** $p<0.0001$

Chapter 3:

Data were analysed using GraphPad Prism 9 software (GraphPad Software, San Diego, CA, USA). For analysis of metabolite concentrations in OA patient synovial fluids, normal distribution was checked by Shapiro–Wilk normality tests. Gaussian distributions were not assumed and Mann–Whitney tests were used to examine differences between obese and normal weight values. Groups were compared using one-way analysis of variance (ANOVA) with Dunnett's test for multiple comparisons. Data are presented as the mean ± SEM, with p-values < 0.05 defining statistically significant differences.

Chapter 4:

Data were analysed using GraphPad Prism 9 software (GraphPad Software, San Diego, CA, USA). Distribution of data was analysed using Shapiro–Wilk normality tests. Groups were compared using one-way analysis of variance (ANOVA) with

post-hoc test corrected for multiple comparisons. Data are presented as the mean ± SD, with P values < 0.05 defining statistically significant differences.

Chapter 6:

Data were analysed using GraphPad Prism 9 software (GraphPad Software, San Diego, CA, USA). Distribution of data was analysed using Shapiro–Wilk normality tests. Groups were compared using one-way analysis of variance (ANOVA) with Dunnett's test for multiple comparisons or 2-way ANOVA with Tukey's HSD post hoc test following Levene's Test of Equality of Error Variances (to test the null hypothesis which is error variance of the dependant variable is equal across groups) depending on the number of independent variables within analysis using SPSS Version 27 (Armonk, NY: IBM Corp). Data are presented as the mean ± SEM, with P values < 0.05 defining statistically significant differences.

CHAPTER 3

METABOLOMICS ANALYSIS OF OSTEOARTHRITIC SYNOVIAL FLUID AND SYNOVIAL FIBROBLAST SECRETOMES USING ^{1}H NMR SPECTROSCOPY

3.1 Introduction

3.1.1 Metabolomics

Metabolomics is amongst the latest “omics” techniques following genomics, proteomics and transcriptomics, which utilize high throughput analytical methods to generate large scale datasets that are examined using bioinformatics, to provide a comprehensive and extensive outlook on cellular processes. These methodologies, including genomics and transcriptomics, are amongst the earliest changes observed prior to changes in cellular phenotype and thus provide insight into both the cellular and molecular pathways that mediate changes to cell phenotype.

The use of the term “metabolome” was first introduced in 1998 and was adopted by the field to match with existing terminology used to describe the complete set of genes (genome), the complete set of proteins (proteome) and the complete set of transcripts (transcriptome). Thus, the term “metabolome” was coined, to describe the complete set of metabolites. Metabolites are small molecules identified within biological samples which have a molecular weight below 1500 Da and are not proteins or RNA/DNA.

Metabolomics analysis can be separated into two categories: Untargeted and targeted analysis. Untargeted metabolomics is a comprehensive analysis of all measurable compounds in a sample. However, due to its extensive datasets, multivariate analysis must be performed. Targeted metabolomics, however, is a measurement of specific groups such as biochemically annotated metabolites, using an internal standard (for example Sodium trimethylsilylpropanesulfonate (DSS) or Tetramethylsilane (TMS)).

By identifying changes in the metabolome of various biological fluids between, for example healthy controls and disease, we can gain insight into the metabolic phenotype or “metabotype” of particular diseased cells or tissues and the potential to identify particular biomarkers of a diseased condition, or a biomarker to stratify patient cohorts, or a biomarker to indicate response to a therapeutic treatment.

An advantage of metabolomics is the capacity to thoroughly analyse potential metabolic biomarkers through non-invasive or easily accessible biofluids such as urine and saliva, allowing for the ability to stratify and investigate pathological perturbations in patients when compared to healthy or normal patients. The technique also has the potential to observe ongoing changes in metabolic features and biomarkers upon receival of therapeutic treatment, providing insight into progression or regression of disease pathology within patients. This is especially useful when the metabolic biomarkers are involved in disease pathology which is often observed in metabolic disorders such as metabolic syndrome, diabetes and obesity (Joseph, Ayeleso and Mukwevho, 2017; Molepo *et al.*, 2018; Mosana *et al.*, 2020). Metabolomics has also been applied to other chronic disease conditions and has been proposed as a means to allow for the early disease diagnosis in inflammatory joint disorders such as rheumatoid arthritis and osteoarthritis (Dudka *et al.*, 2021) (Carlson *et al.*, 2018), in cardiovascular diseases (X. S. Li *et al.*, 2018), neurodegenerative diseases such as Alzheimer’s Disease (AD) (Yilmaz *et al.*, 2017) and in cancer (Shang, Zheng and Tong, 2020).

Unlike the other omics methodologies, metabolomics is relatively new and therefore the ability to identify all or most of the metabolites using metabolomics technologies is limited. This is due to several reasons including but not limited to incomplete metabolite identification libraries and limitations in sensitivity of metabolomic

techniques. However, development within the field of metabolomics and widespread adoption of the techniques is increasing as research costs decrease and access to instruments increase.

Metabolomics can be conducted using a number of technologies however two have arisen as the primary technologies to conduct metabolomics experiments, namely NMR spectroscopy and mass spectroscopy. Each technology has its unique advantages and disadvantages which have been described in table 3.1. Although these technologies have primarily been used separately for analysing biological material, they are not mutually exclusive and the use of hyphenated techniques including chromatography (liquid chromatography (LC)/gas chromatography (GC)) alongside mass spectrometry (MS) and NMR spectroscopy allow for high-throughput profiling of hundreds of metabolites simultaneously within biological fluid (Ussher *et al.*, 2016).

Table 3.1: Advantages and Disadvantages of using NMR Spectroscopy compared to Mass Spectroscopy (Emwas, 2015; Aderemi *et al.*, 2021)

	NMR	Mass Spectrometry
Sample Preparation	Sample filtration (3kDa molecular weight cut-off) and dilution in NMR buffer containing chemical shift standard	Metabolite extraction is required and optimisation of ionisation techniques
Time	Shorter time for sample analysis	Requires longer periods of time per sample
Database	Few comprehensive metabolite database	More comprehensive metabolite database
Sample Recovery	Non-destructive; multiple runs can be taken from the sample	Destructive; Due to hyphenated techniques (HPLC, LC) samples chromatographically separated
Solid phase analysis	Possible using magic angle spinning NMR spectroscopy	Requires tissue extraction
Sensitivity	Can identify and measure a smaller number of metabolites and detect at micromolar concentrations	Can identify and measure larger number of metabolites and detect at nanomolar concentrations

3.1.2 Metabolomics in Inflammation and Obesity

3.1.2.1 Metabolomics in Cardiovascular Disease

Cardiovascular diseases (CVD) are the leading causes of premature death and disability in humans and the incidence rate is increasing worldwide (Flora and Nayak, 2019). The underlying pathogenesis of CVDs is predominantly of atherosclerotic origin which then develops into coronary artery diseases (CAD), venous thromboembolism and peripheral vascular disease, which subsequently lead to myocardial infarction, cardiac arrhythmias and stroke (Flora and Nayak, 2019). CVD is associated with several markers of systemic inflammation such as C reactive protein (CRP) and proteins within the coagulation cascade (Berg and Scherer, 2005). These proteins are also elevated with obesity, diabetes mellitus and other metabolic diseases, which are often comorbidities associated with CVD. Metabolomics within a CVD context has become particularly popular, likely due to the strong association between CVD and metabolic diseases.

Ischemic heart disease (IHD) is the most common cause of CVD and remains the single largest cause of death in countries of all income groups (Nowbar *et al.*, 2019). IHD occurs as a result of inadequate perfusion of the myocardium and includes stable and unstable anginas. One aspect of IHD metabolism is the restriction of oxygen and nutrient supply to the myocardium and therefore, like other oxygen restricted tissues, there is reduction in oxidative metabolism and reliance on glycolysis to produce ATP. This was observed in LC/MS blood-based metabolomic profiling in 36 individuals who displayed myocardial ischemia, which found a reduced number of Krebs cycle metabolites(Sabatine *et al.*, 2005).

Another aspect of IHD metabolism is the reduction in fatty acid oxidation, again as a result of poor oxygen delivery to ischemic sites (Ussher *et al.*, 2016). Furthermore, LC/MS/MS metabolomic profiling of serum from age and sex matched CAD patients, compared to healthy individuals, show elevated Branched Chain Amino Acid (BCAA) levels (Yang *et al.*, 2015). It should be noted, patients with CVD will often have associated comorbidities like obesity and type 2 diabetes (T2D), which have the potential to independently or synergistically alter the metabolomic profile of these patients, thus adding further complexity to any analysis performed in such patient cohorts. For instance, metabolomic analysis has revealed BCAA and aromatic amino acids are currently emerging as predictors of future T2D, which could suggest contribution of T2D to aberrant BCAA metabolism in CAD patients (Shah and Newgard, 2015). Using samples unique to CVD such as sampling arterial blood and the coronary sinus for the heart, could provide more information on the local metabolic changes observed within CVD patients. Likewise, the application of metabolomics techniques to large scale population-based epidemiological cohorts allows for robust statistical analysis which will adjust for potential cofounding factors such as comorbidities (Ussher *et al.*, 2016).

3.1.2.2 Metabolomics in Neurological Disease

Another application of metabolomic technology which has developed recently, is the study of neurological and neurodegenerative diseases. Central nervous system (CNS) disorders are linked to aberrant neurotransmitter signalling, fatty acids such as arachidonic acid-cascade, oxidative stress and mitochondrial function (Quinones and Kaddurah-Daouk, 2009). High performance liquid chromatography coupled with electrochemical coulometric array detection profiling of plasma from 66 Parkinson's disease (PD) patients compared to 25 controls found elevated markers of oxidative

damage (8-OHdG) and the antioxidant metabolite glutathione (Bogdanov *et al.*, 2008). Clinical samples from Huntington's disease (HD) patients and a transgenic mouse model of HD were analysed using GC-MS. Metabolic differences were identified between HD patients and controls including aberrant amino acid metabolism and the accumulation of ethylene glycol and its oxidation product, oxalate (Underwood *et al.*, 2006). Metabolites such as malonate and 2-amino-n-butyrate, were elevated in both PD and HD, which could be indicative of generic neurodegenerative markers (Underwood *et al.*, 2006). Depression is a disorder associated with increased inflammatory activation of the immune system, affecting both the periphery and the central nervous system. GC-MS analysis of blood plasma found several fatty acids, glycerol and gamma-aminobutyric acid (GABA) were altered in depressed patients compared to never-depressed older adults (Paige *et al.*, 2007). Metabolomics analysis of cerebrospinal fluid of patients with multiple sclerosis (MS) found increased levels of glutamate and 3-hydroxybutyrate when compared to healthy controls (Porter *et al.*, 2020).

CNS disorders are likely due to dynamic dysregulations of multiple gene regulatory networks and metabolic alterations and therefore there is an increasing need to further investigate CNS pathology through omics technologies.

3.1.2.3 Metabolomics in Metabolic Disorders

The prevalence of T2D is increasing at an alarming rate due to an ongoing obesity epidemic and an ageing population (Paneni *et al.*, 2013; Hu, Satija and Manson, 2015). T2D, like other metabolic diseases, increases the risk of developing severe conditions such as CVD, liver and pancreatic cancers (Rahman, Athar and Islam, 2021). The use of high throughput metabolomic techniques has generated quite a lot of interest within the field, with potential for gaining insight into novel modifiable

disease pathways and the possibility of identifying biomarkers predictive of incident T2D.

It is well known that plasma hexose sugars are positively associated with T2D and are responsible for elevations in glucose (Gonzalez-Franquesa *et al.*, 2016). Likewise, intracellular metabolite perturbations have been observed within several tissues, one such example being glucose-stimulated insulin secretion (GSIS) requiring increased late glycolytic and early TCA cycle metabolites (Spégel *et al.*, 2011).

A longitudinal study which followed 2422 normoglycemic individuals for 12 years, found 201 developed diabetes (Wang *et al.*, 2011). Metabolomic profiling of blood samples from these subjects found five branched-chain and aromatic amino acids that had highly significant associations with the development of future diabetes, namely isoleucine, leucine, valine, tyrosine and phenylalanine (Wang *et al.*, 2011). A similar study in a young cohort of normoglycemic adults found branched-chain and aromatic amino acids are markers of development of insulin resistance, particularly within men (Wurtz *et al.*, 2013). Another aspect of metabolomics is lipidomics analysis. Novel lipids have been identified as plasma biomarkers and contributors of T2D pathophysiology, including free fatty acids (C14:0, C16:1, C16:0, C18:1, C20:4) which are increased in obesity (Gonzalez-Franquesa *et al.*, 2016). Non-targeted metabolomics identified elevation of long chain lipids (adrenate and arachidonate, C22:4 and C20:4) in impaired fasting glucose (Menni *et al.*, 2013).

In summary, metabolomics analysis of biological fluids have been critical in investigating the pathogenesis of T2D and related risk factors. Research within this area has highlighted perturbations in amino acid and lipid profiles within T2D

samples and murine models, which could suggest impaired amino acid and fatty acid metabolism contributes to reduced anaplerotic flux and complete oxidative metabolism and therefore contributes to decreased cellular energetics in insulin resistance and T2D (Gonzalez-Franquesa *et al.*, 2016).

Obesity is widely recognised as a worldwide public health crisis, an ongoing epidemic and is significantly associated with development of several metabolic disorders including cancer, T2D, cardiovascular disease, and dyslipidaemia (Bagheri *et al.*, 2018).

Like T2D, metabolomics analysis has also been applied to obese subjects in order to understand systemic changes associated with obesity and relevance to distal tissues and associated disorders. In a Japanese cohort, subjects with high visceral fat area had elevated levels of amino acids alanine, glycine, glutamate, tryptophan and tyrosine as wells as BCAA (Yamakado *et al.*, 2012). Tissue specific metabolomics also provides further insight into altered metabolite profiles in obesity. Ultra-high performance LC-MS-MS of subcutaneous abdominal white adipose tissue from 52 obese women compared to 29 non-obese controls showed 6 polar metabolites were significantly altered including glutamine (Petrus, *et al.*, 2020). Further stratification of obese patients into those who are considered “metabolically healthy” (reduced blood pressure, lipid profiles and insulin resistance and elevated high-density lipoprotein cholesterol (HDL-C)) and those who are “metabolically unhealthy”, has led to some interesting developments within the field of obesity. LC-MS targeted metabolomics shows BCAA, tyrosine, glutamate, diacyl-phosphatidylcholines C32:1 and C38:3 were directly associated with “metabolically healthy” phenotype and acyl-carnitine C18:2, acyl-lysophosphatidylcholines C18:1 and C18:2, and alkyl-

lysophosphatidylcholines C18.0 were inversely associated with this “metabolically healthy” phenotype (Bagheri *et al.*, 2018).

Metabolomics within animal models also provides direct insight into metabolic changes within tissues *in vivo*. TCA cycle intermediates are reduced in liver and skeletal muscle within obese murine model and glycolytic metabolites are increased within muscle (Giesbertz *et al.*, 2015). High fat diet (HFD) fed mice have reduced TCA intermediates derived from labelled glucose within skeletal muscle (Kowalski *et al.*, 2015). Analysis of biological fluids from animal models also offers insight into systemic changes associated with obesity. NMR spectroscopy of urinary samples from a diabetic mouse model identified elevated glucose, lactate and other TCA cycle intermediates (Connor *et al.*, 2010). Additionally, plasma amino acids such as glutamine-glutamate, aspartate-asparagine and alanine are also elevated within an obese HFD rodent model (Gonzalez-Franquesa *et al.*, 2016). Increases in circulating amino acid levels including BCAA, are particularly interesting and may be explained by low expression of LAT1 transporter in obese subjects, which is responsible for the transport of large natural amino acids within cells (Payab *et al.*, 2021).

By shifting towards a multi-omics analysis including both transcriptomics and metabolomics, further understanding of what underpins the altered metabolism within obesity, may result in improved therapeutic interventions, which could prove to be particularly useful in combatting this obesity epidemic.

3.1.3 Multivariate Analysis using Soft Independent Modelling by Class Analogy (SIMCA)

A key step within the metabolomics pipeline, is multivariate analysis. Due to the large quantity of data collected from hundreds of metabolites and multiple variables to compare, the best method of analysis involves looking for the greatest contributing variables or components within the dataset and plotting the data using models.

Principal component analysis (PCA) models the correlation structure of a dataset and observations are represented as scores. Using this method, large quantities of data are refined to a handful of plots. From this data, 2 or 3 score vectors are calculated and then plotted against each other resulting in t/t plots, giving a holistic overview of process behaviour over time and a strong model of variation within the data (SIMCA, 2020). Scores are sorted in descending order of importance (i.e., t1> t2>t3). From these t/t plots, trends/patterns in data can be observed.

Score plots alongside loading plots, are an indicator of responsible variables for deviation from normal operation. From PCA plots it is possible to derive residuals (deviations from data), through which one can generate DModX plots (distance to model), which shows distance to the model plane for each observation (SIMCA, 2020). If the DModX are greater than the DCrit, then this is regarded as an outlier. DModX plots are a detection tool which are used to identify moderate outliers within data (SIMCA, 2020). However, Hotelling's T^2 distribution (multivariate generalisation of Student's t-distribution), is used to identify clear outliers in data (<95% confidence interval).

PCA plots can also be diagnosed using R^2 values and Q^2 values for each component within the model. R^2 values estimate the “goodness” of the fit and Q^2 values estimate the “goodness” of prediction (SIMCA, 2020). It is common practice to keep modelling the data to increase the fit (R^2 values) until the Q^2 values decreases, which would reduce prediction and result in an overfitted model. Overfitting the model is a tendency to describe too much variation within the data, thereby including non-informative variation and results in lower quality of prediction (SIMCA, 2020). The higher the R^2 and Q^2 values the better the model. Q^2 values of approximately 0.5 are an indicator of a good model and those around 0.9 suggest an excellent model, which is often observed in calibration (SIMCA, 2020).

Another method used in multivariate analysis is the Partial Least Squares Projections to Latent Structures (PLS). When trying to analyse large datasets that have multiple input/process variables (X) which are responsible for alterations in output/results variables (Y), identifying the relationships between these variables using multivariate regression is fraught with issues (including correlated variables) (SIMCA, 2020). In this scenario, regression analysis provides an output for every result variable (Ym) separately and can therefore result in hundreds of different regression analysis for one dataset. One solution to this issue is the use of a different classification method, namely PLS analysis. PLS analysis requires the specification of which variables are predictors (X) and which are dependant (Y) and will then identify the relationship between the 2 groups of variables. Orthogonal Partial Least Squares (OPLS) analysis is an extension of PLS and is a regression and prediction method. Regression in this instance refers to (i) how things vary as a whole (covariance) and (ii) a prediction being how well the known information is predicted (SIMCA, 2020). OPLS splits systemic variation in X into two components,

with the one being the correlated (predictive) to Y and the other being components unique in X but uncorrelated (orthogonal) to Y, giving better model interpretability (Sthle and Wold, 1990). When referring to predictive variation within data, this is correlated variation between X and Y variables. Orthogonal variation refers to uncorrelated variation between X and Y variables. Random variation is not included in OPLS analysis and is left within residuals. OPLS is a supervised method of multivariate analysis, which finds information in the X data that is related to known information in the Y data (SIMCA, 2020). The multivariate analysis undertaken in this study deals with discrete or categorical variables and is therefore OPLS-discriminant analysis (OPLS-DA). Although OPLS-DA is easiest to interpret with two classes (e.g., normal weight vs obese), the analysis can be extended and used in cases of multiple classes. Amongst the benefits of using OPLS-DA is the ability to identify which particular variables are responsible for class discrimination and is often used in identifying biomarkers in metabolomics experiments (SIMCA, 2020). Also, OPLS-DA model can handle unwanted variation within datasets which is critical when analysing samples with large variation like biological samples.

Vector	Type	Description
SS (Sum of Squares)	Total corr (Total corrected)	SS of the Y of the workset corrected for the mean.
	Regression	Fraction of Total Corrected SS accounted for by the model, estimated via the cross-validation principle.
	Residual	Difference between Total Corrected and Regression SS, i.e., the fraction of Total Corrected unaccounted for by the model.
DF (Degrees of freedom)	Total corr, Regression, residual	The number of degrees of freedom (DF). This is an approximate number based on the experience that PLS needs half the components to reach the same explanation of Y as principal components regression.
MS (Mean Squares)	Total corr, Regression, residual	By dividing each SS by the respective DF, the corresponding mean squares (MS), or variances, are obtained.
p		The p-value indicates the probability level where a model with this F-value may be the result of just chance. The common practice is to interpret a p-value lower than 0.05 as pointing to a significant model.
SD (Standard Deviation)	Standard deviation.	Square root of MS.

Table 3.2: Terminology of Cross-Validated (CV) ANOVA explained

(adapted from SIMCA (Umetrics, Germany)) and (Sthle and Wold, 1990; Eriksson, Trygg and Wold, 2008)).

Metabolomics has been used as an effective tool to investigate the systemic and local effects of altered cell metabolism in disease conditions and as such would be ideally placed to investigate and interpret the role obesity and inflammation plays in the inflammatory joint condition, osteoarthritis.

3.2 Hypothesis

We hypothesised that

- OA synovial fluid from normal weight and obese patients have distinct metabolomic profiles
- The metabolome of OA synovial fibroblast from normal weight and obese OA patients would reflect the differences observed in OA synovial fluid
- The metabolic differences between stimulated and unstimulated OA synovial fibroblasts would contribute to their activated state and inflammatory microenvironment

3.3 Methods

3.3.1 Patient Characteristics and Anthropometric Data

Table 3.3: Patient characteristics from OA synovial fluid from obese (n = 5) and normal weight (n = 6) patients

		Obese	Normal weight	P-value
Age (years)		63 ± 4	72 ± 2.0	0.05
Female:Male		5:3	5:3	
BMI (kg/m^2)		33.6 ± 1.2	22.9 ± 0.7	<0.0001
Waist circumference (cm)		106.5 ± 5.1	86.6 ± 3.2	<0.01
Hip circumference, (cm)		116.4 ± 3.6	94.4 ± 2.1	<0.001
Waist:Hip ratio		0.91 ± 0.03	0.92 ± 0.03	0.93
KL Grade	**Median (IQR)**	4 (3-4)	3.5 (3-4)	
	KL3 (%)	37.5	37.5	
	KL4 (%)	62.5	62.5	
Joint Space (mm)		1.4 ± 0.7	1.8 ± 0.3	0.60

Table 3.4: Patient Characteristics from OA synovial fibroblast conditioned media from obese (n = 6) and normal weight (n = 5) patients

		Obese	Normal weight	P-value
Age (years)		68 ± 4.5	70 ± 5.2	0.79
Female:Male		6:1	4:1	
BMI (kg/m^2)		34.8 ± 2.6	22.9 ± 0.7	0.003
Waist circumference (cm)		101.6 ± 4.6	81.2 ± 4.9	0.01
Hip circumference, (cm)		115.3 ± 2.4	95.7 ± 4.0	0.005
Waist:Hip ratio		0.88 ± 0.04	0.86 ± 0.07	0.78
KL Grade	**Median (IQR)**	4 (3-4)	4 (3-4)	
	KL3 (%)	20	25	
	KL4 (%)	80	75	
Joint Space (mm)		2.1 ± 1.1	2.5 ± 1.1	0.60

Grade	Definition
0	Definite absence of x-ray changes of osteoarthritis
1	Doubtful joint space narrowing and possible osteophytic lipping
2	Definite osteophytes and possible joint space narrowing
3	moderate multiple osteophytes, definite narrowing of joint space and some sclerosis and possible deformity of bone ends
4	Large osteophytes, marked narrowing of joint space, severe sclerosis and definite deformity of bone ends

Table 3.5: Kellgren and Lawrence system for classification of osteoarthritis (KELLGREN and LAWRENCE, 1957)

3.4 Results

3.4.1 Univariate Metabolite Analysis from OA synovial fluid and OA Synovial Fibroblast Conditioned Media

Following NMR spectroscopy analysis of OA synovial fluid and synovial fibroblast conditioned media, 8 metabolites from synovial fluid were significantly increased when comparing obese OA patients to normal weight OA patients and no metabolites were decreased in the same comparison. From those metabolites which had the highest fold change was 1,3-Dimethylurate which increased by 46-fold ($p = 0.024$) when comparing obese and normal weight OA synovial fluid (Figure 3.1) (table 3.6). Metabolites associated with energy metabolism were also increased including Glucose (3-fold, $p = 0.043$), Pyruvate (3-fold, $p = 0.018$), Lactate (3-fold, $p = 0.016$) and Succinate (3.8-fold, $p = 0.013$) (Figure 3.1) (table 3.6). Amino acids were also found to be significantly increased in obese OA synovial fluid compared to normal weight OA synovial fluid including Tyrosine (3-fold, $p = 0.025$) and Glycine (2-fold, $p = 0.019$) (Figure 3.1) (table 3.6).

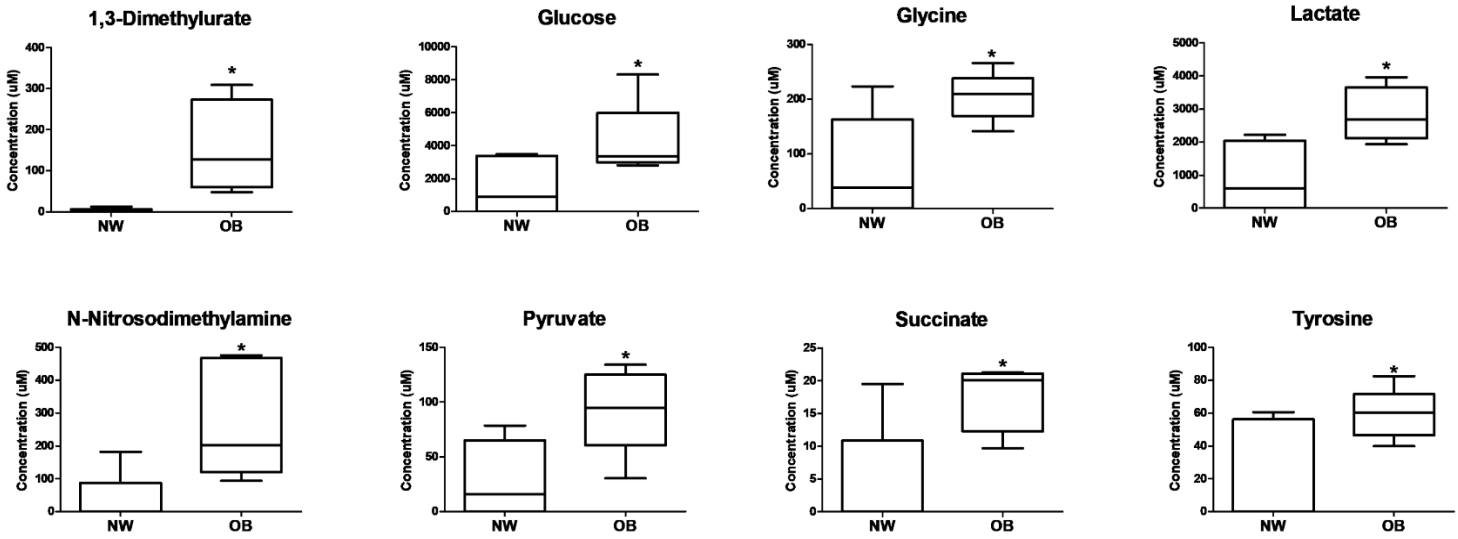

Figure 3.1: Boxplot of significantly increased metabolites in obese OA synovial fluid (n = 5) compared to normal weight (n = 6) OA synovial fluid (Farah *et al.*, 2022)[1]

[1] **Statistical analysis using two tailed unpaired Student T test using Prism 9.0 (GraphPad).**

Table 3.6: Full list of detected metabolite concentrations from normal weight (NW) (n = 5) and obese (OB) (n = 6) OA synovial fluid. (n.d: not detectable)

Metabolite	NW (μM)	OB (μM)	Fold-Change	P-Value
Succinate	4.6	17.4	3.8	0.013
Lactate	899	2819	3.1	0.016
N-Nitrosodimethylamine	39.8	276	6.9	0.016
Pyruvate	28.5	93.1	3.3	0.018
Glycine	73.7	205	2.8	0.019
1,3-Dimethylurate	2.8	128	46.4	0.024
Tyrosine	19.2	59.2	3.1	0.025
Glucose	1440	4253	3.0	0.043
Phenylalanine	15.9	42.0	2.6	0.050
Valine	69.5	227	3.3	0.064
Urea	1392	3584	2.6	0.067
Acetoacetate	n.d	24.8	>100	0.067
Guanidoacetate	33.1	89.6	2.7	0.069
Methanol	34.2	n.d	>100	0.085
sn-Glycero-3-phosphocholine	7.9	172	21.7	0.093
Creatine phosphate	50.7	249.4	4.9	0.093
1,3-Dihydroxyacetone	n.d	10.0	>100	0.104
Glycylproline	n.d	176	>100	0.104
2-Hydroxyisocaproate	n.d	10.8	>100	0.104
N,N-Dimethylglycine	0.3	139	554.2	0.105
Pantothenate	3.8	436	116.2	0.107
Alloisoleucine	n.d	180	>100	0.108

Metabolite	NW (μM)	OB (μM)	Fold-Change	P-Value
Glycolate	52.3	208	4.0	0.110
Threonate	n.d	17.0	>100	0.110
Caprate	n.d	38.2	>100	0.111
Lysine	n.d	117	>100	0.116
Cadaverine	n.d	57.4	>100	0.122
2-Hydroxyvalerate	n.d	18.8	>100	0.123
Malonate	566	n.d	>100	0.125
Formate	71.8	184	2.6	0.126
5-Aminolevulinate	3.4	159	47.1	0.138
O-Phosphocholine	n.d	45.4	>100	0.153
Glutamate	47.5	563	11.8	0.154
Galactarate	22.5	192	8.5	0.162
Succinylacetone	2.8	227	82.5	0.174
Ethylene glycol	1671	n.d	>100	0.189
Alanine	65.3	192	2.9	0.194
N-Methylhydantoin	0.5	2.8	6.2	0.201
Oxypurinol	n.d	138	>100	0.206
Galactonate	30.4	n.d	>100	0.207
Hypoxanthine	1.5	7.9	5.5	0.221
3-Hydroxyisovalerate	11.7	26.8	2.3	0.230
Hydroxyacetone	7.3	n.d	>100	0.235
Riboflavin	n.d	10.0	>100	0.251
Trimethylamine N-oxide	24.2	n.d	>100	0.283
1,7-Dimethylxanthine	0.5	83.7	173.2	0.294
N-Acetylglucosamine	1.5	463	312.0	0.295
2-Oxoisocaproate	n.d	4.9	>100	0.297
Caprylate	n.d	5.5	>100	0.297
Butanone	n.d	81.9	>100	0.297

Metabolite	NW (µM)	OB (µM)	Fold-Change	P-Value
Thymidine	n.d	0.8	>100	0.297
3,5-Dibromotyrosine	n.d	1.2	>100	0.297
Methylamine	n.d	1.7	>100	0.297
UDP-N-Acetylglucosamine	n.d	2.6	>100	0.297
Nα-Acetyllysine	n.d	2.6	>100	0.297
N-Acetylaspartate	n.d	2.8	>100	0.297
Propylene glycol	n.d	3.3	>100	0.297
N-Acetylcysteine	n.d	3.5	>100	0.297
N-Acetylglutamate	n.d	4.7	>100	0.297
Choline	n.d	8.9	>100	0.297
ADP	n.d	9.2	>100	0.297
Isoleucine	n.d	10.5	>100	0.297
Methionine	n.d	15.0	>100	0.297
Histidine	n.d	15.3	>100	0.297
Aspartate	n.d	16.1	>100	0.297
Galactose	n.d	16.5	>100	0.297
Valerate	n.d	17.0	>100	0.297
Isobutyrate	n.d	21.3	>100	0.297
N-Acetyltyrosine	n.d	24.6	>100	0.297
Lactulose	n.d	40.5	>100	0.297
Ascorbate	n.d	45.2	>100	0.297
myo-Inositol	n.d	107	>100	0.297
Isocitrate	n.d	165	>100	0.297
Glucitol	n.d	170	>100	0.297
N-Acetylglycine	n.d	182	>100	0.297
Glycerate	n.d	465	>100	0.297
Lactose	n.d	662	>100	0.297
Arabinose	n.d	709	>100	0.297

Metabolite	NW (µM)	OB (µM)	Fold-Change	P-Value
Acetone	21.0	3.7	-5.6	0.305
Threonine	12.8	720	56.4	0.305
3-Hydroxybutyrate	126.8	262	2.1	0.316
3-Methylxanthine	8.4	25.0	3.0	0.332
Anserine	41.1	116	2.8	0.345
Glutamine	294.6	481	1.6	0.347
4-Hydroxy-3-methoxymandelate	6.4	0.9	-6.8	0.372
5-Hydroxyindole-3-acetate	0.6	n.d	>100	0.389
2-Hydroxyisovalerate	0.7	n.d	>100	0.389
N-Acetylserotonin	0.7	n.d	>100	0.389
Dimethylamine	1.0	n.d	>100	0.389
N-Acetylornithine	1.3	n.d	>100	0.389
Theophylline	2.4	n.d	>100	0.389
Carnosine	2.5	n.d	>100	0.389
Isopropanol	3.0	n.d	>100	0.389
N-Acetylglutamine	7.1	n.d	>100	0.389
Sebacate	8.1	n.d	>100	0.389
Ethanol	11.3	n.d	>100	0.389
Homovanillate	12.7	n.d	>100	0.389
Dimethyl sulfone	19.8	n.d	>100	0.389
Leucine	23.5	n.d	>100	0.389
Carnitine	25.4	n.d	>100	0.389
Isoeugenol	34.8	n.d	>100	0.389
cis-Aconitate	67.1	n.d	>100	0.389
2-Phosphoglycerate	302	n.d	>100	0.389
Xylose	672	n.d	>100	0.389
2-Hydroxyisobutyrate	108.0	2.0	-55.1	0.395
Acetate	38.8	66.3	1.7	0.427

Metabolite	NW (μM)	OB (μM)	Fold-Change	P-Value
Pyridoxine	1.9	7.9	4.2	0.438
Galactitol	8.9	37.2	4.2	0.439
N-Isovaleroylglycine	1.7	6.3	3.8	0.459
4-Pyridoxate	8.0	19.2	2.4	0.467
Xanthine	12.1	2.1	-5.7	0.479
Acetamide	0.9	2.9	3.2	0.499
3-Methylhistidine	9.6	19.7	2.0	0.508
Creatine	13.9	32.2	2.3	0.566
N,N-Dimethylformamide	10.6	4.0	-2.6	0.605
1-Methylhistidine	76.9	115	1.5	0.658
Syringate	0.3	0.5	1.8	0.684
Histamine	14.4	8.0	-1.8	0.706
Thymine	1.8	3.0	1.6	0.719
O-Acetylcarnitine	5.0	7.2	1.4	0.733
Trimethylamine	4.2	2.6	-1.6	0.738
3-Methyl-2-oxovalerate	24.5	14.4	-1.7	0.745
Imidazole	8.9	6.4	-1.4	0.749
Creatinine	22.3	27.7	1.2	0.757
O-Acetylcholine	15.0	20.8	1.4	0.782
3,4-Dihydroxymandelate	1.7	1.2	-1.4	0.821
Methylguanidine	1.3	0.9	-1.4	0.842
Sarcosine	9.9	7.5	-1.3	0.842
Betaine	209	165	-1.3	0.844
Caffeine	13.5	14.2	1.1	0.972
Glutaric acid monomethyl ester	33.0	34.5	1.0	0.975
2-Hydroxybutyrate	18.8	19.2	1.0	0.982

Having identified these metabolites as significantly altered in OA synovial fluid in obesity, the next step was to look at whether these same metabolites were altered in OA synovial fibroblasts, and therefore NMR spectroscopy of conditioned media following stimulation with TNFα (10ng/ml for 24 hrs) was analysed. However, these same 8 metabolites were not significantly increased or decreased in any of the groups (figure 3.2).

When analysing the NMR spectroscopy data from OA synovial fibroblast conditioned media, some metabolites were significantly altered following stimulation with TNFα (10ng/ml for 24 hrs) in both normal weight and obese patients. 4 metabolites were significantly increased in normal weight OA synovial fibroblast secretomes following TNFα (10ng/ml for 24 hrs) stimulation, including Formate ($p = 0.0258$), 1,7-dimethylxanthine ($p = 0.047$), N-Acetlyglycine ($p = 0.035$) and Galacterate ($p = 0.0206$) (figure 3.3) (table 3.7). Likewise, 3 metabolites were significantly altered in obese OA synovial fibroblast conditioned media following TNFα (10ng/ml for 24 hrs) stimulation, including Phenylalanine which was significantly decreased ($p = 0.0097$), Imadizole ($p = 0.0347$) and Glycolate ($p = 0.0404$) which were significantly increased (figure 3.4) (table 3.8).

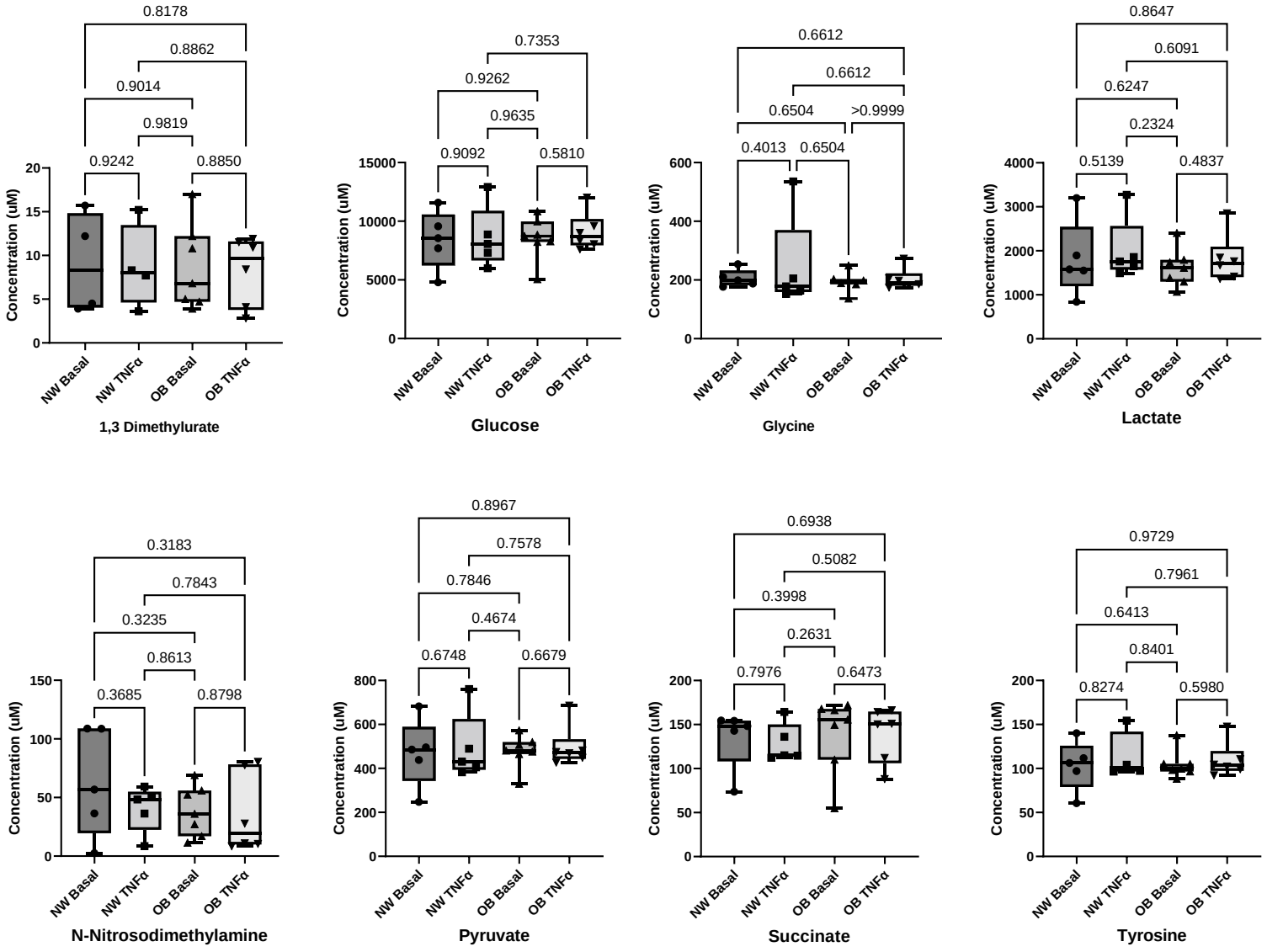

Figure 3.2: Boxplot of metabolites in OA synovial fibroblast conditioned media unstimulated and stimulated (10ng/ml TNFα for 24hrs) from obese (OB) (n = 6) and normal weight (NW) (n = 5) patients which were identified to be altered in OA synovial fluid1.

[1] **Statistical analysis using one-way ANOVA with Tukey Post Hoc test using Prism 9.0 (GraphPad).**

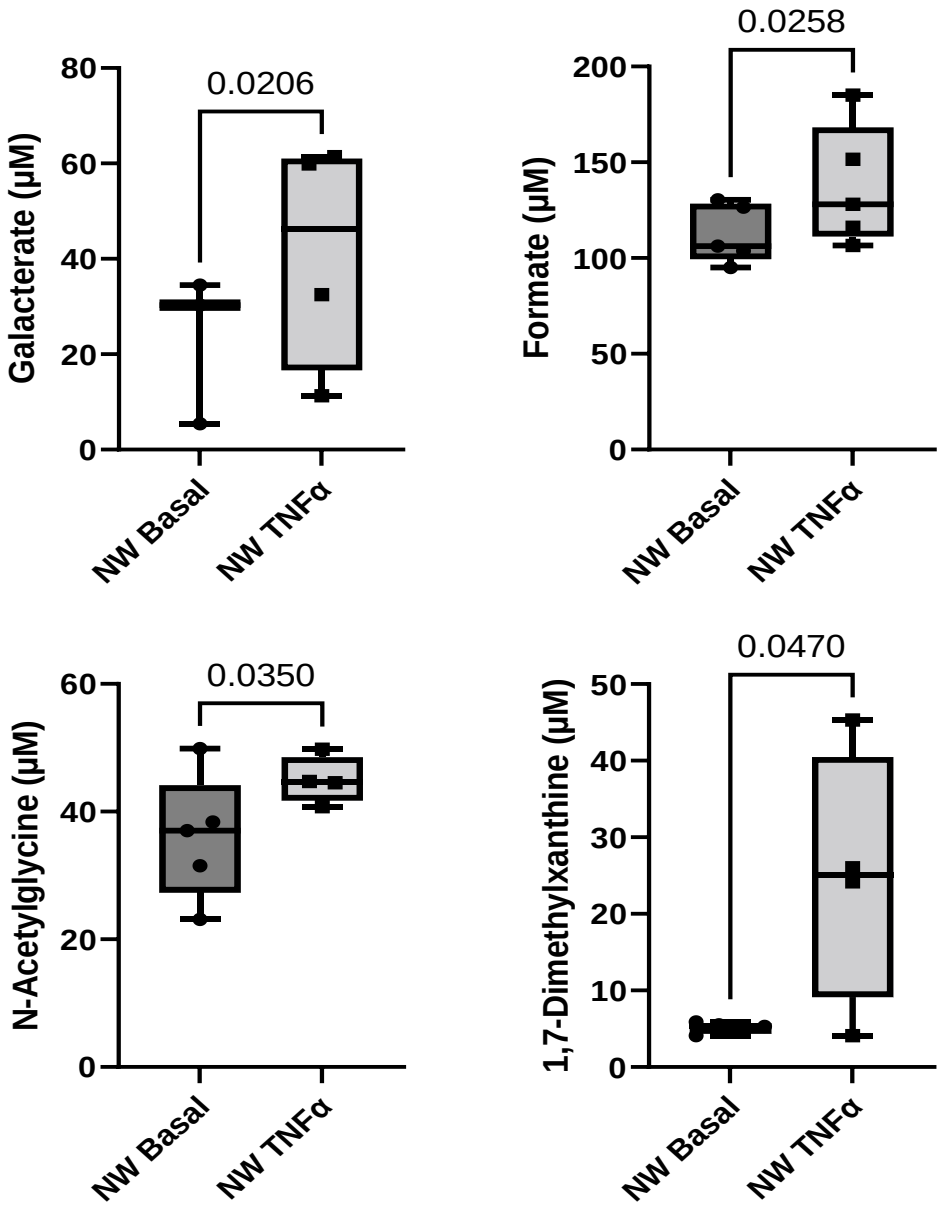

Figure 3.3: Boxplot of significantly increased metabolites in OA synovial fibroblast conditioned media unstimulated and stimulated (10ng/ml TNFα for 24hrs) from normal weight (NW) patients (n= 5).

[1] **Statistical analysis using one tailed paired student T test (following confirmation of normal distribution using Shapiro-Wilk test) using Prism 9.0 (GraphPad).**

Metabolite	NW Basal (μM)	NW TNFα (μM)	Fold-Change	P Value
Galactarate	23.4	41.275	1.763888889	0.010304
Formate	112.38	137.42	1.222815448	0.025816
N-Acetylglycine	35.98	44.95	1.24930517	0.034956
1,7-Dimethylxanthine	5.08	24.9	4.901574803	0.047012
Guanidoacetate	128.8	156.52	1.215217391	0.054043
myo-Inositol	577.85	680.2	1.177122091	0.054781
Galactitol	148.2	51.05	0.344466937	0.095484
cis-Aconitate	14.36	20.775	1.446727019	0.099316
Valine	160.3333333	176.6	1.101455301	0.102816
Allantoin	42.475	86.125	2.027663331	0.122794
Hydroxyacetone	76.12	48.26	0.633998949	0.12609
Dimethyl sulfone	5.08	6.26	1.232283465	0.153295
Galactonate	109.88	103.35	0.940571533	0.174515
Lactate	1812.66	2006.06	1.10669403	0.188281
Succinylacetone	328.9666667	12.96666667	0.039416354	0.196237
Creatine phosphate	43.74	35.275	0.80647005	0.203442
Pyridoxine	2.48	37.9	15.28225806	0.209667
Ethanol	4441.95	4144.86	0.933117212	0.210188
Citraconate	119.525	117.4	0.982221293	0.217474
N-Nitrosodimethylamine	62.66	40.58	0.647622087	0.222194

Table 3.7: Top 20 detected metabolite concentrations from normal weight (NW) Basal and normal weight TNFα (10ng/ml for 24hrs) synovial fibroblast conditioned media. Statistical analysis using one tailed paired Student T test.

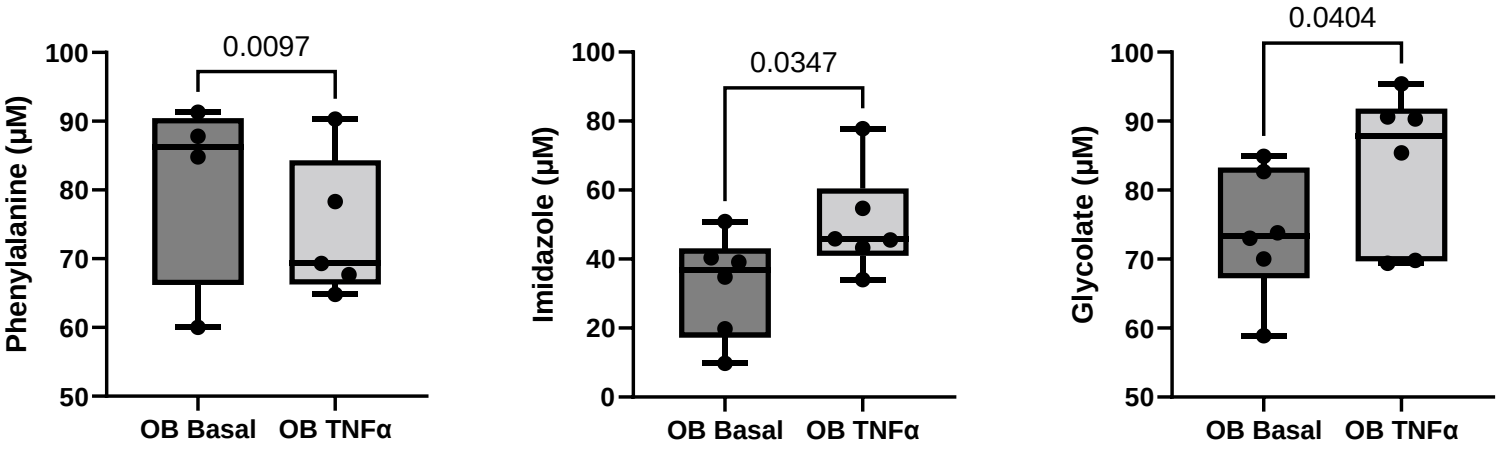

Figure 3.4: Boxplot of significantly increased metabolites in OA synovial fibroblast conditioned media unstimulated and stimulated (10ng/ml TNFα for 24hrs) from obese (OB) patients (n= 6)[1].

[1] **Statistical analysis using one tailed paired student T test (following confirmation of normal distribution using Shapiro-Wilk test) using Prism 9.0 (GraphPad).**

Table 3.8: Top 20 detected metabolite concentrations from obese (OB) Basal and obese TNFα (10ng/ml for 24hrs) synovial fibroblast conditioned media. Statistical analysis using one tailed paired Student T test.

Metabolite	OB Basal (μM)	OB TNFα (μM)	Fold-Change	P Value
Phenylalanine	72.4	76.4	1.055248619	0.009714
Imidazole	43.1	53.44	1.239907193	0.034718
Glycolate	71.1	82.12	1.154992968	0.040425
Valine	151.32	163.8	1.082474227	0.050744
Glutamine	2265.46	2531.14	1.117274196	0.056332
O-Acetylcholine	66.18	45.7	0.690540949	0.066172
Lactate	1624.64	1811.98	1.1153117	0.067555
Galactitol	40.03333333	256	6.394671107	0.069623
Ethanol	6282.32	7412.7	1.179930344	0.075327
Galactarate	16.26666667	43.2	2.655737705	0.108067
Arginine	865.62	969.76	1.120306832	0.108659
N-Methylhydantoin	17.92	37.55	2.095424107	0.111307
1,7-Dimethylxanthine	9.225	11	1.192411924	0.115127
myo-Inositol	541.85	544.96	1.005739596	0.118535
Creatine	32.08	42.35	1.320137157	0.121315
Threonine	192.575	551.775	2.865247306	0.129632
Cadaverine	110.725	105.7	0.954617295	0.130205
3-Hydroxyisovalerate	25	31.48	1.2592	0.133033
Tyrosine	106.56	112.78	1.058370871	0.149017
Allantoin	25.46666667	29.225	1.147578534	0.149372

3.4.2 Linear Regression Analysis of Significantly Altered Metabolites in OA Synovial Fluid

Having identified 10 metabolites from the NMR spectroscopy analysis with significantly different concentrations between synovial fluid from obese and normal-weight OA patients, we further examined these metabolites by subjecting them to simple linear regression models to determine their relationship to adiposity/body composition parameters. These parameters included body mass index , waist circumference, hip circumference and waist to hip ratio.

When analysing the relationships between metabolite concentrations and body mass index, 4 of the 10 metabolites showed a significant linear relationship. Glycine showed a strong positive correlation with body mass index, with those patients with the highest body mass index having significantly higher synovial fluid glycine concentrations (P= 0.006, r^2 = 0.58) (table 3.9, Figure 3.7 A). Likewise, Lactate (P= 0.046, r^2 = 0.41) (table 3.9, Figure 3.8 A), succinate (P= 0.015, r^2 = 0.5) (table 3.9, Figure 3.12 A) and tyrosine (P= 0.046, r^2 = 0.39) (table 3.9, Figure 3.13 A) also showed positive correlation with body mass index. Amongst these metabolites Glucose (P= 0.052, r^2 = 0.36) (table 3.9, Figure 2.2 A), Pyruvate (P= 0.07, r^2 = 0.32) (table3.9, Figure 2.6 A), and N-Nitrosodimethylamine (P= 0.051, r^2 = 0.36) (table 3.9, Figure 2.5 A) displayed a positive trend with body mass index however this was not statistically significant.

Following BMI analysis, the next adiposity parametric was to determine whether there was a linear relationship with waist circumference. From the 10 metabolites, 5 were found to have a statistically significant linear relationship to waist

circumference. Glycine again showed a strong positive correlation with waist circumference (P= 0.009, r^2 = 0.6) (table 3.9, Figure 3.7 C). Likewise, Lactate (P= 0.02, r^2 = 0.56) (table 3.9, Figure 3.8 C), N-Nitrosodimethylamine (P= 0.02, r^2 = 0.51) (table 3.9, Figure 3.10 C), succinate (P= 0.01, r^2 = 0.57) (table 3.9, Figure 3.12 C) and Glutamine:Glutamate (P= 0.036, r^2 = 0.55) (table 3.9, Figure 3.16 C) all showed strong positive correlation with waist circumference. Tyrosine displayed a positive trend with waist circumference however this was not statistically significant (P= 0.06, r^2 = 0.37) (table 3.9, Figure 3.13 C).

Linear regression analysis between metabolite concentrations and hip circumference showed only one metabolite with a statistically significant relationship, which was succinate (P= 0.04, r^2 = 0.42) (table 3.9, Figure 3.12 D). Additionally, Glycine (P= 0.05, r^2 = 0.39) (table 3.9, Figure 3.7 D), N-Nitrosodimethylamine (P= 0.08, r^2 = 0.34) (table 3.9, Figure 3.10 D) and the Glutamine:Glutamate ratio (P= 0.051, r^2 = 0.49) (table 3.9, Figure 3.16 D) all displayed a positive trend with hip circumference, however this was not statistically significant.

Finally, when comparing metabolite concentrations with waist to hip ratio, of the 10 significantly altered metabolites, 5 showed a significant linear relationship. Glycine showed a strong positive correlation with waist to hip ratio (P= 0.004, r^2 = 0.66) (table 3.9, Figure 3.7 B). Lactate (P= 0.0001, r^2 = 0.9) (table 3.9, Figure 3.8 B), N-Nitrosodimethylamine (P= 0.02, r^2 = 0.51) (table 3.9, Figure 3.10 B), succinate (P= 0.019, r^2 = 0.52) (table 3.9, Figure 3.12 B) and Tyrosine (P= 0.019, r^2 = 0.52) (table 3.9, Figure 3.13 B) all showed a strong positive correlation with waist to hip ratio. Pyruvate (P= 0.059, r^2 = 0.38) (table 3.9, Figure 3.11 B) and Glutamate (P= 0.07, r^2

= 0.45) (table 3.9, Figure 3.15 B) both displayed a positive trend with waist to hip ratio, however this was not statistically significant.

Table 3.9: Regression analysis of synovial fluid metabolite concentrations with parameters of OA patient adiposity/body composition (n = 15 patients)[1].

	BMI			WC (cm)			HC (cm)			WHR		
	R^2	Slope	p-value	R^2	Slope	p-value	R^2	Slope	p-value	R^2	Slope	p-value
1,3 Dimethylurate	**0.28**	**9.0 ± 4.8**	**0.09**	**0.13**	**2.0 ± 1.8**	**0.30**	**0.13**	**2.9 ± 2.7**	**0.31**	**0.10**	**390 ± 415**	**0.38**
Glucose	**0.36**	**249 ± 110**	**0.052**	**0.22**	**60 ± 40**	**0.17**	**0.13**	**67 ± 62**	**0.31**	**0.30**	**15700 ± 8400**	**0.1**
Glycine	**0.58**	**13.2 ± 3.7**	***0.006****	**0.60**	**4.0 ± 1.1**	***0.009****	**0.39**	**4.7 ± 2.1**	**0.05**	**0.66**	**935 ± 236**	***0.004****
Lactate	**0.41**	**145 ± 61**	***0.046****	**0.56**	**50 ± 17**	***0.02****	**0.26**	**51 ± 33**	**0.16**	**0.90**	**14500 ± 1900**	***0.0001*****
N-Nitrosodimethylamine	**0.36**	**18.4 ± 8.2**	**0.051**	**0.51**	**7.0 ± 2.4**	***0.02****	**0.34**	**8.4 ± 4.1**	**0.08**	**0.51**	**1560 ± 542**	***0.02****
Pyruvate	**0.32**	**4.8 ± 2.3**	**0.07**	**0.25**	**1.3 ± 0.8**	**0.15**	**0.13**	**1.4 ± 1.3**	**0.31**	**0.38**	**355 ± 161**	**0.059**
Succinate	**0.50**	**1.1 ± 0.4**	***0.015****	**0.57**	**0.38 ± 0.11**	***0.01****	**0.42**	**0.47 ± 0.2**	***0.04****	**0.52**	**80 ± 28**	***0.019****
Tyrosine	**0.39**	**3.4 ± 1.4**	***0.046****	**0.37**	**1.0 ± 0.47**	**0.06**	**0.20**	**1.1 ± 0.8**	**0.20**	**0.52**	**267 ± 92**	***0.019****
Glutamine	**0.11**	**-12.3 ± 14.4**	**0.43**	**0.03**	**-2.1 ± 4.7**	**0.17**	**0.04**	**-3.5 ± 6.6**	**0.61**	**0.02**	**-379 ± 1161**	**0.75**
Glutamate	**0.04**	**22.0 ± 43.7**	**0.63**	**0.29**	**18.4 ± 11.7**	**0.17**	**0.13**	**17.4 ± 18.3**	**0.38**	**0.45**	**5586 ± 2542**	**0.07**
Glutamine:Glutamate	**0.36**	**-0.20 ± 0.11**	**0.11**	**0.55**	**-0.08 ± 0.03**	***0.036****	**0.49**	**-0.10 ± 0.04**	**0.051**	**0.38**	**-15.4 ± 8.0**	**0.11[1]**

[1] Statistical analysis of these general linear models was conducted on SPSS Statistics (version 27) (Farah et al., 2022).

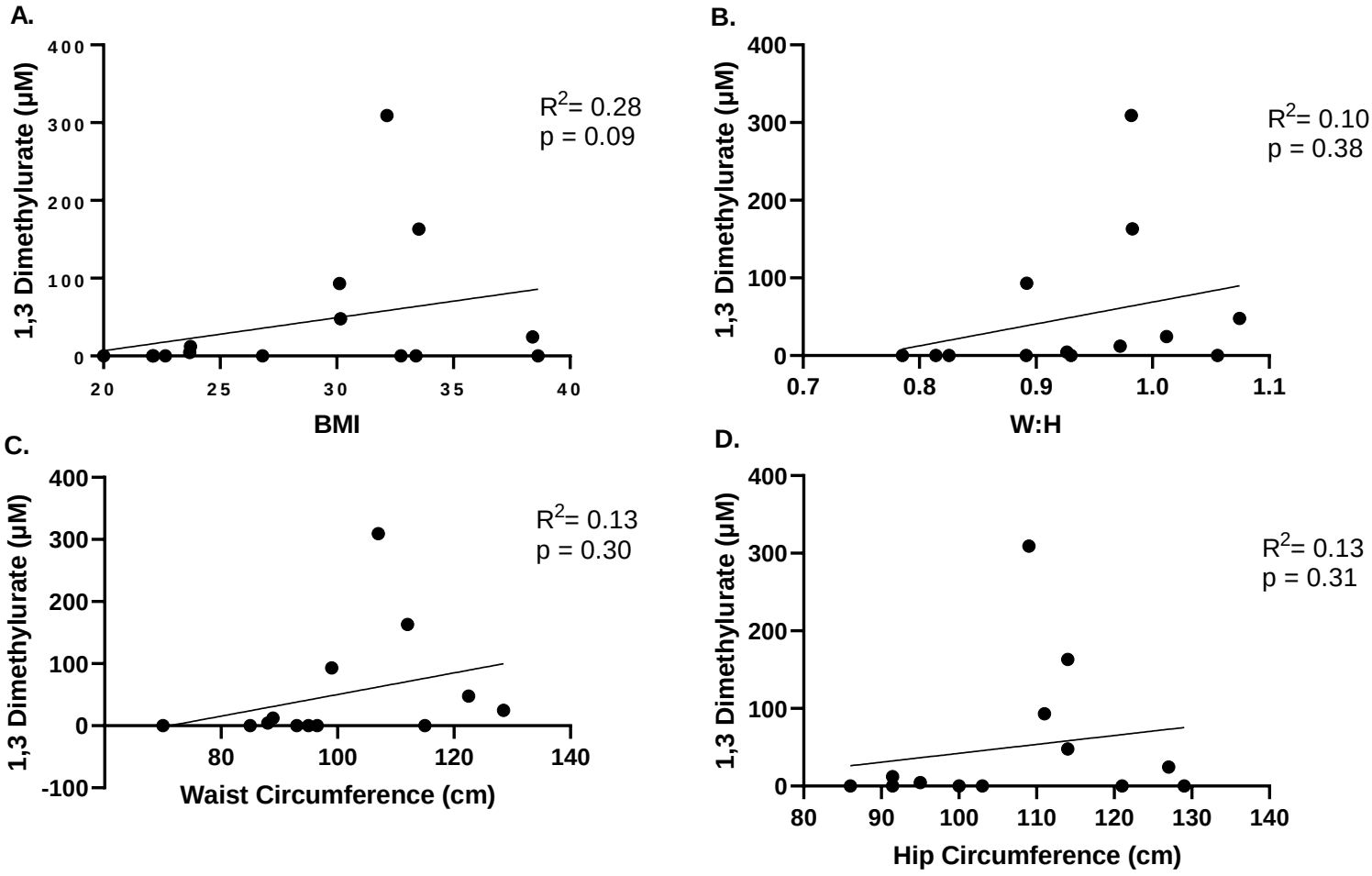

Figure 3.5: Regression analysis of the relationship between the synovial fluid concentration of 1,3-Dimethylurate and (A). BMI, (B) W:H (C) WC and (D) HC. (n = 15 patients).

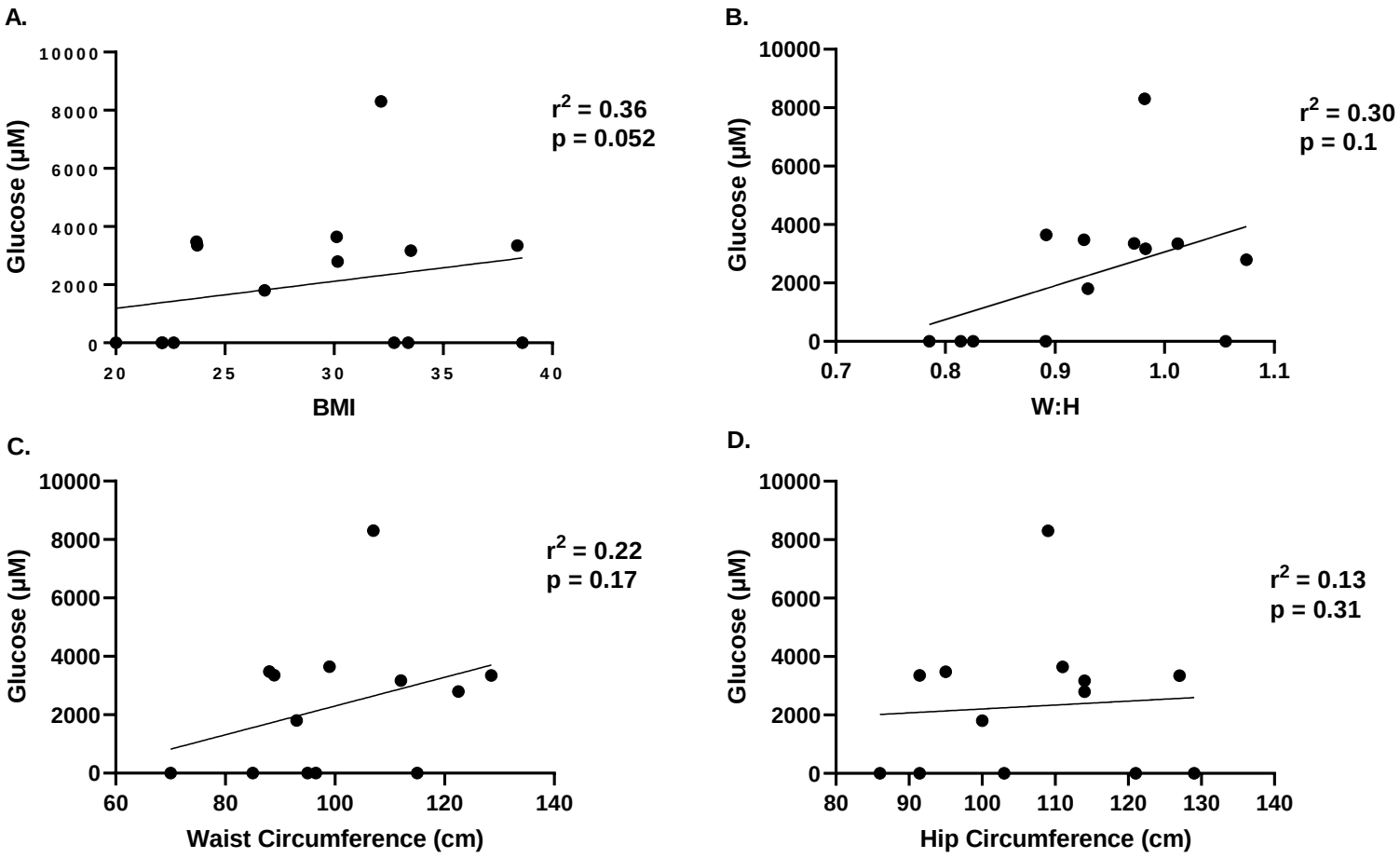

Figure 3.6: Regression analysis of the relationship between the synovial fluid concentration of Glucose and (A). BMI, (B) W:H (C) WC and (D) HC. (n = 15 patients).

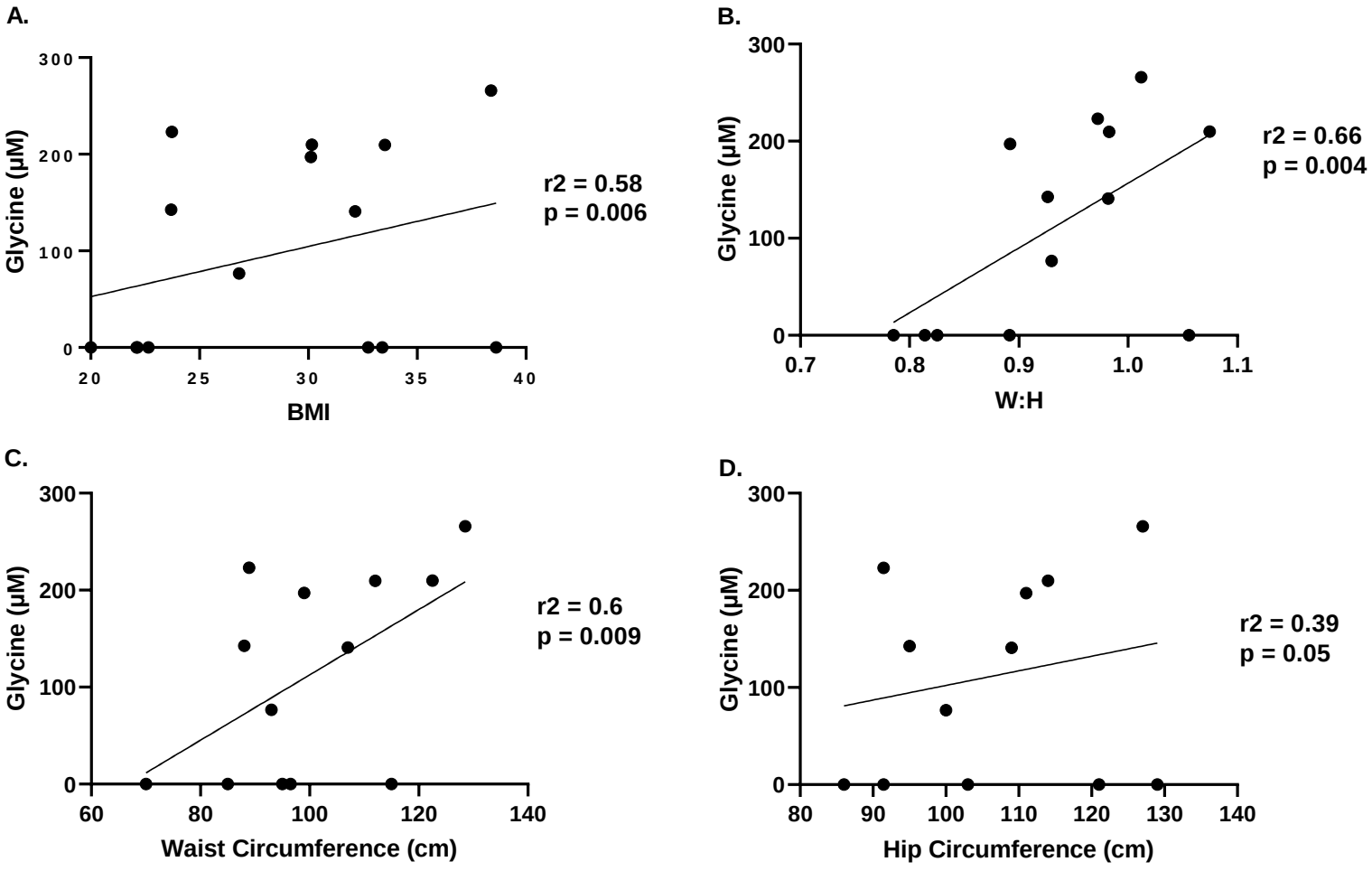

Figure 3.7: Regression analysis of the relationship between the synovial fluid concentration of Glycine and (A). BMI, (B) W:H (C) WC and (D) HC. (n = 15 patients).

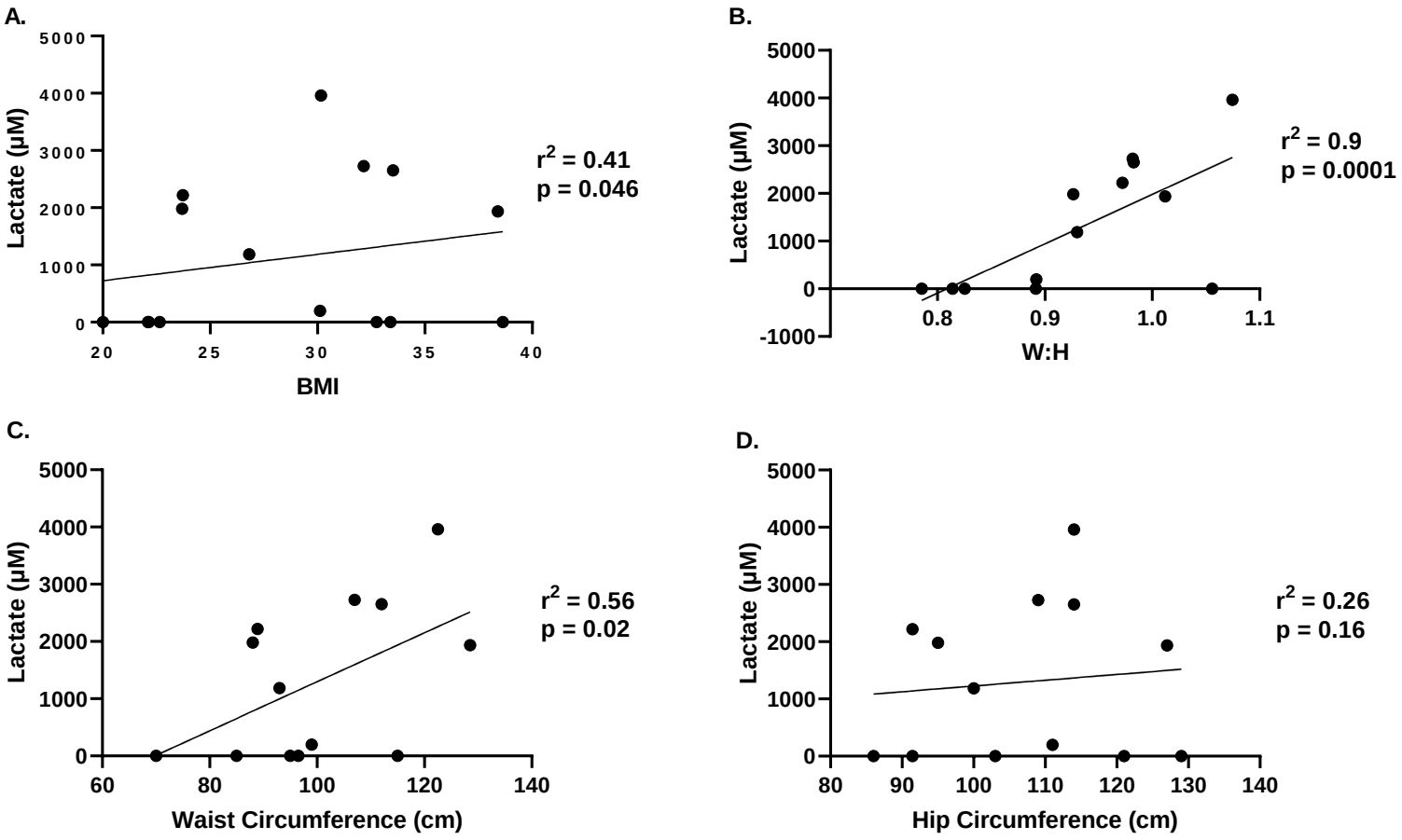

Figure 3.8: Regression analysis of the relationship between the synovial fluid concentration of Lactate and (A). BMI, (B) W:H (C) WC and (D) HC. (n = 15 patients).

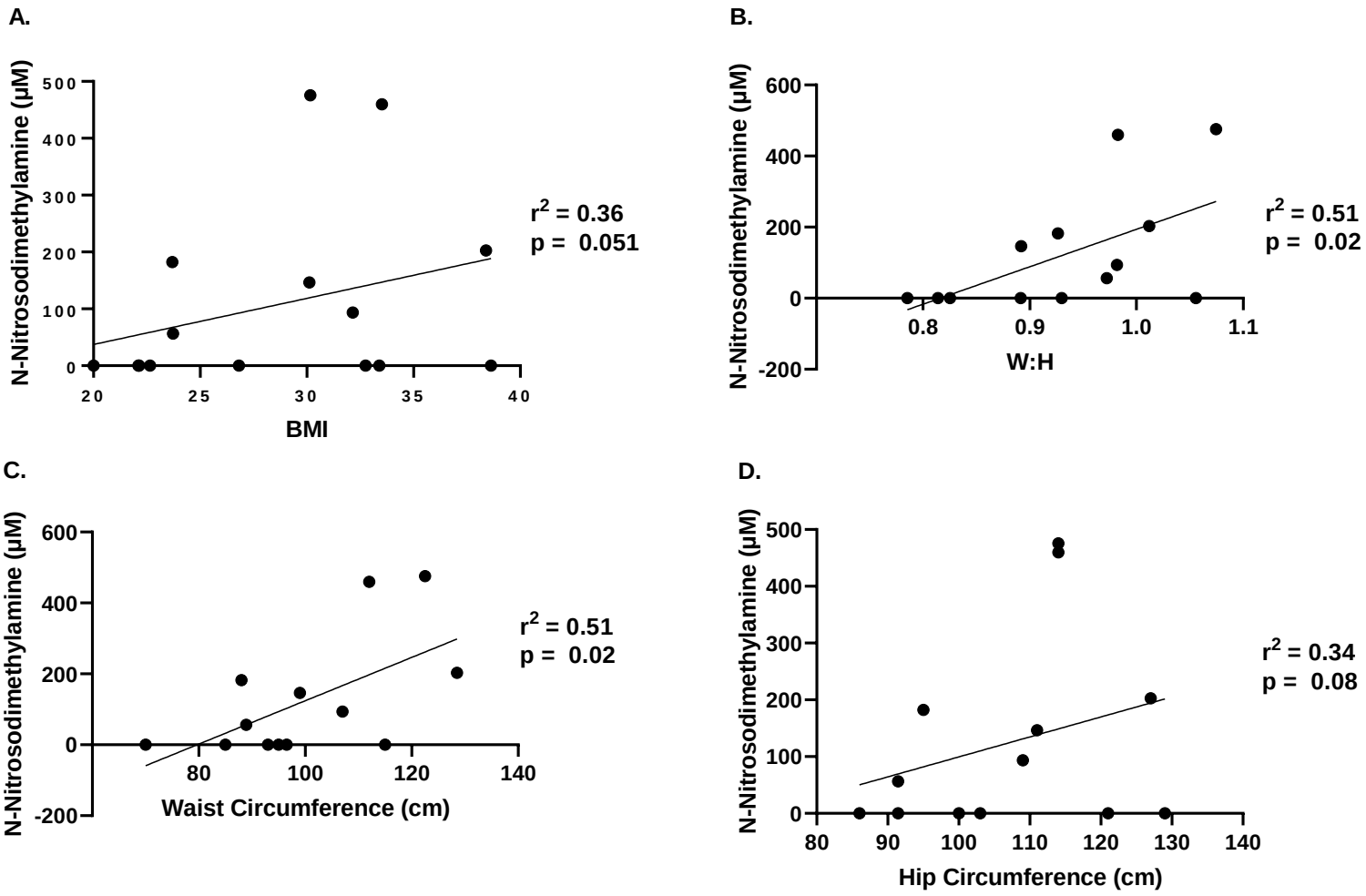

Figure 3.10: Regression analysis of the relationship between the synovial fluid concentration of N-Nitrosodimethylamine and (A). BMI, (B) W:H (C) WC and (D) HC. (n = 15 patients).

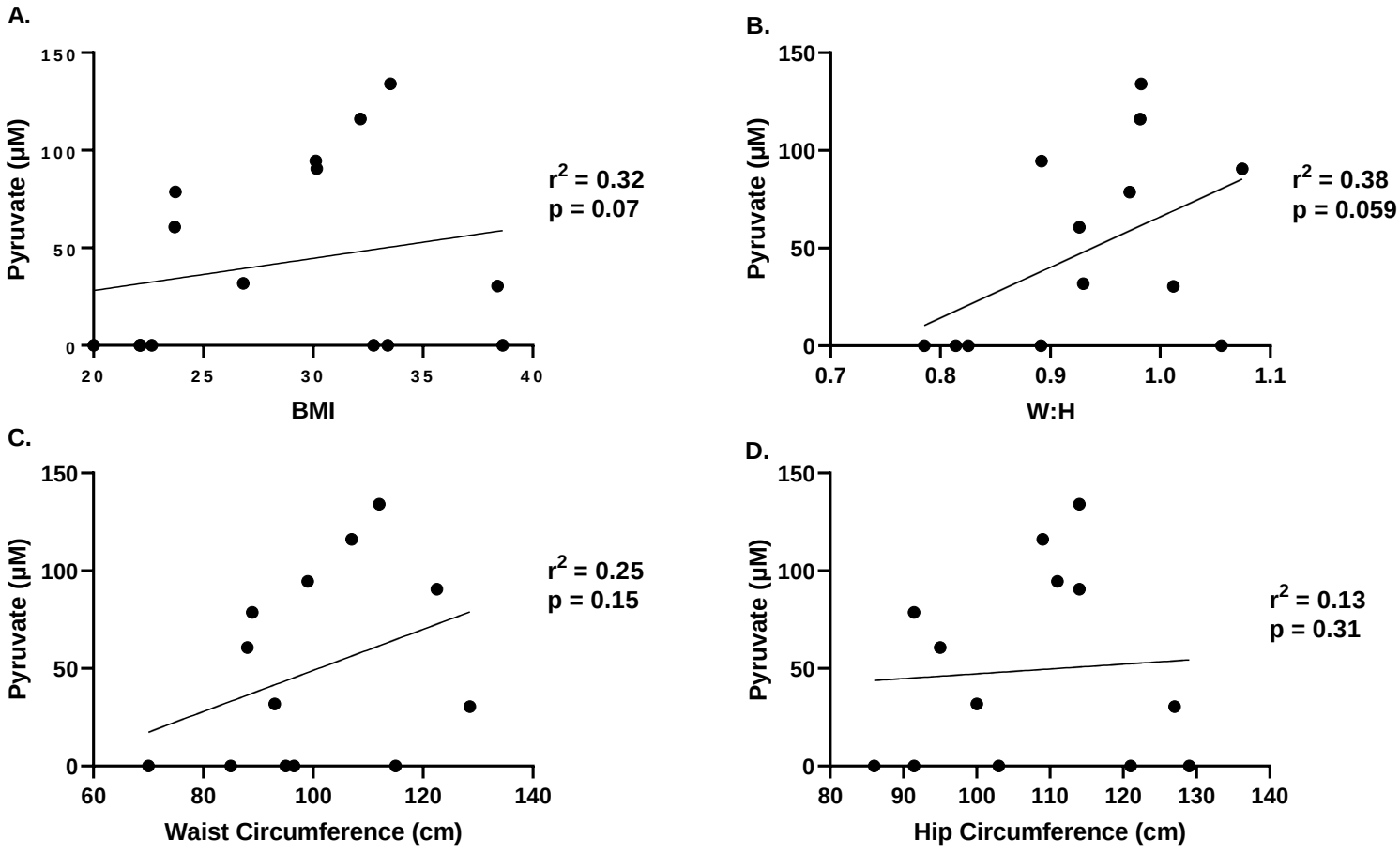

Figure 3.11: Regression analysis of the relationship between the synovial fluid concentration of Pyruvate and (A). BMI, (B) W:H (C) WC and (D) HC. (n = 15 patients).

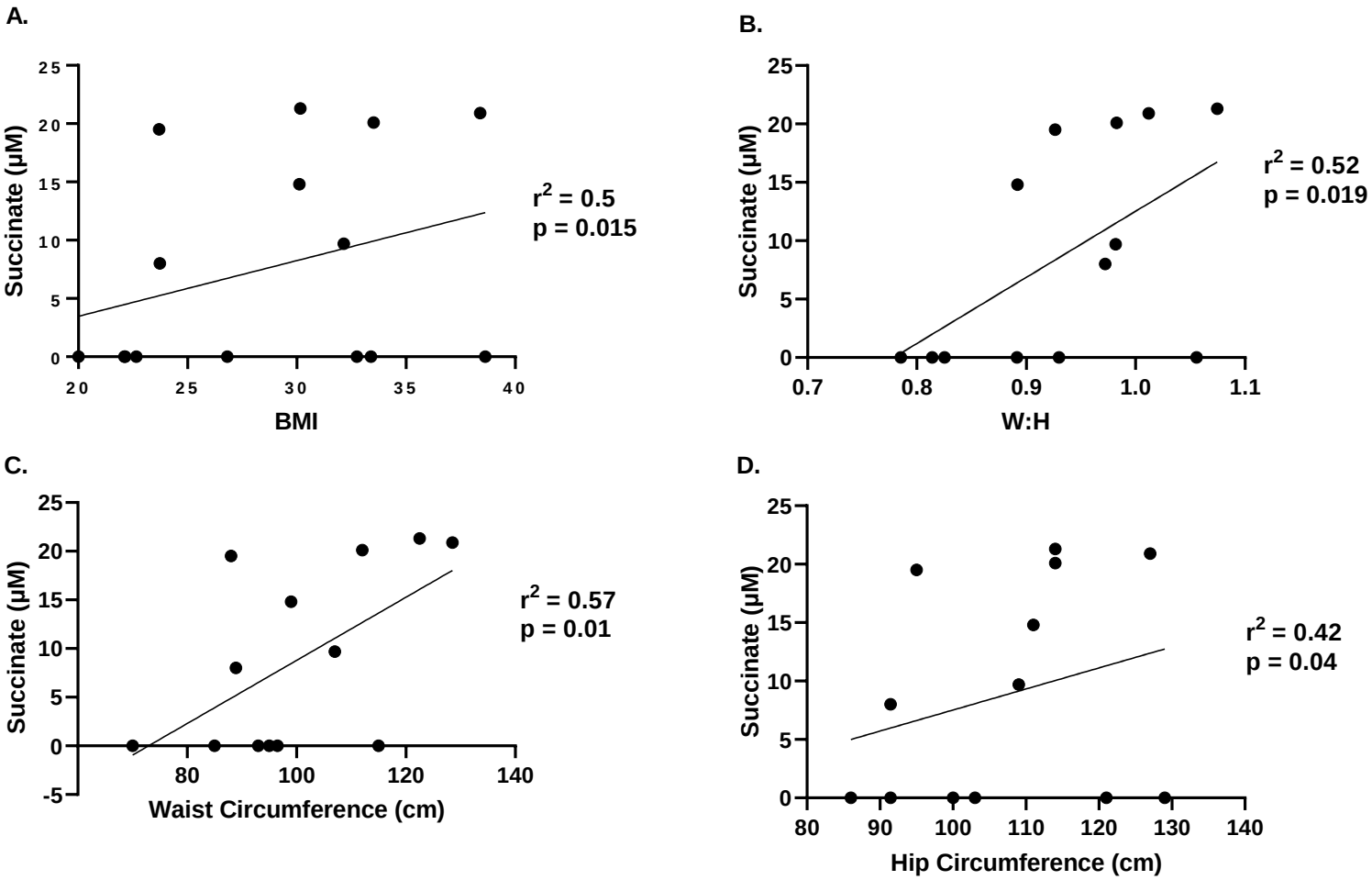

Figure 3.12: Regression analysis of the relationship between the synovial fluid concentration of Succinate and (A). BMI, (B) W:H (C) WC and (D) HC. (n = 15 patients).

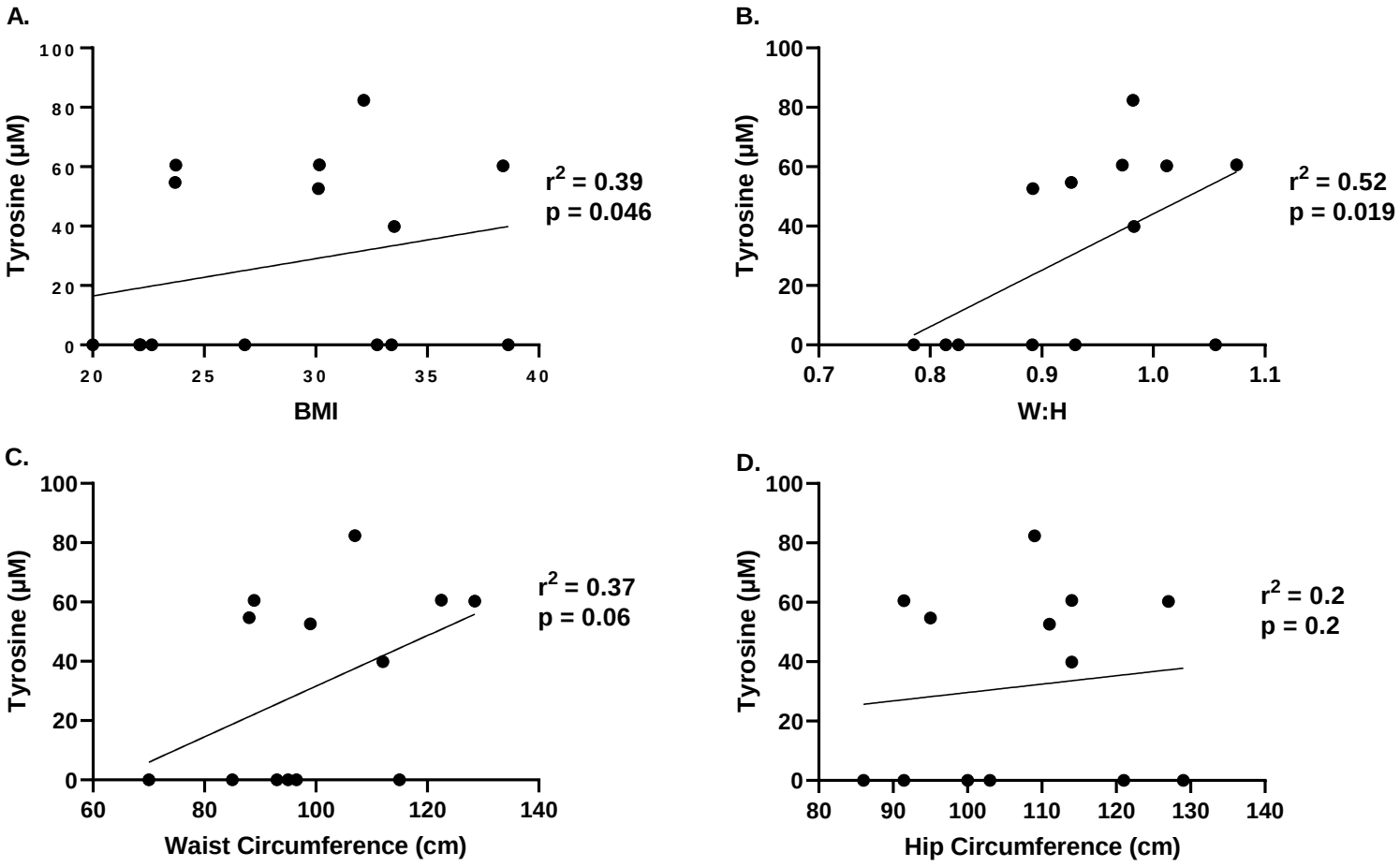

Figure 3.13: Regression analysis of the relationship between the synovial fluid concentration of Tyrosine and (A). BMI, (B) W:H (C) WC and (D) HC. (n = 15 patients).

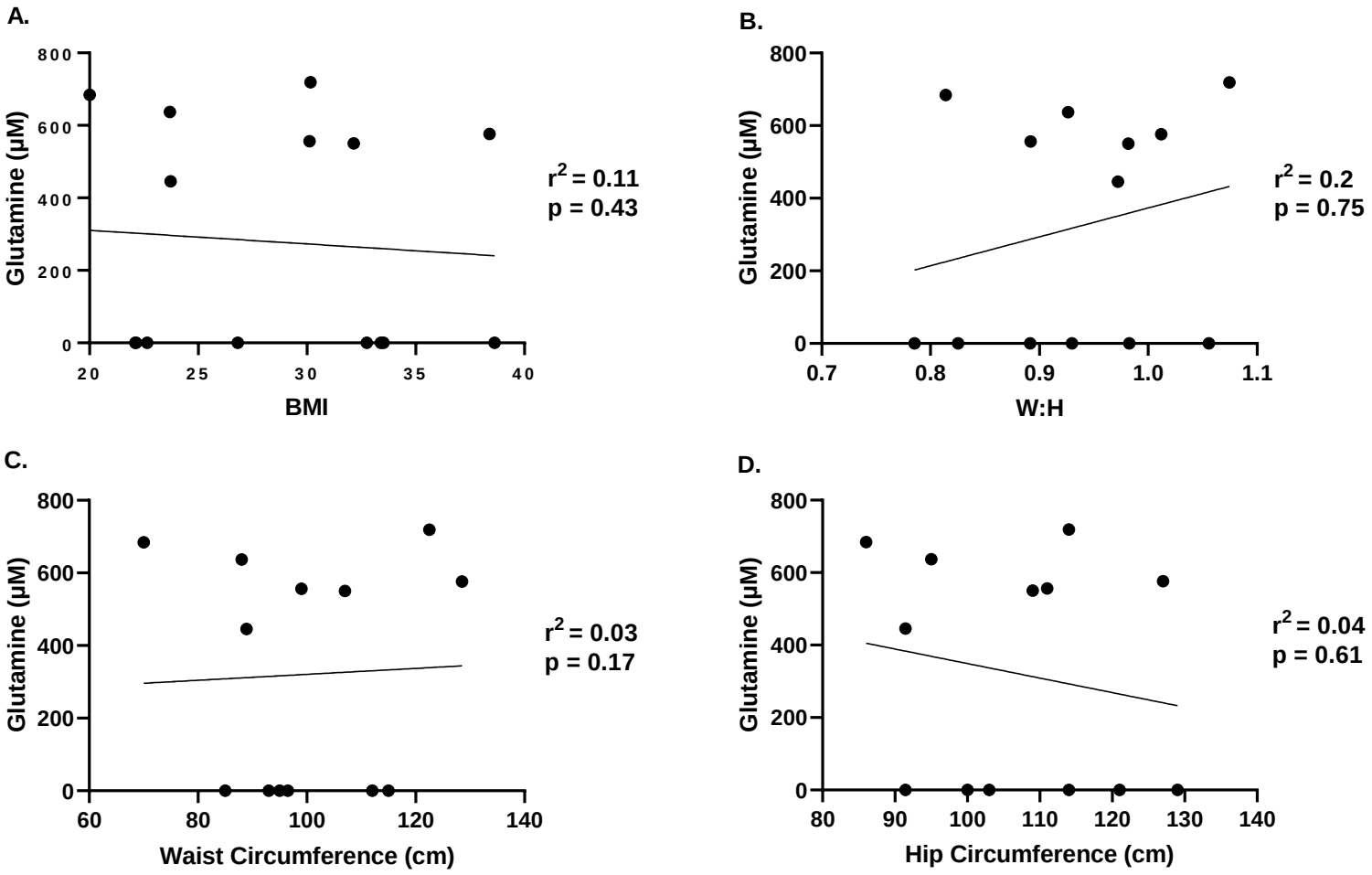

Figure 3.14: Regression analysis of the relationship between the synovial fluid concentration of Glutamine and (A). BMI, (B) W:H (C) WC and (D) HC. (n = 15 patients).

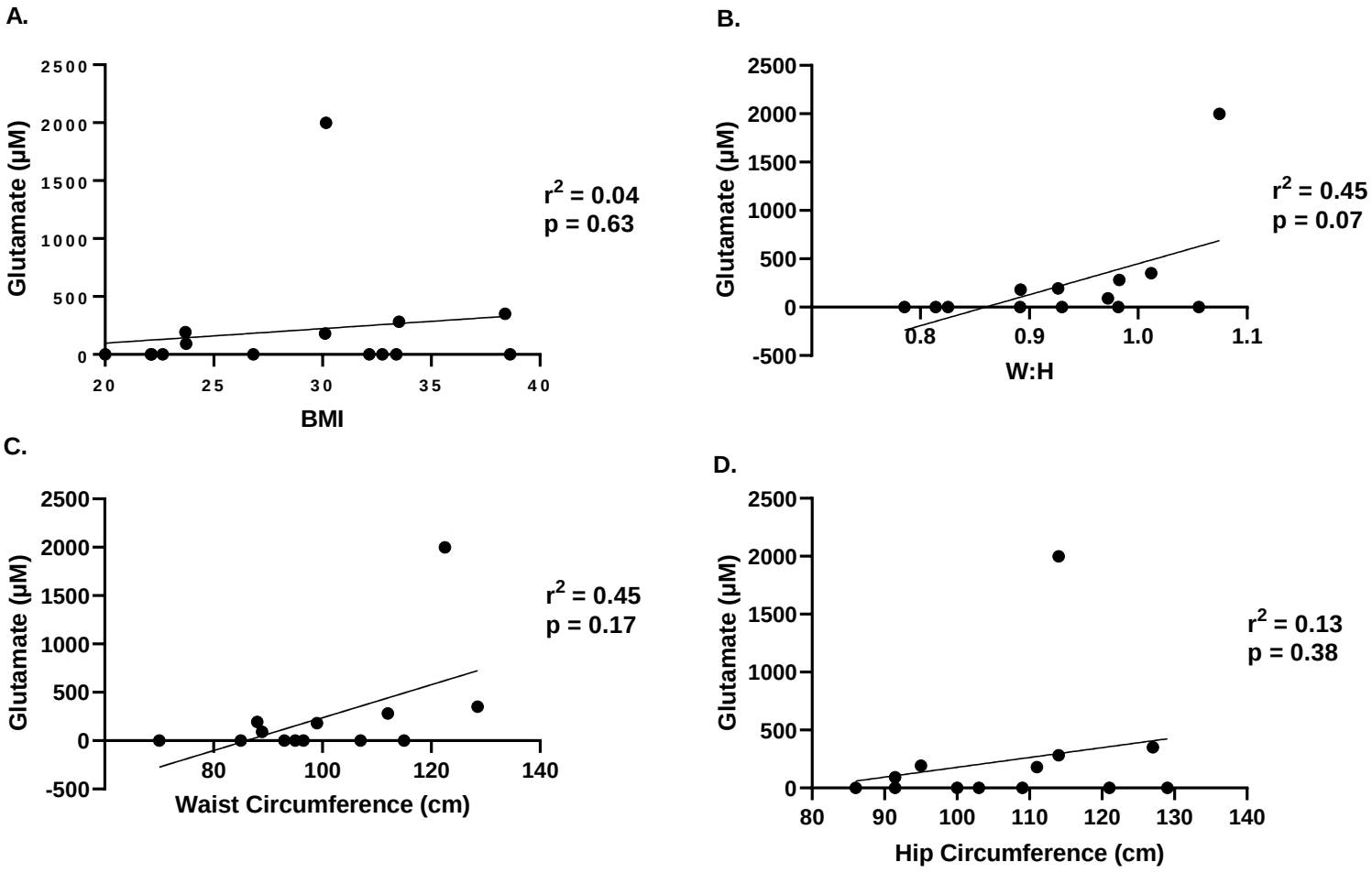

Figure 3.15: Regression analysis of the relationship between the synovial fluid concentration of Glutamate and (A). BMI, (B) W:H (C) WC and (D) HC. (n = 15 patients).

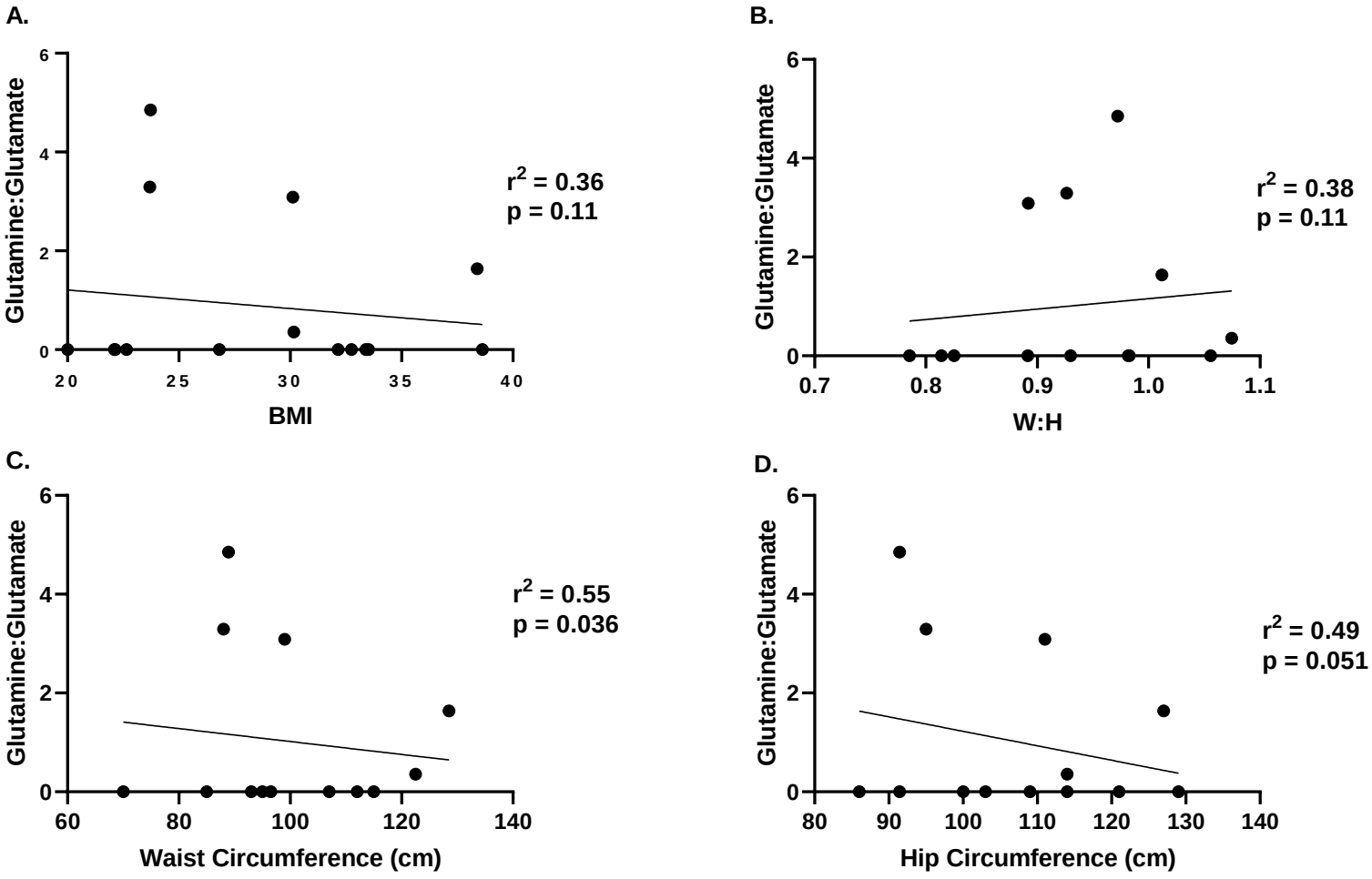

Figure 3.16: Regression analysis of the relationship between the synovial fluid concentration of Glutamine:Glutamate and (A). BMI, (B) W:H (C) WC and (D) HC. (n = 15 patients).

3.4.3 Metabolomic multivariate analysis of obese OA synovial fluid compared to normal weight OA synovial fluid

Having identified and annotated metabolite peaks detected by Chemonx (Edmonton, Canada), concentrations of each metabolite were assorted into a matrix and imported into SIMCA (Umetrics, Germany). OA synovial fluid from normal weight and obese patients (table 3.3) underwent multivariate analysis. PCA was used to plot the data (figure 3.17), and from this initial analysis no obvious clustering was observed, however all patients fell within Hoteling's T^2 range (displays a measure of how far each observation is from the model centre) suggesting no clear outliers within dataset. Model diagnostics of the PCA analysis (figure 3.18) show a low R^2 and Q^2, suggesting further multivariate analysis was required.

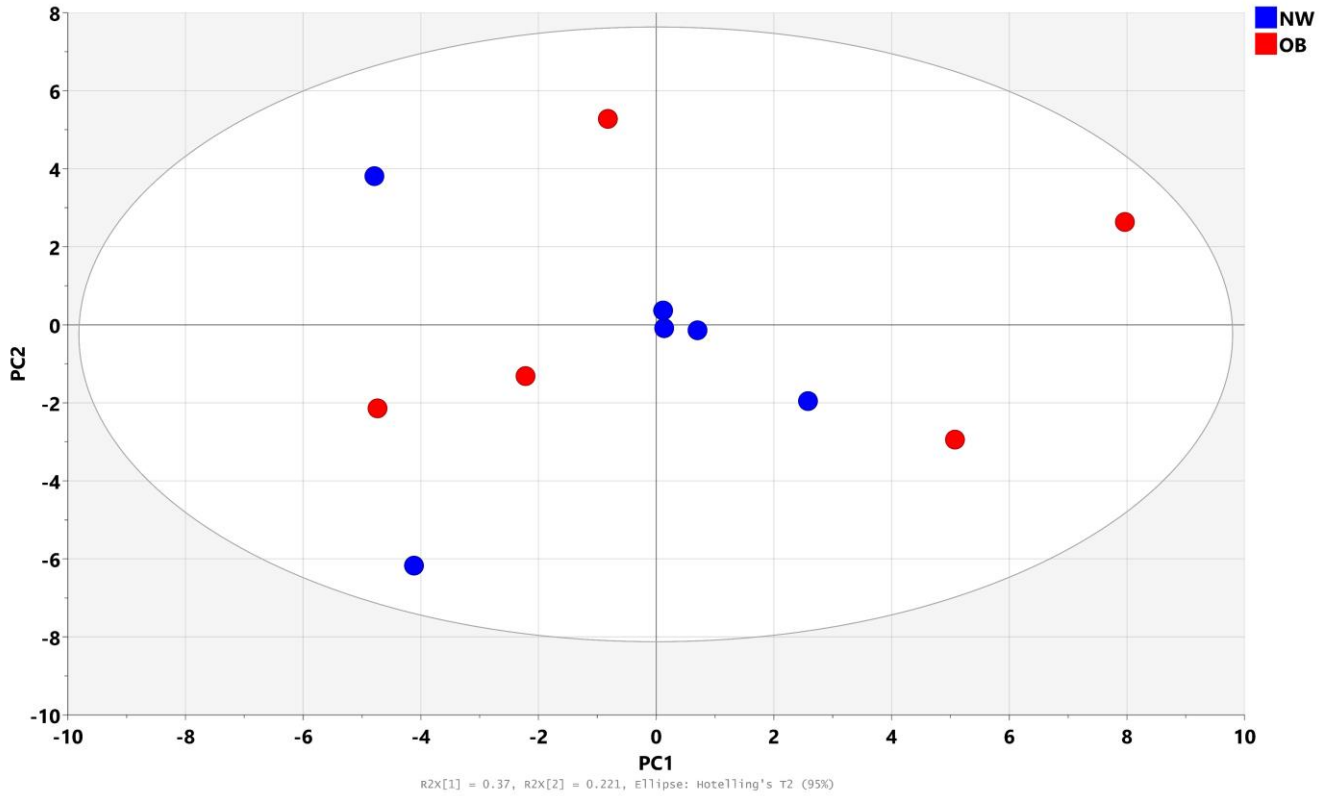

Figure 3.17: Scores plot of 1D 1H NMR spectra of normal weight (NW) and obese (OB) OA synovial fluid subjected to PCA-X plot.

The values on the axis labels indicate the proportion of the variance captured by each principal component.

OPLS-DA was used as a classification model providing supervised regression. This model (figure 3.19) showed no obvious outliers using Hotelling T^2 range, with further clustering of normal weight and obese patients and lower inter group variability with an increase of variation within the group. However, model diagnostics of the OPLS-DA model (figure 3.20) showed a low predictive ability and low fit. Statistical analysis of this OPLS-DA model using CV-ANOVA (Table 3.10) shows a p value of 0.6 and therefore cannot be concluded that the observed effect isn't due to random variations within the data.

A possible explanation for this low fit and predictive ability of the model might be the inclusion of metabolites which do not contribute to the response. One method of altering this is by introducing a cut-off score to remove metabolites which contribute the least to the model. These metabolites are ranked based on their variable influence of projection (VIP), which displays the overall importance of each variable (x or metabolites) on all responses (Y) cumulatively over all components. Therefore, metabolites with a VIP score <1 were excluded from the analysis (figure 3.21).

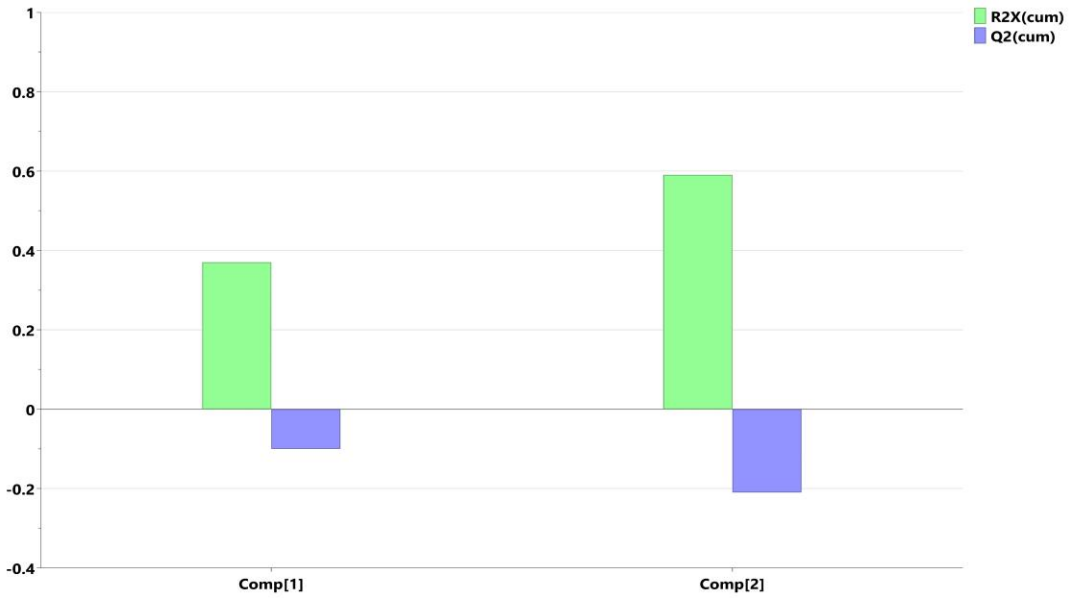

Figure 3.18: Summary of fit of 1D 1H NMR spectra of normal weight and obese OA synovial fluid subjected to PCA-X plot.

The R^2 and Q^2 values for both components are 0.37 and -0.1 and 0.59 and -0.21 respectively suggesting a bad fit and poor predictive ability for this model.

Table 3.10: Cross Validation Analysis of Variance (CV-ANOVA) performed on OPLS-DA model of normal weight and obese OA synovial fluid (Terminology can be found in Table 3.2)

M4	SS	DF	MS	F	p	SD
Total corr.	14	14	1			1
Regression	3.04482	4	0.761206	0.694837	0.612449	0.872471
Residual	10.9552	10	1.09552			1.04667

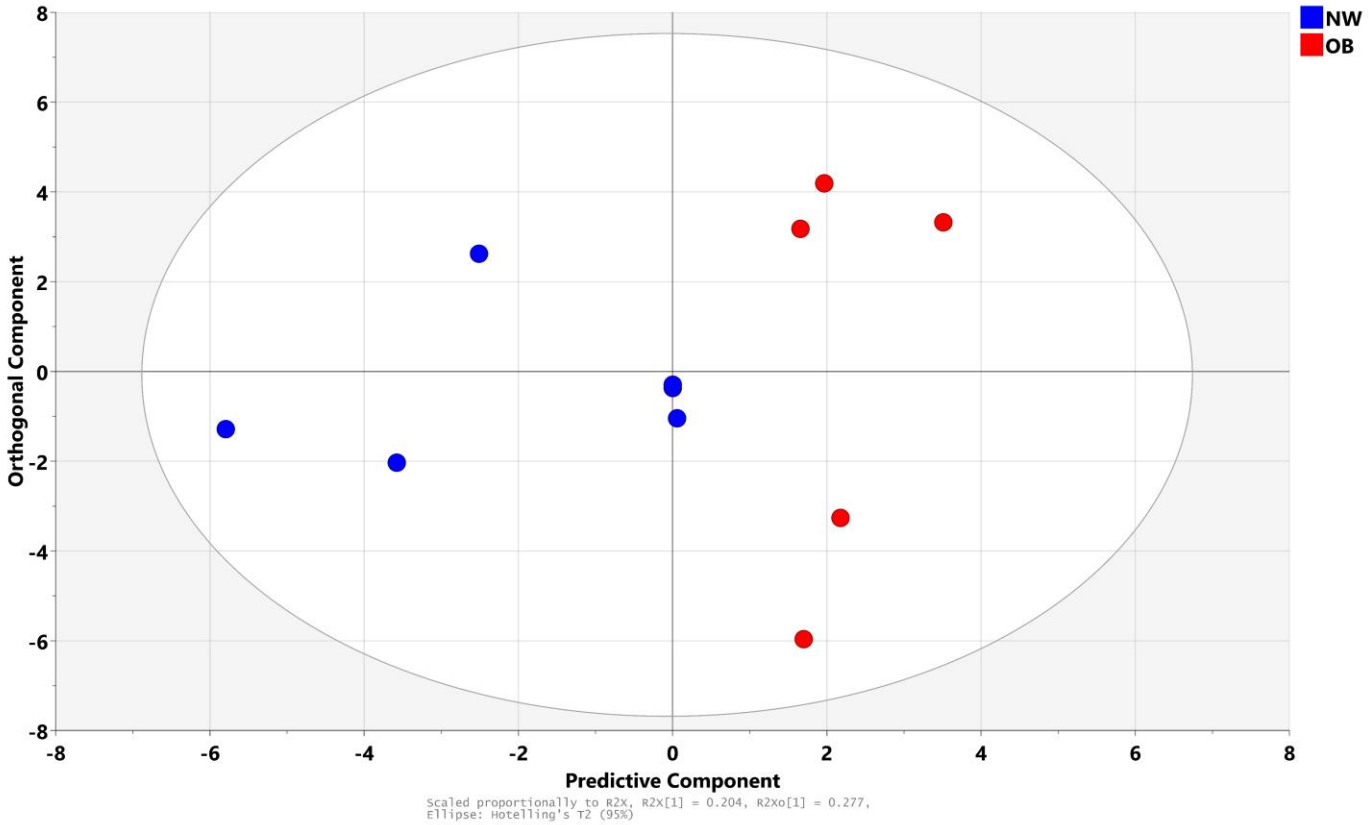

Figure 3.19: Scores plot of 1D 1H NMR spectra of normal weight (NW) and obese (OB) OA synovial fluid subjected to OPLS-DA plot.

The values on the axis labels indicate the predictive component (between group variation) and orthogonal component (within group variation). The separation of classes is maximized along the predictive component, while there is some intra-class variability within orthogonal component.

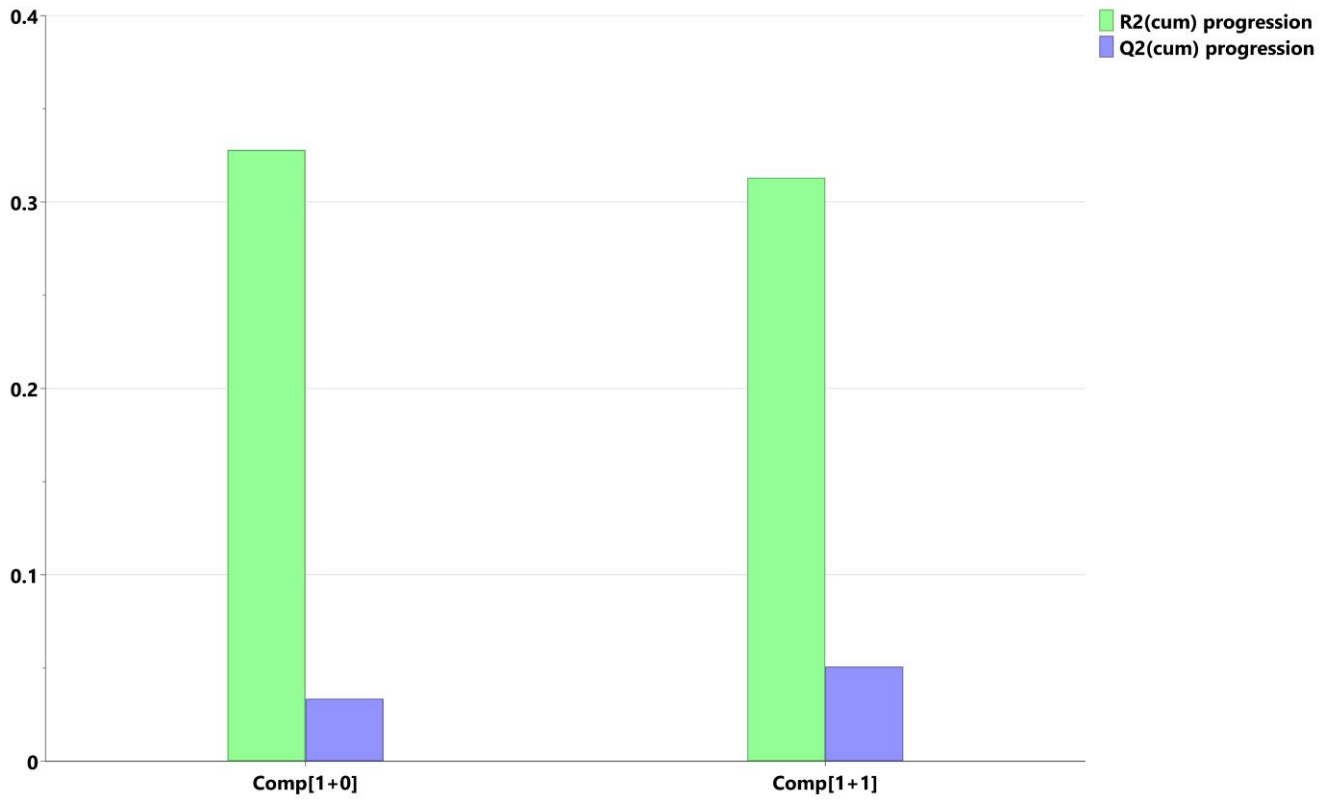

Figure 3.20: Summary of fit of 1D 1H NMR spectra of normal weight and obese OA synovial fluid subjected to subjected to OPLS-DA plot.

The R^2 and Q^2 values for both components are 0.34 and 0.03 and 0.31 and 0.05 respectively suggesting a poor fit and poor prediction for this model.

Figure 3.21: VIP scores for metabolites derived from 1H NMR spectra of normal weight and obese OA synovial fluid subjected to OPLS-DA plot.

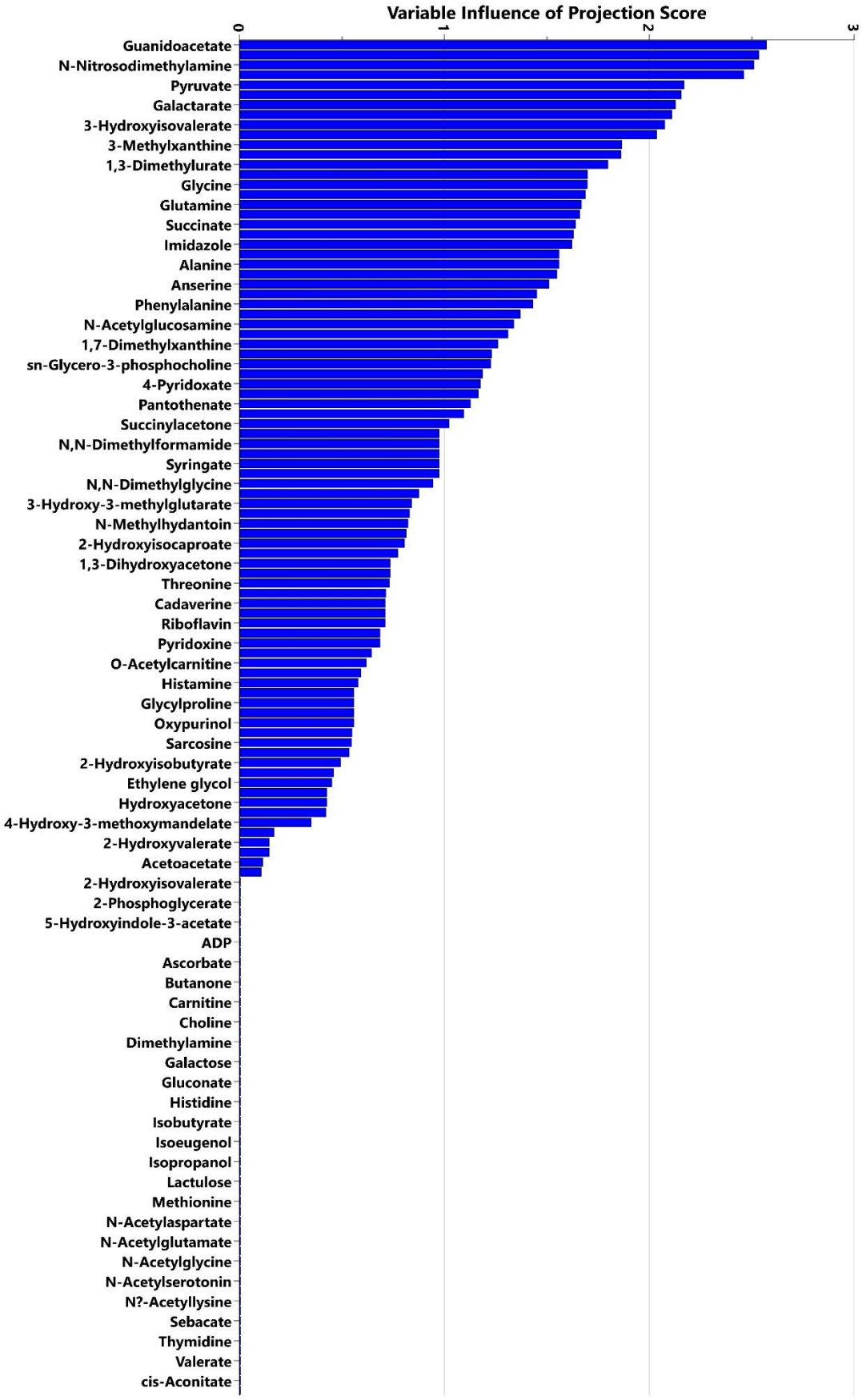

Following this exclusion criteria using VIP cut-off of ≥1, a new OPLS-DA model was generated (figure 3.22). This OPLS-DA model shows a reduced intra-class variation within the normal weight OA synovial fluid but a similar between group variation. Model diagnostics of this OPLS-DA model show an increased fit and predictive ability of the data (figure 3.22) and statistical analysis using CV-ANOVA (table 3.11) show a p value of 0.06. Further analysis was not performed on the data so as not to overfit the model. Those metabolites which had a VIP score of ≥1 (figure 3.24) where included in metabolite set enrichment analysis (MSEA) using MetaboAnalyst 5 (Montreal, Canada).

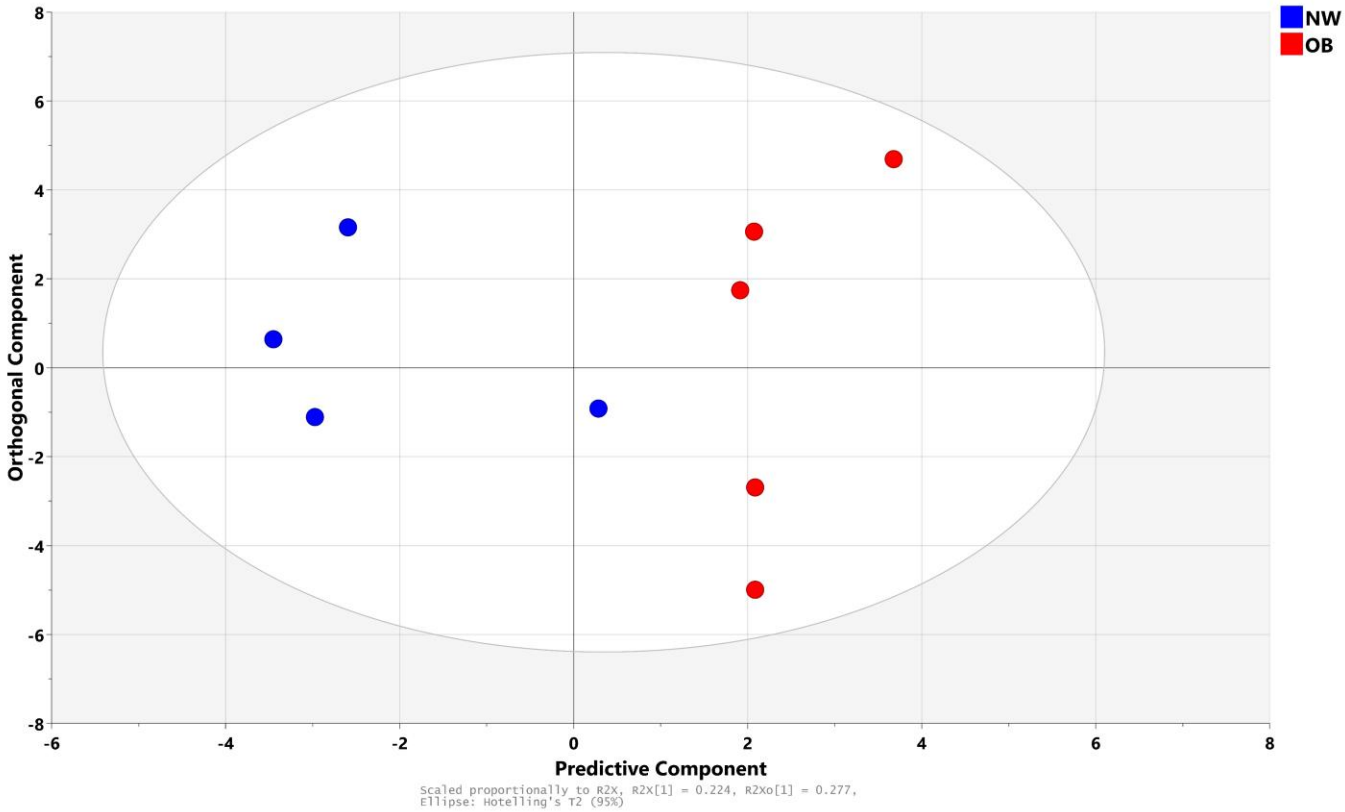

Figure 3.22: Scores plot of 1H NMR spectra of normal weight and obese OA synovial fluid subjected to OPLS-DA plot with a VIP cut-off of ≥ 1.

The values on the axis labels indicate the predictive component (between group variation) and orthogonal component (within group variation). The separation of classes is maximized along the predictive component, while there is some intra-class variability within orthogonal component.

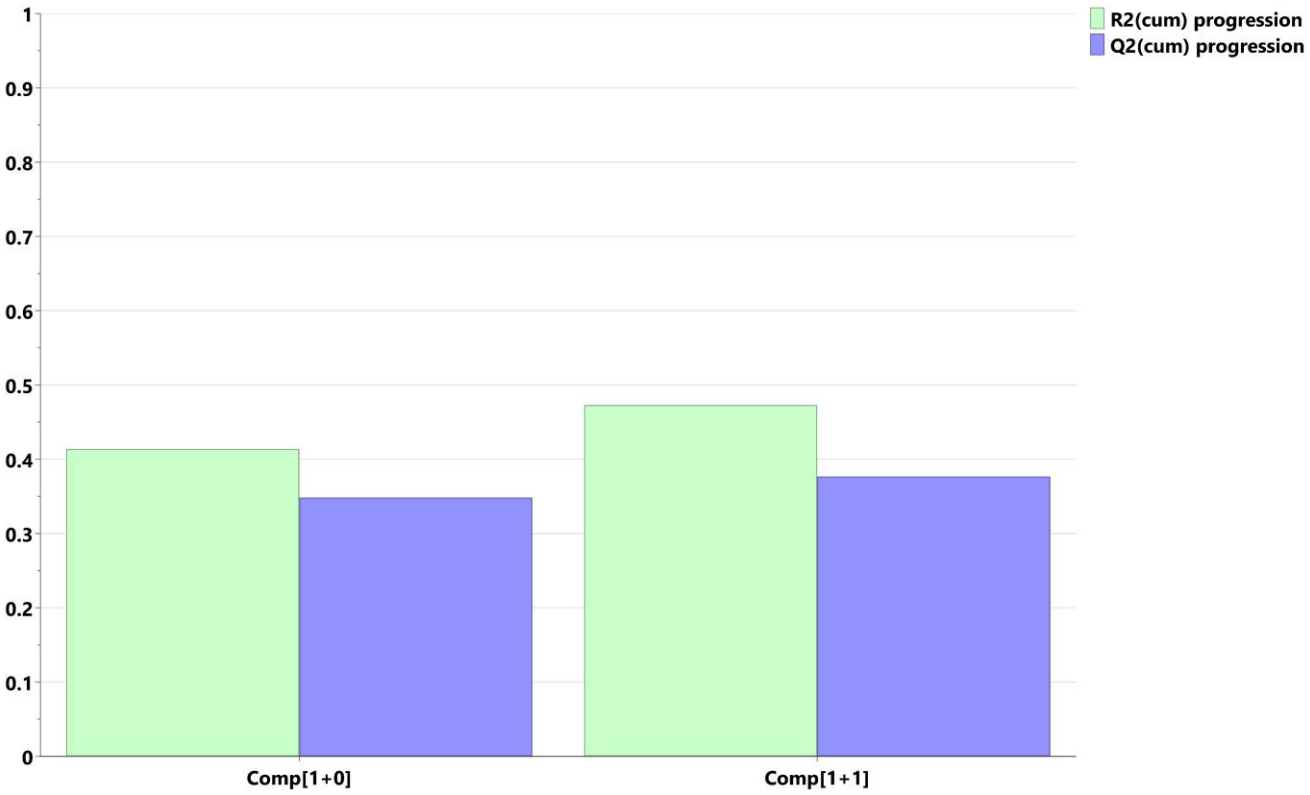

Figure 3.23: Summary of fit of 1H NMR spectra of normal weight and obese OA synovial fluid subjected to OPLS-DA plot with a VIP cut-off of ≥ 1.

The R^2 and Q^2 values for both components are 0.41 and 0.35 and 0.47 and 0.38 respectively suggesting a good fit and good prediction for this model.

Table 3.11: Cross Validation Analysis of Variance (CV-ANOVA) performed on OPLS-DA model of normal weight and obese OA synovial fluid with a VIP cut-off of ≥ 1 (Terminology can be found in Table 3.2)

M5	SS	DF	MS	F	p	SD
Total corr.	14	14	1			1
Regression	9.91833	6	1.65305	3.23996	0.0639622	1.28571
Residual	4.08167	8	0.510209			0.714289

Figure 3.24: VIP scores for metabolites derived from 1H NMR spectra of normal weight and obese OA synovial fluid subjected to OPLS-DA plot with a VIP cut-off of ≥ 1.

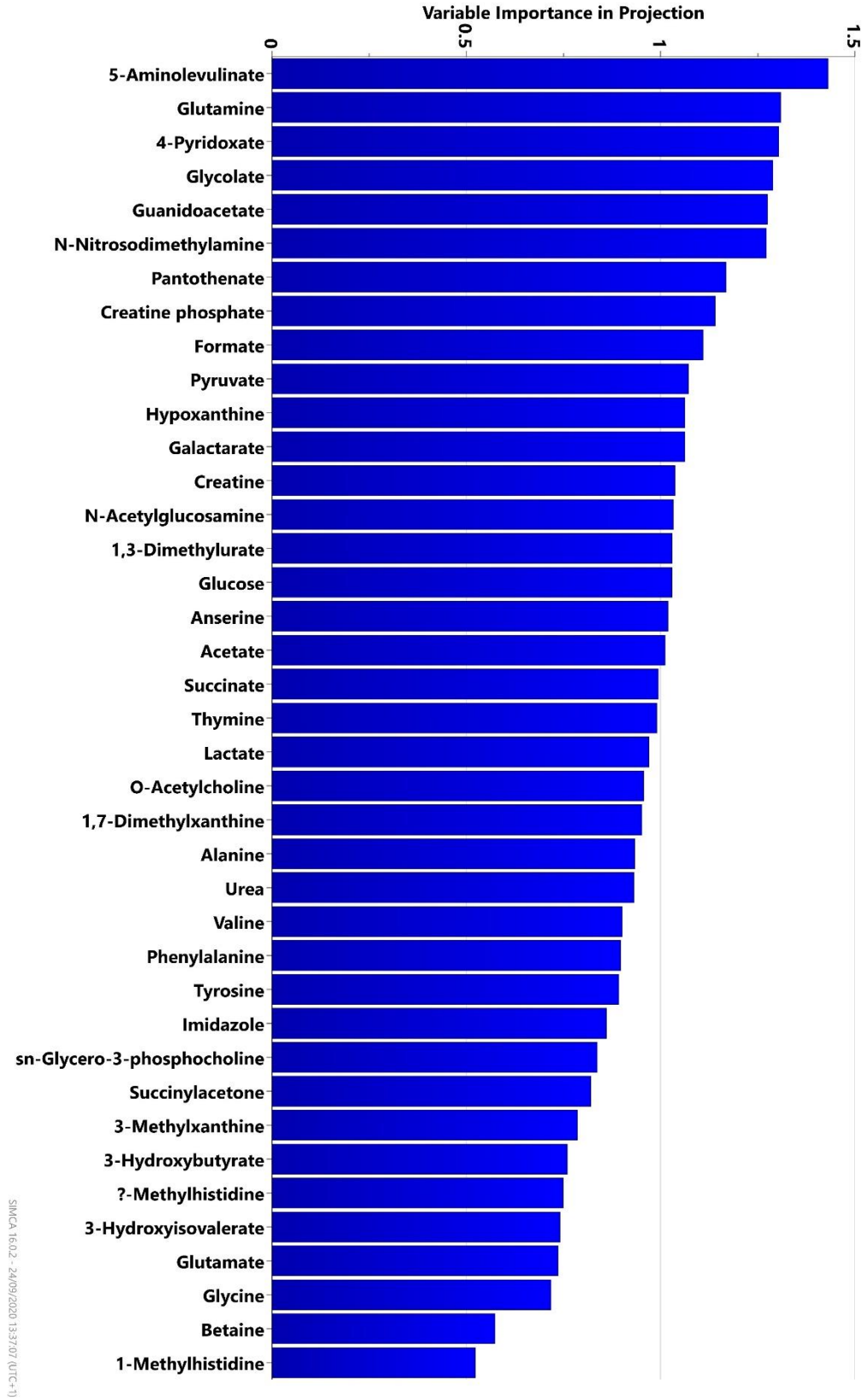

3.4.4 Metabolic Pathway Analysis of OA synovial fluid and synovial fibroblast conditioned media from obese patients compared to normal weight patients

3.4.4.1 OA Synovial Fluid

3.4.4.2

Following multivariate analysis of OA synovial fluid and OA synovial fibroblast conditioned media from obese and normal weight patients, metabolic pathway analysis was conducted using the KEGG database on MetaboAnalyst 5.0. A number of metabolic pathways were altered in obese OA synovial fluid compared to normal weight OA synovial fluid, including Alanine, Aspartate and Glutamate metabolism, Caffeine metabolism, Valine, Leucine and Isoleucine metabolism and Histidine metabolism (figure 3.25).

Metabolite set enrichment analysis was also conducted using the KEGG database on MetaboAnalyst 5.0. The top 5 significantly enriched metabolites (table 3.12) were metabolites involved in Glutamine and Glutamate metabolism ($p = 5.34x\ 10\text{-}6$), Glyoxylate and Dicarboxylate Metabolism ($p = 1.06x\ 10\text{-}4$), Glycine, Serine and Threonine metabolism ($p = 1.27x\ 10\text{-}4$), Aminoacyl-tRNA biosynthesis ($p = 1.42\ x\ 10\text{-}4$), and Alanine, Aspartate and Glutamate Metabolism ($p = 5.42x\ 10\text{-}4$). Likewise, MSEA also identified significantly enriched pyruvate metabolism and glycolysis.

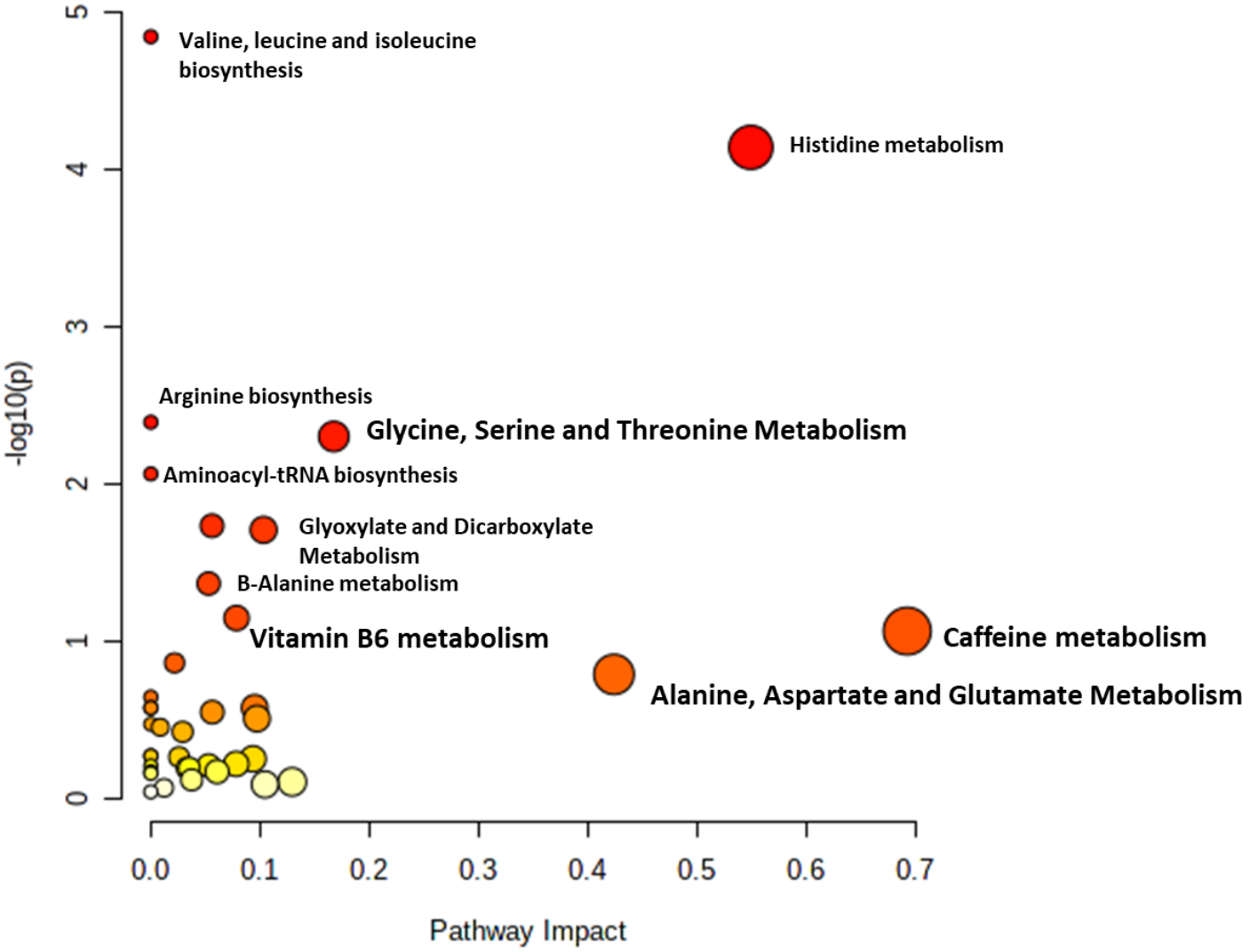

Figure 3.25: Pathway analysis of the most altered metabolic pathways in obese OA synovial fluid (n = 5) compared to normal weight OA synovial fluid (n = 6) patients.

Metabolic pathways are arranged by p values on Y-axis and pathway impact values (from pathway topology analysis) on X-axis. The node colour is based on p values and the node radius is based on pathway impact values

Table 3.12: Metabolomics pathway analysis of normal weight and obese OA synovial fluid using KEGG metabolomics library on MetaboAnalyst 5.0.

	Metabolite Set	Total	Hits	Expect	P value	Holm P	FDR
	D-Glutamine and D-glutamate metabolism	6	4	0.154	5.34E-06	4.48E-04	4.48E-04
	Glyoxylate and dicarboxylate metabolism	32	6	0.82	1.06E-04	0.00879	0.00298
	Glycine, serine and threonine metabolism	33	6	0.846	1.27E-04	0.0104	0.00298
	Aminoacyl-tRNA biosynthesis	48	7	1.23	1.42E-04	0.0115	0.00298
	Alanine, aspartate and glutamate metabolism	28	5	0.717	5.42E-04	0.0434	0.00911
	Arginine and proline metabolism	38	5	0.974	0.00229	0.181	0.0321
	Phenylalanine, tyrosine and tryptophan biosynthesis	4	2	0.102	0.00372	0.29	0.0446
	Arginine biosynthesis	14	3	0.359	0.00466	0.359	0.0489
	Nitrogen metabolism	6	2	0.154	0.009	0.684	0.084
	Pyruvate metabolism	22	3	0.564	0.0171	1	0.144
	Phenylalanine metabolism	10	2	0.256	0.0253	1	0.188
	Glycolysis / Gluconeogenesis	26	3	0.666	0.0269	1	0.188

3.4.4.2 OA Synovial Fibroblast Secretomes

Following multivariate analysis OA synovial fibroblast conditioned media from obese and normal weight patients stimulated with and without TNFα (10ng/ml for 24 hrs), metabolic pathway analysis was conducted using the KEGG database on MetaboAnalyst 5.0. Several metabolic pathways were altered in the secretomes of normal weight stimulated compared to unstimulated OA synovial fibroblasts including Alanine, Aspartate and Glutamate metabolism, Phenylalanine, Tyrosine and Tryptophan biosynthesis, Glycine, Serine and Threonine metabolism and Glycolysis (figure 3.26).

Metabolite set enrichment analysis shows Aminoacyl-tRNA biosynthesis ($p = 2.62 \times 10^{-6}$), Glycine, Serine and Threonine metabolism ($p = 8.82 \times 10^{-5}$), Glyoxylate and Dicarboxylate metabolism ($p = 6.04 \times 10^{-4}$), Arginine Biosynthesis ($p = 1.01 \times 10^{-3}$), Valine, Leucine and Isoleucine Biosynthesis ($p = 1.97 \times 10^{-3}$) as the top 5 most significantly enriched metabolites (table 3.13). Likewise, Metabolite set enrichment analysis also identified significantly enriched pyruvate metabolism ($p = 0.0385$), and Glycolysis ($p = 0.0111$) and Glutamine and Glutamate metabolism ($p = 0.0163$) (table 3.13).

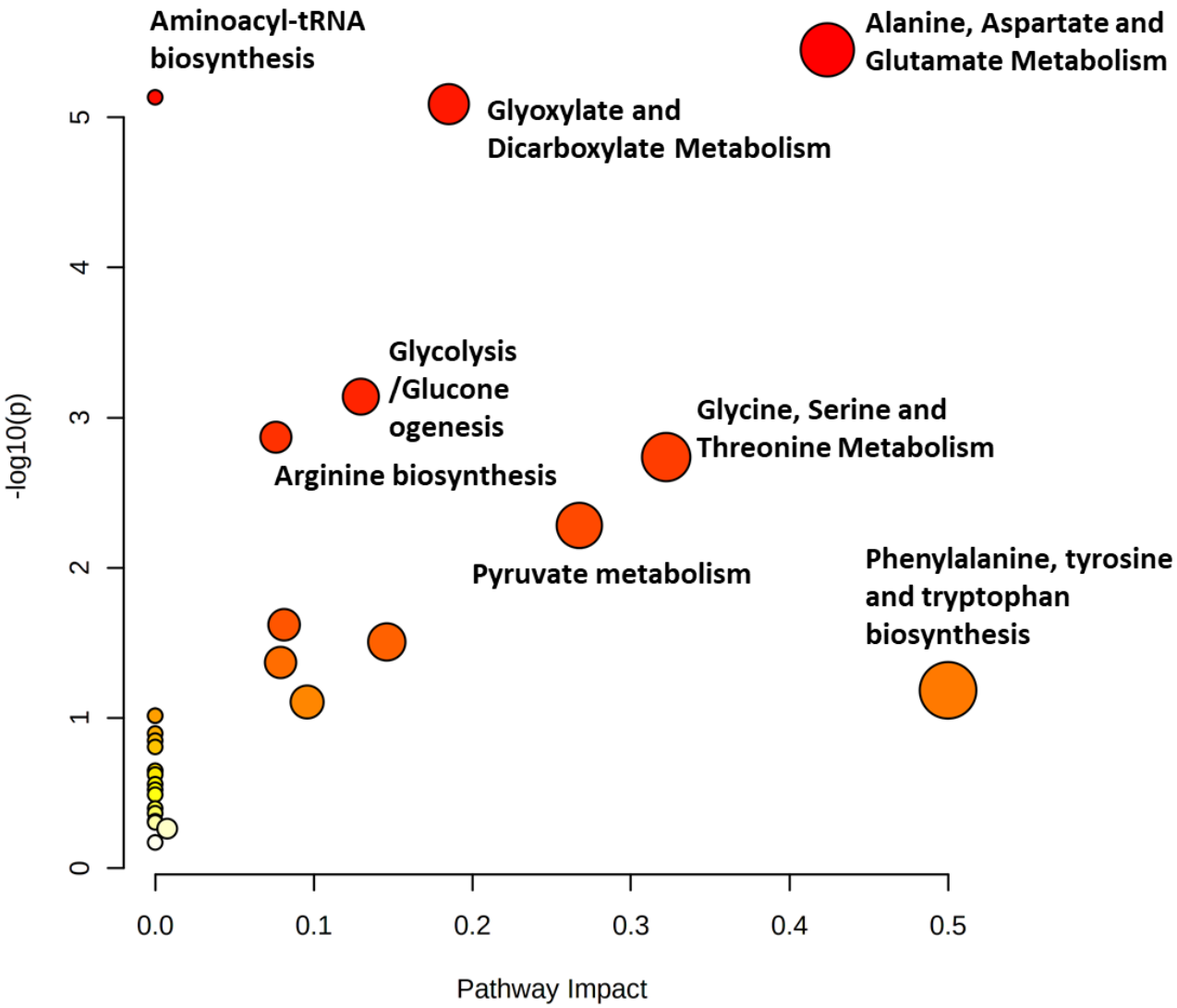

Figure 3.26: Pathway analysis of OA synovial fibroblast conditioned media with the most altered metabolic pathways in normal weight TNFα stimulated synovial fibroblasts secretomes compared to unstimulated synovial fibroblasts (n = 5).

Metabolic pathways are arranged by p values on Y-axis and pathway impact values (from pathway topology analysis) on X-axis. The node colour is based on p values and the node radius is based on pathway impact values

Table 3.13: Metabolomics pathway analysis of normal weight basal synovial fibroblast conditioned media compared to normal weight TNFα (10ng/ml for 24hrs) synovial fibroblast conditioned media.

	Metabolite Set	Total	Hits	Expect	P value	Holm P	FDR
	Aminoacyl-tRNA biosynthesis	48	10	1.67	2.62E-06	2.20E-04	2.20E-04
	Glycine, serine and threonine metabolism	33	7	1.15	8.82E-05	0.00732	0.00371
	Glyoxylate and dicarboxylate metabolism	32	6	1.11	6.04E-04	0.0496	0.0169
	Arginine biosynthesis	14	4	0.488	0.00101	0.0821	0.0213
	Valine, leucine and isoleucine biosynthesis	8	3	0.279	0.00197	0.158	0.0316
	Alanine, aspartate and glutamate metabolism	28	5	0.975	0.00226	0.179	0.0316
	Phenylalanine, tyrosine and tryptophan biosynthesis	4	2	0.139	0.00683	0.533	0.0819
	Arginine and proline metabolism	38	5	1.32	0.00886	0.682	0.093
	Glycolysis / Gluconeogenesis	26	4	0.905	0.0111	0.843	0.104
	D-Glutamine and D-glutamate metabolism	6	2	0.209	0.0163	1	0.137
	Citrate cycle (TCA cycle)	20	3	0.696	0.0299	1	0.228
	Vitamin B6 metabolism	9	2	0.313	0.0366	1	0.249
	Pyruvate metabolism	22	3	0.766	0.0385	1	0.249
	Caffeine metabolism	10	2	0.348	0.0448	1	0.251
	Phenylalanine metabolism	10	2	0.348	0.0448	1	0.251

Metabolic pathway analysis of OA synovial fibroblast conditioned media from obese patients stimulated with and without TNFα (10ng/ml for 24 hrs) was also conducted using the KEGG database on MetaboAnalyst 5.0. Amongst the altered metabolic pathway in obese TNFα secretomes compared to unstimulated secretomes are Alanine, Aspartate and Glutamate metabolism, Phenylalanine, Tyrosine and Tryptophan biosynthesis, Glycine, Serine and Threonine metabolism and Arginine Biosynthesis (figure 3.27).

Metabolite set enrichment analysis (table 3.14) shows Aminoacyl-tRNA biosynthesis ($p = 8.92 \times 10\text{-}8$), Glycine, Serine and Threonine metabolism ($p = 4.55x\ 10\text{-}5$), Histidine metabolism ($p = 0.0012$), Glyoxylate and dicarboxylate metabolism ($p = 0.00268$) and Phenylalanine, Tyrosine and Tryptophan biosynthesis ($p = 0.00561$). Likewise, metabolite set enrichment analysis also identified significantly enriched pyruvate metabolism ($p = 0.0298$), and Glycolysis ($p = 0.00782$) and Glutamine and Glutamate metabolism ($p = 0.0135$).

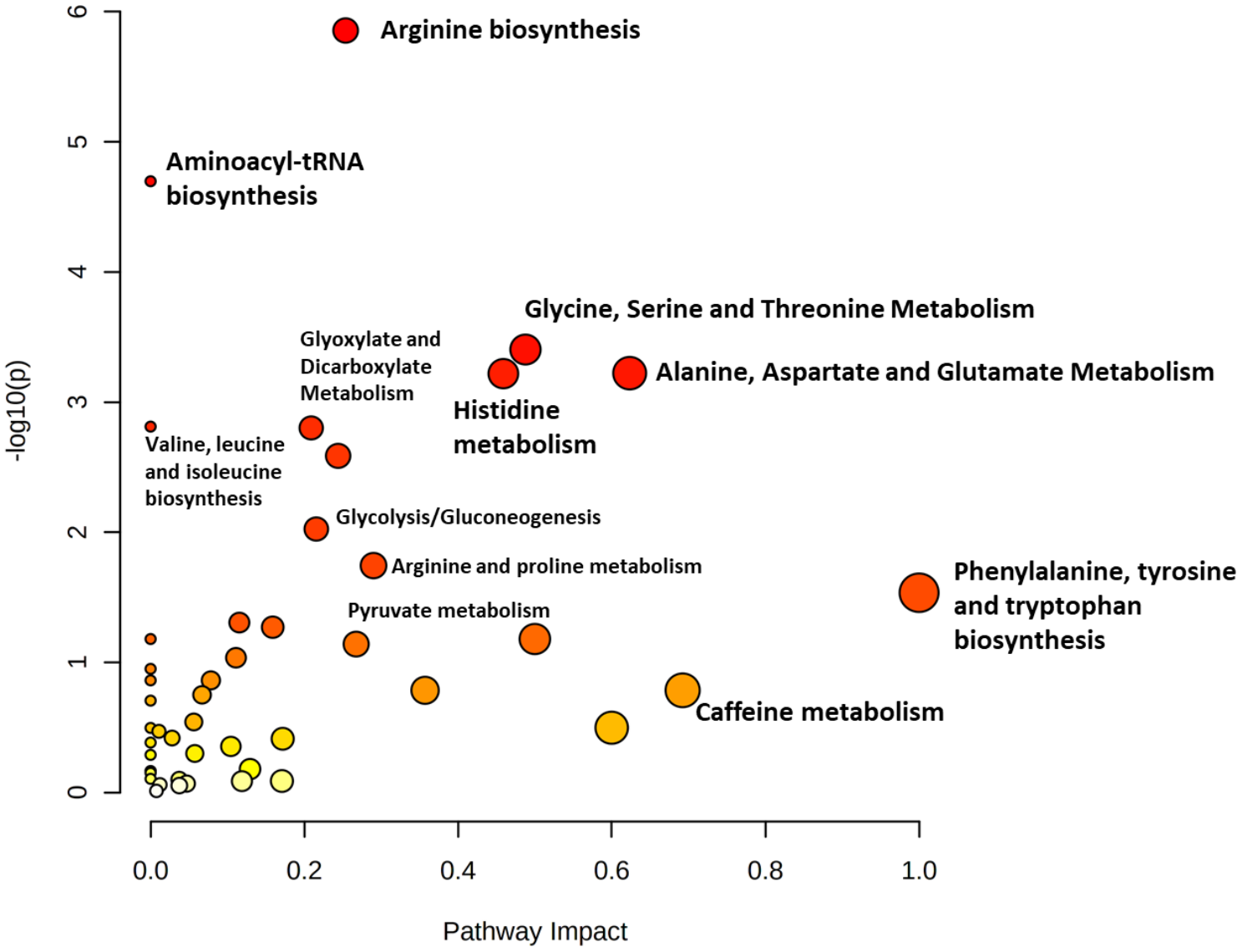

Figure 3.26: Pathway analysis of OA synovial fibroblast conditioned media with the most altered metabolic pathways in obese TNFα stimulated synovial fibroblasts secretomes compared to unstimulated synovial fibroblasts (n = 6).

Metabolic pathways are arranged by p values on Y-axis and pathway impact values (from pathway topology analysis) on X-axis. The node colour is based on p values and the node radius is based on pathway impact values

Table 3.14: Metabolomics pathway analysis of obese basal synovial fibroblast conditioned media compared to obese TNFα (10ng/ml for 24hrs) synovial fibroblast conditioned media.

	Metabolite Set	Total	Hits	Expect	P value	Holm P	FDR
	Aminoacyl-tRNA biosynthesis	48	11	1.51	8.92E-08	7.50E-06	7.50E-06
	Glycine, serine and threonine metabolism	33	7	1.04	4.55E-05	0.00378	0.00191
	Histidine metabolism	16	4	0.505	0.0012	0.0985	0.0336
	Glyoxylate and dicarboxylate metabolism	32	5	1.01	0.00268	0.217	0.0562
	Phenylalanine, tyrosine and tryptophan biosynthesis	4	2	0.126	0.00561	0.449	0.0943
	Glycolysis / Gluconeogenesis	26	4	0.82	0.00782	0.618	0.101
	Arginine biosynthesis	14	3	0.442	0.0084	0.655	0.101
	Alanine, aspartate and glutamate metabolism	28	4	0.883	0.0102	0.787	0.107
	D-Glutamine and D-glutamate metabolism	6	2	0.189	0.0135	1	0.126
	Valine, leucine and isoleucine biosynthesis	8	2	0.252	0.0242	1	0.203
	Arginine and proline metabolism	38	4	1.2	0.0292	1	0.208
	Pyruvate metabolism	22	3	0.694	0.0298	1	0.208
	Phenylalanine metabolism	10	2	0.315	0.0373	1	0.241
	Galactose metabolism	27	3	0.852	0.0506	1	0.304

3.5 Discussion

3.5.1 The impact of obesity on the metabolome of synovial joint fluid and synovial joint tissue in hip osteoarthritis patients

3.5.1.1 Metabolomics of biological fluids in OA patients and animal models

Since OA is generally a localised inflammatory joint disorder, the synovial fluid, which surrounds the joints, represents an appropriate biological fluid to identify any changes in joint pathology and inflammatory state. In contrast, other joint disorders such as rheumatoid arthritis, involve systemic inflammatory changes and can therefore be identified using circulating blood (plasma/serum). However, with the inflammation in osteoarthritis largely being localised to the specific diseased joint, determinants of circulating markers are deemed less relevant to the diseased joint pathology. A few previous studies have examined changes in the metabolome of synovial fluid in either OA patients or in OA preclinical animal models, and these are discussed below in the context of the present dataset

3.5.1.2 Preclinical animal model data

Synovial fluid was collected in an ovine model of OA joint damage induced, following anterior cruciate ligament (ACL) surgery, and analysed using NMR spectroscopy (Mickiewicz, Heard, *et al.*, 2015). 24 metabolites were increased with ACL OA and Sham surgery including alanine, lysine, **tyrosine**, threonine, arginine, phenylalanine,

serine, leucine, isoleucine, valine, hypoxanthine, methionine, hydroxyproline, proline, aspartate, asparagine, glutamate, 2- hydroxybutyrate, choline, **lactate**, **succinate**, formate, tryptophan and acetate) (Mickiewicz, Heard, *et al.*, 2015) (table 3.6). Six metabolites were decreased compared to non-operated sheep including 2-oxovalerate, 2-oxoglutarate, ethanol, **glucose, pyruvate** and 3- hydroxybutyrate (Mickiewicz *et al.*, 2015) (table 3.6). Metabolic pathway analysis was conducted and those samples which were impaired in early degenerative joint diseases were Glycine, serine, and threonine metabolism, Aminoacyl-tRNA biosynthesis, Arginine and proline metabolism, Alanine, aspartate and glutamate metabolism. NMR spectroscopy conducted in this study comparing obese OA synovial fluid to normal weight to obese OA synovial fluid, also had significant enrichment on all these pathways (Mickiewiczet al., 2015) (table 3.12).

Following on from the preclinical ovine study, the same group then collected synovial fluid samples from symptomatic chronic knee OA patients and normal human cadaveric knee joints and conducted 1H NMR spectroscopy and GC-MS on the samples (Mickiewicz *et al.*, 2015). Following multivariate analysis of OA vs non-OA controls, 11 metabolites were found to be the most significantly discriminant metabolites. Those highlighted were also found to be increased or decreased respectively within the modelling of OA synovial fluid samples of this study. There was an increase in fructose and citrate and a decrease in O-acetylcarnitine, N-phenylacetylglycine, methionine, ethanol, creatine, malate, ethanolamine, 3-hydroxybutyrate and hexanoylcarnitine (Mickiewicz *et al.*, 2015) (table 3.6).

In other metabolomics study by the same group looking into the protective role of integrin α1β1 role and the inhibitory role of epidermal growth factor receptor (EGFR) in OA, serum was collected from wild type and integrin α1-null mice that underwent

surgical destabilization of the medial meniscus (DMM), a post traumatic osteoarthritis (PTOA) model (Mickiewicz *et al.*, 2016). NMR spectroscopy conducted showed, an increase in the concentration of dimethyl sulfone (DMSO) and **glutamine** regardless of sex and a reduction in concentration of serotonin, 3-hydroxyisovalerate, phenylalanine in both α1-null female and male groups when compared to wild type mice (Mickiewicz *et al.*, 2016) (table 3.6). Likewise amongst the pathways that where most disturbed in α1-null compared to wild type mice include **alanine, aspartate and glutamate metabolism**, **arginine and proline metabolism**, tryptophan metabolism, valine, leucine and isoleucine degradation, **phenylalanine metabolism**, **phenylalanine, tyrosine and tryptophan biosynthesis, glycine, serine, alanine and threonine metabolism** (Mickiewicz *et al.*, 2016) (table 3.12).

Interestingly, HR-NMR spectroscopy of synovial fluid collected from canine model of OA using ACL surgery compared to normal joint SF showed an increase in Alanine, isoleucine, **lactate,** lipoprotein associated fatty acid, ketone bodies (3-D-hydroxyisobutyrate and **3-D-hydroxybutyrate**), **pyruvate**, acetate, glycerol and N acetyl-glycoproteins and a decrease in glucose concentration (Damyanovich *et al.*, 1999) (table 3.6).

3.5.1.3 Clinical patient data

A previous study comparing the serum metabolome of knee OA patients to non-OA controls using electrospray ionisation tandem MS found 14 metabolite ratios were significantly associated with knee OA, including the ratios of Valine: Histidine and Leucine: Histidine (Zhai *et al.*, 2010). These ratios remained after adjustment for age and BMI and are a potential clinical OA biomarker. These metabolites are associated with BCAA and cannot be synthesised within the body. This increase in BCAA levels could suggest an increased rate of protein breakdown or an indirect effect associated with collagen breakdown. BCAA are known to increase the production of cytokines such as IFN, TNF, IL1 and IL2 (Bassit *et al.*, 2000) and therefore this could suggest a link between metabolite levels, collagen degradation and inflammation associated with knee OA.

Other metabolomics studies, such as high-resolution magnetic angle spinning (HRMAS) of human knee cartilage from end stage OA compared to gender matched cadaveric cartilage show a decrease in alanine concentration (a marker of degradation of collagen framework) and N-Acetyl levels (a marker of total proteoglycan content) (Shet *et al.*, 2012; Tufts *et al.*, 2015). N-Acetyl levels (including N-Acetylglucosamine, N-Acetylaspartate, N-Acetylglutamate and N-Acetyltyrosine) were increased, although not significantly, in OA synovial fluid in obese patients compared to normal weight patients suggesting higher degradation of collagen and proteoglycan content in OA joints in obese patients compared to normal weight patients (table 3.6).

The use of MS and its hyphenated techniques have also been employed in inflammatory joint disease metabolomics. One study used HPLC-MS for global metabolomic profiling of healthy (n = 5), OA (n = 5) and RA (n=3) synovial fluid and found distinct clustering between OA/RA synovial fluid samples compared to controls in PCA model of metabolite intensities (Carlson *et al.*, 2018). Pathway analysis of OA vs healthy synovial fluid showed altered **arginine and proline metabolism**, chondroitin sulfate degradation, amino oxidase reactions, COX reactions, and creatine biosynthesis (Carlson *et al.*, 2018). UPLC/MS performed on plasma of human knee OA patients (n = 64) compared to non-OA controls (n = 45) showed a 65% decreased plasma concentration of arginine compared to the healthy controls (Zhang *et al.*, 2016).

In conclusion, research within OA and other inflammatory joint disorders in both preclinical animal models and clinical samples show distinct differences in the metabolome of healthy compared to inflammatory joint disease patients within serum and synovial fluid. Many of these altered metabolic pathways were also enriched within the OA synovial fluid of obese OA patients within this study. These differences may be indicative of an altered metabolic status observed in the resident and infiltrating cells within the tissues of the OA synovial joint in obese individuals.

3.5.1.4 Metabolomics of OA synovial fibroblast conditioned media

Another aspect of this study was to analyse the metabolome of OA synovial fibroblast from obese and normal weight patients following stimulation with and without (TNFα at 10ng/ml for 24hrs) as a model of inflammatory cells.

3.5.1.5 Formate Metabolism

Amongst the changes in metabolite concentrations observed in normal weight OA synovial fibroblast secretomes upon stimulation was an increase in Formate levels ($p= 0.0258$) (figure 3.3). Formate levels however remained constant within stimulated obese OA synovial fibroblast secretomes compared to unstimulated obese OA synovial fibroblast. Formate is an intermediate metabolite in one carbon metabolism and is a mediator between mammalian organisms, the diet, and the gut microbiome as formate is a by-product of anaerobic fermentation of some enteric bacterial species (Pietzke, Meiser and Vazquez, 2020).

Formate has been shown to contribute towards the one carbon metabolite demands of purine and thymidylate synthesis in proliferating cells which require purine for the synthesis of RNA, DNA and the free ATP pool (Ducker *et al.*, 2016). Formate is known to have different fates depending on the metabolic needs of the cell and so the exact role formate plays in the OA synovial fibroblast metabolism is unknown however this would be an interesting metabolite to investigate further, possibly through carbon labelling mass spectroscopy, to follow its fate throughout one carbon metabolism.

3.5.1.6 Galactose Metabolism

The most significantly altered metabolite within unstimulated normal weight OA synovial fibroblast compared to stimulated OA synovial fibroblast secretomes was Galactarate. Galactarate is a metabolite within the galactose metabolic pathway. Galactose can be metabolised to form glucose-1-phosphate which can then be converted into glucose-6-phosphate, and therefore could be a metabolite which is

utilised by cells to generate glucose for glycolysis (Elsas Ii and Lai, 1998). Several studies have been conducted on the disorders of galactose metabolism and alterations in Leloir metabolism and although interesting, metabolite set enrichment analyses of OA synovial fibroblast secretomes shows galactose metabolism has consistently low false discovery rate suggesting this is not the most significantly enriched metabolic pathway within the secretomes of OA synovial fibroblasts and therefore does not warrant further investigation.

3.5.1.7 Caffeine Metabolism

From the key metabolites altered in normal weight OA synovial fibroblast secretomes upon stimulation was 1,7 dimethylxanthine or paraxanthine which is a caffeine derivative that is generated through liver biotransformation of caffeine and amounts to 80% of caffeine derivatives produced by caffeine in humans (Lelo *et al.*, 1986). Paraxanthine has similar sympathomimetic and ergogenic effects to caffeine and has been shown to suppress neutrophil and monocyte chemotaxis (Horrigan, Kelly and Connor, 2006) and reduce the production of TNFα from human blood (Horrigan, Kelly and Connor, 2004). Caffeine was also identified amongst the key metabolites with high VIP scores (≥1). Caffeine has been shown to reduce human lymphocyte function through decreased T cell proliferation and reduced production of T helper (Th) cell cytokines from Th1 (IL2 and IFN-y), Th2 (IL4, IL5) and Th3 (IL-10) cells (Horrigan, Kelly and Connor, 2006). Likewise, metabolite set enrichment analysis of stimulated normal weight OA synovial fibroblasts secretomes show caffeine metabolism was significantly enriched ($p = 0.00448$) (table 3.13). This suggests the presence of caffeine derivatives may be a negative feedback mechanism, released

by the normal OA synovial fibroblast challenged with TNFα, as a means of reducing the inflammatory microenvironment through its anti-inflammatory properties.

3.5.1.8 N-Acetylglycine

Amongst the changes observed in normal weight OA synovial fibroblast secretomes upon stimulation was increased N-Acetylglycine levels ($p = 0.035$) (figure 3.3). N-Acetylglycine is a N-terminal capped form of the alpha amino acid glycine and an amino acid derivative. N-terminal protein acetylation is one of 2 distinct mechanism of protein acetylation. Acetylation of proteins is a form of post-translational modification of proteins were an acetyl group (CH_3CO) is added to a molecule. This acetylation maybe a mechanism of post-translational modification, providing acetyl groups for neighbouring cells or could simply be a transitional step within glycine metabolism. Glycine was also significantly increased in obesity within OA synovial fluid, possibly suggesting glycine metabolism is increased due to inflammatory challenge in the OA synovial joint.

Interestingly several studies have shown alterations within glucose metabolism can regulate histone acetylation and there are key molecular links between cellular metabolism and histone acetylation (Cai *et al.*, 2011; Lu and Thompson, 2012; Evertts *et al.*, 2013). Notably, OA synovial fibroblast that have been isolated from OA synovial membrane and cultured for a few passages, retain their metabolic and inflammatory phenotype *in vitro*. A possible explanation for this phenomenon could be epigenetic changes. Although not decisive proof, this preliminary data could suggest any epigenetic changes within OA synovial fibroblast from obese patients

could be maintained via protein acetylation, however further research would be required to substantiate this hypothesis.

3.5.1.9 Imidazole

Another metabolite which was significantly increased in obese OA synovial fibroblast secretomes upon inflammatory challenge was Imidazole. Imidazole is an aromatic heterocycle species which contains a ring structure (heterocycle) that is incorporated into several metabolites such as histidine and the hormone histamine. Metabolite set enrichment analysis of obese OA synovial fibroblast secretomes upon inflammatory stimulation, shows increased enrichment of Histidine metabolism ($p = 0.0012$) (table 3.14). This suggests imidazole may be a biological building block for the generation of the amino acid histidine. Histamine is a well-known mediator of inflammation and its enzyme, histidine decarboxylase is induced at inflammatory sites in late and chronic phases of non-allergic and allergic inflammation (Hirasawa, 2019).

3.5.1.10 Phenylalanine

Amongst the metabolites which were significantly different in metabolome of obese OA synovial fibroblast upon inflammatory challenge was phenylalanine, which was significantly decreased ($p = 0.009$, table 3.8). Phenylalanine metabolism is altered in both inflammatory conditions like inflammatory bowel diseases and in ageing (Julià *et al.*, 2016). Phenylalanine metabolism is dysregulated in the serum of elderly persons suggesting systemic changes in phenylalanine metabolism is a an indicator of ageing (Capuron *et al.*, 2011). Serum inflammatory markers IL6 and CRP were found to be associated with increased phenylalanine levels (Capuron *et al.*, 2011).

Phenylalanine metabolism is also altered in obesity. Obese patients who have hyperglycemia, hypertension and dyslipidemia have altered serum phenylalanine metabolism compared to obese patients without these conditions, suggesting in intimate link between “metabolically abnormal” obesity and phenylalanine metabolism (Chen *et al.*, 2015). Pathway analysis of the metabolome of these “metabolically abnormal” obese patients also showed significant enrichment of phenylalanine metabolism which was also observed in the metabolome of obese OA synovial fibroblast secretomes upon inflammatory challenge ($p = 0.037$, table 3.14) (Chen *et al.*, 2015).

Another aspect of this study was to see whether the OA synovial fluid metabolome and metabolites was similar to the metabolites identified in OA synovial fibroblast secretomes in normal weight and obese patients. Univariate analysis of OA synovial fibroblast secretomes show that those metabolites significantly altered in OA synovial fluid are not significantly altered in OA synovial fibroblast secretomes from normal weight or obese patients (figure 3.2). There are a few possible explanations for this divergence in metabolomes from these samples. OA synovial fluid is a biological fluid which encompasses the entire synovial joint and therefore is in contact with several cell types and tissues including articular cartilage, which contributes to the metabolome of the synovial fluid. In contrast, the synovial fibroblast conditioned media metabolome comes from one source i.e., cultured synovial fibroblast cells. Furthermore, OA is a chronic inflammatory condition, with the synovial fluid representing metabolites that have accumulated over time and in some cases may have developed an equilibrium homeostatic state. In contrast, the synovial fibroblast conditioned media was collected over a 24-hour period and may therefore not be fully representative of the chronic state of OA. Additionally, OA

synovial fibroblast conditioned media was collected using RPMI-1640 cell culture media, which although underwent normalisation, will still result in a different metabolome to OA synovial fluid. Another difference is the number of cells within tissue which contribute to OA synovial fluid which is exponentially higher than the 40,000 cells which were used to generate the conditioned media from OA synovial fibroblast.

3.5.2 Metabolomics Studies in OA

Following collection of metabolite concentrations from OA synovial fluid, multivariate analysis was undertaken using PCA which allows for identification of any anomalous metabolites or samples. Following PCA analysis, further modelling was conducted using OPLS-DA, which was used to identify whether there was clustering of samples and which metabolites contributed the most to the variability between obese and normal weight OA synovial fluid. This was obtained by looking at VIP scores (figure 3.24).

The metabolite with the highest VIP score, 5-aminolevulinic acid (5ALA) is a precursor to heme in humans (Gardner and Cox, 1988). It is synthesised using glycine and succinyl-CoA using the Shemin pathway at the mitochondria (Gardner and Cox, 1988). 5ALA has been shown to increase ATP levels in murine model through increased aerobic energy metabolism via COX signalling, which could suggest a possible role for 5ALA in energy metabolism within obese OA synovial fluid compared to normal weight synovial fluid (Ogura *et al.*, 2011). Notably, metabolites such as glycolate, N-Nitrosodimethylamine, formate, lactate, pyruvate, glucose and galactarate amongst others all appeared to have a high VIP score and

were also found to be significantly different upon univariate analysis between OA synovial fluid and within OA synovial fibroblast secretomes.

Another aspect of this study was to investigate the contribution OA synovial fibroblast to the metabolome at the synovial joint. A key question was whether there were clear differences between the metabolome of OA synovial fibroblast cultured from the synovium of normal weight patients compared to obese patients. To further model the inflammatory microenvironment observed in synovial inflammation during OA, these same synovial fibroblasts were treated with TNFα for 24hrs at 10ng/ml. Following collection of conditioned media from synovial fibroblasts, NMR spectra were obtained and underwent analysis.

Clear clustering of samples within the same group/class was observed upon modelling of OA synovial fibroblast secretomes comparing unstimulated with stimulated OA synovial fibroblast (data not shown), however upon statistical analysis of these OPLS-DA models using CV-ANOVA (data not shown), none of these models came up as statistically significant due to overfitting the model as a result of low sample number (n=5 patients per group) and therefore requires further samples to be inputted into the model to see whether the variation observed between samples of different groups is consistent with what was observed in the first data analysis.

On the other hand, this study did provide data for further power analyses to be conducted and to work out the potential number of samples required to run a second study which would provide more robust results (data not shown).

3.5.3 Pathway analysis

3.5.3.1 Aminoacyl-tRNA Biosynthesis

Amongst the most significantly altered metabolic pathways identified using metabolite set enrichment analysis, comparing normal weight and obese OA synovial fibroblast secretomes and OA synovial fluid was amino acyl-tRNA biosynthesis. Aminoacylation of transfer RNAs (tRNAs) is generated by enzymes called aminoacyl-tRNA synthetases (AARS), which implement the correct assignment of amino acids to their corresponding codons and therefore are an essential link in establishing the genetic code. Consequently, by linking tRNA molecules to their amino acids, they are critical for protein synthesis. Although much has been discovered regarding AARS, their involvement in novel functions and pathological processes has yet to be fully determined.

Because the enrichment of amino acyl-tRNA biosynthesis was present across all analysis in the OA synovial fibroblast conditioned media samples and was observed within the OA synovial fluid analysis, this could suggest that dysregulation of this metabolic pathway within the OA joint is potentially driven by the metabolic phenotype of the OA synovial fibroblast. However, confirmation of this would require further metabolomics analysis to be conducted on the other resident cells within the synovial joint.

One possible and simple suggestion for the enrichment of amino acyl-tRNA biosynthesis could be to support the proliferation and adhesion of OA synovial fibroblast *in vitro*. Aminoacyl-tRNA synthetase-associated factor, p43 has been shown to induce cell-cell adhesion through PI3 kinase-ERK and p38 MAP kinase

dependant upregulation of ICAM-1 (Park *et al.*, 2002), however this does not explain the enrichment of this metabolic pathway in OA synovial fluid.

Recent research has shown a relationship between enrichment of amino acyl-tRNA biosynthesis and OA. A recent study by (Xiao Z *et al.*, 2021) (preprint), collected serum from a rabbit knee OA model and conducted LC-MS/MS metabolomics analysis, identified aminoacyl-tRNA biosynthesis as being increased alongside the biosynthesis of amino acids when compared to normal controls (Xiao Z *et al.*, 2021).

One possible reason for the enrichment of aminoacyl-tRNA biosynthesis, is the production of tRNA derived fragments (tRFs). These tRFs regulate gene expression through several means including but not limited to ribosome biogenesis, apoptosis, transcription, translation and cell proliferation (Zacharjasz *et al.*, 2021). tRFs act in an Argonaute dependant manner and are therefore involved in the formation of RNA-induced silencing complex (RISC) to silence mRNA. tRNA is cleaved by the dicer enzyme in similar fashion that pre-miRNA's are cleaved. These tRFs are then incorporated into the RISC complex and regulate gene expression (Zacharjasz *et al.*, 2021). Aberrant expression of tRFs is implicated in a number of pathologies such as neurodegenerative diseases and multiple types of cancers (Zacharjasz *et al.*, 2021).

tRF's have also been implicated in age-associated OA (Sacitharan and Vincent, 2016). In an equine model of knee OA, there were 81 differentially expressed tRFs when comparing aged chondrocytes to young chondrocytes with 44 increased and 37 decreased in aged chondrocytes (Balaskas *et al.*, 2020). In addition to this, when comparing high grade OA degradation of cartilage to low grade, 8 tRFs were induced and 3 tRFs were reduced (Zacharjasz *et al.*, 2021). Additionally, in a model of inflammatory OA, human chondrocytes stimulated with IL-1β showed an increase in

the expression of 14 tRFs and a reduction in 4 tRFs (Green *et al.*, 2020). This study showed the most upregulated 3'-tRF, which originates from tRNA-Cys-GCA, post-transcriptionally regulates Janus kinase 3 (JAK3) expression via AGO/RISC formation (Green *et al.*, 2020). The JAK-STAT kinase signalling pathway is known to regulate the expression of several pro-inflammatory cytokines such as IL6, which plays a major role in the inflammatory environment observed in synovitis and in OA. JAK3 inhibition through this tRFs (tRF-3003a) resulted in decreased IL6 expression and this tRF has been shown to be decreased in OA cartilage compared to normal cartilage, providing further evidence of tRFs involvement in inflammation observed within OA (Green *et al.*, 2020).

In summary, tRNAs and their corresponding tRFs have been shown to play a role in OA and inflammation, however despite these recent revelations, the understanding regarding tRNA and tRFs function in osteoarthritis still requires further research.

Whether the synthesis of aminoacyl-tRNAs is a possible pathological process identified in OA synovial fibroblast or simply an inherent observation of cellular function being undertaken by these fibroblasts such as ribosome biogenesis and cellular proliferation is unknown, though its role in OA and inflammation suggest further investigation could be worthwhile.

3.5.3.2 Glutamine-Glutamate Metabolism

Amongst the key metabolite changes observed in amino acid metabolism within OA synovial fibroblast secretomes and in OA synovial fluid, was changes in the glutamine-glutamate metabolic pathway. Glutamine is intricately involved in many biosynthetic and metabolic processes such as the generation of nucleotides,

maintaining intracellular redox homeostasis, epigenetic regulation and is involved in generation of extracellular matrix proteins (Pallett et al, 2021)

Metabolomics studies of OA synovial fluid have shown altered glutamine-glutamate metabolism. Glutamate concentrations were found to be increased in the synovial fluid of arthritic patients with synovitis compared to healthy patients suggesting glutamine-glutamate metabolism may be involved in synovial inflammation at the arthritic joint (McNearney *et al.*, 2000). Global metabolomics analysis of OA synovial fluid showed glutamine was strongly associated with OA (Zheng *et al.*, 2017).

Glutamine is also involved in inflammation and has been shown to supress the expression of inflammatory cytokines through activation of MKP-1 and through inhibition of NF-κB and MAPK pathways (Kim *et al.*, 2015).

Another cell type which utilises glutamine within the synovial joint are chondrocytes which are resident cells within the articular cartilage. These cells use glutamine as a precursor of glucosamine and therefore increasing glutamine levels may contribute to synthesis of glucosamine. Glucosamine has already been shown to decrease cartilage destruction and increase the biosynthetic activity of chondrocytes (Varghese *et al.*, 2007; Jerosch, 2011).

Furthermore, glutamine is also involved in reductive oxidative species (ROS) homeostasis through glutathione. Exogenous glutamine supplementation has been shown to increase glutathione levels during stress loading thereby protecting cells from injury (Unneberg *et al.*, 1997) (Rodas *et al.*, 2012). Oxidative stress is known to play a role in OA pathology and analysis of knee OA synovial fluid shows altered activity of antioxidant enzymes (superoxide dismutase, both isoenzymes zinc-copper superoxide dismutase and manganese superoxide dismutase) and glutathione

transformation enzymes (glutathione peroxidase, glutathione reductase and glutathione-S-transferase) (Ostalowska *et al.*, 2006).

Glutamine levels also influence infiltrating and circulating cells. Extracellular glutamine is essential for activation of T cells and its absence impairs cytokine secretion and reduces proliferation (Carr *et al.*, 2010), suggesting another possible role for glutamine in supporting immune cell function in an inflammatory microenvironment. Additionally, glutaminolysis generates α-ketoglutarate, Krebs cycle intermediates and acetyl-CoA, which in turn influence epigenetic landscape of the cell and the metabolic flux within the cell (Wong, Qian and Yu, 2017).

This data collected within this thesis has shown alterations in metabolites associated with glutamine-glutamate metabolism when challenged with pro-inflammatory cytokine TNFα and therefore warrants enough evidence to investigate this pathway further *in vitro*.

3.5.3.3 Glycine, serine and threonine metabolism

Glycine, serine and threonine metabolism was amongst the most enriched metabolic pathways identified in obesity and upon inflammatory challenge in OA synovial fluid and synovial fibroblast secretomes respectively.

This metabolic pathway is particularly interesting for its role in fibrosis. Collagen is the main structural protein in the extracellular space and is produced in excess in fibrotic diseases. One third of collagen is made up of glycine and it is the most abundant amino acid in collagen. The high glycine content stabilises the structural confirmation of collagen's helices through the formation of stabilising hydrogen bonds. Glycine is the smallest amino acid and is a non-essential amino acid. Glycine is produced from Serine via the serine biosynthetic pathway. There are two enzymes involved serine to glycine synthesis, namely SHMT1 (cytoplasmic isozyme) and SHMT2 (mitochondrial isoenzyme). Human lung fibroblasts when stimulated with TGF-β differentiate into activated myofibroblasts and increase the expression of activated marker, α-smooth muscle actin (α-SMA). These same fibroblasts when in an activated state, increase glycolysis and collagen-1 levels (Nigdelioglu *et al.*, 2016). Blocking glycolysis was shown to reduce collagen 1 production (COL1A1 expression) and α-SMA expression (Nigdelioglu *et al.*, 2016). TGF-β-induced up-regulation of the enzymes of de novo serine synthesis pathway is SMAD3 dependent and de novo serine synthesis pathway is required for TGF-β-induced collagen protein production (Nigdelioglu *et al.*, 2016).

Recent research has also shown the master metabolic regulator mTORC1 is implicated in fibrosis, through upregulation of the de novo serine-glycine pathway

(Selvarajah *et al.*, 2019; O'Leary *et al.*, 2020). RNA sequencing analysis was performed on human lung fibroblasts exposed to TGF-β1 and mTOR inhibitor rapamycin as well as the highly selective ATP-competitive mTOR inhibitor, AZD8055 (Selvarajah *et al.*, 2019). Pathway analysis shows the most enriched pathway as serine-glycine biosynthesis pathway (Selvarajah *et al.*, 2019). Enzymes involved in the serine-glycine pathway increased following TGF-β1 stimulation including PSAT1, PHGDH, PSPH and SHMT2 (Selvarajah *et al.*, 2019). This increase was inhibited by AZD8055 treatment, whereas rapamycin had no effect (Selvarajah *et al.*, 2019). TGF-β1 stimulation of lung fibroblast increases SMAD3 and mTOR signalling which increases ATF4 transcription factor expression and protein levels which increases the expression of PSAT1, PHGDH, PSPH and SHMT2 (Selvarajah *et al.*, 2019). Furthermore, increased glycine is incorporated into collagen (Selvarajah *et al.*, 2019).

This association between glycine-serine metabolism, activated fibroblasts and increased cellular metabolism through glycolysis is particularly interesting as the latter two observations have been identified within these OA synovial fibroblast, however further research on the glycine-serine metabolic pathway would be required before postulating a hypothesis.

3.5.3 Limitations

This metabolomic and analytical methods follow on from well-established protocols which aided in streamlining workflow and critically analysing the data generated from NMR spectroscopy. This study is the first to examine differences in the metabolome

of OA patient synovial fluid and synovial fibroblast secretomes with respect to obesity. However, there were limitations to the work generated within this study. One such limitation was the reduced number of patient samples that could be run on NMR spectrometer, due to budget, the impact of Covid19 on patient recruitment and the subsequent time limitations. Increasing patient numbers would have provided additional data to input into the model, thus increasing its reliability and reducing the variation within the classes.

Another limitation within this study was the missing data values in the NMR spectroscopy analysis. This could be due to several possibilities including but not limited to (i) the metabolite was not present within the sample, (ii) the metabolite was present but was below the concentration required for detection, (iii) the metabolite was not recorded, or (iv) the metabolite was present and within range of detection however due to incorrect peak annotation the metabolite was not labelled. Although large percentages of missing values do have negative impact on statistical analyses, exclusion criteria with low sample size reduce the power of the test that is used for statistical analysis. One way to overcome this limitation is by imputing missing values within the dataset. This can be conducted by a number of approaches including K-nearest neighbours (KNN), small value replacement and Random Forest. There are multivariate statistical test which have been developed and modified to handle data which contains large percentage of missing values such as Support Vector Machines, Random Forest, probabilistic PCA and Bayesian PCA. In regard to this study, missing values were replaced by 1/5 of minimum positive values of their corresponding variables and samples with more than 50% missing values were excluded from data analysis.

The samples collected from this study only included OA synovial fluid from end stage OA patients undergoing total hip replacement surgery. This study was limited to samples from end stage OA synovial fluid as in early OA, the volume of synovial fluid in the patient precludes collection of an adequate volume for analysis. Also, the use of normal controls such as synovial fluid samples from neck of femur fracture patients might have provided insight into the metabolic changes associated with long term chronic inflammatory microenvironment compared to acute inflammation observed at the synovial joint.

Another aspect of this study was the focus on hip OA synovial fluid. From observations on the metabolic state of OA synovial fibroblast in different joints, at the hand knee and hip, there are clear cut differences in the metabolism or metabotypes of these cells. Therefore, not including these samples does limit the scope of the study, however due to limitations in which patient samples were available for analyses, it seemed in the best interest to increase patient numbers of hip OA synovial fluid samples, thereby giving the study stronger weight and more power. Furthermore, the majority of data collected within this study used OA synovial fibroblast cultured from hip OA patients and therefore by matching the samples for this metabolomics chapter, allows for the possibility for comparison of other datasets which utilised hip OA synovial fibroblast including transcriptomics analyses.

Another limitation was the differences in mean ages of the normal weight and obese OA patients. On average, the normal weight OA patients were older than the obese OA patients, and although this study did try to control for age and other possible confounding factors, limitations in patient sample numbers meant that these samples could not be excluded without reducing the power of the statistical tests.

3.5.4 Summary

In this study we demonstrated that there are distinct differences in the metabolome of OA synovial fluid from obese and normal weight patients and have highlighted the metabolic pathways which have been enriched within obese OA patients compared to normal weight OA patients. This was also observed in OA synovial fibroblast from normal weight and obese patients when challenged with inflammatory cytokine TNFα. Although a shared common dysregulated metabolite(s) could not be found following metabolomic analysis of both datasets, there were common/shared enriched metabolic pathways such as Aminoacyl-tRNA biosynthesis, Glycine, serine and threonine metabolism, pyruvate metabolism and finally glutamine and glutamate metabolism. These metabolically enriched pathways were shared in obesity and following inflammatory challenge suggesting their importance in synovitis and in obesity associated OA. Further *in vitro* work was conducted on one of these key metabolic pathways, namely glutamine and glutamate metabolism, to see what role glutamine-glutamate metabolism plays in obesity and in inflammation within an OA context.

CHAPTER 4

MODULATING GLUTAMINE METABOLISM TO CONTROL INFLAMMATORY PHENOTYPE OF THE OA SYNOVIAL FIBROBLAST

4.1 Introduction

Glutamine is a neutral α-amino acid which is used within several biosynthetic and metabolic pathways that are fundamental for cell function. These pathways include synthesis of nucleotides/hexosamines and other non-essential amino acids, maintaining redox balance through glutathione production, glycosylation and epigenetic regulation(Pallett *et al*, 2021) . It is the most abundant circulating amino acid (~500μM), contributing to 40% of the amino acid pool in muscle and 20% in blood (Altman, Stine and Dang, 2016). Glutamine is regarded as a conditionally essential amino acid, which is synthesised endogenously from glutamate and ammonia by glutamine synthetase (GLUL), but during catabolic stressed conditions (e.g., postoperative period, injury and sepsis), glutamine requirements exceed the individual's ability to endogenously produce sufficient amounts (Lacey and Wilmore, 1990). Glutamine dependence in cells is such that deprivation of glutamine results in cell death for a number of cell types, including fibroblasts, and induces apoptosis in cancerous cells (Eagle *et al.*, 1956; Altman, Stine and Dang, 2016). Circulating glutamine levels are maintained at high levels within the blood as ready supply of carbon and nitrogen. It is transported into cells through protein transporters such as SLC1A5 (ASCT2) and exported out of cells in exchange with other amino acids by antiporters such as L-type amino acid transporter 1 (LAT1) or SLC7A11 (Nicklin *et al.*, 2009; Howden *et al.*, 2019). Glutamate is a well-known neurotransmitter and signals through several receptors including metabotropic/GPCRs ($mGluR_{1-8}$) and ionotropic receptors (NMDA, Kainate and AMPA). These receptors are highly expressed in neuronal tissues however have relatively low expression in connective

and soft tissues (Sjöstedt *et al.*, 2020). Interestingly, introducing expression of neuronal isoforms of GRIK2/$GluR_6$ into fibroblasts resulted in immediate cessation of cell proliferation and induced a state of senescence (Zhawar, Kandpal and Athwal, 2020). Activated myofibroblasts have recently been shown to primarily utilise glutamate for collagen production and not energy metabolism, with cytoplasmic enzymes phosphoserine aminotransferase (PSAT1) and Δ1-pyrroline-5-carboxylate synthetase (P5CS) producing amino acids serine, glycine and proline thereby contributing to fibrosis (O'Leary *et al.*, 2020). This was validated in a mouse model of pulmonary fibrosis, which showed increased expression of key glutamine metabolic enzyme glutaminase 1 (GLS1), which converts glutamine to glutamate (glutaminolysis), and inhibition of this enzyme reduced both bleomycin and transforming growth factor-β1–induced pulmonary fibrosis (Cui *et al.*, 2019).

Furthermore glutamine-glutamate metabolism is well known to play a role in other pathophysiological conditions including obesity and immune-mediated inflammation. White adipose tissue from obese individuals have reduced glutamine levels and reduced expression of the enzyme glutamine synthetase (GLUL), which synthesis glutamine from glutamate and ammonia (Petrus *et al.*, 2020). In an obesity murine model in which mice were fed a high fat diet and supplemented with glutamine, there was a reduction in markers of inflammation (IL6 and IL1β) and macrophage markers (CD68) in white adipose tissue compared to a high fat diet control (Petrus *et al.*, 2020). Adipocytes incubated with high (10mM) glutamine show reduced expression and secretion of pro-inflammatory markers such as IL6, IL1β and CCL2 due to reduced glycolysis and through post-transcriptional regulation of these markers (via protein O-GlcNAcylation) (Petrus *et al.*, 2020). This suggests glutamine is an immunometabolic regulator in white adipose tissue which links obesity to

inflammation. Likewise, metabolomics analysis of the serum of RA patients shows TNF-inhibitor therapy with etanercept increases glutamine levels, suggesting glutamine plays a role in inflammatory arthritis (Priori et al, 2015). The use of glutamine supplementation to manage disease course in clinical trials or as a drug intervention for patients has had mixed effect. Plasma glutamine levels have been shown to decrease markedly following major surgery and is significantly correlated with the production of IL6 (Parry-Billings *et al.*, 1992). Patient with low admission illness severity who underwent major abdominal surgery and were given parental L-alanyl-L-glutamine supplementation showed a reduction in plasma IL6 levels (Lin *et al.*, 2005). However, in inflammatory bowel disease, glutamine supplementation in clinical trials was shown to have no effect on disease course, disease activity, biochemical parameters, oxidative stress and inflammation markers (CRP) in patients (Soares Severo *et al.*, 2021). Four studies within this meta-analysis however reported no change in plasma glutamine concentrations and the majority of these studies were short term (4 weeks) suggesting further research on long term glutamine supplementation maybe appropriate to validate these findings (Soares Severo *et al.*, 2021).

Glutaminolysis is catalysed in mammalian tissues by the aforementioned GLS. There are two glutaminase enzymes, GLS which is broadly expressed in normal tissues whereas GLS2/LGA expression is limited to liver, brain, pituitary gland and pancreas (Altman, Stine and Dang, 2016). Although there is high degree of similarities in their amino acid sequences, GLS and GLS2 are products of different genes (Curthoys and Watford, 1995). Furthermore, there is alternative splicing of GLS pre-mRNA into either glutaminase C (GAC) or kidney-type glutaminase (KGA) isoforms (Altman, Stine and Dang, 2016). These proteins are regulated differently. GLS isoforms KGA

and GAC as well as GLS2 are activated by inorganic phosphate (Altman, Stine and Dang, 2016). GLS is inhibited by glutamate in a negative feedback loop whereas GLS2 isn't and GLS2 alone is activated by ammonia *in vitro* (Krebs, 1935). GLS2 is increased during starvation, diabetes and consumption of high-protein diet whereas GLS is involved in maintenance of acid-base homeostasis and is increased in the kidney in response to metabolic acidosis (Curthoys and Watford, 1995). In neurones, loss of function mutations of GLS and its counteracting enzyme GLUL causes a disturbance in maintaining homeostasis of neurotransmitter glutamate and results in severe neonatal encephalopathy (Rumping *et al.*, 2019). As a key enzyme within the glutamine-glutamate metabolic pathway, GLS is the ideal target for disrupting normal function of this pathway. It can be inhibited pharmacologically by cell permeable, selective and non-competitive allosteric inhibitors Bis-2-(5-phenylacetamido-1,3,4-thiadiazol-2-yl)ethyl sulphide ($C_{24}H_{24}N_6O_2S_3$) (BPTES), which induces an inactive GLS1 tetrameric conformation, and Telaglenastat ($C_{26}H_{24}F_3N_7O_3S$) (CB-839), with the latter currently being tested in phase II clinical trials primarily for cancerous conditions such as clear cell and advanced renal cell carcinoma, triple negative breast cancer and metastatic prostate cancer (Ferreira *et al.*, 2013; Ramachandran *et al.*, 2016).

4.2 Hypothesis

We hypothesised that:

- Inhibition of the glutamine-glutamate metabolic pathway would reduce the inflammatory phenotype of OA synovial fibroblasts and impact on their proliferative capacity and viability

4.4 Results

Metabolomics analysis of OA synovial fluid in obese patients compared to normal weight patients identified glutamine-glutamate metabolism as the most significantly enriched metabolic pathway (chapter 3). Following this analysis, modulation of glutamine-glutamate metabolism in OA synovial fibroblasts was undertaken to observe changes in the inflammatory phenotype of OA synovial fibroblasts.

Genes involved in glutamine-glutamate metabolism were identified and analysed to determine differential gene expression in hip OA synovial fibroblasts using bulk RNA sequencing data characterised further in the following chapter (chapter 5). Glutamine receptors were not highly expressed in OA synovial fibroblasts (figure 4.1), however glutamine transporters and enzymes, including the neutral amino acid transporter SLC1A5 and glutaminase (GLS), were highly expressed in OA synovial fibroblasts (figure 4.2 and 4.3).

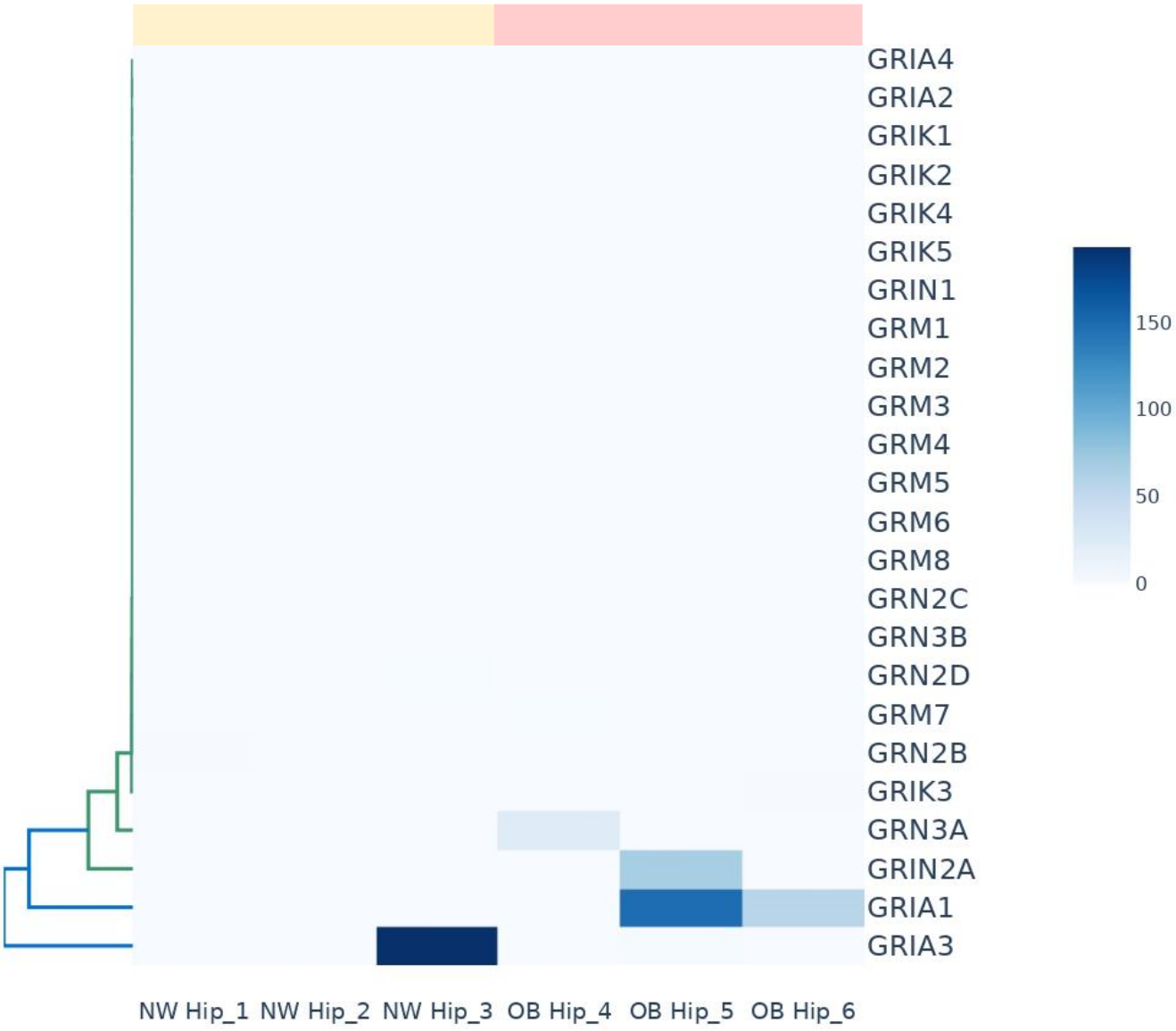

Figure 4.1: Glutamine receptors expression is not altered in obese and normal weight OA synovial fibroblasts

Fibroblasts are from normal weight (NW) (yellow) and obese (OB) (pink) (n = 3 patients per BMI category) hip OA patients. Differential gene expression analysis taken from normalised counts of bulk RNA sequencing data.

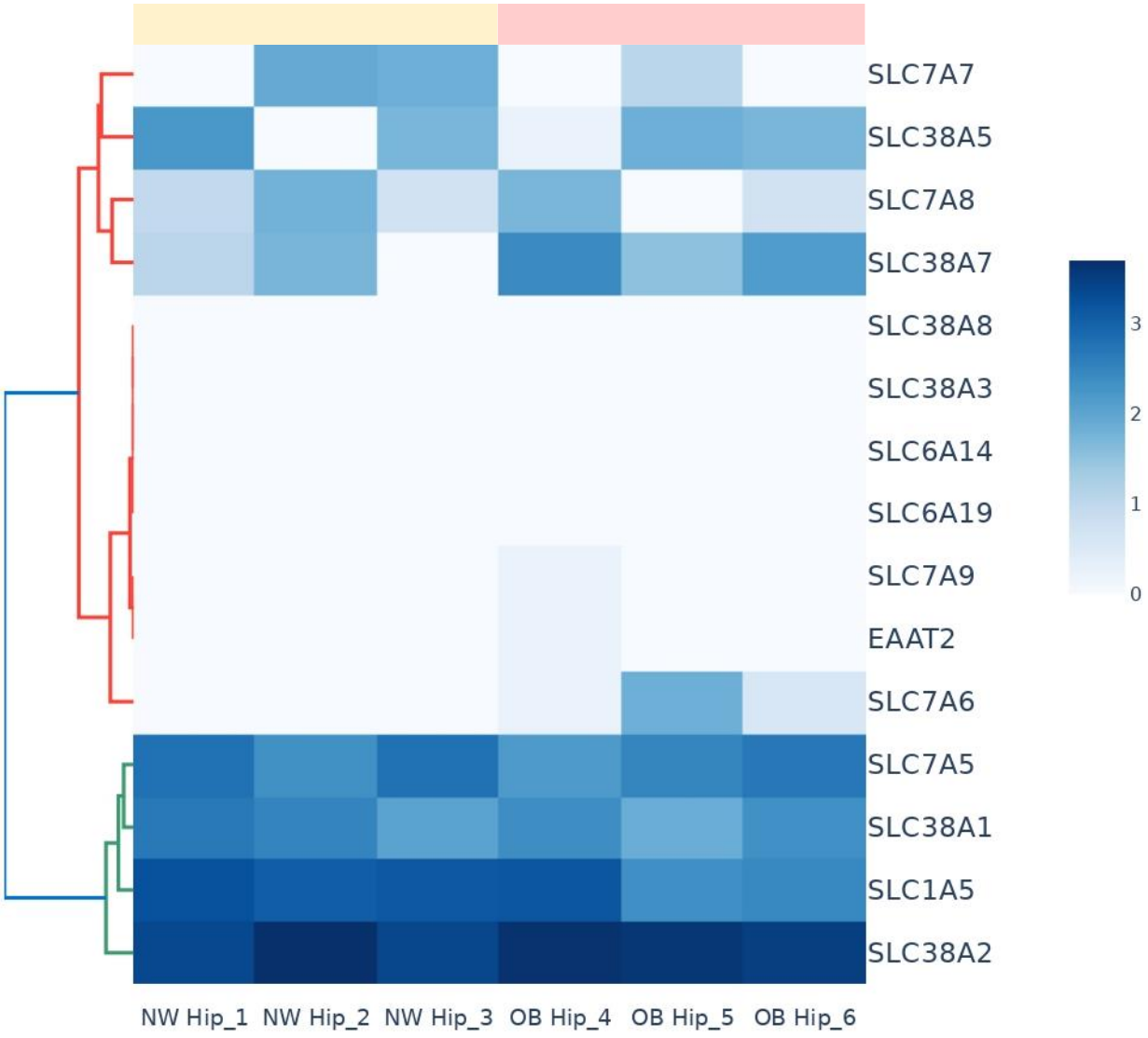

Figure 4.2: OA synovial fibroblasts express primary glutamine transporter expression in obese and normal weight patients

Fibroblasts are from normal weight (NW) (yellow) and obese (OB) (pink) (n = 3 patients per BMI category) hip OA patients. Differential gene expression analysis taken from normalised counts of bulk RNA sequencing data.

Figure 4.3: OA synovial fibroblasts express key glutamine enzyme GLS

Fibroblasts are from normal weight (NW) (yellow) and obese (OB) (pink) (n = 3 patients per BMI category) hip OA patients. Differential gene expression analysis taken from normalised counts of bulk RNA sequencing data.

As previously mentioned, GLS1, as a critical enzyme within this pathway, was targeted *in vitro* using a non-competitive pharmacological inhibitor, Bis-2-(5-phenylacetamido-1,3,4-thiadiazol-2-yl) ethyl sulfide (BPTES), which blocks the conversion of glutamine to glutamate (Farah *et al.*, 2022).

OA synovial fibroblasts were cultured for 24 hours either in normal growth media, or stimulated with TNFα (10 ng/mL) or TNFα (10 ng/mL) in combination with BPTES (20 μM) (Farah *et al.*, 2022). GLS1 inhibition significantly attenuated TNFα mediated IL6 protein secretion in normal weight OA synovial fibroblasts and on average reduced IL-6 protein secretion in obese OA fibroblasts, albeit this did not reach statistical significance (figure 4.4a). To validate this effect, a loss of function study was conducted using siRNA directed against GLS1. siRNA knockdown using GLS1 siRNA for 24 hours at 5 nM and 100 nM significantly reduced GLS expression by 65% and 35%, respectively, compared to transfection using a non-targeting control (NTC) siRNA (figure 4.4b) (Farah *et al.*, 2022). Immunoblotting of OA synovial fibroblasts lysates following siRNA transfection showed a reduction in GLS1 protein expression at both 24 and 48 hour timepoint (figure 4.4c) (Farah *et al.*, 2022). Furthermore, fibroblasts treated with GLS1 targeting siRNA exhibited significantly reduced IL-6 expression by between 40–65%, supporting the role of GLS1 in mediating IL-6 production and the inflammatory response in OA synovial fibroblasts (figure 4.4d) (Farah *et al.*, 2022).

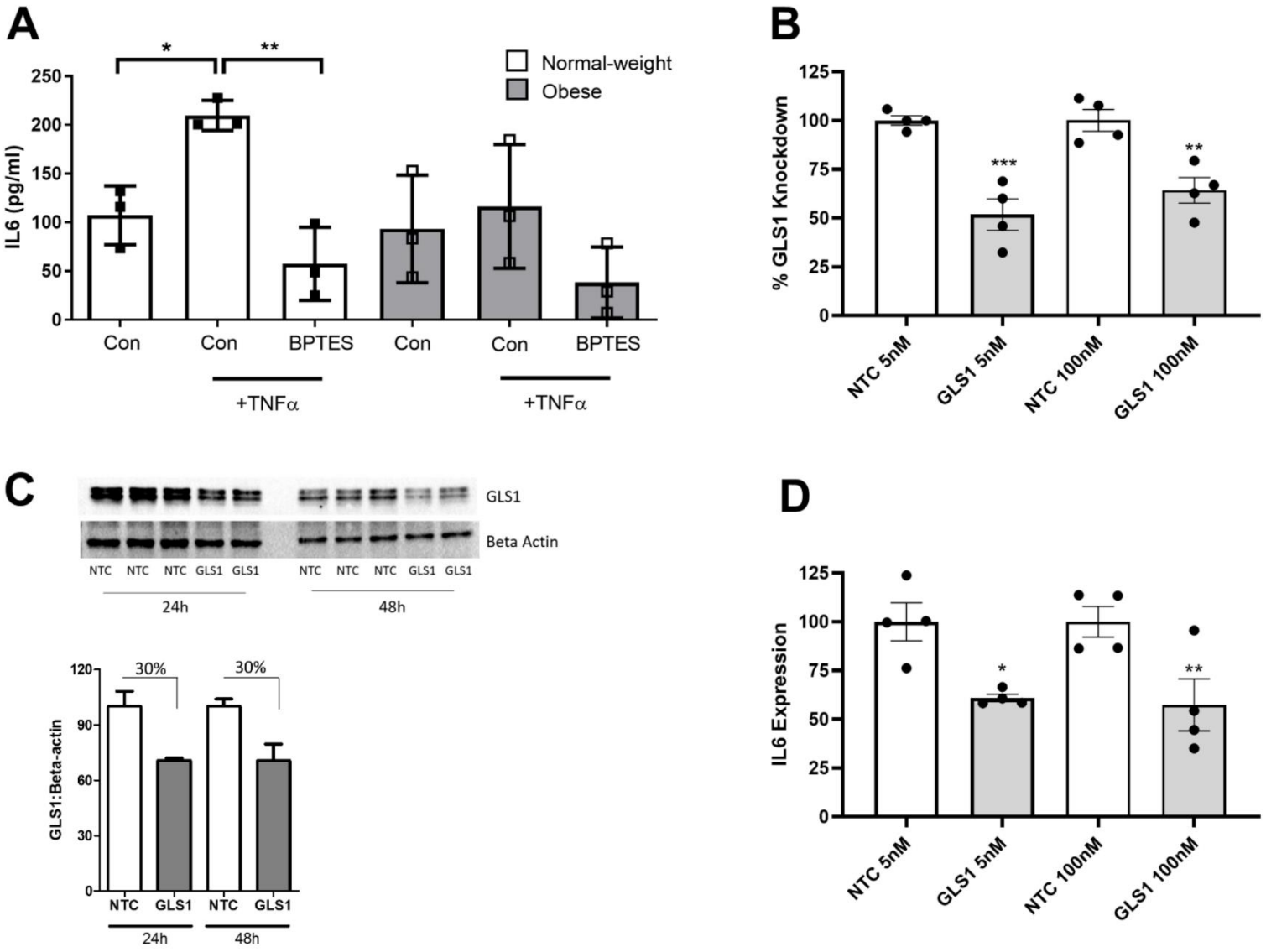

Figure 4.4: Inhibition of GLS1 attenuates IL6 inflammatory response in OA synovial fibroblasts

(A) GLS1 inhibitor, BPTES (20 μM), attenuates TNFα induced IL-6 secretion in synovial fibroblasts from normal weight and obese hip OA patients (n = 3 patients). Bars represent mean IL-6 secretion (pg/mL). **(B)** % knockdown of GLS1 expression in OA synovial fibroblasts after 24 hours post-transfection with a GLS1 targeting siRNA (5 nM or 100 nM), compared to a non-targeting control (NTC) siRNA (n = 4 patients). **(C)** Confirmation of siRNA-mediated GLS1 protein knockdown at 24 hours and 48 hours post-transfection using 100 nM siRNA. **(D)** Effect of sRNA-mediated knockdown of GLS1 on IL-6 expression in OA synovial fibroblasts at 24 hours post-transfection (n = 4 patients). Data are presented as mean ± SEM. * = $p < 0.05$, ** = $p < 0.01$, *** = $p < 0.001$. (Farah *et al.,* 2022).

Having identified an association between IL6 mediated inflammation and glutamine-glutamate metabolism in OA synovial fibroblasts, further investigation into the role GLS1 and glutamine-glutamate metabolism plays in OA synovial fibroblast function and phenotype was conducted.

In an attempt to understand how reliant these synovial fibroblasts were on glutamine-glutamate metabolism, a long-term culture experiment was conducted using fibroblasts from normal weight and obese patients cultured in the presence of either low glutamine (2mM), high glutamine (20mM) or high glutamine supplemented with the GLS1 inhibition (BPTES 20µM) and their morphology, proliferation and viability determined.

Within 24 hours, cells exposed to the GLS1 inhibitor BPTES exhibited increased cell death (based on phase-contrast microscopy analysis of membrane blebbing and appearance of apoptotic bodies) (figure 4.6), and after 2-4 days of GLS1 inhibition the vast majority of fibroblasts were dying whether from normal weight or obese patients, compared to cells exposed to vehicle control (DMSO 0.5%) (figure 4.7 and 4.8).

Having investigated cell morphology, we next measured cell proliferation using BrdU labelling ELISA. Fibroblasts incubated with high glutamine (20mM) showed significantly increased proliferation, which was diminished by GLS1 inhibition (figure 4.9).

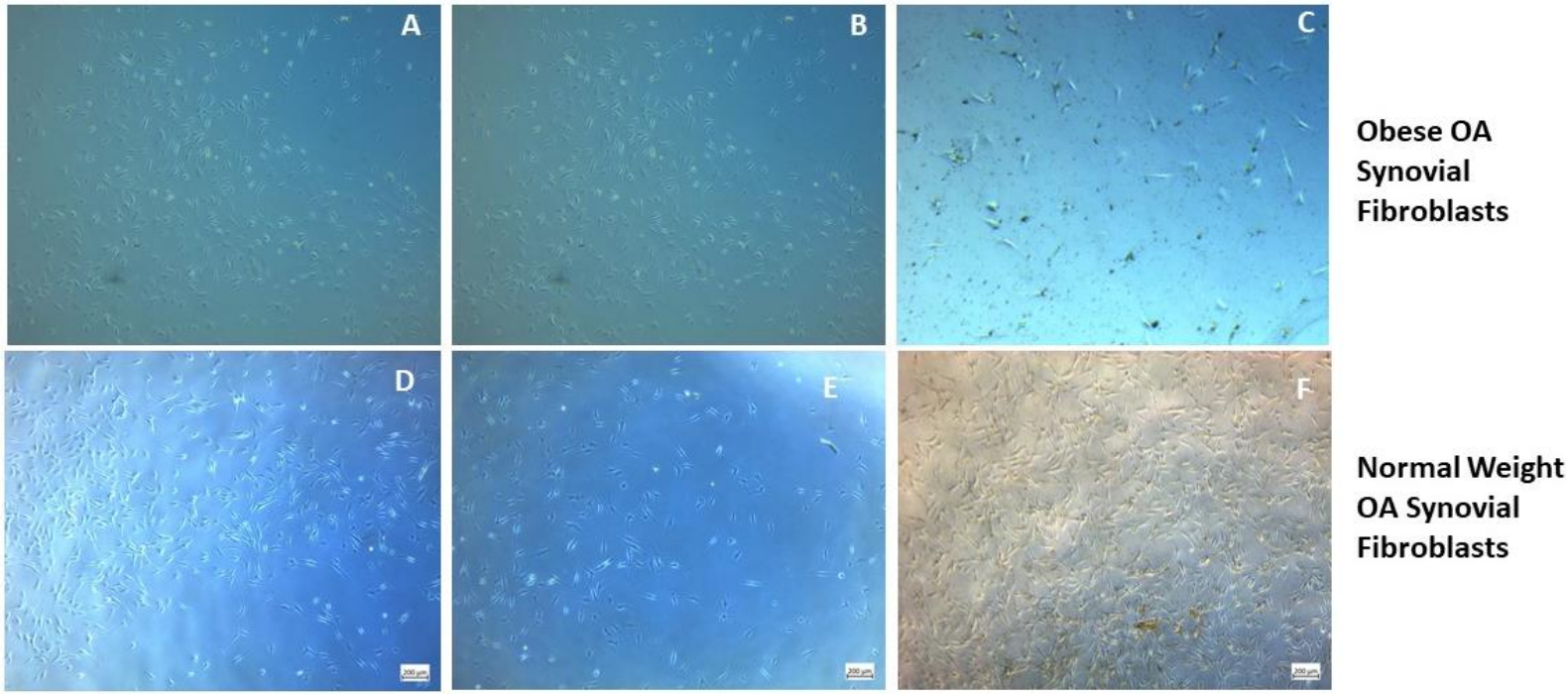

Figure 4.5: Inhibition of GLS1 in OA synovial fibroblasts alters cellular morphology

Representative images of fibroblasts from normal weight and obese patients treated with GLS1 inhibitor, BPTES (20 µM), across time (6 hours - 4 days) show altered cell morphology possibly due to increased cell death. Fibroblasts were treated with (**A** and **D**) low glutamine (2mM), (**B** and **E**), high glutamine (20mM) and (**C** and **F**) BPTES (20µM). Normal weight (n= 2 patients) and obese (n = 3 patients) used for this experiment.

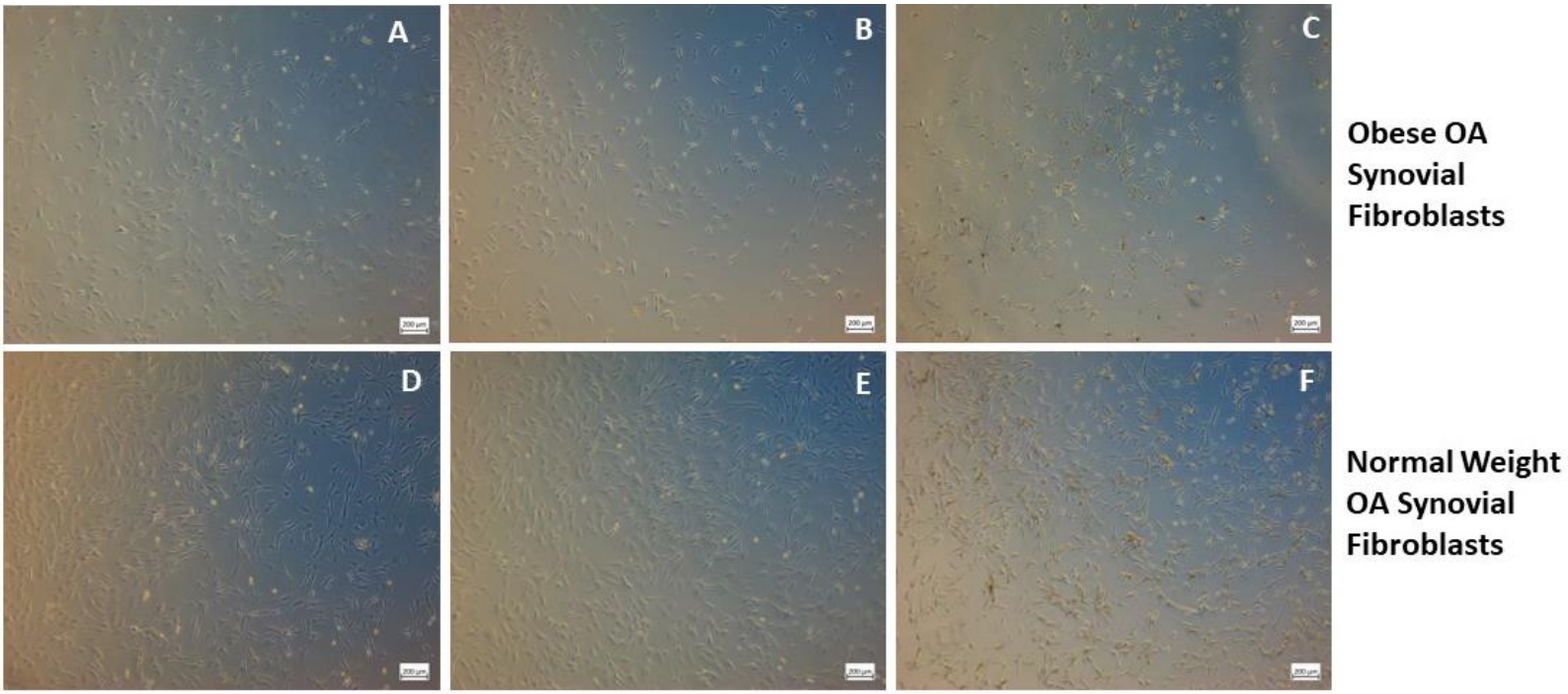

Figure 4.6: 1-day inhibition of GLS1 in OA synovial fibroblasts alters fibroblast morphology

Representative images of fibroblasts from normal weight and obese patients treated with GLS1 inhibitor, BPTES (20 µM), across time (6 hours - 4 days) show altered cell morphology possibly due to increased cell death. Fibroblasts were treated with (**A** and **D**) low glutamine (2mM), (**B** and **E**), high glutamine (20mM) and (**C** and **F**) BPTES (20µM). Normal weight (n= 2 patients) and obese (n = 3 patients) used for this experiment.

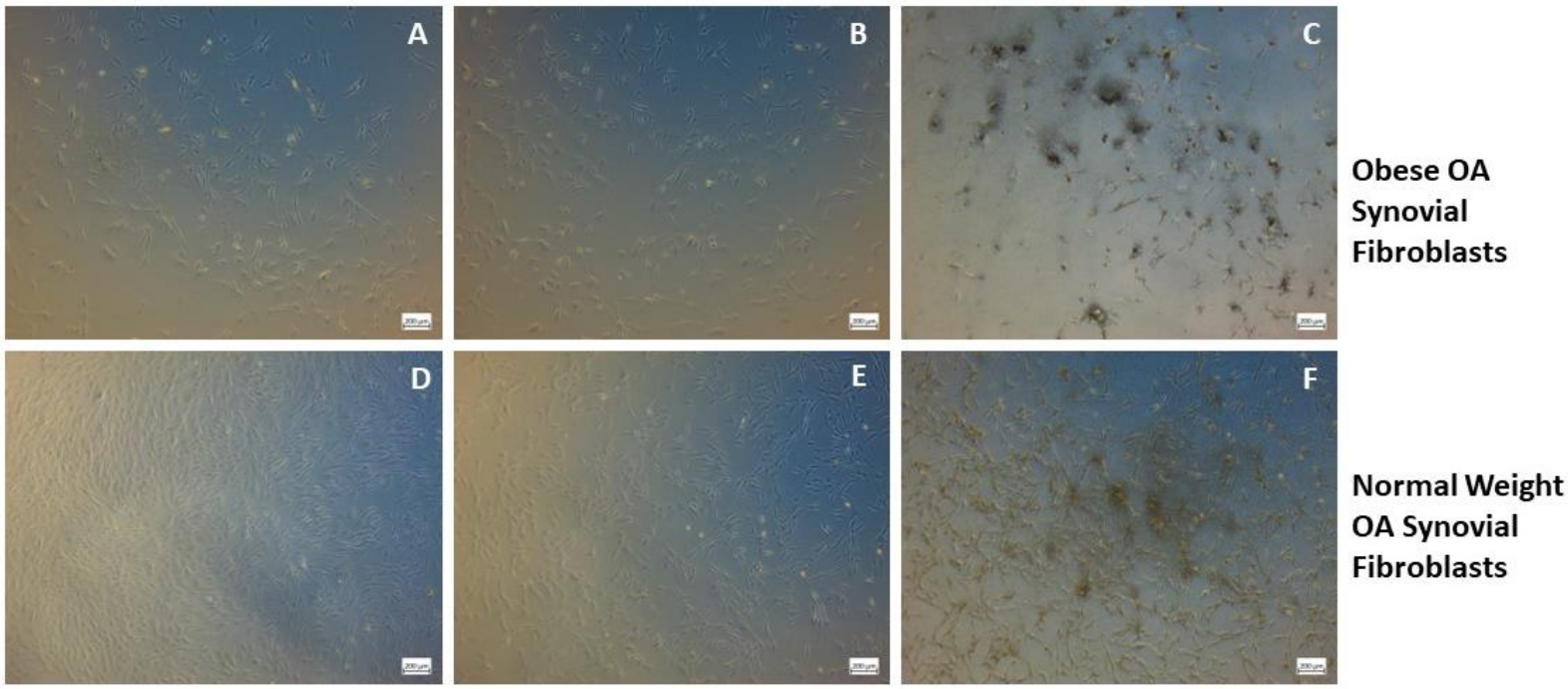

Figure 4.7: 2-day inhibition of GLS1 in OA synovial fibroblasts alters fibroblast morphology

Representative images of fibroblasts from normal weight and obese patients treated with GLS1 inhibitor, BPTES (20 µM), across time (6 hours - 4 days) show altered cell morphology possibly due to increased cell death. Fibroblasts were treated with (**A** and **D**) low glutamine (2mM), (**B** and **E**), high glutamine (20mM) and (**C** and **F**) BPTES (20µM). Normal weight (n= 2 patients) and obese (n = 3 patients) used for this experiment.

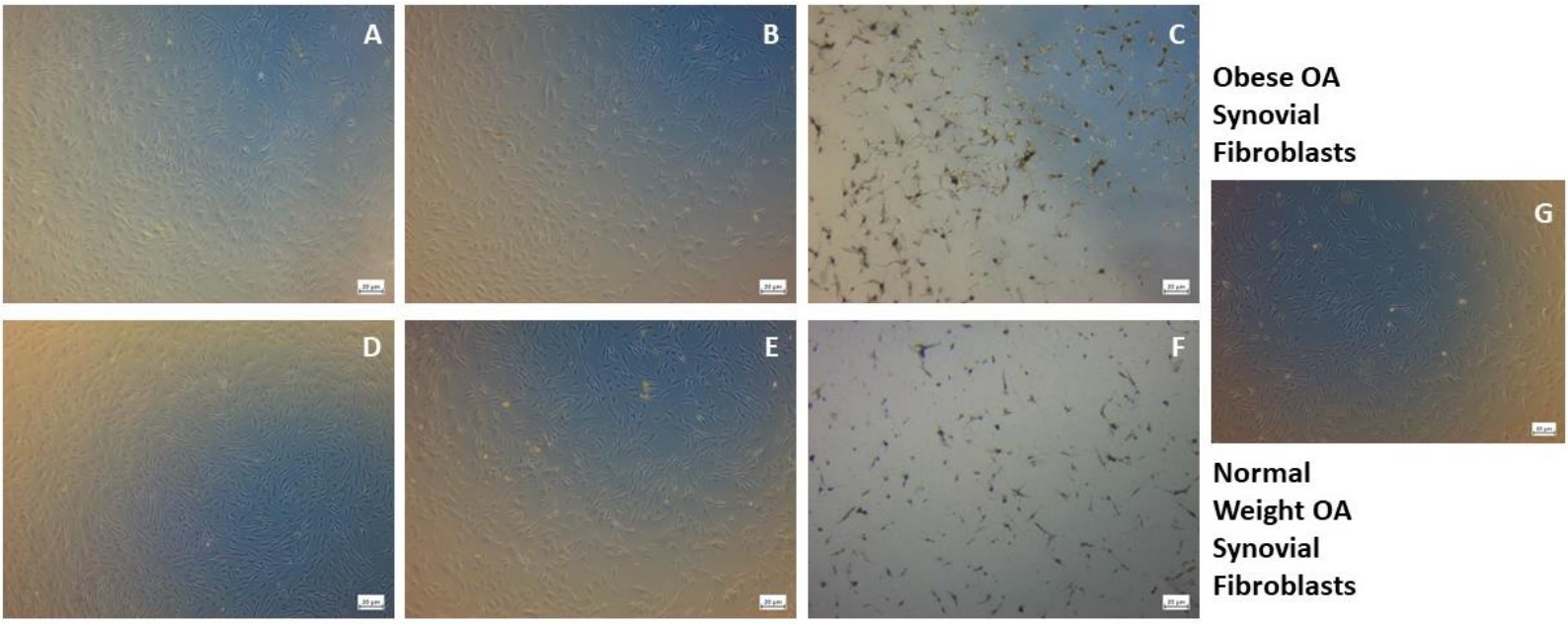

Figure 4.8: 4-day inhibition of GLS1 in OA synovial fibroblasts alters fibroblast morphology

Representative images of fibroblasts from normal weight and obese patients treated with GLS1 inhibitor, BPTES (20 µM), across time (6 hours - 4 days) show altered cell morphology possibly due to increased cell death. Fibroblasts were treated with (**A** and **D**) low glutamine (2mM), (**B** and **E**), high glutamine (20mM) and (**C** and **F**) BPTES (20µM). (**G**) DMSO vehicle control (0.5%). Normal weight (n= 2 patients) and obese (n = 3 patients) used for this experiment.

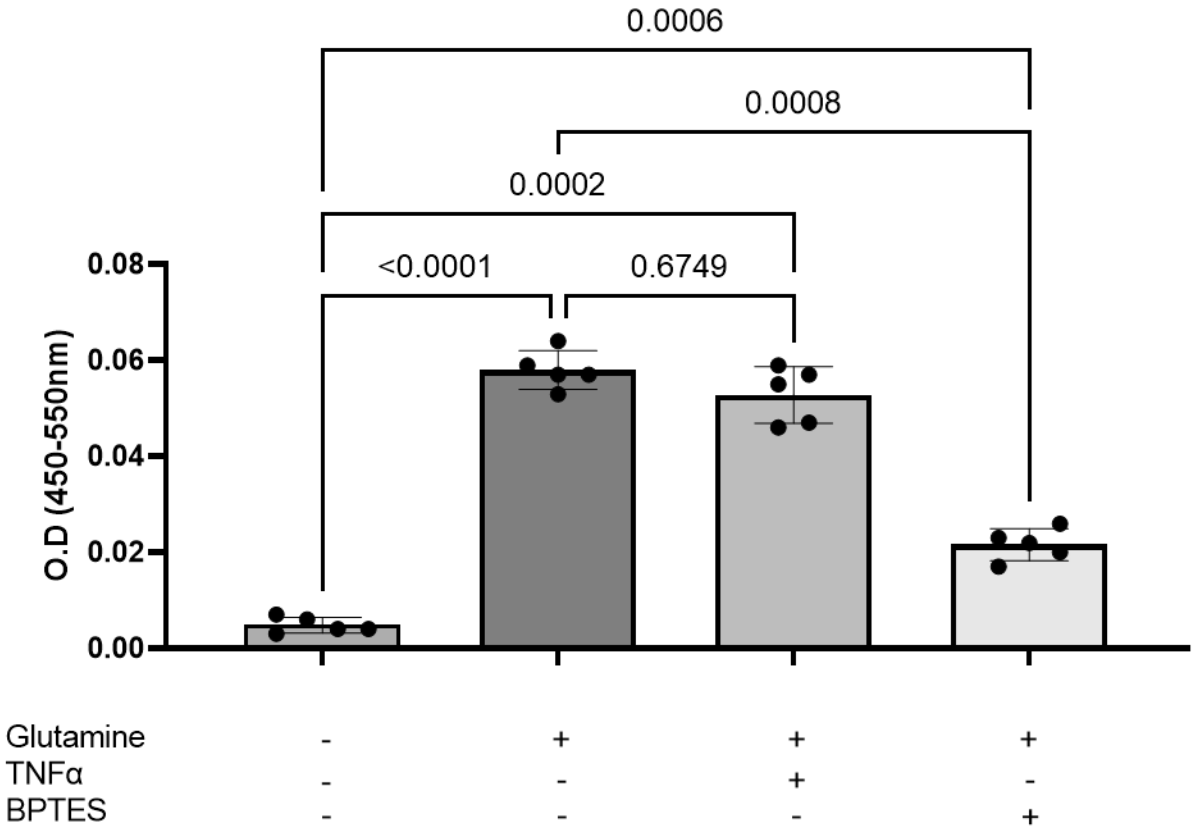

Figure 4.9: Synovial fibroblast proliferation increases with glutamine treatment and decreases with GLS1 inhibition

OA synovial fibroblasts were treated glutamine (2mM) and TNFα (10ng/ml for 24 hrs) stimulation show increased cell proliferation compared to fibroblasts treated with GLS1 inhibitor BPTES (20μM for 24 hours) (n= 5 biological replicates). Repeated measures ANOVA with Tukey's multiple comparisons test. All data presented as mean ± SD.

Following this investigation into the long-term effects of GLS1 inhibition *in vitro* on cell phenotype, short term inhibition of GLS1 in OA synovial fibroblasts was examined. Long term inhibition of GLS1 affected cell proliferation and most probably cell death. However, a quantifiable approach was required to measure cell death following short term GLS1 inhibition in fibroblasts. Annexin V was used as signal for detecting apoptosis and propidium iodide (PI) was used to detect necrotic/late apoptotic cells due to increased permeability of plasma and nuclear membranes as previously described (figure 4.10) (Rieger *et al.*, 2011). OA synovial fibroblasts were treated with varying concentrations of GLS1 inhibitor BPTES (5-5000nM) and spanned the IC_{50} of BPTES (60nM). Short term inhibition of GLS1 (1 hour) did not increase apoptosis or necrosis in dose-dependent manner (figure 4.12). Furthermore, GLS1 inhibition did not decrease cell proliferation in normal weight and obese OA synovial fibroblasts in dose-dependent manner (figure 4.14), however it did significantly reduce IL6 secretion in both normal weight and obese OA synovial fibroblasts in a dose-dependent manner (figure 4.15). Glucose uptake was significantly altered in OA synovial fibroblasts treated with BPTES (20µM for 1 hour) however there was no effect on mitochondrial mass (figure 4.16)

Finally, short term GLS1 inhibition did increase NAD(P)H-dependant oxidoreductase activity in dose-dependent manner as measured by MTS assay, however there was no significant change in ROS production following GLS1 inhibition (figure 4.17).

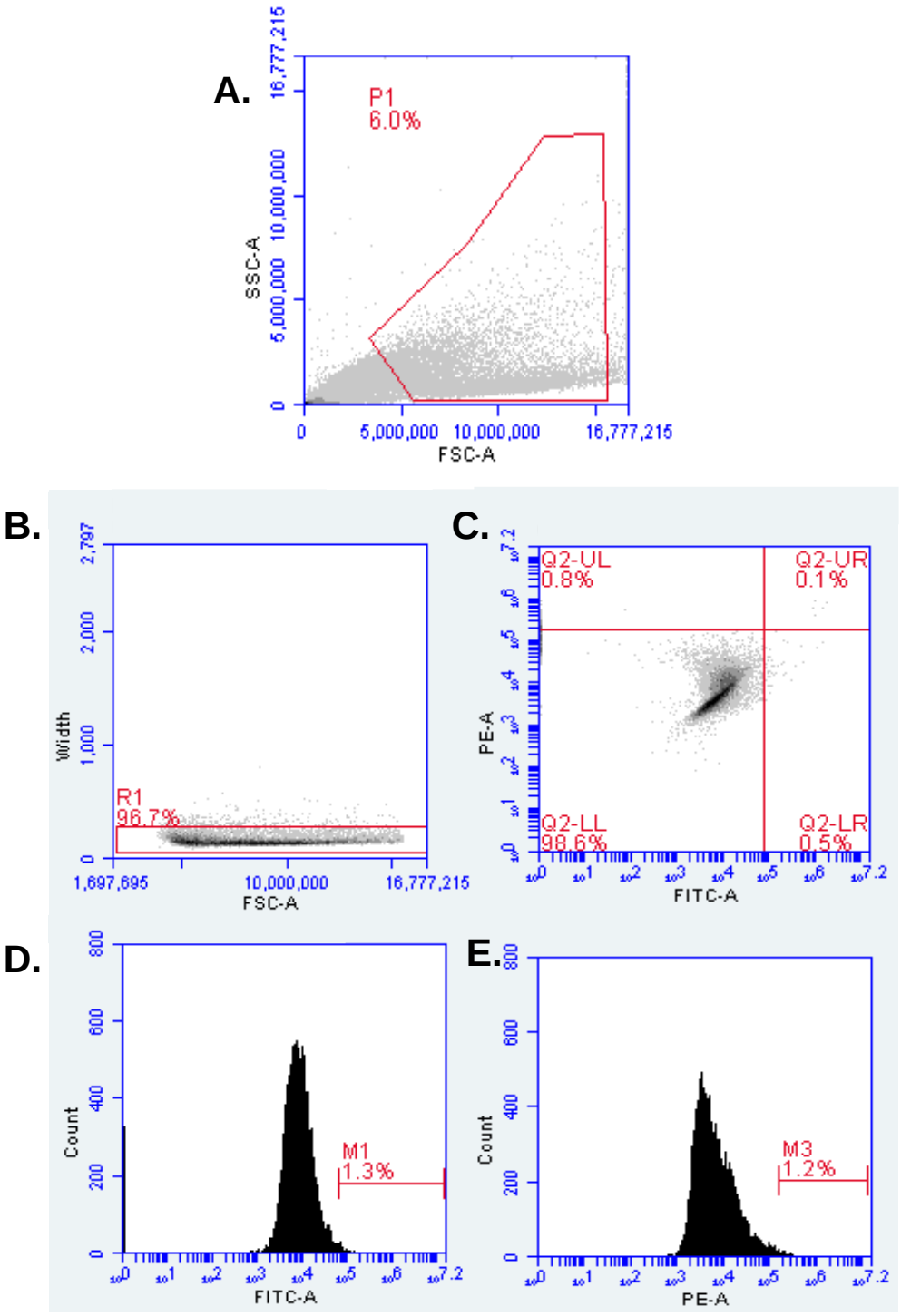

Figure 4.10: Unstained cells displayed in gating strategy used for annexin V:Pi staining as measure of apoptosis in fibroblasts

Live: Dead stain was achieved using Annexin V and Propidium iodide (n =2 repeats). Fibroblasts in this figure were not stained and live cells shown were mixed with heat killed cells in 1:1 ratio as a positive control for apoptosis. Flow cytometry conducted using FACSvia™. **(Primary data analysis conducted by Joshua Price).**

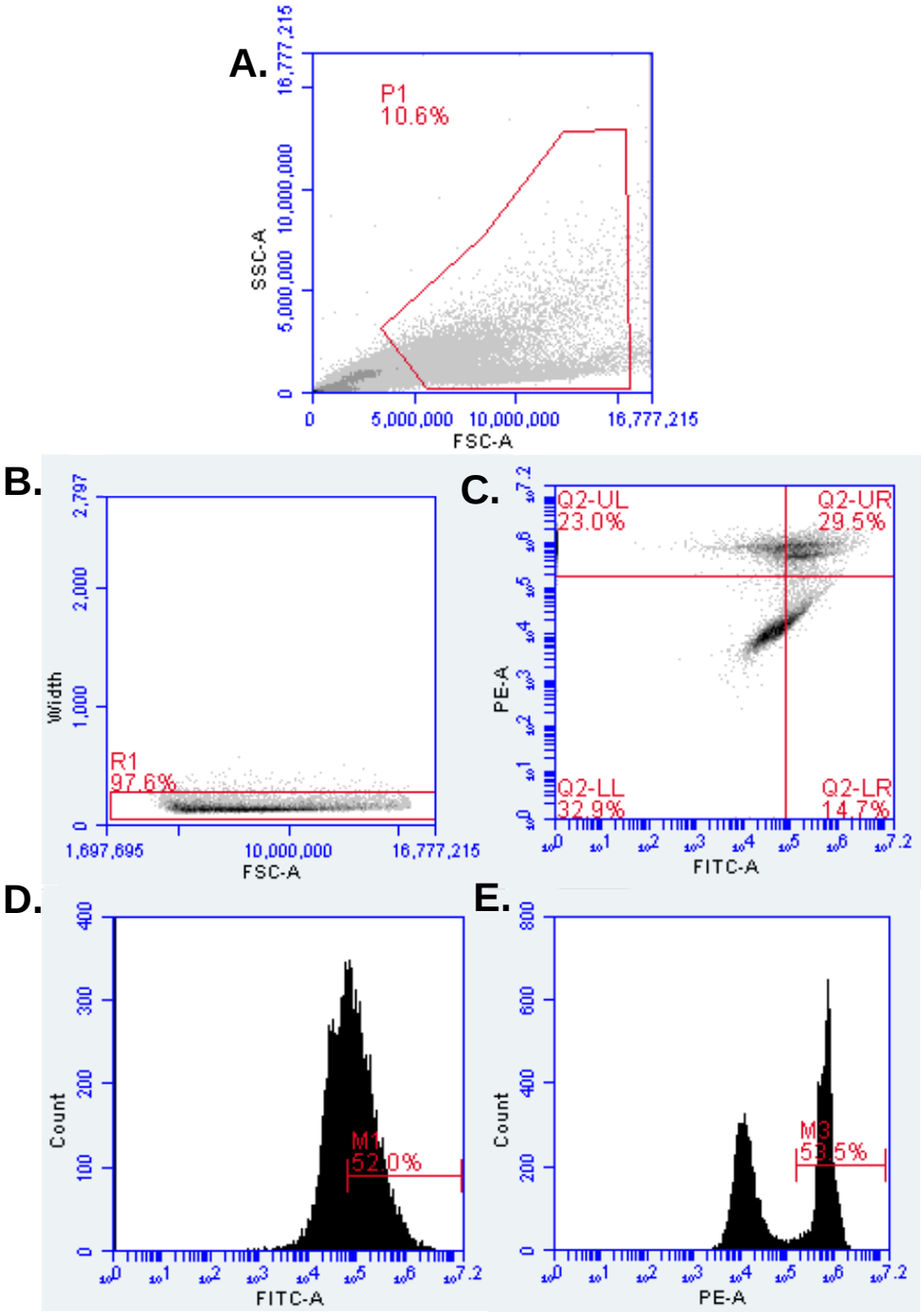

Figure 4.11: Gating strategy used for Annexin V:Pi staining as measure of apoptosis in fibroblasts

Live: Dead stain was achieved using Annexin V and Propidium iodide (n =2 repeats). Gating strategy shown was used to identify fibroblasts on cell size, removing doublets and determining apoptosis by staining cells which are Annexin V^+ (FITC) and Pi^+. Live cells shown were mixed with heat killed cells in 1:1 ratio as a positive control for apoptosis. In panel C fibroblasts in lower left quadrant were labelled live, fibroblasts in lower right quadrant were labelled early apoptotic, fibroblasts in upper right quadrant were labelled late apoptotic and fibroblast in upper left quadrant were labelled necrotic. Flow cytometry conducted using FACSvia™. **(Primary data analysis conducted by Joshua Price).**

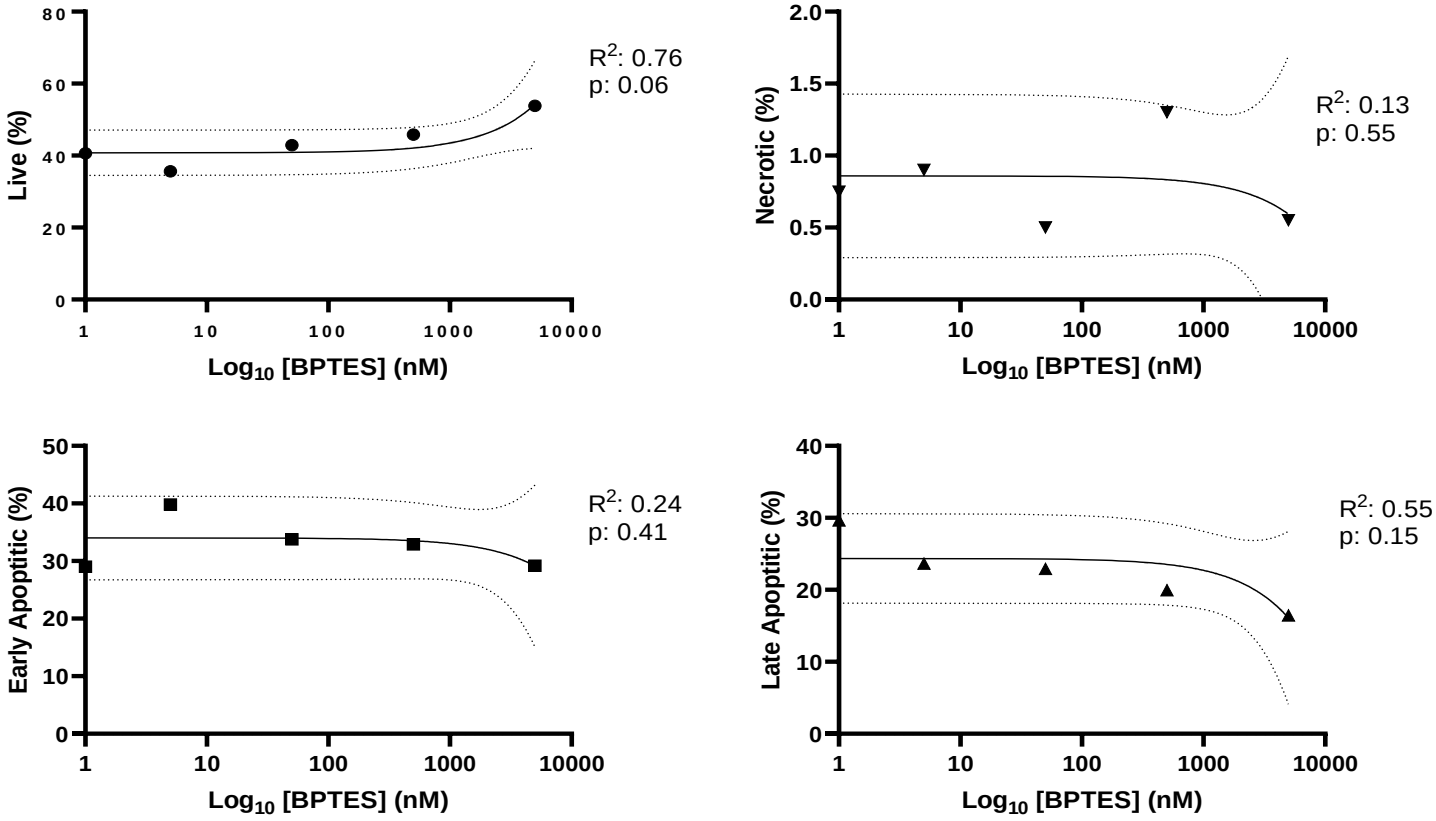

Figure 4.12: Short term GLS1 inhibition does not increase apoptosis

Fibroblasts incubated with GLS1 inhibitor BPTES (5-5000nM) for 1 hour do not show significant relationship between cell death and BPTES concentration (n = 2 repeats). Cell death was measured using annexin V:Pi staining on FACSvia™ as described in figure 4.10. **(primary data analysis performed by Joshua Price).**

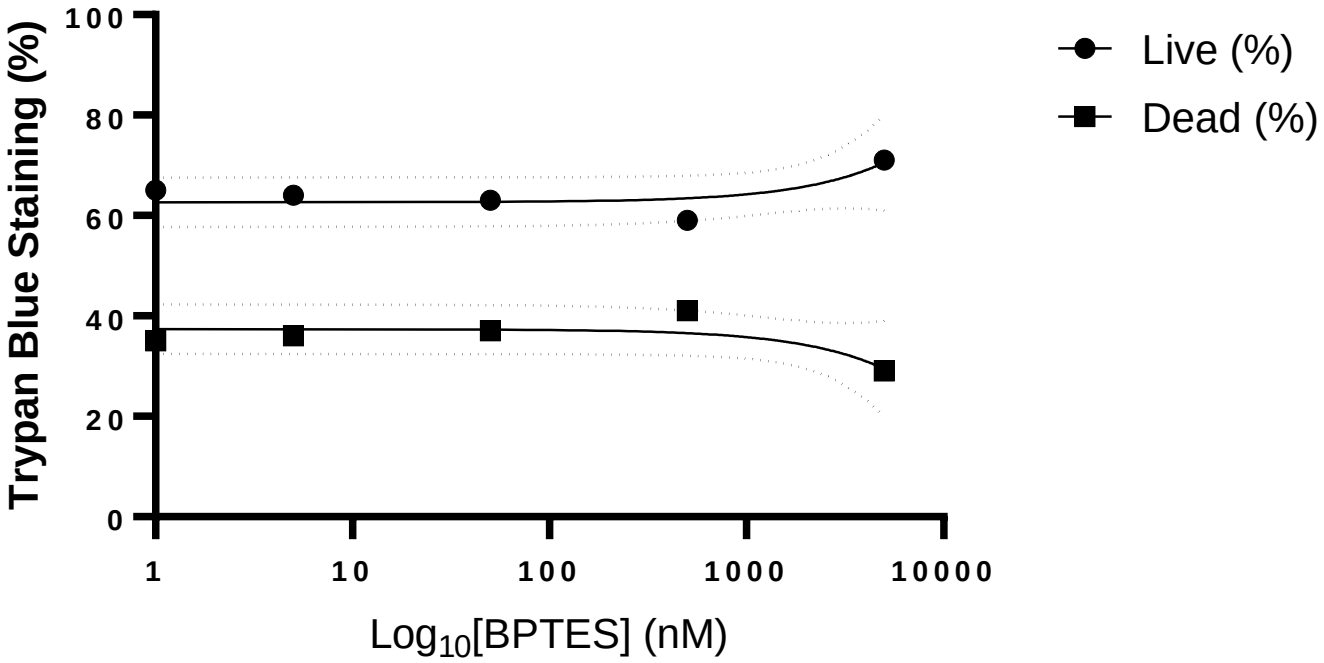

Figure 4.13: Short term GLS1 inhibition does not increase cell death

Fibroblasts incubated with GLS1 inhibitor BPTES (5-5000nM) for 1 hour do not show significant relationship between cell death and BPTES concentration (n = 2 repeats). Cell death was measured using trypan blue stain and calculated using Countess™ 3 automated cell counter.

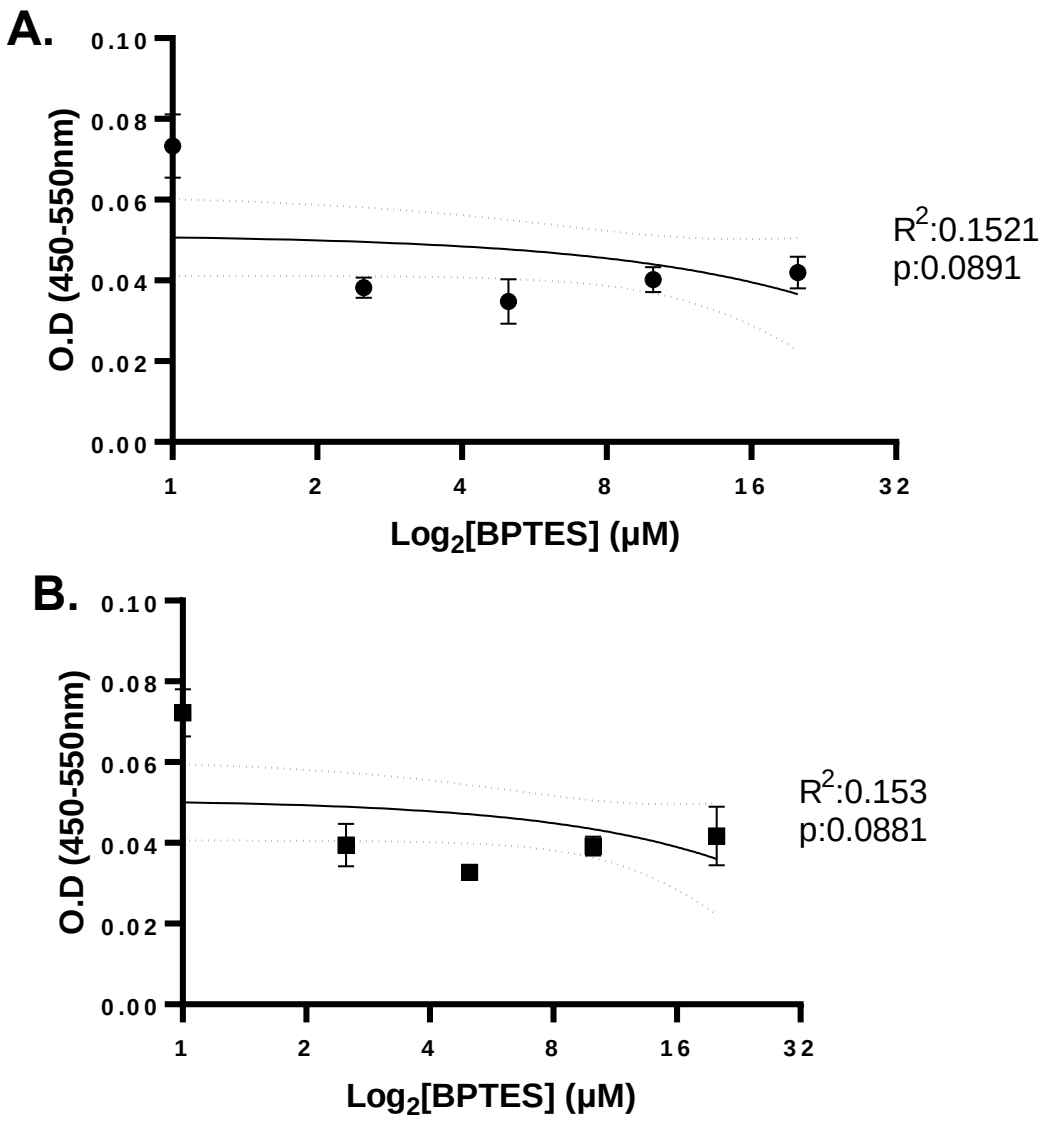

Figure 4.14: Short term GLS1 inhibition does not alter cell proliferation

Fibroblasts from normal weight **(A)** and obese **(B)** patients were incubated with GLS1 inhibitor BPTES (2.5-20μM) for 1 hour do not show significant relationship between cell proliferation and BPTES concentration (n = 4 biological replicates). Cell proliferation was measured using BrdU ELISA and absorbance was measured and normalised at 450-550nm. All data presented as mean ± SD.

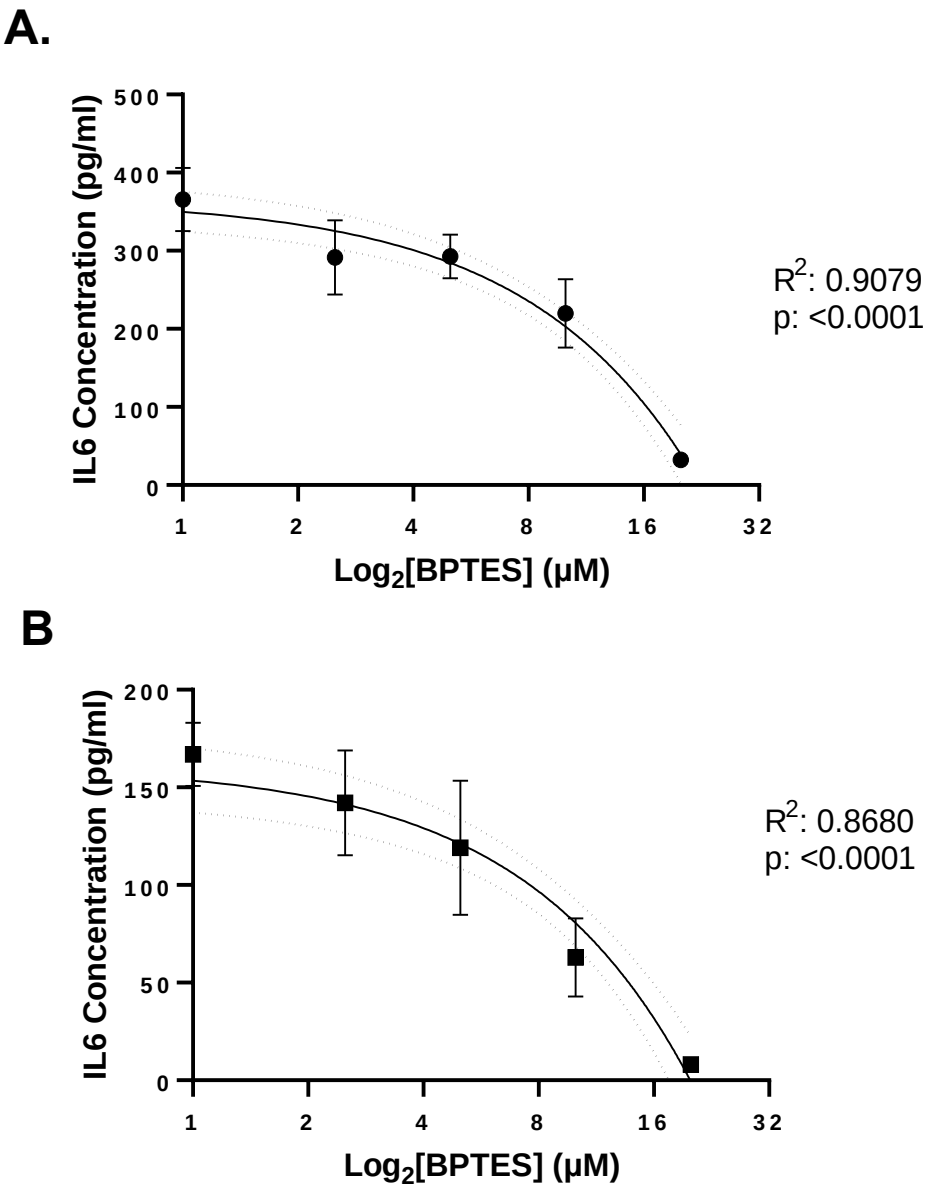

Figure 4.15: Short term GLS1 inhibition attenuates IL6 mediated inflammation in dose-dependent manner

Fibroblasts from normal weight **(A)** and obese **(B)** patients were incubated with GLS1 inhibitor BPTES (2.5-20μM) for 1 hour show significant decrease in IL6 secretion (n = 4 biological replicates). IL6 secretion was measured using ELISA and absorbance was measured and normalised. All data presented as mean ± SD.

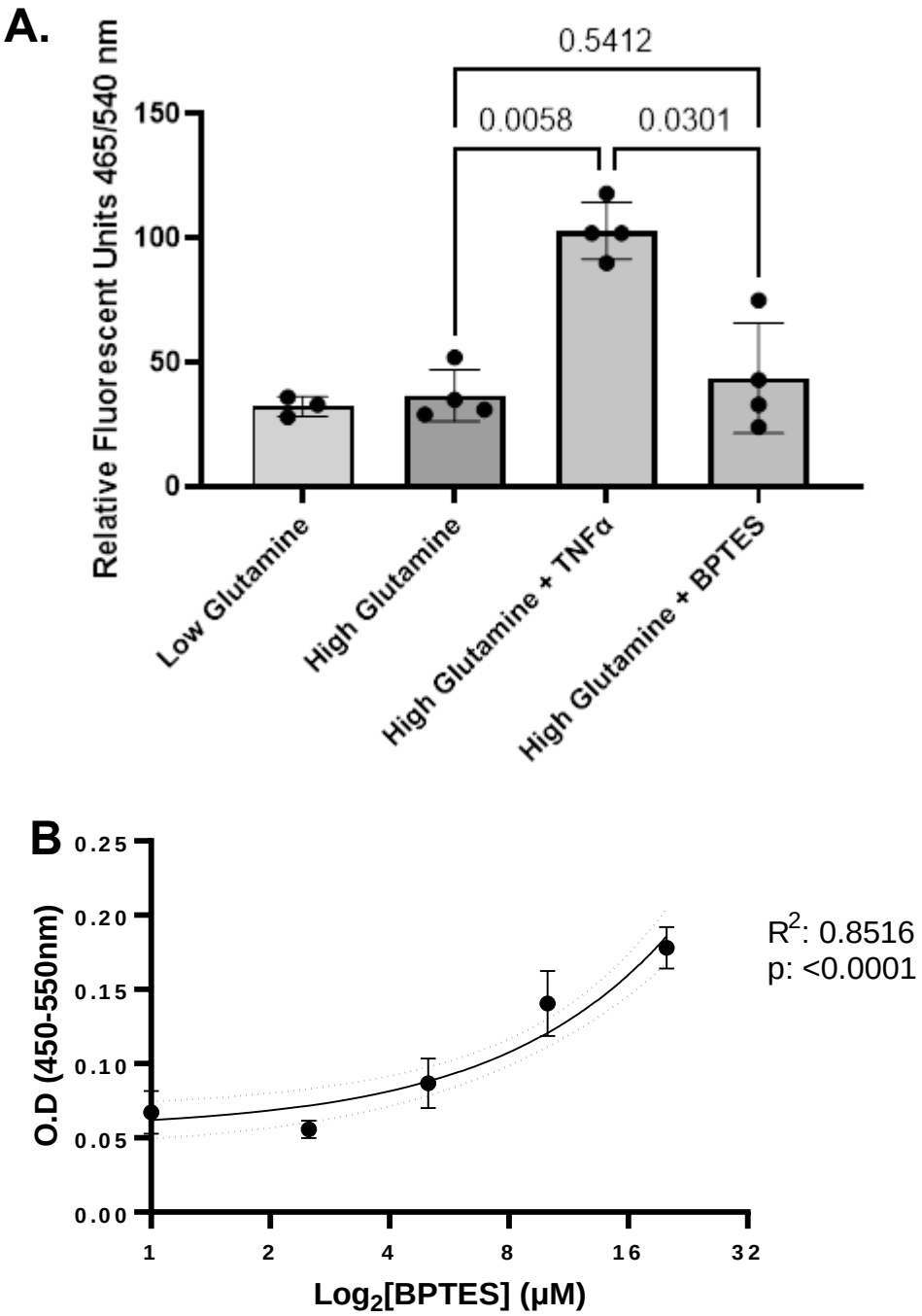

Figure 4.16: Short term GLS1 inhibition increases NAD(P)H-dependent oxidoreductase activity in dose-dependent manner but does not increase ROS generation

Fibroblasts from normal weight **(A)** and obese **(B)** patients were incubated with GLS1 inhibitor BPTES (2.5-20μM) for 1 hour show significant decrease in IL6 secretion (n = 4 biological replicates). IL6 secretion was measured using ELISA and absorbance was measured and normalised. All data presented as mean ± SD.

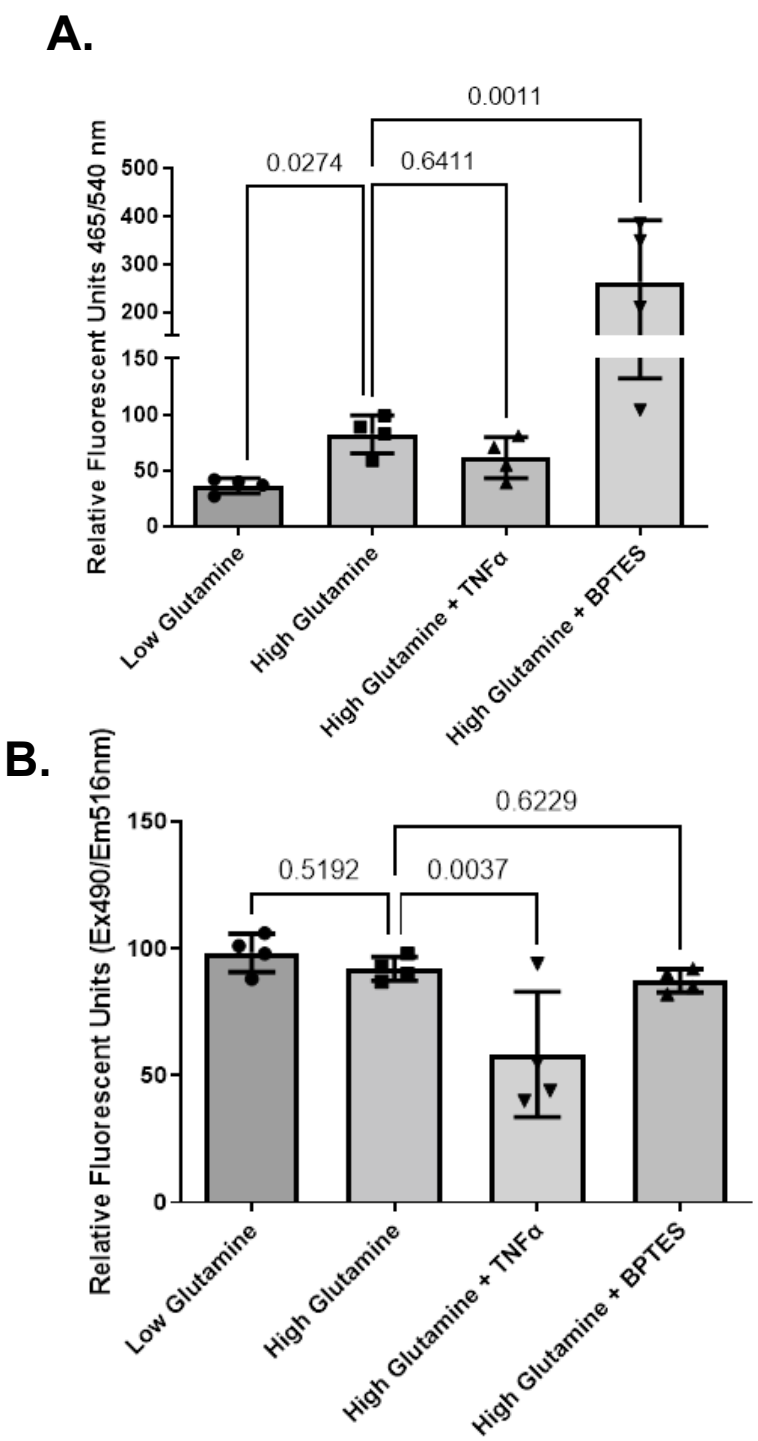

Figure 4.17: Glutamine supplementation and GLS1 inhibition increases glucose uptake but not mitochondrial mass

Fibroblasts were incubated low glutamine (2mM) or high glutamine (20mM) for 24 hours and stimulated with TNFα (10ng/ml for 24 hours) or with GLS1 inhibitor BPTES (20µM for 1 hour) (n = 4 biological replicates). A. Glucose uptake was measured using fluorescent glucose analog 6NBDG and B. mitochondria were stained using Mitotracker Green. Fluorescence was measured and normalised using vehicle control and background. All data presented as mean ± SD.

4.5 Discussion

Having identified glutamine-glutamate metabolism as the most significantly enriched metabolic pathway in obese OA patients following metabolomics analysis of OA synovial fluid, further investigation was undertaken to see whether this metabolic pathway influences the inflammatory profile of OA synovial fibroblasts as previously described in other cell types (Petrus *et al.*, 2020)

GLS1, a mitochondrial enzyme, has received much attention as a critical enzyme within the glutamine-glutamate metabolic pathway and therefore was the ideal target for inhibition of this pathway. Inhibiting GLS1 pharmacologically using BPTES in OA synovial fibroblasts reduced TNFα mediated IL6 secretion in normal weight OA synovial fibroblasts but not in obese OA synovial fibroblasts. This was an interesting development and a result which was concurrent with other experiments within this thesis (discussed further in chapters 5 and 6). This could be due to the inherent nature of the OA synovial fibroblasts in obese patients to be less responsive to TNFα stimulation. This reduced responsiveness could be a consequence of overstimulation as a result of the chronic low grade inflammation observed in obese state with the associated increased localised inflammation in obese OA joint, compared to normal weight OA joint (Dominika E. Nanus *et al.*, 2020). This link between glutamine-glutamate metabolism and IL6 mediated inflammation was confirmed with siRNA knockdown of GLS, indicating that the BPTES mediated amelioration of IL6 was not because of off-target effects but was indeed due to GLS inhibition. Another interesting development following short-term BPTES inhibition was an increase in NAD(P)H-dependent oxidoreductase activity (measured via MTS assay) after 1 hour. This link between NAD(P)H-dependent oxidoreductase activity and BPTES inhibition

might suggest changes in oxidation and reduction activity due to changes in NAD(P)H levels within OA synovial fibroblasts as a consequence of increased glycolysis. However, this would require further investigation before confirming this as the mechanism through increased NAD(P)H-dependent oxidoreductase activity.

Investigation into possible off-target effects of BPTES was investigated with experiments on cell proliferation and apoptosis. Long-term GLS1 inhibition resulted in cell death. However, short-term inhibition of GLS1 (1 hour) did not result in increased cell death or cell proliferation but did decrease IL6 levels in dose dependant manner in both obese and normal weight OA synovial fibroblasts. Breast cancer cell lines which underwent glutamine deprivation for 4 days have been reported to show increased oxidative stress, aberrant mitochondrial membrane potential and apoptosis induction (Gwangwa, Joubert and Visagie, 2019). This could also explain why altered cell morphology (membrane blebbing and apoptotic bodies) following 4 days GLS1 inhibition increased in the synovial fibroblasts in this thesis. Likewise, confirmation of recent work on the inhibition of glutaminolysis via BPTES and the increase in glucose consumption suggested BPTES inhibition of GLS1 was similar to that observed in other cell types and disease models (Elgogary *et al.*, 2016).

4.5.1 Limitations

As with the majority of studies, the design of the current study is subject to limitations. Amongst the limitations of this study is the quantification of cell death with long term inhibition of GLS1 visualised using phase contrast microscopy. Labelling with an antibody such as annexin V as a marker of apoptosis or staining with a marker of cell death like propidium iodide would have allowed for the quantification of cell death. However, as the fibroblasts are adherent cells, upon cell death there is

detachment which would not allow for cell staining. Likewise, due to low cell numbers a fourth condition of low glutamine and BPTES inhibition in the long-term culture experiment was not included.

Another limitation would be the low patient numbers used within this study and the use of fibroblasts cell line for the apoptosis flow cytometry. However, as the principal hypothesis for these experiments *in vitro* was mechanistic in nature and observing whether the treatment had an effect on the cells, the adoption of biological replicates was logical.

4.5.2 Future Studies

Having completed this study, there were areas of interest which were not pursued which could yield interesting insights into glutamine-glutamate metabolism and inflammation in OA synovial fibroblasts. Namely looking into the mechanism of how GLS1 inhibition drives changes in IL6 production and whether it effects the production of other cytokines and chemokines. This could be achieved by conducting a Luminex or multiplex based assay which would reveal any changes in cytokines and chemokines levels, thereby giving some information on non-IL6 mediated inflammation. Likewise, siRNA knockdown of GLS1 in myofibroblasts has been shown to reduce collagen 1 production (O'Leary *et al.*, 2020). Another potential area of investigation would be to look into markers of fibroblast function in OA synovial fibroblast such as collagen levels/ECM production following GLS1 inhibition or knockdown to see whether there is a similar effect.

CHAPTER 5

INTEGRATION OF THE SYNOVIAL FIBROBLAST TRANSCRIPTOME AND METABOLOME PROVIDES UNIQUE INSIGHTS TO PATHWAYS ASSOCIATED WITH OBESITY AND OSTEOARTHRITIS

5.1 Introduction

Osteoarthritis (OA) has historically been considered a “wear and tear” disease with degradation of articular cartilage being attributed to increased chronic biomechanical loading of the joint. On the other hand, rheumatoid arthritis (RA) is viewed primarily as a disease driven by synovial inflammation. Although OA does result in destruction of articular cartilage, a number of additional pathological changes that are associated with the development of OA have been overlooked, including the deleterious effects of chronic local inflammation of the synovial membrane (synovitis) (Tonge, Pearson and Jones, 2014; Mathiessen and Conaghan, 2017). This historically narrow view of OA as a non-inflammatory condition has likely hindered the development of disease-modifying OA drugs (DMOADs), with studies having predominantly focused on catabolic and anabolic pathways of cartilage tissue to limited success.

Recently, particular focus has been placed on understanding the molecular biology of OA, and there has been a change in perspective from degradation of cartilage as the only cause of disease towards investigation of causes from different tissues within the joint. One technique to deconvolute the molecular changes observed within the tissues of the OA joint is to use transcriptomics, i.e analysis of the complete set of RNA transcripts using next-generation sequencing techniques, such as RNA sequencing (RNAseq). For example, transcriptomic analysis of articular knee OA cartilage has been performed to better understand the heterogeneity of OA, identifying four distinct clusters (Yuan *et al.*, 2020). These 4 clusters were developed into a classification model that was correlated with OA symptoms, resulting in four distinct OA subtypes; glycosaminoglycan metabolism disorder,

collagen metabolism disorder, activated sensory neurons and inflammation (Yuan *et al.*, 2020). This suggests transcriptomic analysis, when paired with patient characteristics data, can yield insights into the pathways and molecular mechanisms that drive OA pathology and provide potential stratification of knee OA patients, which will facilitate the development of DMOADs.

Transcriptomic analysis has been applied to primary human OA chondrocytes cells (Ji *et al.*, 2019). To define cell populations and identify genome-wide gene expression patterns, 1,464 chondrocytes were sequenced at single cell resolution and were compared with clinical outcome using severity index (Ji *et al.*, 2019). Different subsets of chondrocytes were identified, including “proliferative chondrocytes”, “pre-hypertrophic chondrocytes” (pre-HTCs), “hypertrophic chondrocytes” (HTCs) and three novel populations; “effector chondrocytes” (ECs), “regulatory chondrocytes” (RegCs) and “homeostatic chondrocytes” (HomCs) (Ji *et al.*, 2019). Gene set enrichment analysis (GSEA) found an increase in metabolic pathways such as steroid biosynthesis, fatty acid metabolism, mTOR signalling and chemokine signalling in EC’s compared to RegCs (Ji *et al.*, 2019). The RegC population of cells showed enrichment of cell signalling pathway regulation such as Toll-like receptor, mTOR, TGF-β, p53, JAK/STAT, WNT and chemokine signalling (Ji *et al.*, 2019). Finally, HomCs enriched mainly with process relating to maintaining cellular homeostasis through regulation of the cell cycle, development, RNA metabolism and biosynthesis (Ji *et al.*, 2019). The relationship between these OA chondrocytes disease severity was determined using a combination of Hospital for Special Surgery (HSS) knee scoring system and the scoring of cartilage using Osteoarthritis Research Society International (OARSI) and International Cartilage Regeneration and Joint Preservation Society (ICRS) grading system. In total, 336

predictive genes were identified and classified into those associated with favourable outcomes (199) and unfavourable outcomes (137) (Ji *et al.*, 2019). Favourable genes were found mainly expressed in ECs, RegCs and HomCs cell populations, whereas unfavourable genes were expressed in a large proportion of ProCs, pre-HTCs and fibrocartilage chondrocytes (Ji *et al.*, 2019). By creating a cell atlas of cartilage OA chondrocytes, with their respective transcriptional programmes and their relationship to disease severity, we are improving our understanding of the disease pathology and this may provide the rationale for new personalised therapeutic strategies.

Alongside transcriptomic analysis of OA chondrocytes, synovial fibroblasts isolated from the synovium of OA patients have also been subjected to similar high-throughput sequencing. Obese patients have been shown to have higher levels of pro-inflammatory cytokines in OA synovial fluid and to exhibit synovial fibroblasts with a more inflammatory phenotype (Pearson *et al.*, 2017). Bulk RNA sequencing of OA synovial fibroblast from obese patients (BMI ≥30) compared to normal weight patients (BMI 18-24.9) found inflammatory pathways were the most upregulated canonical pathways in obese OA patient's fibroblasts which included cytokine–cytokine interactions, nucleotide-binding oligomerization domain–like receptor signalling, Toll- like receptor signalling, and chemokine signalling pathways (Nanus *et al.*, 2020). When comparing normal weight and obese hip OA patients synovial fibroblasts, 19 differentially expressed long-non coding (lnc) RNAs were identified, 9 upregulated long intergenic non-coding RNAs (lincRNAs) and 6 downregulated lincRNAs with MALAT1 demonstrating the largest absolute increase in expression (Nanus *et al.*, 2020). MALAT1 was the most responsive lincRNA to pro-inflammatory challenge and was transiently increased suggesting it may play a role in regulating

synovial fibroblast inflammation. Indeed, depletion of MALAT1 reduced proliferative capacity of synovial fibroblast as well as CCL8 expression indicating that targeted inhibition of MALAT1 in the synovial joint could both reduce synovial inflammation and hyperplasia (Nanus *et al.*, 2020). However, this study was only in hip OA patients, and further characterisation of the transcriptome of OA fibroblasts from different joints including non-load bearing joints could reveal globally altered OA signalling pathways or lncRNAs common to obesity.

Animal models are widely used to study joint biology and allow the opportunity to study early stages of OA. Such studies are difficult in humans, where access to joint tissues are largely limited to patients undergoing arthroscopy and/or total joint replacement in patients with late-stage disease. RNA sequencing has been used in murine models to investigate post-traumatic osteoarthritis (PTOA) (Sebastian *et al.*, 2018). Three different mouse strains with varying susceptibility to OA, STR/ort (highly susceptible), C57BL/6J (moderately susceptible), and MRL/MpJ (not susceptible), underwent a non-invasive tibial compression (TC) injury model which represents anterior cruciate ligament (ACL) rupture in humans (Sebastian *et al.*, 2018). In the highly susceptible STR/ort model, 497 genes were upregulated compared to the moderately susceptible C57BL/6J and not susceptible MRL/MpJ mice (Sebastian *et al.*, 2018). GO analysis found that 33 of those genes were associated with inflammatory responses and 78 genes were associated with apoptotic processes (Sebastian *et al.*, 2018). Several members of the Wnt signalling pathway, which are intricately associated with skeletal development and bone metabolism, were upregulated in all strains at weeks 1 and 2 post-injury (Sebastian *et al.*, 2018). Previous research has shown inflammatory programs following joint injury may be a key factor in the progression of PTOA (Sokolove and Lepus, 2013).

This study shows that pre-injury STR/ort joints expressed elevated inflammatory markers (IL1β, IL6, CCL2, and CXCL1) and post-injury these same inflammatory markers were further amplified suggesting persistent inflammation could be a major factor in PTOA (Sebastian *et al.*, 2018).

High-throughput single cell RNA sequencing (scRNA-seq) has also been performed on primary chondrocytes from the ACL injury murine OA model compared to healthy controls in order to identify and stratify chondrocyte subtypes within OA (Sebastian *et al.*, 2021). Although cartilage appeared histologically normal at 3 days post injury, scRNA-seq analysis identified several significant injury-induced transcriptional changes in chondrocyte subpopulations (Sebastian *et al.*, 2021). Transcripts encoding for enzymes involved in oxidative phosphorylation pathways were significantly enriched 3 days post injury suggesting early metabolic changes in these cells are upregulated post injury and could suggest reactive oxygen species (ROS) produced by OXPHOS could contribute to cellular stress and reduced chondrocyte viability early in OA development (Sebastian *et al.*, 2021). During the analysis, 9 transcriptionally distinct chondrocyte subpopulations were identified and in an attempt to evaluate the extent of cross-species translatability, the murine chondrocyte subtypes were compared to human chondrocytes isolated from OA cartilage resulting in 6 mouse chondrocyte subtypes, which had highly molecular fidelity to the human subtypes (Sebastian *et al.*, 2021). The next steps in *in vivo* testing of these ACL mice would involve identifying which of these 6 subtypes are actively involved in cartilage degradation and knocking out key genes which are highly involved in these chondrocyte subtypes to discover whether this may ameliorate or reverse the disease course early on in OA development.

In summary, transcriptomic analysis of OA joint tissues, including single cell RNA sequencing, is yielding novel insights into resident cell populations and the changes these cells undergo during disease pathology. By targeting these altered pathologic cell populations, through future therapeutic treatments, there could be opportunities to ameliorate the disease course observed in OA, intervening at an early stage to avoid the progression and requirement for the invasive joint replacement surgery.

5.1.2 Biomechanical loading of joint

Although much of the data within OA points towards a multi-faceted pathology in OA, there is no doubt biomechanical loading does play a role in shaping the transcriptome of joint resident cell types. Previous research has focused on the role chemical stimuli, adhesion signals, transcription factors and how their co-regulators control transcriptional regulation however the use of chemical signalling alone does not provide spatiotemporal control of transcriptional activities within tissues and organs. Cells will sense mechanical cues such as physical forces (tension, compression or shear stress), extracellular matrix mechanics and alterations in cell morphology and will modulate transcriptional activities to respond to these changes in environment (Mammoto, Mammoto and Ingber, 2012). Mechanosensitive transcriptional control mechanisms are known to contribute to the maintenance of pluripotency, determination of cell fate, pattern formation and organogenesis as well as controlling cellular function throughout embryogenesis and in adulthood (Mammoto, Mammoto and Ingber, 2012). The human joint undergoes several distinct types of mechanical loads throughout the lifetime- including tension, compression, fluid shear, and/or torsional shear stresses, all of which chronically may induce cartilage damage resulting in OA. Researching the effect of these mechanical cues

on resident cells of the joint, such as fibroblasts and chondrocytes, would elucidate the pathological changes which occur due to repeated load through physical forces on the joint such as through biomechanical loading and those which are due to other contributing factors to OA pathology.

Another determinant of fibroblast transcriptional diversity is based on anatomical position within tissues and organs. Fibroblasts have site-specific variations in gene expression that are associated with their positional/geometric identities in three dimensional axis; namely anterior-posterior, proximal-distal, and dermal versus non-dermal (Rinn *et al.*, 2006). Likewise, these adult fibroblasts are known to maintain key features of *HOX* gene expression patterns, which are established during embryogenesis (Chang *et al.*, 2002; Rinn *et al.*, 2006). Fibroblasts isolated from human vocal folds (VFF) are exposed to high inertial stresses and are therefore are ideal for comparison to fibroblast isolated from tissues which remain absent of such mechanical trauma (Titze *et al.*, 2004). Transcriptomic analysis of VFFs have upregulation of several functional themes, which varied across transcription factors for signalling pathways regulating pluripotency of stem cells, ECM components of cell signalling, migration, proliferation, and differentiation potential when compared to fibroblast isolated from neighbouring tissues with shared developmental origins but which do not normally undergo similar high inertial stresses (Foote *et al.*, 2019). Murine synovial fibroblasts from knee (lineage descending from mesoderm) and temporomandibular joint (TMJ) (lineage descending from ectoderm) treated *in vitro* with experimental dynamic stretching assay as a model of mechanical stress, underwent gene expression profiling via RT-qPCR (Nazet *et al.*, 2021). Gene expression profiles due to different dynamic stretching protocols are strongly dependant on the origin of synovial fibroblast, with those derived from TMJ having a

reduced *Rankl/Opg* gene expression ratio after moderate and mixed dynamic stretching (Nazet *et al.*, 2021). Notably, knee-derived synovial fibroblasts which underwent moderate stretching exhibited increased *Ptgs2* and *IL1-Ra* gene expression which was not observed in TMJ derived synovial fibroblast. Demonstrating that mechanical forces can have a differential effect on the inflammatory profile of fibroblasts derived from different joints (Nazet *et al.*, 2021). Murine synovial fibroblasts maintain distinct *HOX* gene expression, which corresponds to anatomical origin suggesting *HOX* gene expression may influence inflammation via NF-κB pathway while tissue specific expression patterns of inflammation and cell-cell interactions are aggravated by mechanical stress (Frank-Bertoncelj *et al.*, 2017; Nazet *et al.*, 2021).

Animal models of mechanical stress have also been applied to other cell types within the joint. Mechanical stress applied to IL-1β-induced rodent chondrocytes using a four-point bending device were subjected to RNA sequencing analysis (B. Xu *et al.*, 2019; Zhang *et al.*, 2022). Transcriptomal analysis found 5,022 differentially expressed mRNAs, 88 differentially expressed micro RNAs, 1,259 differentially expressed lncRNAs and 393 differentially expressed circRNAs (Zhang *et al.*, 2022). KEGG enrichment analysis of lncRNAs found enrichment of cAMP signalling pathway, insulin signalling, PPAR signalling, glycine, serine and threonine metabolism and apoptosis suggesting a link between mechanical stress and cellular metabolism (Zhang *et al.*, 2022). Chondrocytes are known to be involved in the immune response by altering T cell proliferation and indirectly inhibiting monocyte differentiation (Pereira *et al.*, 2016) however this study demonstrated involvement in immune pathways in chondrocytes undergoing mechanical stress which could

possibly underlie immune-relevant mechanism of chondrocytes in OA pathogenesis (Zhang *et al.*, 2022)

5.1.3 The use of integrative Multi-Omics in Inflammatory Joint Diseases

In recent years, due to the availability and economic feasibility of the technologies, there has been an exponential increase in studies featuring multi-omics, which has been greatly facilitated by analytical tools for data integration. Within the OA field, a recent study by Steinberg et al, employed the use of epigenomic, transcriptomic and proteomic analysis on primary chondrocytes isolated from knee and hip OA articular cartilage from degraded (high OARSI grade score) compared to “normal” (low OARSI grade score) cartilage (Steinberg *et al.*, 2017). DNA methylation and RNASeq were utilised to identify differentially methylated regions (DMRs) and DEGs, which, with a cut-off at a false discovery rate (FDR) of 5%, resulted in 271 DMRs and 349 DEGs respectively (Steinberg *et al.*, 2017). Proteomics on these same samples found 209 proteins, with evidence of differential abundance and subsequent GO annotation of these proteins found 31 proteins that were also differentially expressed at the RNA level (Steinberg *et al.*, 2017). Five of these genes were overexpressed in the degraded tissue including *COL4A2, CXCL12, FGF10, HTRA3* and *WNT5B* (Steinberg *et al.*, 2017). Pathway analysis using KEGG libraries and Reactome found extracellular matrix organisation, collagen catabolism and angiogenesis as biological pathways significantly associated with disease progression (Steinberg *et al.*, 2017). Having identified these regions and pathways of interest, they next sought to identify existing therapeutics as candidates for repurposing. Of the 49 genes that were differentially regulated, 10 drug agents with investigational or established

actions on 9 of the dysregulated proteins (which are already FDA approved) were identified including NSAIDs against prostacyclin synthase, which is already authorised for symptomatic treatment of OA, phylloquinone (vitamin K1) and Periostin (Vitamin K dependant protein induces cartilage degradation) (Steinberg *et al.*, 2017). This study shows the integrative functional genomics approach when applied to disease relevant tissue and cells may provide potential therapeutic targets and highlight existing therapies that may have clinical efficacy in OA (Steinberg *et al.*, 2017).

As a result of its common comparison to RA, the focus on identifying systemic factors which contribute to OA disease development and progression hasn't been as popular. However, when compared to healthy controls, there are several systemic changes to circulating metabolites which are associated with OA (Huang *et al.*, 2020). However, identifying systemic changes in OA patients and then finding the connection between these alterations and

local changes at the OA joint tissues has been particularly challenging. Multi-omics data analysis using plasma untargeted metabolomics data from 12 OA patients compared to 20 healthy controls and synovial tissue transcriptomic dataset (GSE55235) of 10 OA patients and 10 healthy controls underwent limited integrative analysis and found 58 differential metabolites and the 726 DEGs (Huang *et al.*, 2020). Subsequent analysis using MetaboAnalyst, found enrichment of pathways including T cell receptor signalling pathway, c epsilon RI (FcεRI) signalling pathway and thermogenesis (Huang *et al.*, 2020). Pathways associated with inflammation, joint destruction and energy metabolism were also identified which provides confirmation of the pathophysiological changes observed in other OA related studies (Huang *et al.*, 2020). When investigating potential metabolic pathways, three metabolites including succinic acid, xanthurenic acid and L-tryptophan were altered in OA, which could potentially be diagnostic biomarkers in OA patients (Huang *et al.*, 2020). However, an issue with this study was the lack of integrative analysis which could be performed on these datasets, with the conclusions drawn using conceptual integration only and an increase in patient numbers would be required before labelling these metabolites as circulating biomarkers of OA.

Although OA is the most common chronic condition associated with ageing, obesity and progressive joint dysfunction, it does not have approved disease-modifying drugs, emphasizing a clear unmet need. To meet this need, likely requires a paradigm shift in our understand of OA, including identifying the pathological changes to cells within the joint that contribute to tissue dysfunction and disease progression. The shift towards employment of these high-throughput techniques to map out and understand OA pathology has begun to yield interesting insights into

OA pathology, and through these means, potential therapeutic interventions may arise.

The approach conducted within this thesis used bulk RNA sequencing of OA patient synovial fibroblasts isolated from OA at different joint sites and in both lean and obese OA patients to identify the role obesity, load-bearing and anatomical site plays in the altered OA synovial fibroblast cellular phenotype.

5.2 Hypothesis

We hypothesised that

- Transcriptomics analysis of hip OA synovial fibroblast from normal weight and obese patients would reveal differentially expressed genes within enriched metabolic pathways identified in OA synovial fibroblast conditioned media from normal weight and obese patients
- Transcriptomics analysis of normal weight and obese OA synovial fibroblast from different joints would reveal common altered metabolic pathways
- Joint pathway analysis using transcriptomics and metabolomics data from normal weight and obese hip OA synovial fibroblasts will reveal significantly enriched metabolic pathways

5.3 Methods

5.3.1 Patient Characteristics and Anthropometric Data

Table 5.1 Patient Characteristics Data

1.	**Normal Weight (N = 11)**	**Obese (N = 12)**	**P Value**	**Load Bearing (n = 18)**	**Non-loadbearing (n =6)**	**P Value**
Age (years)	65.8 ± 9.26	63.92 ± 8	0.606	66.67 ± 8.34	58.17 ± 4.96	0.025
Female:Male	8:3	8:4		12:6	4:2	
BMI (kg/m^2)	22.95 ± 1.56	33.77 ± 1.96	<0.000001	28.63 ± 5.81	28.14 ± 5.78	0.810
Weight (kg)	60.37 ± 5.55	92.78 ± 12.1	<0.000001	78. 08 ± 19.69	77.03 ± 17.36	0.974
Height (cm)	162.2 ± 8.03	164.47 ± 10.36	0.575	163.77 ± 9.73	165.65 ± 11.28	0.986

1. Shapiro-Wilk and Kolmogorov-Smirnov Normality test computed to test for normal distribution of data. Multiple unpaired t test with Welch correction performed for normal weight vs obese comparison. Multiple Mann-Whitney t test performed for loadbearing vs non-loadbearing comparison

5.4 Results

Transcriptomics analysis was conducted on primary human OA synovial fibroblasts from normal weight (BMI 18.5 to 24.9) and obese (BMI ≥30) patients undergoing joint replacement surgery for the hip, knee, foot and hand. Following Bulk RNA sequencing of these OA synovial fibroblasts, differential expression analysis and $\log_2$ fold change data was computed using DESeq2 R package (Love, Huber and Anders, 2014). Data was visualised using Venn diagram comparing differentially expressed genes identified in OA synovial fibroblast within obesity to those found in loadbearing joints (hip, knee and foot) compared to non-loadbearing joints (hand) (figure 5.1). 726 genes were found to be differentially expressed in obesity within OA synovial fibroblasts and 819 genes were differentially expressed in loadbearing joints when compared to non-loadbearing joints within OA synovial fibroblasts (figure 5.1). Amongst those genes were 19 DEGs were shared across obesity and loadbearing comparison (figure 5.1).

Figure 5.1: Venn Diagram of differentially expressed genes in obesity and loadbearing OA synovial fibroblasts

Fibroblasts from obese vs normal weight (n = 18) compared to load bearing vs non-load bearing (n= 6) with $\log_2$ fold change ≥0.48 or ≤-0.48 and with p value >0.05 (Heberle *et al.*, 2015).

GENE ID	LOG_2FC OB	P VALUE	LOG_2FC LB	P VALUE	DAVID GENE NAME
AC005410.2	2.32	0.03	-6.37	0.05	N/A
AC015712.2	-3.06	0.01	-4.88	0.03	N/A
AC025164.1	4.29	0	-5.72	0.01	N/A
ADAM12	-1.09	0.05	-1.49	0	ADAM metallopeptidase domain 12
ANKRD40	0.77	0.05	0.81	0.02	ankyrin repeat domain 40
DNAJC10	-0.35	0.05	-0.41	0.02	DnaJ heat shock protein family (Hsp40) member C10
EFHD1	1.85	0.04	6.98	0 .003	EF-hand domain family member D1
IL32	0.97	0.04	-1.03	0.05	interleukin 32
LRRC8C	-2.78	0.05	-4.37	0.01	leucine rich repeat containing 8 VRAC subunit C
MAP3K11	3.34	0.01	-3.19	0.01	mitogen-activated protein kinase 11
MASTL	-3.58	0.01	-4.17	0	microtubule associated serine/threonine kinase like
NAB1	-1.59	0.03	-0.91	0.01	NGFI-A binding protein 1
PCF11	-0.99	0.04	-1.05	0.01	PCF11 cleavage and polyadenylation factor subunit
PIGA	2.79	0.04	-7.03	0	phosphatidylinositol glycan anchor biosynthesis class A
PSMA5	1.44	0.03	-1.1	0.03	proteasome 20S subunit alpha 5
SLC13A3	-2.65	0.02	-6.59	0.01	solute carrier family 13 member 3
SNAPC4	-2.71	0.02	-2.81	0.02	small nuclear RNA activating complex polypeptide 4
TAOK1	0.35	0.04	-0.4	0.04	TAO kinase 1
TFEB	-2.11	0.04	-5.59	0.01	transcription factor EB

Table 5.2: Shared differentially expressed genes in obesity (OB) and loadbearing (LB) comparison

Likewise, a more in-depth analysis of the data was conducted to examine whether there were any DEGs shared across different joints in obese compared to normal weight OA synovial fibroblasts (figure 5.2). From the analysis, 547 genes were found to be differentially expressed in hip OA, 631 genes were found to be differentially expressed within knee OA, 620 genes were found to be differentially expressed in foot OA and 661 genes were found to be differentially expressed in hand OA (figure 5.2). There were no shared DEGs found in all 4 comparisons across the different joints with respect to obesity.

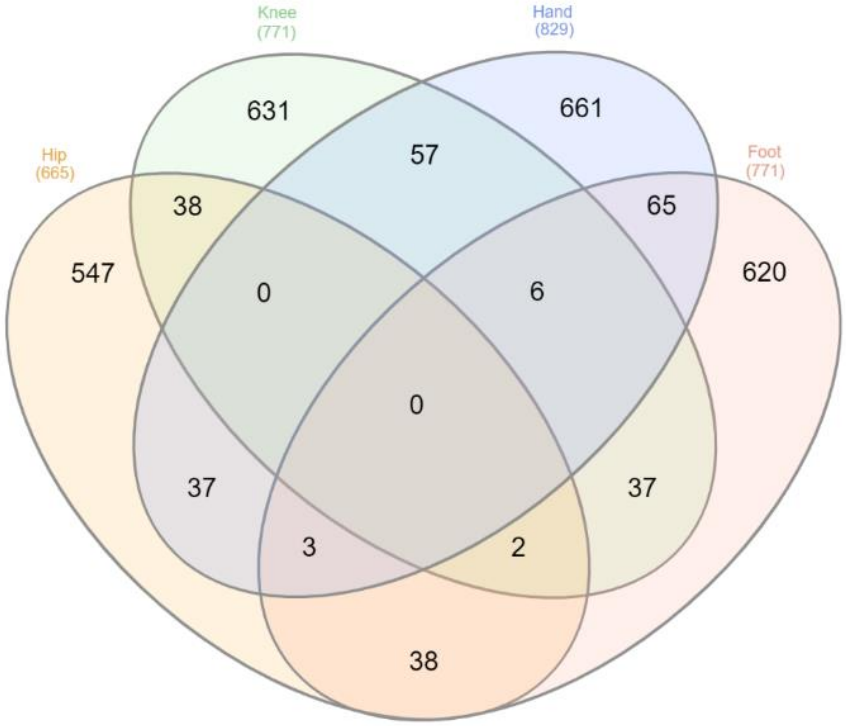

Figure 5.2: Venn diagram of differentially expressed genes (DEGs) in OA synovial fibroblasts from different joints

Analysis of fibroblasts from obese compared to normal weight in hip (n= 6), knee (n= 6), foot (n= 6) and hand (n= 6) with $\log_2$ fold change ≥0.48 or ≤-0.48 and with p value >0.05 (Heberle *et al.*, 2015).

5.4.1 Heatmaps of metabolic pathways identified within metabolomics data of OA synovial fibroblast

Following general analysis of the RNA sequencing data, one question which arose from metabolomics analysis of this data (as mentioned previously within Chapter 1) was whether the proteins and enzymes involved in the enriched metabolic pathways for obese and normal weight OA synovial fibroblast secretomes following TNFα stimulation, were also differentially expressed. To that end, the gene names for these proteins and enzymes were manually filtered and verified using PANTHER functional classification gene list analysis. This pathway analysis was not restricted only to OA synovial fibroblast hip patients but included other OA synovial fibroblasts from different joints to determine whether any obesity associated changes were globally dysregulated or specific to particular anatomical joint sites. The first metabolic pathway investigated was the glycolysis/gluconeogenesis KEGG pathway (map00010) as shown in heatmap form (figure 5.3). Hierarchical clustering analysis of different genes within this pathway did not reveal any clearcut underlying differences in gene expression of OA synovial fibroblast from normal weight and obese patients or within different joints however there was a high expression of alpha enolase (ENO1), lactate dehydrogenase (LDHA) and pyruvate kinase (PKM) across all comparisons relative to expression of other genes within pathway and a slight increase in ALDH2 expression in obese hip compared to normal weight hip OA synovial fibroblast. On the other hand, there was low expression of ALDH7 and ALDH3B2 expression across all comparisons relative to expression of other genes within pathway (figure 5.3).

Another pathway which was highly enriched within the metabolome of OA synovial fibroblast conditioned media (for both obese and normal weight patients) was the Aminoacyl tRNA biosynthesis KEGG pathway (map00970). Hierarchical clustering analysis of this pathway identified a set of highly expressed aminoacyl tRNA synthetase compared to other genes within pathway, which include Threonyl-tRNA synthetase (TARS), Tryptophanyl-tRNA synthetase (WARS), Asparaginyl-tRNA synthetase (NARS) and Leucyl-tRNA synthetase (LARS).,However, there were no clear-cut differences in obesity of OA synovial fibroblasts from different joints (figure 5.4).

Another common pathway altered in hip OA synovial fibroblast metabolome was serine, glycine, and threonine metabolism (map00260). Similar hierarchical clustering analysis was applied to this KEGG pathway and found relatively high expression of Phosphoserine Aminotransferase 1 (PSAT1) which is increased in obese knee OA synovial fibroblasts compared to normal weight samples and Serine hydroxymethyltransferase 2 (SHMT2) (figure 5.5).

The final pathway which was significantly enriched within OA synovial fibroblast metabolome of hip patients was alanine, aspartate and glutamate metabolism (map00250). Hierarchical clustering analysis of this metabolic pathway found relatively higher expression of Glutaminase (GLS) in obese hip and knee samples and increased expression of Glutamine synthetase (GLUL), however there was a decrease in expression of Glutamate dehydrogenase 2 (GLUD2) and Glutamate decarboxylase 2 (GAD2) enzymes (figure 5.6).

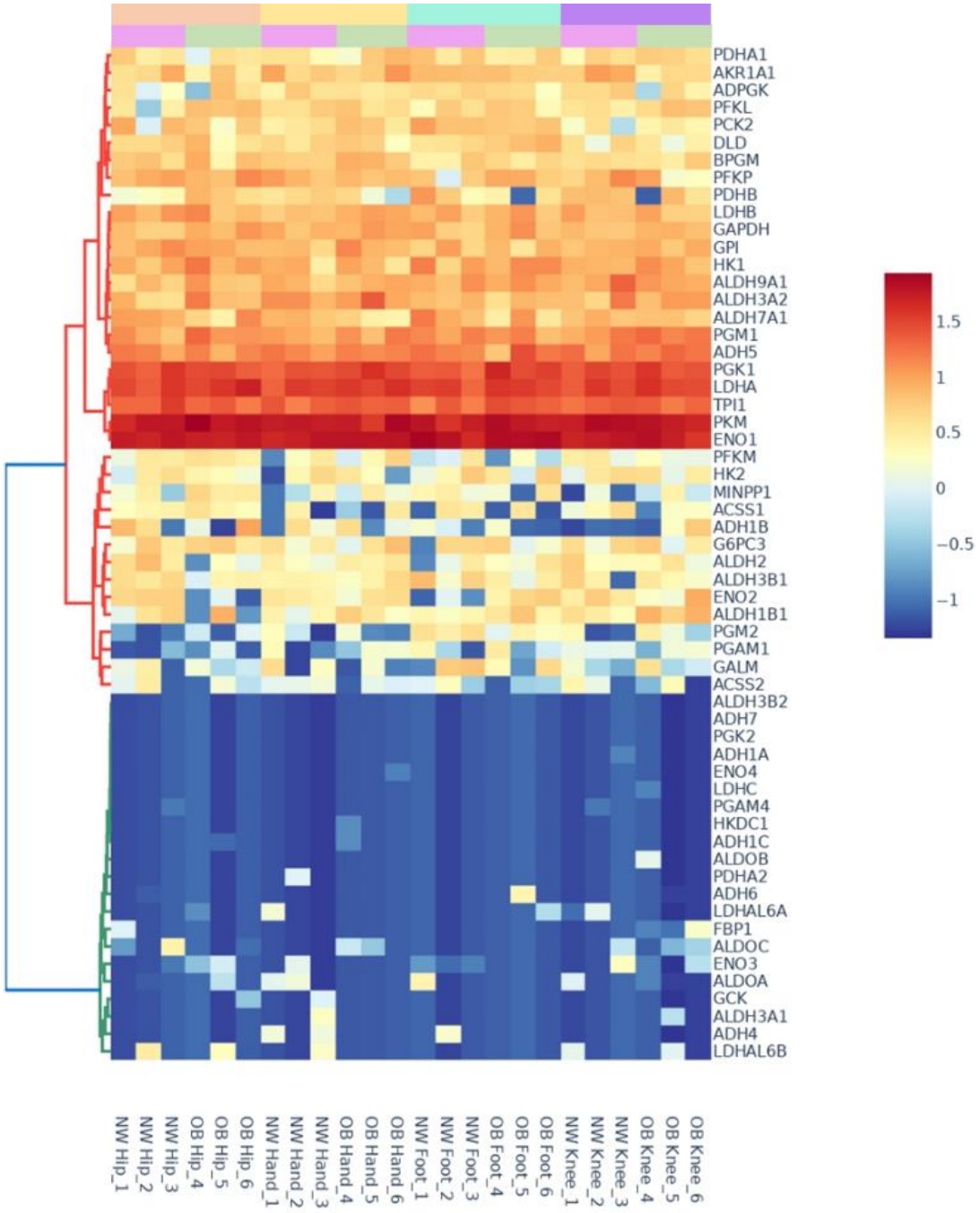

Figure 5.3: Differential Gene Expression of Glycolysis/Gluconeogenesis KEGG pathway

Normalised counts from bulk RNA sequencing data of OA synovial fibroblasts from hip (n = 6) (orange), knee (n = 6) (purple), hand (n = 6) (yellow) and foot (n = 6) (cyan) and different BMI's (normal weight (NW) as pink and obese (OB) in green). Hierarchical Clustering analysis conducted using dendrogram for row clusters using the ward method and cluster distance set as Euclidean. Log_2 transformation of data was utilised to aid interpretation due to large differences in expression levels (counts) of different genes.

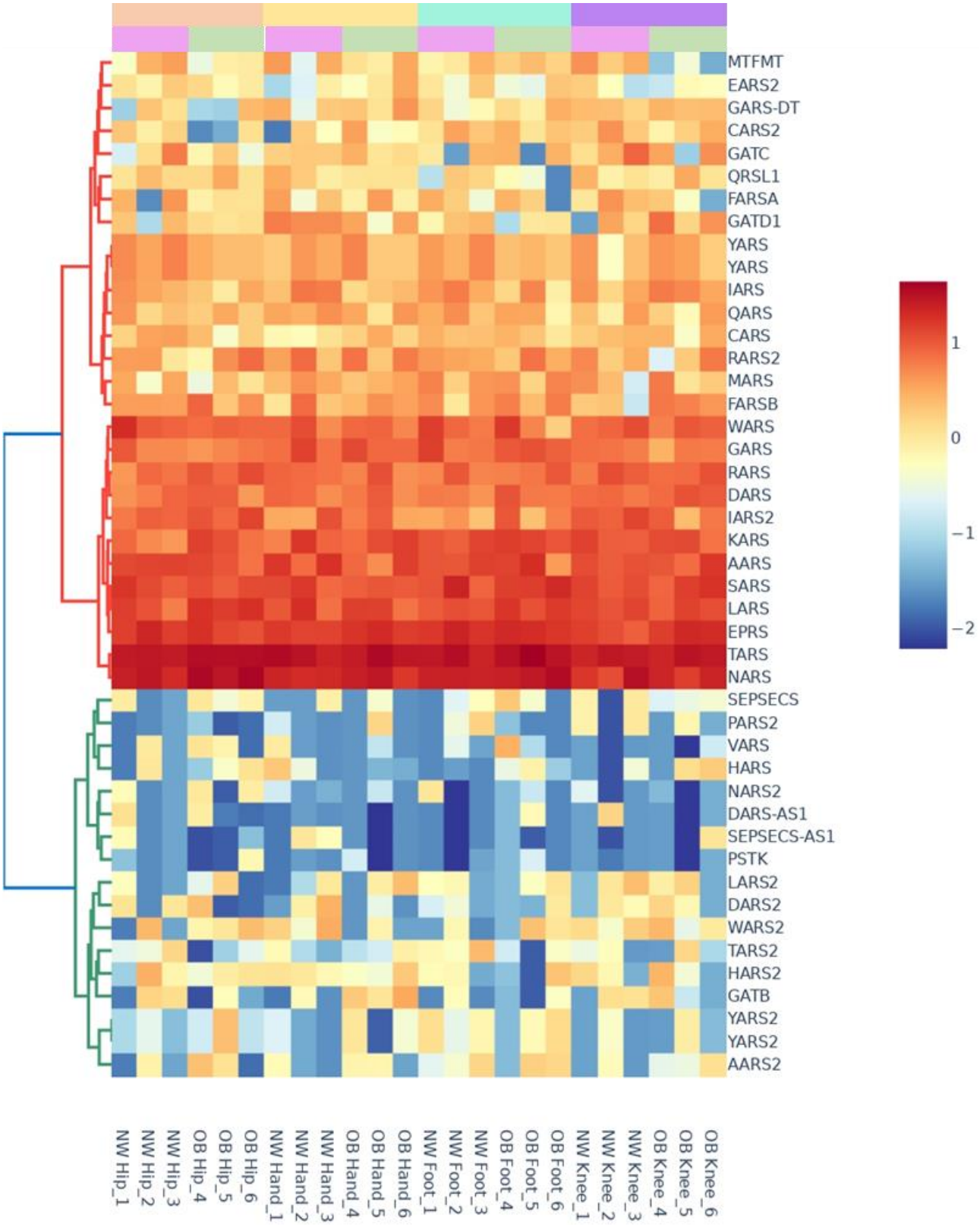

Figure 5.4: Differential Gene Expression of Aminoacyl-tRNA Biosynthesis KEGG pathway

Normalised counts from bulk RNA sequencing data of OA synovial fibroblasts from hip (n = 6) (orange), knee (n = 6) (purple), hand (n = 6) (yellow) and foot (n = 6) (cyan) and different BMI's (normal weight (NW) as pink and obese (OB) in green). Hierarchical Clustering analysis conducted using dendrogram for row clusters using the ward method and cluster distance set as Euclidean. Log_2 transformation of data was utilised to aid interpretation due to large differences in expression levels (counts) of different genes.

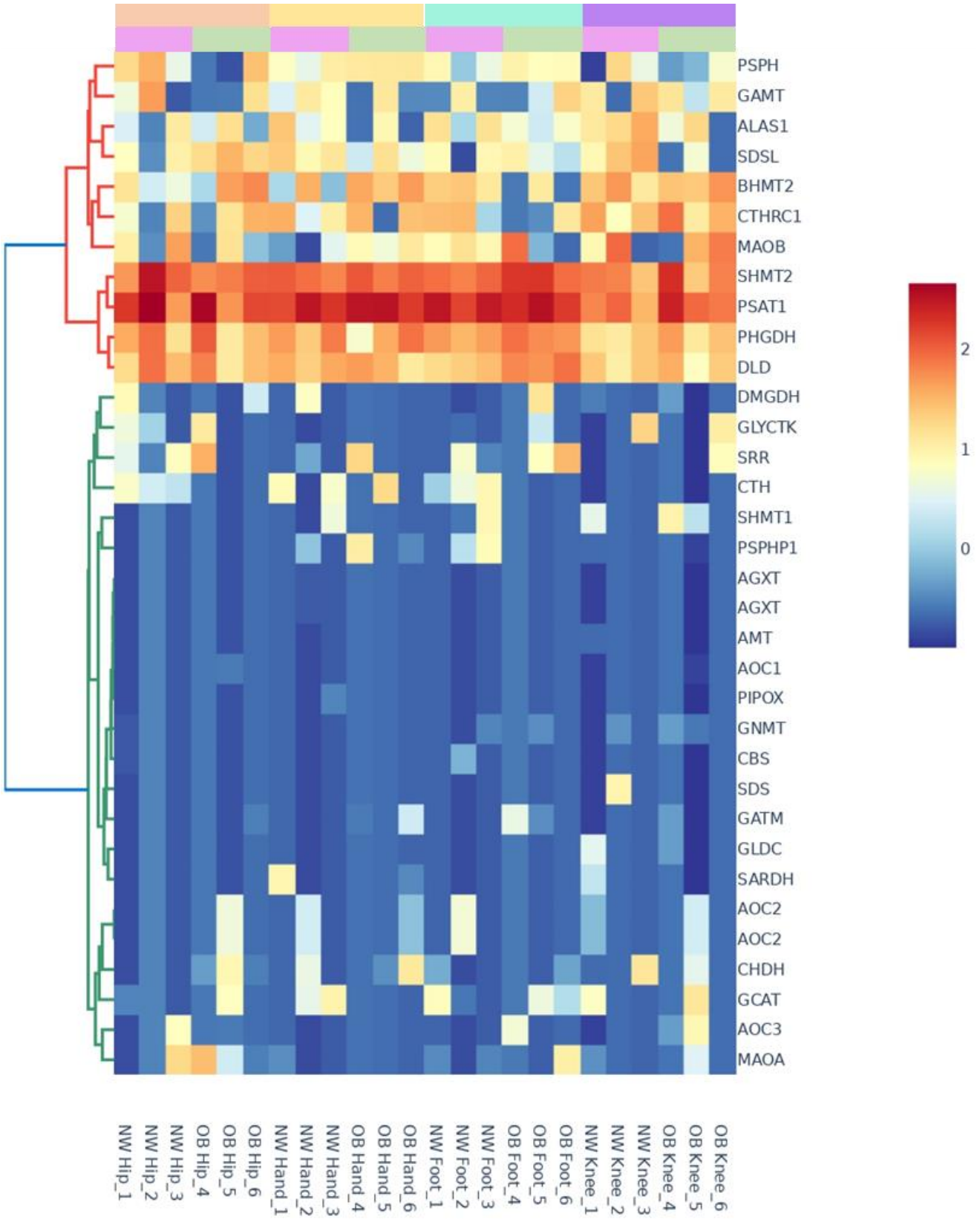

Figure 5.5: Differential Gene Expression of Serine, Glycine and Threonine metabolism KEGG pathway

Normalised counts from bulk RNA sequencing data of OA synovial fibroblasts from hip (n = 6) (orange), knee (n = 6) (purple), hand (n = 6) (yellow) and foot (n = 6) (cyan) and different BMI's (normal weight (NW) as pink and obese (OB) in green). Hierarchical Clustering analysis conducted using dendrogram for row clusters using the ward method and cluster distance set as Euclidean. Log_2 transformation of data was utilised to aid interpretation due to large differences in expression levels (counts) of different genes.

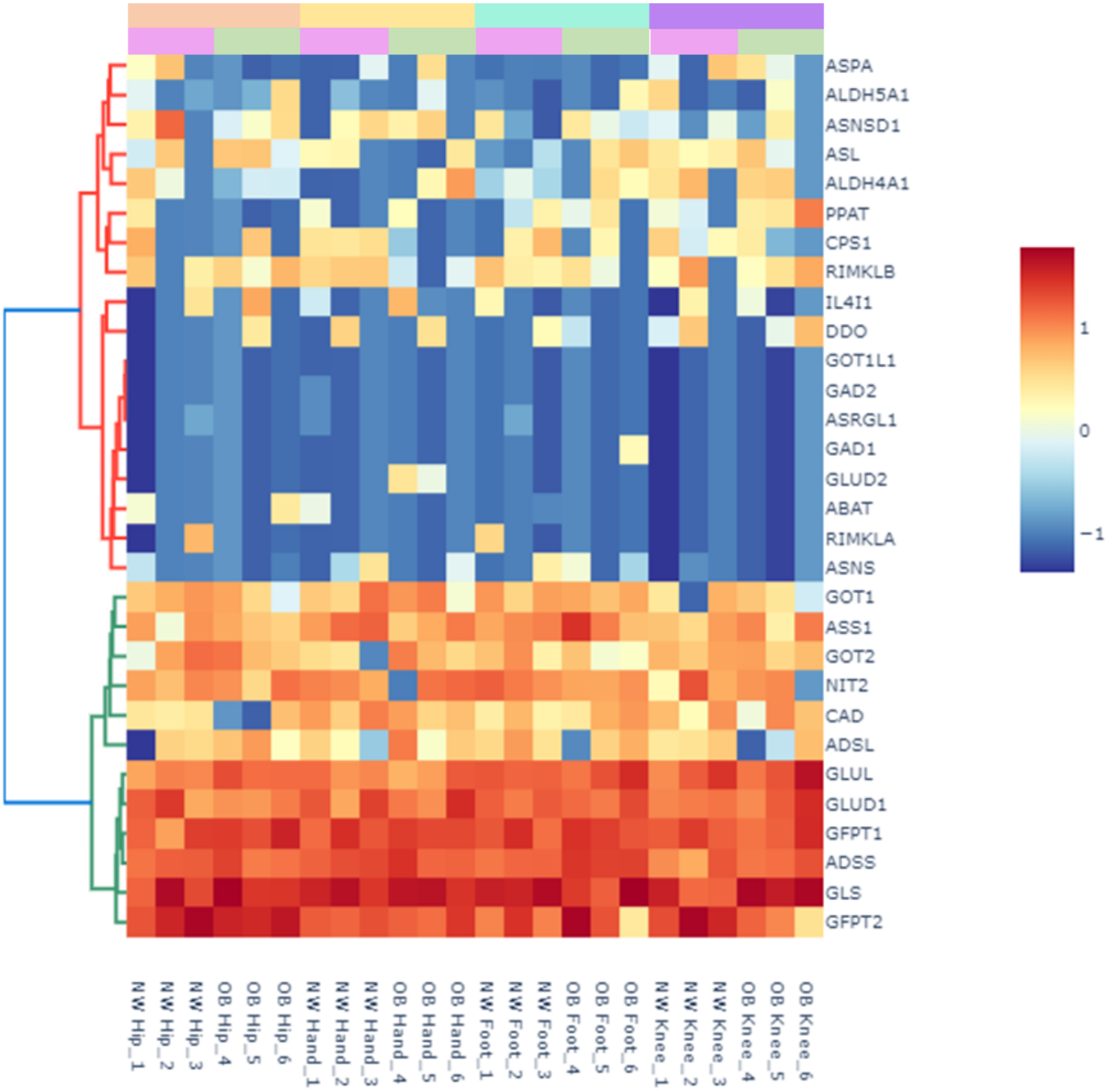

Figure 5.6: Differential Gene Expression of Alanine, Aspartate and Glutamate metabolism KEGG pathway

Normalised counts from bulk RNA sequencing data of OA synovial fibroblasts from hip (n = 6) (orange), knee (n = 6) (purple), hand (n = 6) (yellow) and foot (n = 6) (cyan) and different BMI's (normal weight (NW) as pink and obese (OB) in green). Hierarchical clustering analysis conducted using dendrogram for row clusters using the ward method and cluster distance set as Euclidean. Log_2 transformation of data was utilised to aid interpretation due to large differences in expression levels (counts) of different genes.

5.4.2 Ingenuity Pathway Analysis (IPA) of obese and normal weight OA synovial fibroblast from different joints

Having investigated the metabolic pathways identified in metabolomics data, the next step was to look for significantly altered metabolic pathways based only on the transcriptomics data from OA synovial fibroblasts. In the stacked bar chart option, the number of transcripts which are upregulated are shown in red, those which are downregulated are in green and those in white are transcripts which didn't pass the cut-offs when put through the core analysis of each canonical pathway.

Having been limited in the metabolomics data to only OA synovial fibroblast from hip patients, RNA sequencing data was applied to synovial fibroblasts isolated from the synovium of patients following total joint replacement surgery at the hip, knee and foot as well as hand synovium following arthroscopy. Ingenuity pathway analysis (IPA) was undertaken using canonical pathway analysis which displays the most significant canonical pathways across the entire dataset. These samples were grouped either by obesity (grouping all the joint samples together with the discriminating factor being BMI) or based on biomechanical loading of joint (grouping samples together with the discriminating factor being anatomical location of the joint).

The first analysis undertaken was the later, with loadbearing joints including OA synovial fibroblasts from hip, knee and foot compared to non-loadbearing hand OA synovial fibroblasts (table 5.1). This was to discriminate the transcriptomics differences observed within metabolic pathways in obesity which arise due to increased biomechanical loading of the joint.

Figure 5.7: Canonical Pathway Analysis of loadbearing (n = 18) compared to non-loadbearing (n =6) OA synovial fibroblast.

Blue pathways indicate predicted inhibition and orange pathways indicate predicted activation. White bars are those which either indicate a pathway with a z-score close to zero or are ineligible for analysis due to >4 analysis ready transcripts within the dataset associated with the pathway.

The top metabolic pathway identified within this comparison included salvage pathways associated with pyrimidine deoxyribonucleotides and ribonucleotides and pyridoxal 5’ phosphate (figure 5.7).

Among the DEGs altered within these OA synovial fibroblasts from loadbearing joints and obesity was thymidine kinase and deoxycytidine deaminase which were identified within the salvage pathways of pyrimidine deoxyribonucleotides. The DEGs within these pathways were downregulated however z score from this analysis didn’t suggest a predicted inhibition or activation of this pathway.

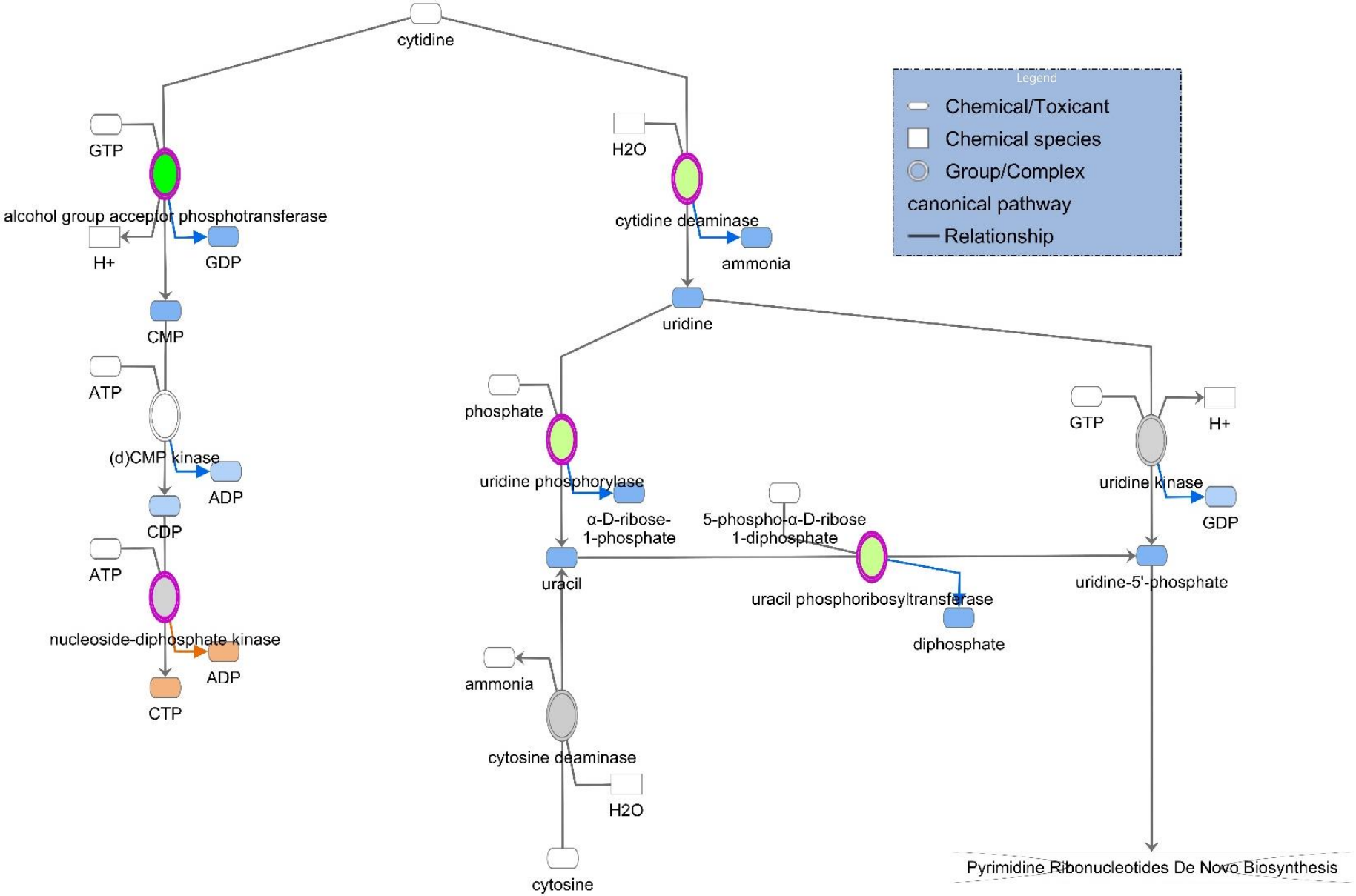

Figure 5.8: Salvage Pathway of Pyrimidine Ribonucleotides highlighted in canonical pathway analysis of loadbearing compared to non-loadbearing OA synovial fibroblast

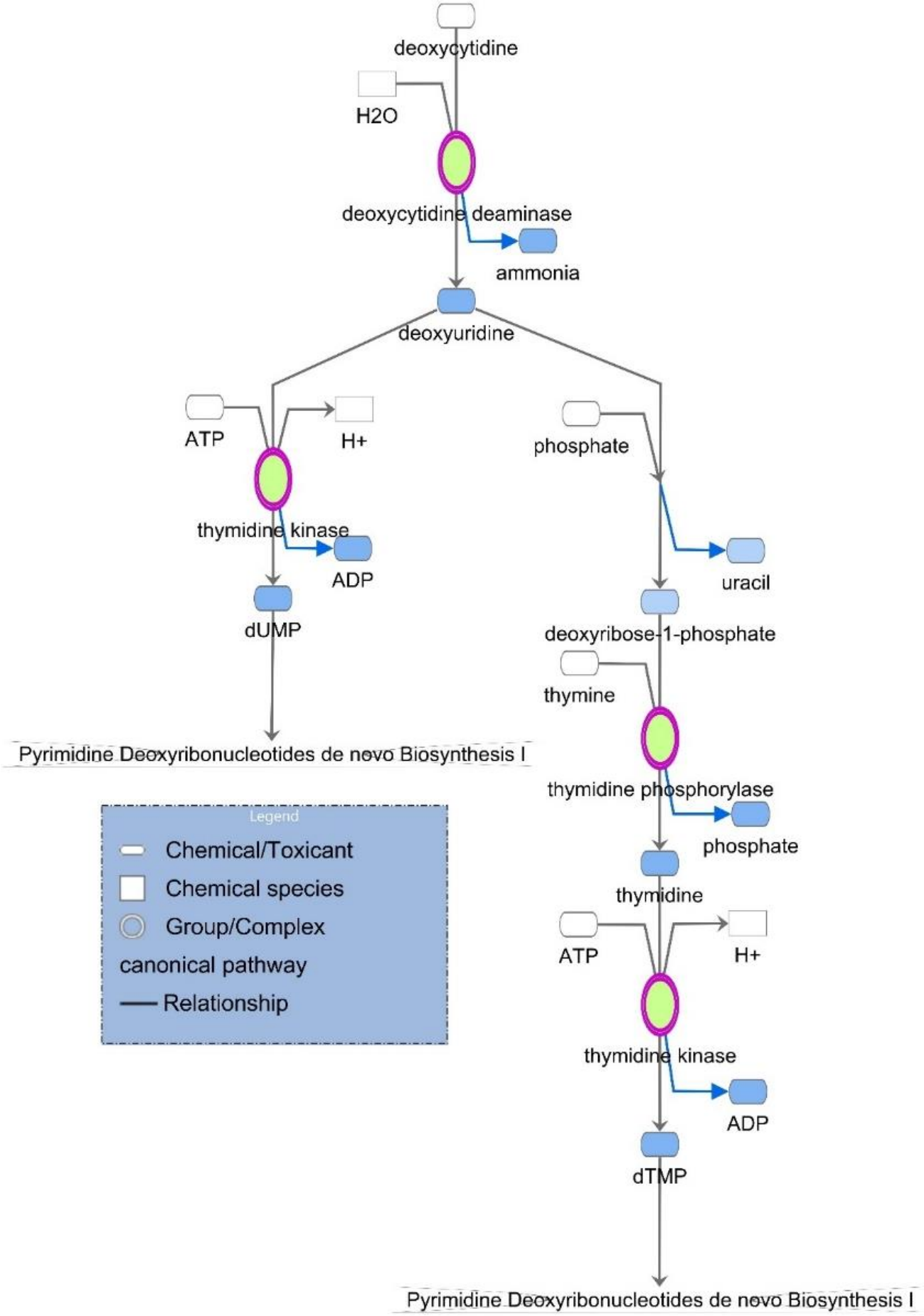

Figure 5.9: Salvage Pathway of Pyrimidine Deoxyribonucleotides highlighted in canonical pathway analysis of loadbearing compared to non-loadbearing OA synovial fibroblast

Figure 5.10: Canonical pathway analysis of obese (n = 12) compared to normal weight (n = 11) OA synovial fibroblast

Blue pathways indicate predicted inhibition and orange pathways indicate predicted activation. White bars are those which either indicate a pathway with a z-score close to zero or are ineligible for analysis due to >4 analysis ready transcripts within the dataset associated with the pathway.

The top altered metabolic pathway in OA synovial fibroblast when investigating obesity is NADH repair although none of the canonical pathways in obesity were highlighted as activated or inhibited (figure 5.10). Another pathway associated with NAD/NADH metabolism, NAD biosynthesis from tryptophan was also significantly altered in obese hand OA synovial fibroblast compared to normal weight hand OA synovial fibroblasts and was predicted to be inhibited based on its z score (figure 5.20).

Likewise, another significantly altered pathway that was commonly identified within canonical pathway analysis of obese compared to normal weight OA synovial fibroblasts was cysteine degradation and biosynthesis, homocysteine degradation and super pathway of methionine degradation. However, the software was not able to make a prediction on its activity status in the overall obesity analysis (figure 5.10). There was predicted activation of the super pathway of methionine degradation in the obese hip and foot OA synovial fibroblasts compared to normal weight OA synovial fibroblasts (figure 5.15 and 5.19).

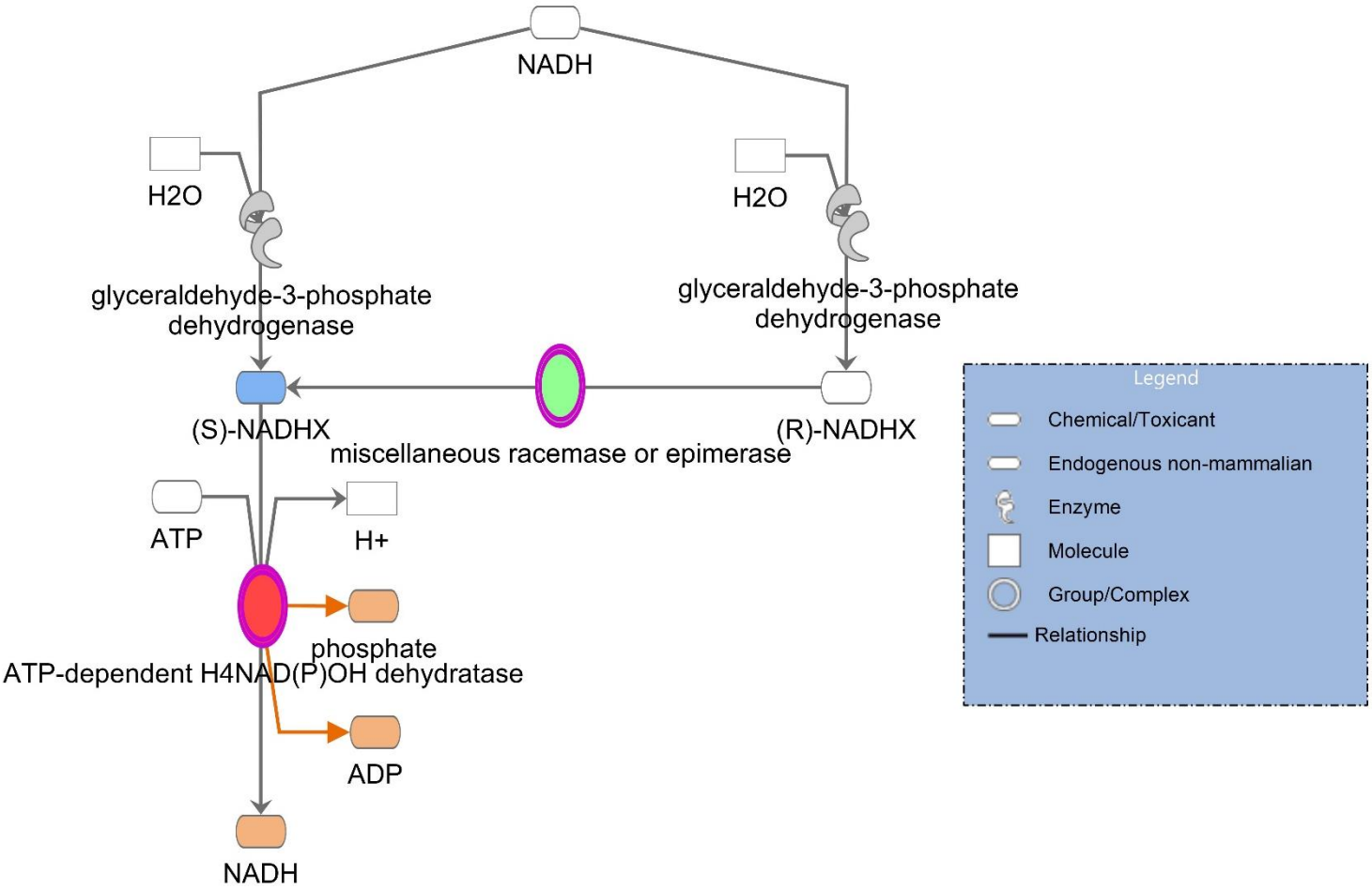

Figure 5.11: NADH repair pathway highlighted in metabolic pathway analysis of obese synovial fibroblast compared to normal weight synovial fibroblast

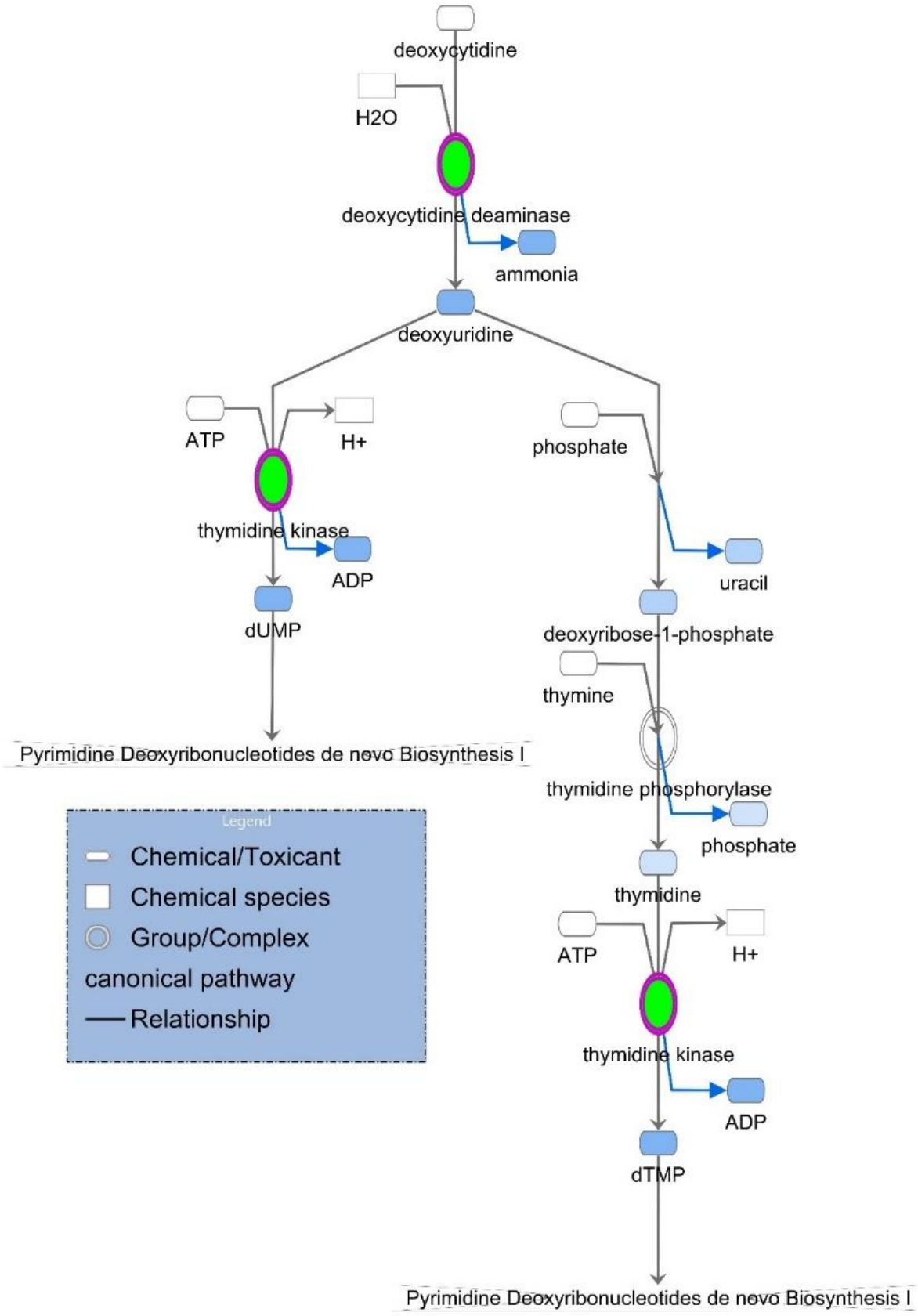

Figure 5.13: Salvage pathway of pyrimidine deoxyribonucleotides pathway highlighted in canonical pathway analysis of obese synovial fibroblasts compared to normal weight synovial fibroblast

Figure 5.14: Percentage upregulated and downregulated DEGs within metabolic canonical pathway analysis of obese (n = 3) compared to normal weight (n = 3) hip OA synovial fibroblast

Figure 5.15: Metabolic canonical pathway activity of obese (n = 3) compared to normal weight hip (n = 3) OA synovial fibroblast

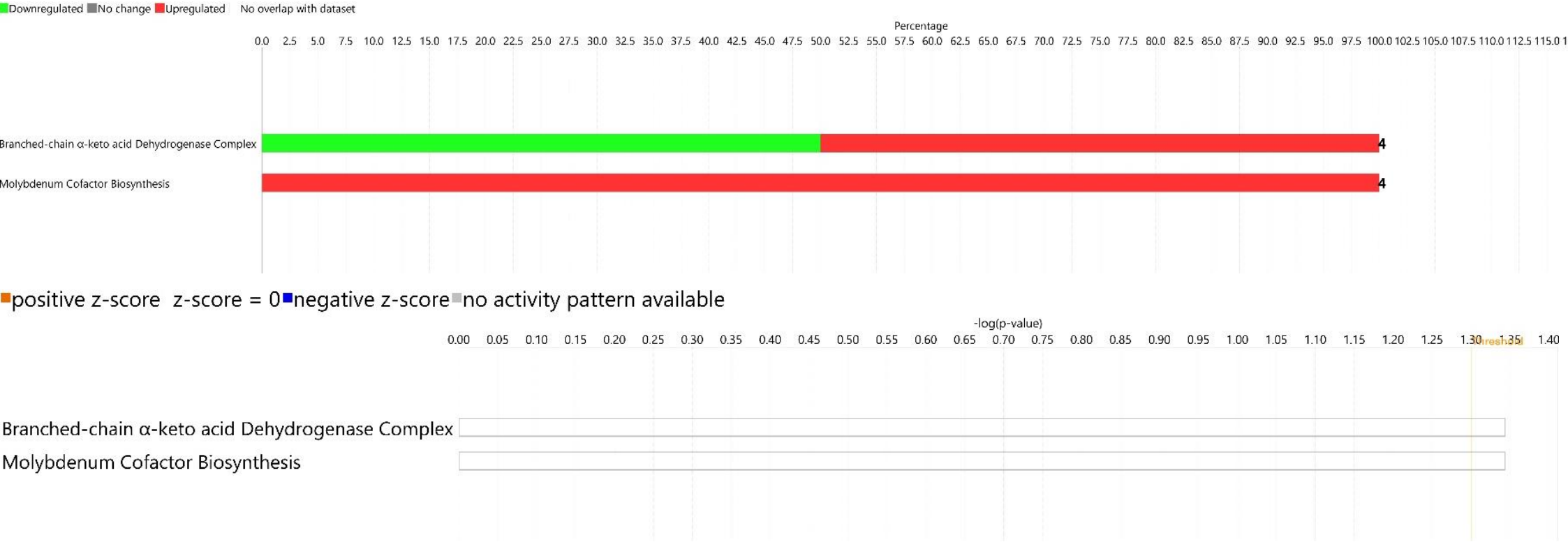

Figure 5.16: Metabolic canonical pathway analysis of obese (n = 3) knee OA synovial fibroblast compared to normal weight (n = 3) knee OA synovial fibroblast

Blue pathways indicate predicted inhibition and orange pathways indicate predicted activation. White bars are those which either indicate a pathway with a z-score close to zero or are ineligible for analysis due to >4 analysis ready transcripts within the dataset associated with the pathway.

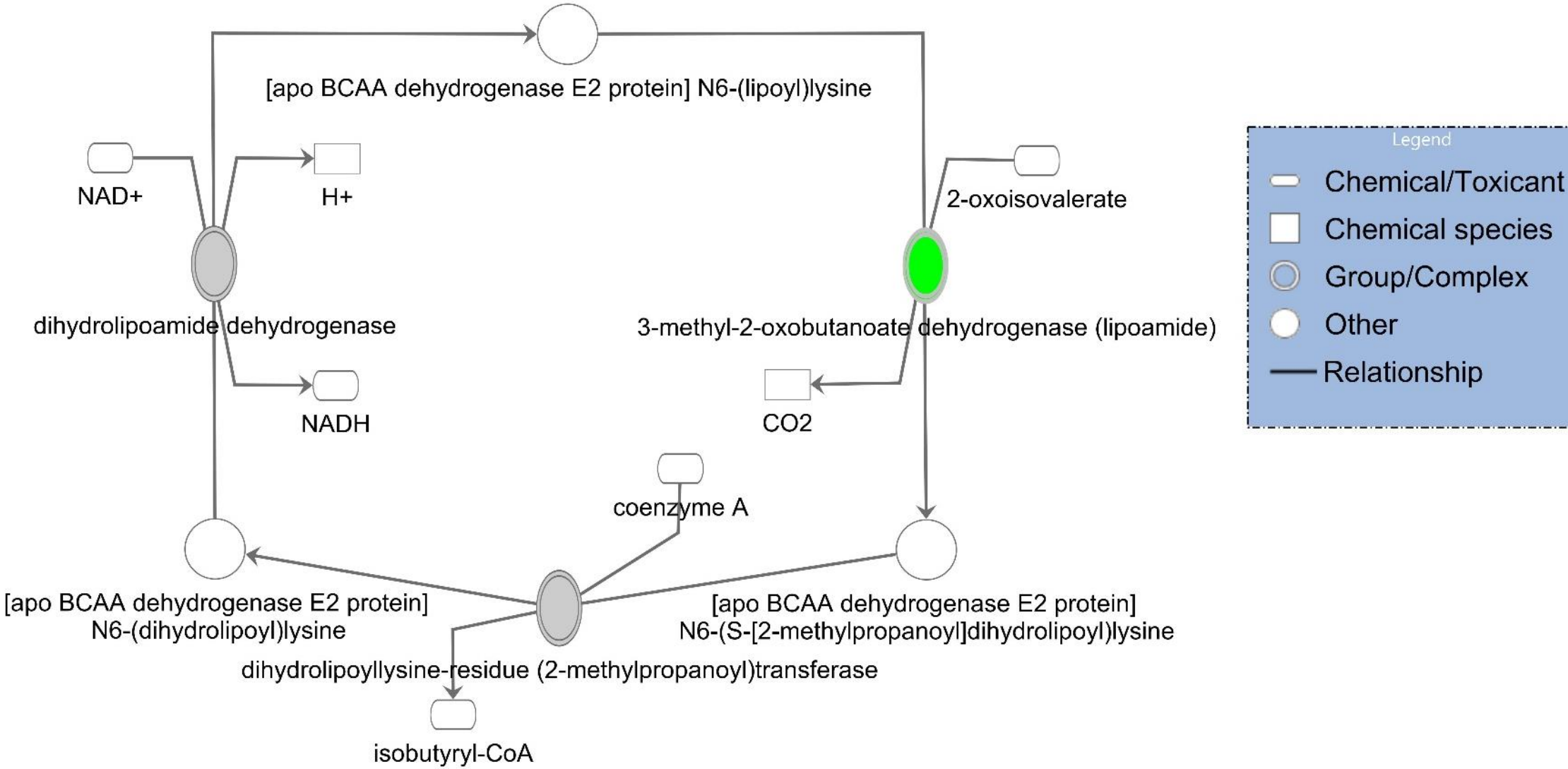

Figure 5.17: Branched chain α ketoacid dehydrogenase complex highlighted in metabolic canonical pathway of obese compared to normal weight knee OA synovial fibroblast

Figure 5.18: Percentage upregulated and downregulated DEGs within metabolic canonical pathway analysis of obese (n = 3) compared to normal weight (n = 3) foot OA synovial fibroblast

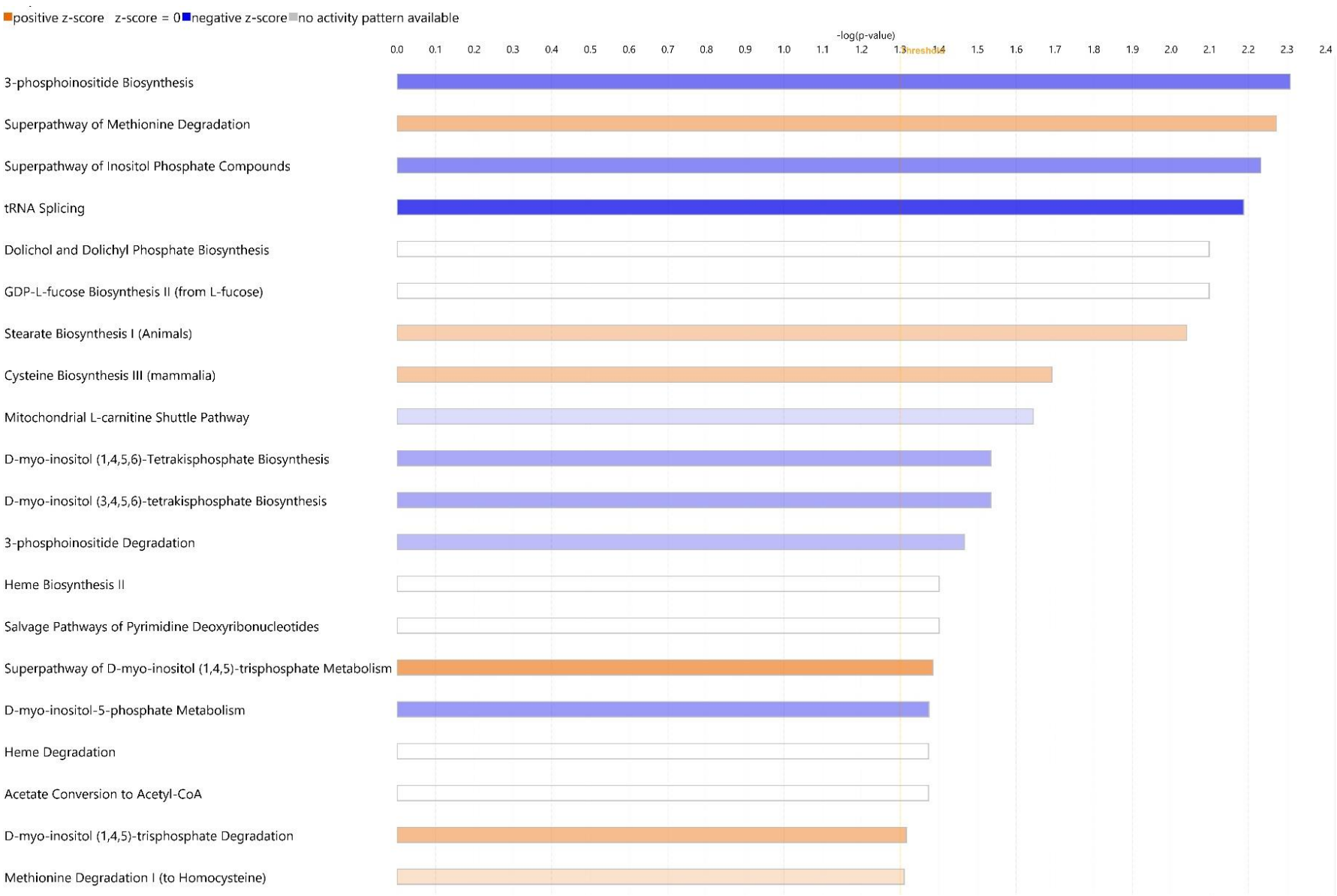

Figure 5.19: Metabolic canonical pathway analysis of obese (n = 3) compared to normal weight (n = 3) foot OA synovial fibroblast

Blue pathways indicate predicted inhibition and orange pathways indicate predicted activation. White bars are those which either indicate a pathway with a z-score close to zero or are ineligible for analysis due to >4 analysis ready transcripts within the dataset associated with the pathway.

Figure 5.20: Metabolic canonical pathway analysis of obese (n = 3) compared to normal weight (n = 3) hand OA synovial fibroblast

Blue pathways indicate predicted inhibition and orange pathways indicate predicted activation. White bars are those which either indicate a pathway with a z-score close to zero or are ineligible for analysis due to >4 analysis ready transcripts within the dataset associated with the pathway.

5.4.3 Joint Pathway Analysis

Having obtained metabolomics data of obese hip OA synovial fibroblast compared to normal weight hip OA synovial fibroblast conditioned media using 1H NMR spectroscopy (described in previous chapter), this data was integrated with transcriptomics RNA sequencing data from obese OA synovial fibroblast compared to normal weight OA synovial fibroblast. This data was restricted to only OA synovial fibroblasts isolated from the synovium of patients who underwent total hip replacement surgery, and the cells were not patient matched but were from the same study patient cohort. This data was then inputted into MetaboAnalyst 5.0 (Pang *et al.*, 2021) joint pathway analysis software to identify significantly enriched metabolic pathways from the transcriptome and secretome of obese OA synovial fibroblasts (figure 5.21).

The top significantly enriched metabolic pathways (based on raw p values) within this joint pathway analysis was Phosphonate and phosphinate metabolism (p = 0.001), Histidine metabolism (p = 0.005), Phosphatidylinositol signalling system (p = 0.005), Inositol phosphate metabolism (p = 0.016), Glycerolipid metabolism (p = 0.039) and Glycolysis or Gluconeogenesis (p = 0.04) (table 5.3). These same pathways however did not reach significance using the more stringent Holm adjusted p value or FDR. Phosphonate and phosphinate metabolism (impact =0.66667), Histidine metabolism (impact =0.3871) and TCA cycle (impact =0.41463) all had the highest pathway impact (table 5.3) suggesting these metabolic pathways have the highest topological impact within the integrated dataset. Although pathway impact scores were computed, identifying whether these pathways were predicted to be activated or inhibited based on z-score was not possible due to software limitations.

However, the actual DEGs and metabolites within these pathways were highlighted as either upregulated or downregulated, giving an indication of how these pathways are altered (figures 5.22-5.26).

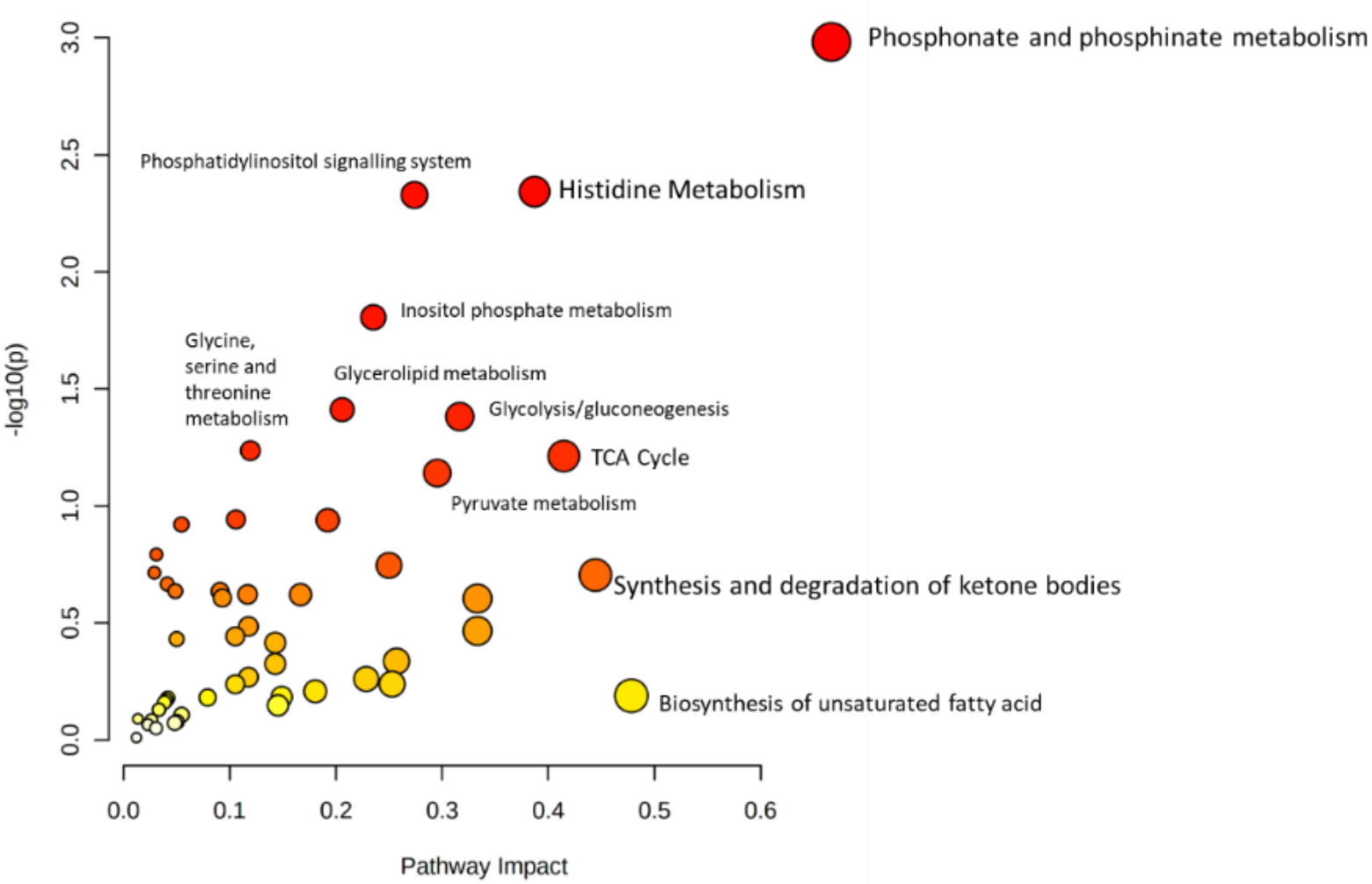

Figure 5.21: Joint pathway analysis using transcriptomics and metabolomics data from obese OA synovial fibroblast compared to normal weight OA synovial fibroblast

Transcriptomics data was collected using RNAseq (n = 6) and metabolomics data was collected using NMR spectroscopy (n = 12). Metabolic pathways are arranged by p values on Y-axis and pathway impact values (from pathway topology analysis) on X-axis. The node colour is based on p values and the node radius is based on pathway impact values

Pathway	Total	Expected	Hits	Raw p	-Log(p)	Holm adjust	FDR	Impact
Phosphonate and phosphinate metabolism	10	0.22	3	0.001	2.98	0.088	0.088	0.67
Histidine metabolism	32	0.70	4	0.0046	2.34	0.38	0.13	0.39
Phosphatidylinositol signalling system	74	1.61	6	0.0047	2.33	0.39	0.13	0.27
Inositol phosphate metabolism	69	1.50	5	0.016	1.81	1	0.33	0.24
Glycerolipid metabolism	35	0.76	3	0.039	1.41	1	0.58	0.21
Glycolysis or Gluconeogenesis	61	1.33	4	0.042	1.38	1	0.58	0.32
Glycine, serine and threonine metabolism	68	1.48	4	0.058	1.24	1	0.64	0.12
Citrate cycle (TCA cycle)	42	0.91	3	0.061	1.21	1	0.64	0.42
Pyruvate metabolism	45	0.98	3	0.072	1.14	1	0.68	0.30

Table 5.3: Multi-omics pathway analysis of obese OA synovial fibroblasts compared to normal weight OA synovial fibroblasts

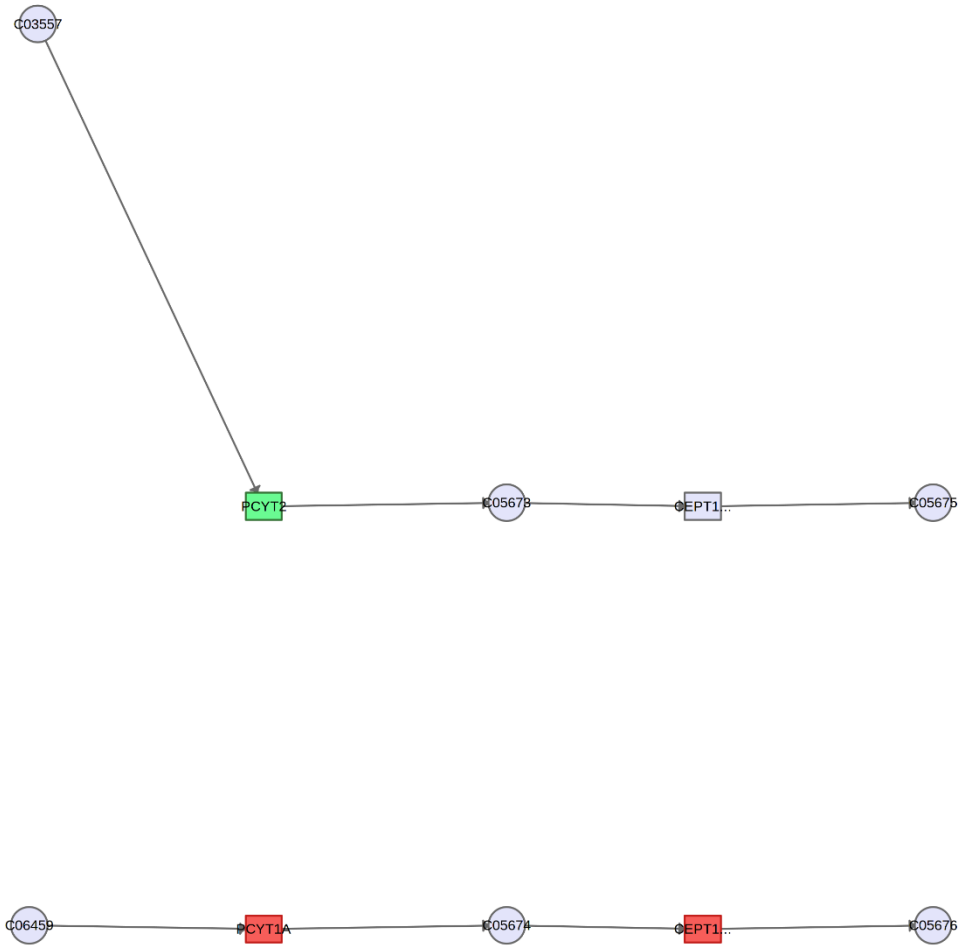

Figure 5.22: Phosphonate and phosphinate metabolism highlighted in multi-omics pathway analysis of obese compared to normal OA synovial fibroblast.

Green is a negative log_2 fold change showing decreased expression or levels and red is a positive log_2 fold change showing increased expression. Symbols in squares refers to genes for enzymes within pathway and circles refers to compounds within pathway.

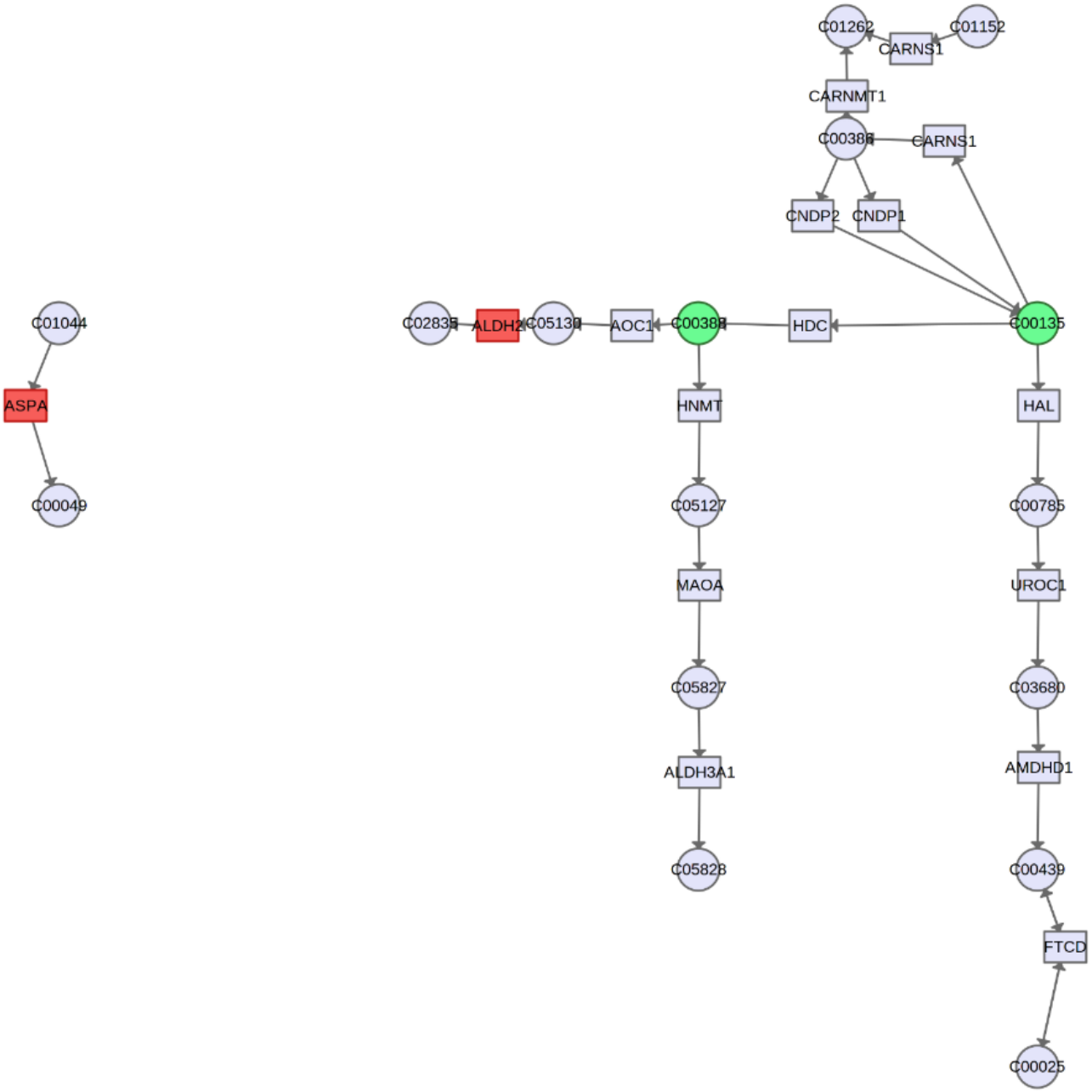

Figure 5.23: Histidine metabolism highlighted in multi-omics pathway analysis of obese compared to normal weight hip OA synovial fibroblast.

Green is a negative log_2 fold change showing decreased expression or levels and red is a positive log_2 fold change showing increased expression. Symbols in squares refers to genes for enzymes within pathway and circles refers to compounds within pathway.

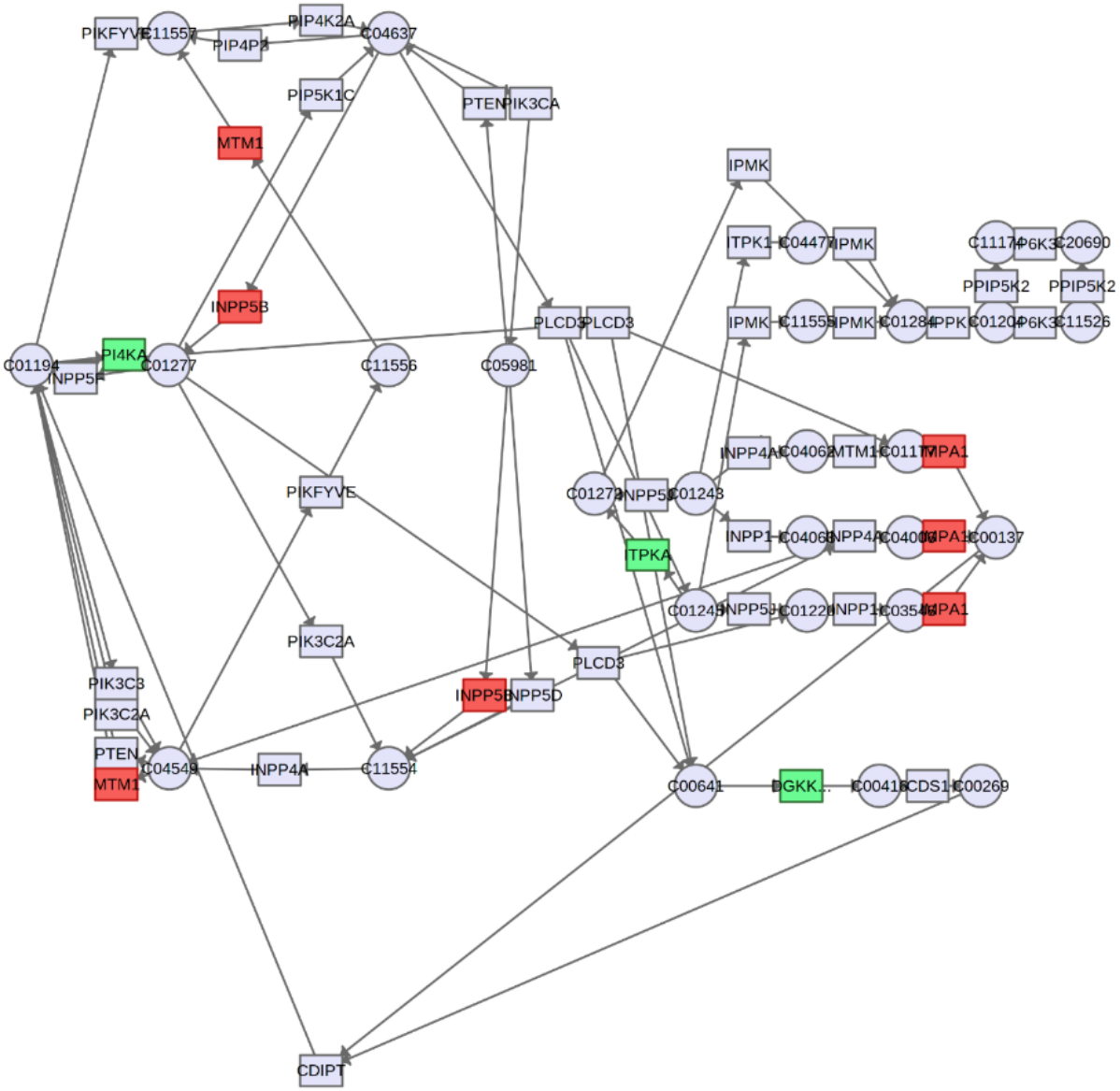

Figure 5.24: Phoshotidylinositol signalling system highlighted in multi-omics pathway analysis of obese compared to normal weight hip OA synovial fibroblast.

Green is a negative log_2 fold change showing decreased expression or levels and red is a positive log_2 fold change showing increased expression. Symbols in squares refers to genes for enzymes within pathway and circles refers to compounds within pathway.

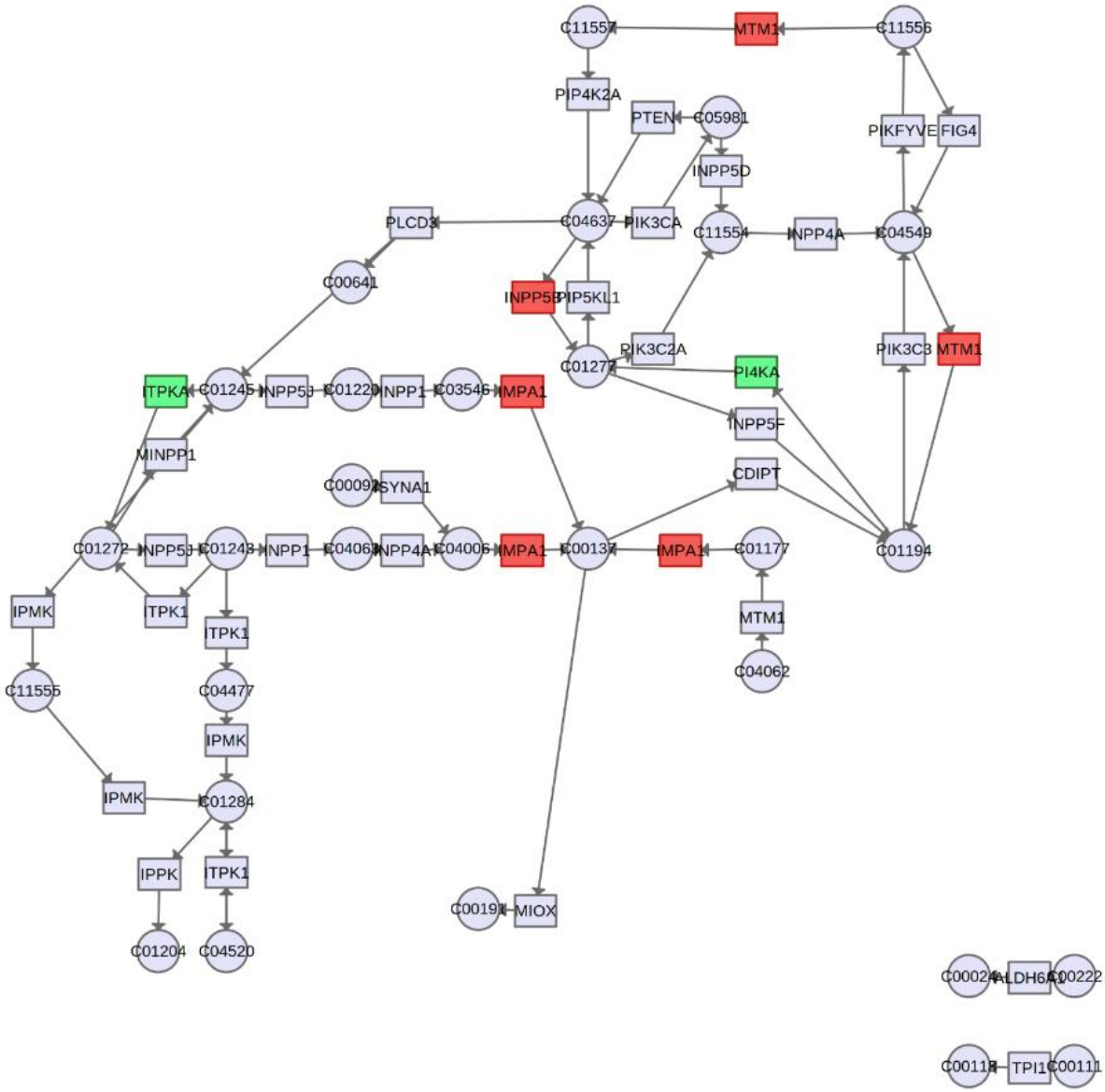

Figure 5.25: Inositol phosphate metabolism highlighted in multi-omics pathway analysis of obese compared to normal weight hip OA synovial fibroblast.

Green is a negative $\log_2$ fold change showing decreased expression or levels and red is a positive $\log_2$ fold change showing increased expression. Symbols in squares refers to genes for enzymes within pathway and circles refers to compounds within pathway.

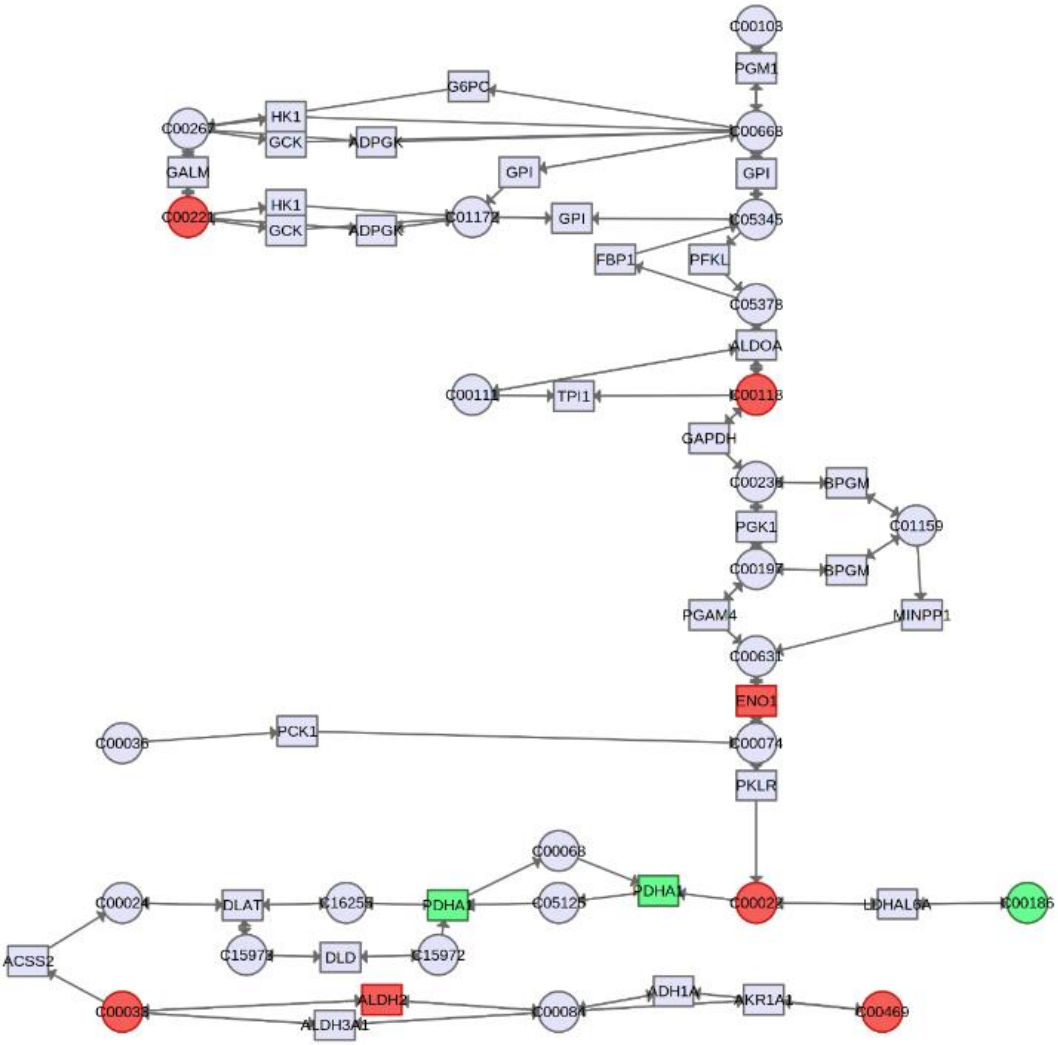

Figure 5.26: Glycolysis highlighted in multi-omics pathway analysis of obese compared to normal weight hip OA synovial fibroblast.

Green is a negative log_2 fold change showing decreased expression/levels and red is a positive log_2 fold change showing increased expression. Symbols in squares refers to genes for enzymes within pathway and circles refers to compounds within pathway.

5.5 Discussion

5.5.1 Shared metabolic gene expression across loadbearing and obesity

Of the 19 shared DEGs in the obesity and loadbearing comparison of OA synovial fibroblasts, Phosphatidylinositol N-Acetylglucosaminyltransferase Subunit A (PIGA) and Solute Carrier Family 13 (Sodium-Dependent Dicarboxylate Transporter), Member 3 (SLC13A3) were highlighted as genes involved in metabolic pathways.

PIGA is involved in synthesis of N-acetylglucosaminyl phosphatidylinositol (GlcNAc-PI), which is the 1st intermediate within the biosynthetic pathway of glycophosphatidylinositol anchor (Bateman *et al.*, 2021). It is the catalytic subunit in glycosylphosphatidylinositol-N-acetylglucosaminyltransferase (GPI-GnT) complex which transfers N-acetylglucosamine from UDP-N-acetylglucosamine onto phosphatidylinositol (Bateman *et al.*, 2021). N-acetylglucosamine and UDP-N-acetylglucosamine were amongst the metabolites increased (p = 0.295 and 0.297) in the synovial fluid of obese OA patients, compared to normal weight OA synovial fluid synovial fibroblasts. The increase in intermediates and altered PIGA expression within obesity (Log_2FC 2.78, p 0.04) could suggest an increase in GPI-anchoring of proteins within cell membranes of obese OA synovial fibroblasts. Amongst the proteins that are known to utilise this post-translational modification is fibroblasts marker Thy-1 (CD90). Thy-1 is glycosyl phosphatidylinositol-anchored glycoprotein and is expressed in a range of cell types including T lymphocytes, thymocytes, neurons and fibroblasts (Shan *et al.*, 2010; Saalbach and Anderegg, 2019). In synovium its expression is mainly limited to the perivascular zone of the sub-lining area and its expression is increased within the inflamed synovium (Adam P Croft *et*

al., 2019). Gene expression data from this study showed no significant change in THY1 expression in obesity, however bulk RNA sequencing would not be the appropriate method of detecting changes in THY1 expression in obese OA synovial fibroblasts. To confirm this theory of altered Thy-1 expression in obese OA synovial fibroblasts and synovium, single cell RNA sequencing of both obese and normal weight OA synovial fibroblasts would need to be conducted and analysis of the sub-lining layer fibroblasts as well as immunofluorescent labelling of THY-1 in obese OA synovium. Likewise, a broader insight into changes in GPI-anchored proteins within these OA synovial fibroblasts might yield insights into the metabolically altered state of these cells .

The second gene which has significantly altered expression in both obesity and loadbearing OA synovial fibroblasts was the protein transporter SLC13A3. SLC13A3 is a mammalian sodium-dicarboxylate cotransporter which is involved in the transport succinate, alpha ketoglutarate and other TCA cycle intermediates (Bateman *et al.*, 2021). Interestingly, its expression is decreased in both obese (Log_2FC -2.64, p 0.0157) and loadbearing (Log_2FC -6.59, p 0.011). Likewise, TCA cycle is among the enriched metabolic pathway observed within obese OA synovial fibroblast although this did not come up as statistically significant in multi-omics analysis. This reduced expression of this transporter and the inference of reduced transport of these TCA cycle metabolites could suggest an increased metabolic need of the cells to accumulate TCA cycle intermediates for its own metabolic needs, through increased mitochondrial respiration. However, further investigation would be needed to corroborate this hypothesis, as data on directional transport of these intermediates and which intermediates are being transported would be required. Likewise, inference of protein transporter function within cells though RNA driven

data is not the best method, as protein transporters have numerous methods of regulation, through post-translational modifications, altered protein expression and internalisation through translocation from the plasma membrane.

5.5.2 Heatmaps of metabolomic pathways highlight differentially expressed genes in obesity

When examining the KEGG glycolysis/gluconeogenesis pathway within the transcriptome of OA synovial fibroblast, alpha enolase (ENO1) and pyruvate kinase (PKM) were largely increased relative to other genes within this pathway. The increase in PKM expression is particularly notable, since it catalyses the final rate-limiting step of glycolysis through the transfer of a phosphoryl group from phosphoenolpyruvate (PEP) to ADP thereby generating ATP. PKM has been widely characterised and the ratio between its highly active tetrameric form and inactive dimeric form governs whether carbons from glucose are funnelled into biosynthetic processes or for energy metabolism thereby generating ATP (Vander Heiden *et al.*, 2010). Increased expression of PKM2 and LDHA have been observed in RA synovial fibroblasts providing not only the energy to sustain the increased cellular proliferation observed in RA synovial fibroblasts but can also modulate transcription through PKM2 nuclear translocation and interaction with NFκB/STAT3 and lactate's ability to activate metalloproteinases and thereby stimulated ECM degradation and angiogenesis via VEGF and HIF1α (D. Xu *et al.*, 2019). This increase in expression of these glycolytic enzymes and LDHA could be simply a mechanism to cope with increased rates of glycolysis. Interestingly, glycolysis/gluconeogenesis metabolic pathway was significantly enriched during joint multi-omics pathway analysis of hip obese compared to hip normal weight OA synovial fibroblasts suggesting glycolysis

is the primary metabolic pathway altered in obesity within hip OA synovial fibroblasts, however confirmation of this requires *in vitro* real time metabolic flux analysis.

The next significantly enriched metabolic pathway identified in the metabolome of OA synovial fibroblasts from hip patients was the amino acyl tRNA biosynthesis pathway. This pathway involves the aminoacylation of transfer RNAs and is synthesised by aminoacyl-tRNA synthetases (AARS). Aminoacylation was found to be significantly enriched in metabolite-gene interactions within a cross-sectional late-stage knee OA cohort (Rockel *et al.*, 2022). AARS have been associated with inflammation and amino acid sensing. For example, KARS acts as a pro-inflammatory cytokines in macrophages (Sang *et al.*, 2005). AARS and their associated protein complexes have been shown to modulate inflammation, apoptosis and gene expression (Pang, Poruri and Martinis, 2014). This pathway is also an essential pathway for protein synthesis through their active role as amino acid sensors (Yu, Han and Kim, 2021). Aminoacyl-tRNA synthetase-interacting multifunctional protein 1 (AIMP1) downregulation in chondrocytes is involved in promoting anabolic cell activity through regulation of TGFβ signalling (Ahn *et al.*, 2016). LARS has recently been identified as a leucine sensor within mammalian target of rapamycin complex 1 (mTORC1) pathway and has been shown to respond to glucose starvation via phosphorylation of Unc-51 like autophagy activating kinase 1 (ULK1) at its leucine binding site, thereby prohibiting protein synthesis and providing leucine for catabolic pathway energy generation (Kim *et al.*, 2017; Yoon *et al.*, 2020). Notably, amino-acyl tRNA biosynthesis was also identified as significant within IPA analysis obese hip OA synovial fibroblasts, compared to normal weight hip OA synovial fibroblasts, and had a predicted inhibition based on its z-score (figure 5.15). Significantly altered transcriptomic metabolic pathways associated with

amino acid metabolism have also been identified within other comparisons including Arginine and Methionine degradation in obese hip OA synovial fibroblasts (figure 5.15), L-Cysteine degradation and biosynthesis in obesity within all OA synovial fibroblasts (figure 5.10) and branched chain α-keto acid dehydrogenase complex within obese knee OA synovial fibroblast (figure 5.16). This could suggest amino acid metabolism plays an essential role in obesity within OA synovial fibroblasts from different joints. However, multi-omics pathway analysis of hip OA synovial fibroblasts did not highlight this as significantly enriched.

Another pathway that was significantly enriched within OA synovial fibroblasts metabolome was serine, glycine and threonine metabolism. Hierarchical clustering analysis highlighted relatively higher expression of genes involved in serine-glycine synthesis and degradation including SHMT2, which catalyses the conversion of serine to glycine within the mitochondria and PSAT1, which catalyses the reversible conversion of 3-phosphohydroxypyruvate to phosphoserine using glutamate and producing the α-keto acid, α-ketoglutarate. Multi-omics analysis of hip OA synovial fibroblasts found serine, glycine and threonine metabolism was not significantly enriched suggesting gene expression data from the transcriptomics dataset doesn't support those differences identified within the metabolomics data. This discrepancy in data integration suggests serine, glycine and threonine metabolism may not be as important to distinguish differences in metabolic phenotype of obese OA synovial fibroblasts as previously thought.

Alanine, aspartate and glutamate metabolism was the final significantly enriched metabolic pathway identified in metabolomics data analysis of hip OA synovial fibroblasts. Hierarchical clustering analysis of the transcriptomics data showed a cluster of relatively highly expressed transcripts including glutaminase 1 (GLS) and

glutamine synthetase (GLUL) as well as lower relative expression of Glutamate dehydrogenase 2 (GLUD2) and Glutamate decarboxylase 2 (GAD2) enzymes. GLS and GLUL enzymes catalyse the glutamine catabolism and synthesis pathway by converting glutamine to glutamate and its opposite reaction respectively. These enzymes have generated much interest due to their clinical significance within the tumour microenvironment and their critical role in cellular senescence making them an attractive target for cancer senolytic therapies (Chen and Cui, 2015; Johmura *et al.*, 2021). Glutamine metabolism and GLS has already been shown to be critical in the function and cellular phenotype of RA synovial fibroblast and has been shown to be critical to the inflammatory response within OA synovial fibroblast which was discussed in the previous chapter of this thesis (Takahashi *et al.*, 2017; Farah *et al.*, 2022).

5.5.3 IPA analysis of the transcriptome of OA synovial fibroblast highlights distinctively altered metabolic pathways in the context of obesity

Having undertaken a metabolomics driven analysis of the transcriptomics data in an attempt to yield conceptual insights into OA synovial fibroblasts metabolism, independent analysis of the transcriptomics data from these cells found unique differences in their metabolism. Amongst the top metabolic canonical pathways significantly altered within load-bearing joints and within obesity was the salvage pathway of deoxyribonucleotides, with a reduction in thymidine kinase and deoxycytidine deaminase expression. This could suggest a reduced capacity for recycling of these deoxyribonucleotides, which would need further investigation, possibly examining changes in DNA synthesis and replication.

Another altered metabolic pathway within obese OA synovial fibroblasts was NADH repair, with NAD biosynthesis predicted as inhibited in hand OA synovial fibroblasts. Nicotinamide adenine dinucleotide (NAD^+) is a critical coenzyme used for redox reactions, which is intricately involved in energy metabolism including glycolysis, TCA cycle and fatty acid oxidation (Covarrubias *et al.*, 2021). NAD^+/NADH ratio depends on the cellular redox state, rates of NAD^+ synthesis and NAD^+ consumption (Xu *et al.*, 2016). Although NAD is well studied within age related diseases, its role within OA is still not well understood. It can be generated de novo through the kynurenine pathway at the liver and can also be generated using nicotinamide (NAM) through the NAD^+ salvage pathway within peripheral cells (Xu *et al.*, 2016). The critical rate-limiting enzyme within this pathway is nicotinamide phosphoribosyl-transferase (NAMPT) and converts NAM into nicotinamide mononucleotide (NMN) (Covarrubias *et al.*, 2021).

Extracellular NAMPT/Visfatin is a highly conserved, globally expressed enzyme which is secreted from visceral adipose tissue. It has multiple potential roles, alongside its catalytic role in converting nicotinamide into NMN, including immunomodulation through activation of human leukocytes and induces pro-inflammatory cytokine production (IL6, TNFα and IL1β) (Moschen *et al.*, 2007). Visfatin has garnered much attention within the field due to its increased expression within age-related diseases, including diabetes and obesity (Philp *et al.*, 2021). However, not much research has been conducted on its role within OA. Previous research within this group has shown visfatin is expressed locally by joint tissues including within synovium and synovial fluid of hip OA patients and it is elevated in the synovial fluid of obese patients (Philp *et al.*, 2021). NAMPT expression is significantly upregulated in obese hip OA synovial fibroblasts compared to normal

weight OA synovial fibroblasts (Q value = 0.0039) (Nanus *et al.*, 2020). This data supports the previous research within this group, on the importance of visfatin and NAD metabolism in hip OA.

Another commonly altered metabolic pathway in OA synovial fibroblasts in the context of obesity was cysteine biosynthesis and degradation, homocysteine degradation and super pathway of methionine degradation. Cysteine, homocysteine and methionine are all sulphur containing amino acids with homocysteine being formed during the conversion of methionine to cysteine in the transsulfuration pathway (Rehman *et al.*, 2020). Cysteine is a proteinogenic amino acid which catalyses several important metabolic reactions including its involvement in lipid biosynthesis, iron-sulphur biosynthesis and is a source for taurine, glutathione and coenzyme A (Rehman *et al.*, 2020). It plays a crucial role in the synthesis of essential fatty acids and therefore is critical for cell membrane formation. It is also involved in DNA methylation, as S-adenosylmethionine (SAM), the activated form of methionine, serves as the most important methyl donor and therefore could be involved in supplying methyl groups for epigenetic modifications of genes (Yang *et al.*, 2018). OA synovial fluid from obese patients had increased methionine levels compared to normal weight OA synovial fluid (p 0.297). However, cysteine and homocysteine were not altered within OA synovial fluid or fibroblasts secretomes, suggesting cysteine, homocysteine metabolism is only altered intracellularly. The role cysteine, homocysteine and methionine metabolism plays within obesity and OA is unknown and warrants further research and investigation.

5.5.4 Joint pathway analysis of hip OA synovial fibroblasts

Having obtained both metabolomics and transcriptomics data from the hip OA synovial fibroblasts, data integration through statistical analysis was conducted using joint pathway analysis software, MetaboAnalyst. Several significantly enriched metabolic pathways were identified in obese hip OA synovial fibroblasts including phosphatidylinositol signalling system and inositol phosphate metabolism. Phosphatidylinositol are a class of short-lived membrane phospholipids composed of an inositol ring and two fatty acid chains linked through a glycerol backbone which secures the molecule to the internal surface of cell membrane (Marat and Haucke, 2016). These molecules are phosphorylated at different hydroxyl positions at the inositol ring by a family of lipid kinases producing the signalling molecules which mediates different aspects of cell function including gating of ions channels, autophagy, cytoskeletal regulation and motility and even regulating vesicular traffic (Balla, 2013; Lystad and Simonsen, 2016). Amongst those pathways most studied that involve phosphatidylinositol's is the receptor tyrosine kinase induced Akt signalling pathway, which is activated upon the synthesis of PI(3,4,5)P3 from PI(4,5)P2 by class I PI3K and is dephosphorylated by PTEN (Lystad and Simonsen, 2016). This results in recruitment of phosphoinositide-dependent protein kinase 1 (PDPK1) to the plasma membrane and PDPK1-mediated phosphorylation of membrane-bound AKT serine/threonine kinase 1 (AKT) (Lystad and Simonsen, 2016). This metabolic pathway which results in the recruitment and activation of the metabolic mTORC1 pathway has been well studied and is involved in regulation of cell growth and metabolism (Takahara *et al.*, 2020). Notably, independent analysis of transcriptomics data from obese hip OA synovial fibroblasts using IPA canonical pathway analysis also highlighted 3-phosphoinositide biosynthesis/degradation and

super pathway of inositol phosphate metabolism, as significantly activated metabolic pathways found in obesity within hip OA synovial fibroblasts. Upon analysing the metabolomic data from these hip OA synovial fibroblasts and synovial fluid, myo-inositol was amongst the metabolites detected. Myo-inositol was increased in obese OA synovial fluid (p 0.297) and with TNFα stimulation in the secretomes of obese (p 0.12) and normal weight (p 0.05) OA synovial fibroblasts, suggesting this pathway is modulated with both obesity and inflammation, making this an interesting area for further investigation.

Furthermore, another significantly enriched metabolic pathway identified in joint pathway analysis was glycolysis. This pathway was also significantly enriched in the metabolomics data, and when integrated with the transcriptomics dataset, suggests a confirmation of the results identified within the first chapter of this thesis. Given this finding, the role of this metabolic pathway in OA synovial fibroblasts was investigated further using real-time metabolic flux analysis within the subsequent chapter.

5.5.5 Limitations

Amongst the limitations associated with this study is the use of a single cell type, namely the synovial fibroblast. The synovial membrane is known to consist of different cell populations including resident and infiltrating immune cells. This study focused specifically on the synovial fibroblast and so might have missed out on some differences in metabolism observed due to cell-cell interactions. *In vitro*, this could have been achieve in-part through the use of co-culture assays, to mimic the interaction between resident fibroblasts and infiltrating immune cells within the synovial membrane. Such analyses was originally intended to be part of the thesis.

However, due to Covid and the subsequent limitations on laboratory access and sample availability this was omitted.

This study only focused only on mRNA transcripts of coding genes (for metabolic proteins). This omits the non-coding transcriptomics aspect, which makes up the majority of the transcripts within RNA sequencing. Many of these non-coding RNA sequences will regulate transcriptomes and therefore, omitting them will leave out much information of the regulation of metabolic pathways. One issue here is the lack of research on the role these non-coding mRNAs and therefore identifying which role these non-coding RNAs play in metabolic regulation or reprogramming is particularly difficult.

RNAseq only focuses on mRNA transcripts whereas as metabolism involves a number of regulatory mechanisms such as post translational modifications of proteins/enzymes and changes in these proteins/enzymes are observed using other omics techniques such as proteomics. However, by utilising multi-omics analysis, such as metabolomics, one can relate changes upstream in cellular phenotype observed in transcriptomics data to those downstream, like metabolite changes, giving further confidence, that those changes observed within transcriptome are a valid reflection of cellular phenotype, which is attempted within this study.

One issue with the metabolomics analysis using transcriptomics dataset was the inability to recognise certain genes using official gene names. Although attempts were made to correct this issue using bioinformatics tools such as PANTHER (Mi *et al.*, 2021), some genes were not recognised and were therefore omitted from the analysis. However, this was not an issue for the metabolomics datasets, as the

known compounds (utilising HMDB database) were already named/labelled when conducting targeted metabolomics.

Multi-omics analysis utilised within this study also contained limitations, as matched samples were not used for the RNA extraction and conditioned cell media. Likewise, cell numbers were not matched as the metabolomics conditioned media was from 40,000 cells/sample, however RNAseq of OA synovial fibroblast was from 250,000 cells per replicate. However, batch effects were not an issue for the samples as samples from both omics datasets were conducted in successive and continuous manner. One way to overcome this issue in future experiments maybe to collect the conditioned media and extract the RNA from the same cells and patients thereby avoiding these potential obstacles when analysing the data.

This study only focused on bulk RNA sequencing, whereas many changes observed within cells, particularly in pathological processes, have altered epigenomic changes, such as DNA methylation and acetylation. As passaged synovial fibroblast where analysed, understanding why these OA synovial fibroblast maintain their cellular phenotype *in vitro* is an important question, which could be answered by using epigenomic analysis. However, the inclusion of epigenomic analysis, is outside of the scope of this study and although interesting would require much analysis and research time

5.5.6 Future Directions

Research by Croft et al, 2019 has shown there are distinct subsets of synovial fibroblast within the synovial membrane based upon lineage markers FAPα, THY1 and PDPN (Croft *et al.*, 2019). Those synovial fibroblasts within the lining layer of the synovial membrane are distinct in their phenotype to those within the sub lining layer of the synovial membrane. These cells may also have a different metabolic phenotype alongside the previously classified differences in their phenotype. Perhaps by conducting bioinformatic metabolic pathway analysis on these cells, one could divulge differences in their metabolism.

Another possible area of future research would be to understand the metabolism of other cells within the synovial joint. As previously mentioned, OA is now regarded as a disease of the whole joint, with pathological changes observed in different tissues within the joint including subchondral bone, synovial membrane, articular cartilage, adipose tissue. By conducting metabolic analysis on the resident and infiltrating cells within these tissues using single cell RNA sequencing alongside integration with established datasets of cell metabolism from metabolomics data for each cell type, one could establish a cell atlas of metabolic and phenotypic changes observed in the OA joint that could be extended to other inflammatory joint diseases, giving us a perspective on shared mechanism and aetiologies.

CHAPTER 6

METABOLIC FLUX ANALYSIS OF OA SYNOVIAL FIBROBLASTS

6.1 Introduction

Recently an increasing number of studies have shown that synovial fibroblast activation and the associated joint damage is accompanied by altered fibroblast metabolism (de Oliveira *et al.*, 2019; Farah *et al.*, 2020). Inflammation and the following cellular activation of synovial fibroblasts is known to alter the metabolism of four major groups of macromolecules associated with cellular metabolism (carbohydrates, proteins, lipids, and nucleic acids) (de Oliveira *et al.*, 2019). This chapter is focused on the first class of macromolecules, namely the breakdown of glucose via glycolysis and the subsequent activation of mitochondrial respiration to generate energy through ATP and NADH. Metabolomic and multi-omic analysis of OA synovial fibroblasts conducted within this study, as shown in previous chapters, highlighted an enrichment in enzymes and metabolites involved in glycolysis and the TCA cycle. Consequently, the next logical steps having obtained this data was to investigate the metabolic state of these cells with a particular focus on their glycolysis and oxidative phosphorylation metabolic activity. This chapter is therefore an in-depth profile of synovial OA fibroblasts and their metabolic state (both basal and activated), to elucidate how these cells adapt to their inflammatory microenvironment.

6.1.1. Glycolysis

Glycolysis is the first step of the canonical and universal pathway for energy metabolism within cells and is in essence the breakdown of glucose into either pyruvate under aerobic conditions (equation below) or lactate under anaerobic conditions, resulting in the generation of potential energy in the form of ATP and NADH (shown below). Glycolysis is a tightly regulated mechanism to maintain constant levels of ATP and the generation of glycolytic intermediates, which are also involved in biosynthetic roles themselves. The rate of flux of glycolysis is maintained and controlled by ATP consumption rates, NADH regeneration and the allosteric regulation of key rate limiting glycolytic enzymes (hexokinase, PFK-1 and pyruvate kinase) as well as the dynamic changes in concentration of glycolytic substrates which mirror the dynamic balance between ATP generation and consumption (Nelson 1942-, 2005). On a longer macro scale, glycolysis is regulated by hormonal changes through hormones insulin, glucagon adrenaline and by changes in gene expression of the rate limiting enzymes.

$$Glucose + 2NAD^+ + 2P_i \rightarrow 2\,Pyruvate + 2NADH + 2H^+ + 2ATP + 2H_2O$$

The use of glycolysis as the primary means of rapid energy generation in inflammatory and activated cells has been well characterised. Synovial fibroblasts are amongst those cell types that upon inflammatory challenge will increase glycolysis, and this is the case in the microenvironment of inflammatory joint diseases such as rheumatoid arthritis. Inhibition of glycolysis not only alters their aggressive cellular phenotype but also reduces the secretion of pro-inflammatory cytokines including IL6, IL8 and chemokines MCP-1, CXCL5 and GRO-α (Biniecka

et al., 2016). This suggests that not only is glycolysis used to generate increased energy metabolism of synovial fibroblasts, but that it also plays a role in maintaining this inflammatory profile.

Hexokinase 2 (HK2), a key enzyme in glycolysis, which catalyses the phosphorylation of glucose to glucose-6-phosphate, is increased in synovial fibroblasts and its ablation decreased invasive phenotype and reduced bone and cartilage damage in a murine model of inflammatory arthritis (de Oliveira *et al.*, 2019). Another glycolytic enzyme altered in the inflammatory synovium is phosphoglycerate kinase 1 (PGK1), which catalyses the transfer of a phosphate group of 1,3-bisphosphoglycerate to ADP, thereby generating ATP and 3-phosphoglycerate (Nelson 1942-, 2005). In a collagen-induced arthritis (CIA) rodent model, PGK1, alpha enolase (ENO1) and HK2 were upregulated and PCK1 and PDK4 were downregulated in synovial tissue (Zhao *et al.*, 2016). High PGK1 levels were found in the blood of RA patients and siRNA knockdowns of PGK1 in synovial fibroblasts resulted in a reduction in cell proliferation, migration as well as inflammatory cytokines IL-1β and IFN-γ (Zhao *et al.*, 2016). This suggest that PGK1 is intricately involved in maintaining synovial fibroblast phenotype in inflammatory joint diseases. Another enzyme involved in glycolysis is 6-phosphofructo-2-kinase/fructose-2,6-bisphosphatase 3 (PFKFB3), which is increased in the synovium and synovial fibroblast in RA. PFKFB3 inhibition reduced fibroblast cell migration, proliferation and invasion as well as decreased the expression of inflammatory cytokines and chemokines including IL6, IL8, CCL2, CXCL10 (Zou *et al.*, 2017). Likewise, inhibition of PFKFB3 supressed TNF-α-induced activation of NF-κB and p38, JNK and ERK/MAPK signals in synovial fibroblasts and reduced the severity of arthritis in a CIA murine model (Zou *et al.*, 2017). This suggest that not only is

glycolysis crucial for maintaining the inflammatory status of synovial fibroblasts through rapid energy generation, but glycolytic enzymes also control inflammatory status of these cells through regulation of downstream signalling pathways via transcription factors.

Another means of glycolysis regulation is through controlling rates of glucose uptake through glucose transporters (SLC2A/GLUT). The facilitative glucose transporters transport glucose across the plasma membrane through facilitated diffusion. The GLUT family of transporters are made up of 14 protein transporters, classified into 3 classes based on sequence similarity and substrate specificity; class one (GLUTs 1-4 and 14), class two (GLUTs 5, 7, 9 and 11) and class three (GLUTs 6, 8, 10, 12 and HMIT) (Zezina *et al.*, 2020). When examining patterns of tissue distribution, GLUT1 and GLUT3 transporters were initially reported to be expressed ubiquitously and within the brain (neuronal) and testis (sperm) respectively (Nelson 1942-, 2005). Amongst all the transporters, GLUT1's role in inflammation has been the primary focus in the context of immune cells and fibroblasts (Bustamante *et al.*, 2017; Rhoads, Major and Rathmell, 2017). Inflammatory stimuli through TNFα or platelet derived growth factor (PDGF) treatment has been shown to increase both glucose metabolism and GLUT1 expression in synovial fibroblasts suggesting this is the main glucose transporter involved in the inflammatory response (Garcia-Carbonell *et al.*, 2016). Alongside this, GLUT1 expression has also been shown to correlate with synovial fibroblast phenotype (cell migration/MMP expression) suggesting a reliance of synovial fibroblasts on glucose metabolism (Garcia-Carbonell *et al.*, 2016). In the arthritic synovium of K/BxN murine model, GLUT1 expression was upregulated as a result of joint hypoxia and inflammation, which could support the glycolytic environment within inflammatory joint diseases (Garcia-Carbonell *et al.*, 2016).

Although there has been much investigation into the role of glycolysis in RA synovial fibroblasts, its role in OA synovial fibroblasts has yet to be explored.

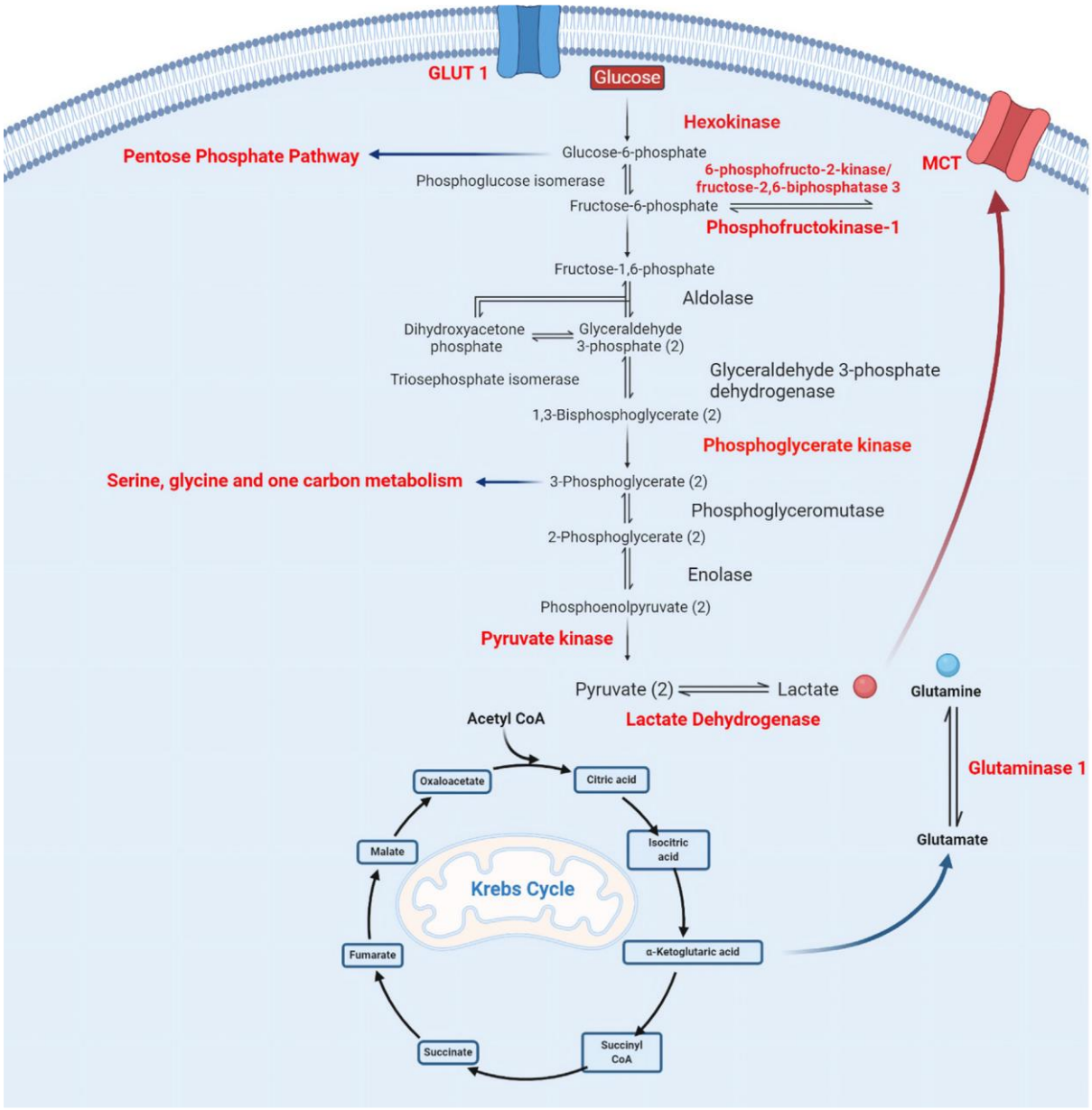

Figure 6.1: Diagram of metabolic changes observed in synovial fibroblasts in inflammatory joint diseases.

Fibroblast upon activation via inflammatory stimuli increase energy metabolism via glycolysis and upregulate key glycolytic enzymes to maintain their inflammatory and invasive phenotype (Farah *et al.*, 2020)

6.1.2 Mitochondrial Respiration

Following glycolysis, pyruvate feeds into another critical metabolic pathway- namely the citric acid cycle (TCA) at the mitochondrial matrix, where pyruvate is oxidised to form an acetyl group (i.e. generating acetyl-co-enzyme A), and then further oxidised into CO_2 within the TCA cycle (Nelson 1942-, 2005). The energy released during these oxidation steps are conserved in the reduced electron carriers and coenzymes nicotinamide adenine dinucleotide (NADH) and flavin adenine dinucleotide ($FADH_2$). The cycle is visualised in figure 1 and consist of eight steps of a cycle of reduction and oxidation reactions, eventually resulting in the formation of the final metabolite within the cycle, oxaloacetate.

Following the TCA cycle, these reduced electron carriers will themselves release their electrons and hydrogen ions, which are transferred to the terminal electron acceptor O_2, through a chain of electron carriers made up of protein complexes (Complex 1-5) located on the mitochondrial inner membrane (IMM) (Nelson 1942-, 2005). This process fuels the proton (H+) translocation in order to generate a proton gradient, which creates a proton motive force consisting of chemical potential energy (difference in concentration of H+ across membrane) and electrical potential energy (results from separation of charge following H+ movement across membrane without counter ion) (Nelson 1942-, 2005). This proton motive force drives the synthesis of ATP from ADP and inorganic phosphate when protons move across the IMM through the proton pore of ATP synthase. This entire molecular process is called oxidative phosphorylation (OXPHOS) and is the primary means of energy generation within synovial fibroblasts.

Metabolites involved in the TCA cycle, whilst originally believed to remain within this cycle in a closed loop fashion, are now known to be contribute as metabolic

precursors to intermediary metabolites involved in cellular growth, nucleotide synthesis, fatty acid synthesis and storage pathways. Metabolites within this cycle are utilised for anabolic processes and replenished through degradative pathways and is tightly regulated and maintained to ensure a constant supply of metabolites for energy transfer (Nelson 1942-, 2005).

These TCA cycle metabolites have also been shown to alter the inflammatory status of cells. Dimethyl fumarate (DMF) for example is an immunomodulatory and anti-oxidative drug which is used for the symptomatic treatment of autoimmune disorders including multiple sclerosis and psoriasis (Tastan *et al.*, 2021). It has been shown to reduce LPS and ATP-induced NLRP3 inflammasome activation through reduced levels of IL-1β, IL-18, caspase-1, reactive oxygen species formation and damage, and inhibiting pyroptotic cell death in N9 murine microglia via Nrf2/NF-κB pathways (Tastan *et al.*, 2021). Succinate, another TCA cycle metabolite, has been shown to enhance IL-1β production in murine macrophages and deficiency of succinate receptor GPR91 attenuates the severity of arthritis in Sucnr1$^{-/-}$ mice (Tannahill *et al.*, 2013; Saraiva *et al.*, 2018). Accumulation of succinate alongside lactate and glutamine has been shown to induce synovial fibroblast invasive phenotype and in a CIA rodent model of arthritis, succinate increased VEGF production and induced angiogenesis in the arthritic synovium (Biniecka *et al.*, 2016; Li *et al.*, 2018). Interestingly, succinate was amongst the most elevated metabolites in OA synovial fluid from obese patients compared to normal weight patients (Farah *et al.*, 2022). This could suggest succinate is not only involved in supplying TCA cycle metabolites to residential and infiltrating cells at the inflamed synovium but could also be exacerbating the inflammatory profile of these cells thereby exacerbating the

inflammation at the arthritic joint, however this would require further investigation before establishing its role outside of energy metabolism.

6.2 Hypothesis

We hypothesise that

- OA synovial fibroblasts from obese patients are metabolically altered compared to fibroblasts from normal weight OA patients
- Differences in metabolic phenotype between obese and normal-weight fibroblasts is not simply as a result of biomechanical loading of the joint but is also due to the non-load bearing effect of obesity
- Obese OA synovial fibroblasts would have a greater capacity to maintain their inflammatory state compared to normal weight OA synovial fibroblast through increased metabolic flux upon inflammatory stimulus

6.3 Methods

6.3.3 Seahorse metabolic analysis explained

Term	Definition
Glycolysis	Glycolysis is measured as the ECAR rate reached by a given cell after the addition of saturating amounts of glucose. Maximum rate before oligomycin injection – last rate before glucose injection
Glycolytic Capacity	This measurement is the maximum ECAR rate reached by a cell following the addition of oligomycin, effectively shutting down oxidative phosphorylation and driving the cell to use glycolysis to its maximum capacity. Maximum rate before FCCP injection- last rate before glucose injection
Glycolytic Reserve	This measure indicates the capability of a cell to respond to an energetic demand as well as how close the glycolytic function is to the cell's theoretical maximum. Glycolytic capacity - Glycolysis
Non glycolytic acidification	This measures other sources of extracellular acidification that are not attributed to glycolysis Last rate before glucose injection

Table 6.1: Definition and calculations of terms used within the Glycolysis stress test (adapted from Agilent User Guide)

Term	Definition
Basal Respiration	Oxygen consumption used to meet cellular ATP demand resulting from mitochondrial proton leak. Shows energetic demand of the cell under baseline conditions. Last measurement before oligomycin – non-mitochondrial oxygen consumption
Maximal Respiration	The maximal OCR attained by adding the uncoupler FCCP. FCCP mimics a physiological "energy demand" by stimulating the respiratory chain to operate at maximum capacity, which causes rapid oxidation of substrates (sugars, fats, and amino acids) to meet this metabolic challenge. Shows the maximum rate of respiration that the cell can achieve. Maximal respiration rate - non-mitochondrial oxygen consumption
Proton Leakage	Remaining basal respiration not coupled to ATP production. Proton leak can be a sign of mitochondrial damage or can be used as a mechanism to regulate the mitochondrial ATP production. Minimum rate after oligomycin injection - non-mitochondrial oxygen consumption
ATP Production	The decrease in OCR upon injection of the ATP synthase inhibitor oligomycin represents the portion of basal respiration that was being used to drive ATP production. Shows ATP produced by the mitochondria that contributes to meeting the energetic needs of the cell. Basal respiration rate – proton leak

Table 6.2: Definition and calculations of terms used within the Mitochondrial stress test (adapted from Agilent User Guide)

6.4 Results

6.4.1 Patient characteristics

OA synovial fibroblasts were collected from different joints following total joint replacement for OA in the hip or knee and following arthroscopy in patients with hand OA. These synovial fibroblasts underwent Seahorse metabolic flux analysis to investigate glycolysis and oxidative phosphorylation of these cells. Cells were grouped into obese and normal weight based on their BMI regardless of joint of origin or grouped into non-loadbearing (hand OA) and loadbearing (hip and knee OA) regardless of BMI. Analysis of patient data showed no significant differences in age, height or waist: hip ratio (W:H) (Table 6.3). There was however a significant difference in BMI, weight, waist and hip circumference between normal weight and obese patients (Table 6.3).

[2]	Normal Weight (n = 9)	Obese (n = 11)	p value	Load Bearing (n = 16)	Non-loadbearing (n = 4)	p value
Age (years)	63 ± 9.8	67.91 ± 10.98	0.31	68.13 ± 10.24	56 ± 4.2	0.0526
Female:Male	8:1	9:2		14:2	3:1	
BMI (kg/m^2)	23.12 ± 1.5	32.35 ± 1.6	<0.0001	28.25 ± 4.67	28.01 ± 6.79	>0.9999
Weight (kg)	59.38 ± 5.28	87.29 ± 11.38	<0.0001	76.06 ± 18.18	73.4 ± 11.65	0.8652
Height (cm)	160.4 ± 10.49	164 ± 9.41	0.4305	162.2 ± 10.01	163.3 ± 10.37	0.8498
Waist Circumference (cm)	84.7 ± 8.06	105.3 ± 10.55	<0.0001	96.15 ± 13.95	95.5 ± 16.38	0.9368
Hip Circumference (cm)	93.75 ± 6.05	117.9 ± 8.2	<0.0001	106 ± 13.86	111 ± 17.32	0.5485
W:H	0.91 ± 0.11	0.89 ± 0.07	0.7347	0.9 ± 0.1	0.86 ± 0.05	0.3395

Table 6.3: Patient Characteristics

1. [2] Shapiro-Wilk and Kolmogorov-Smirnov Normality test computed to test for normal distribution of data. Student unpaired two-tailed t test performed for comparisons. Groups with non-parametric distribution were analysed using Mann-Whitney t test.[2]

6.4.2 Comparative analysis of metabolic flux in OA synovial fibroblasts isolated from lean and obese patients

Seahorse analysis of grouped normal weight compared to obese OA synovial fibroblasts found, on average, an increase in basal glycolysis and an increase in glycolytic capacity in obese OA synovial fibroblasts upon TNFα stimulation, as well as maximal respiration and ATP production. However, this did not reach statistical significance (Figure 6.2 and 6.3).

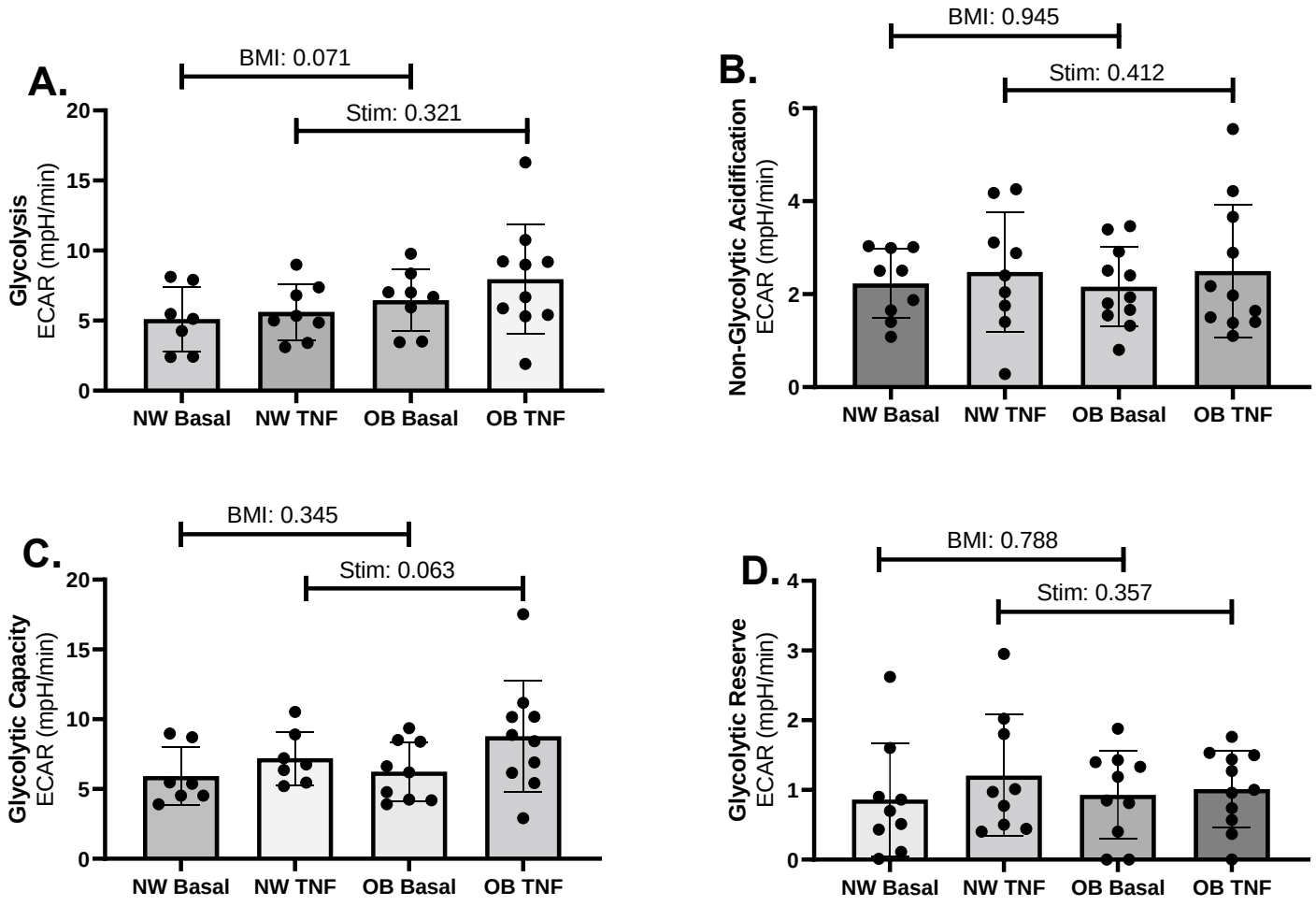

Figure 6.2: Glycolysis stress test of OA synovial fibroblasts from normal weight and obese patients either basal or following TNFα stimulation.

Fibroblasts from n=9 normal-weight (NW) and n=11 obese (OB) patients were either unstimulated (basal) or stimulated for 24 h with TNFα (10 ng/ml). Glycolysis stress test data is represented as (**A**) Glycolysis. (**B**) Non-glycolytic acidification. (**C**) Glycolytic Capacity and (**D**) Glycolytic reserve. Data was analysed by 2-way ANOVA and is presented as mean ± SD. * = $p < 0.05$, ** = $p \leq 0.01$.

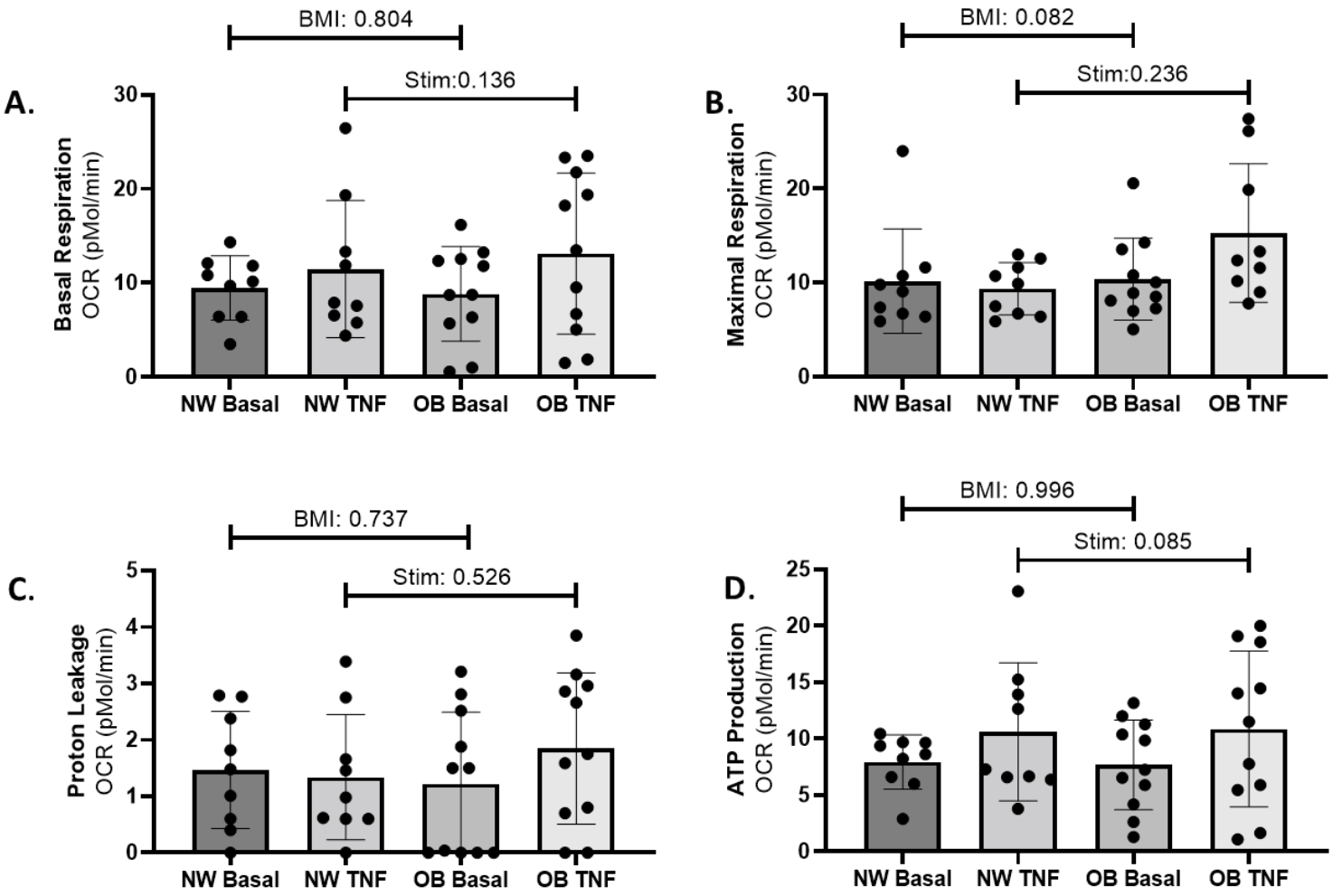

Figure 6.3: Mitochondrial stress test of OA synovial fibroblasts from normal weight and obese patients either basal or following TNFα stimulation.

Fibroblasts from n=9 normal-weight (NW) and n=11 obese (OB) patients were either unstimulated (basal) or stimulated for 24 h with TNFα (10 ng/ml). Mitochondrial stress test data is represented as **(A)** Basal Respiration, **(B)** Maximal respiration, **(C)** Proton leakage and **(D)** ATP production. Data was analysed by 2-way ANOVA and is presented as mean ± SD. * = $p < 0.05$, ** = $p \leq 0.01$

6.4.3 Comparative analysis of metabolic flux in OA synovial fibroblasts isolated from loadbearing and non-loadbearing joints

As there were no differences in the metabolism of OA synovial fibroblast from different joints grouped by BMI, cells were then grouped based on their anatomical location, with non-loadbearing synovial fibroblasts from hand OA patients compared to loadbearing synovial fibroblasts from hip and knee OA (Table 6.3).

Interestingly, although joint loadbearing did not affect glycolysis, there was a significant increase in glycolytic reserve in loadbearing OA synovial fibroblast compared to non-loadbearing hand OA synovial fibroblasts (figure 6.4). Furthermore, there was also a significant increase in basal respiration, proton leakage and ATP production in in loadbearing OA synovial fibroblast compared to non-loadbearing OA synovial fibroblasts (figure 6.5).

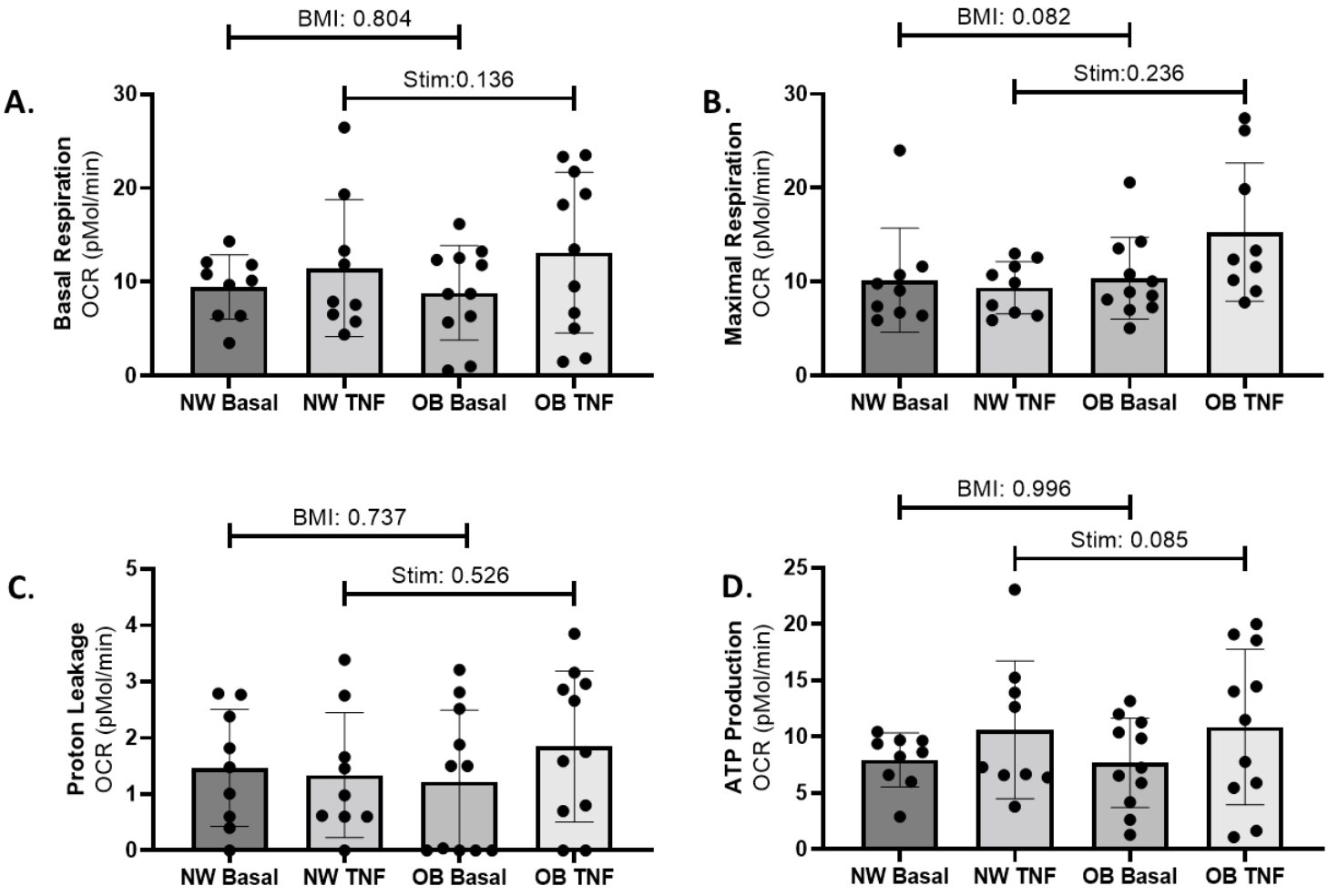

Figure 6.4: Glycolysis stress test of OA synovial fibroblasts from loadbearing and non-loadbearing joints either basal or following TNFα stimulation.

Fibroblasts from n=16 loadbearing (LB) and n=4 non-loadbearing (NLB) joints were either unstimulated (basal) or stimulated for 24 h with TNFα (10 ng/ml). Glycolysis stress test data is represented as **(A)** Glycolysis, **(B)** Non-glycolytic acidification, **(C)** Glycolytic capacity and

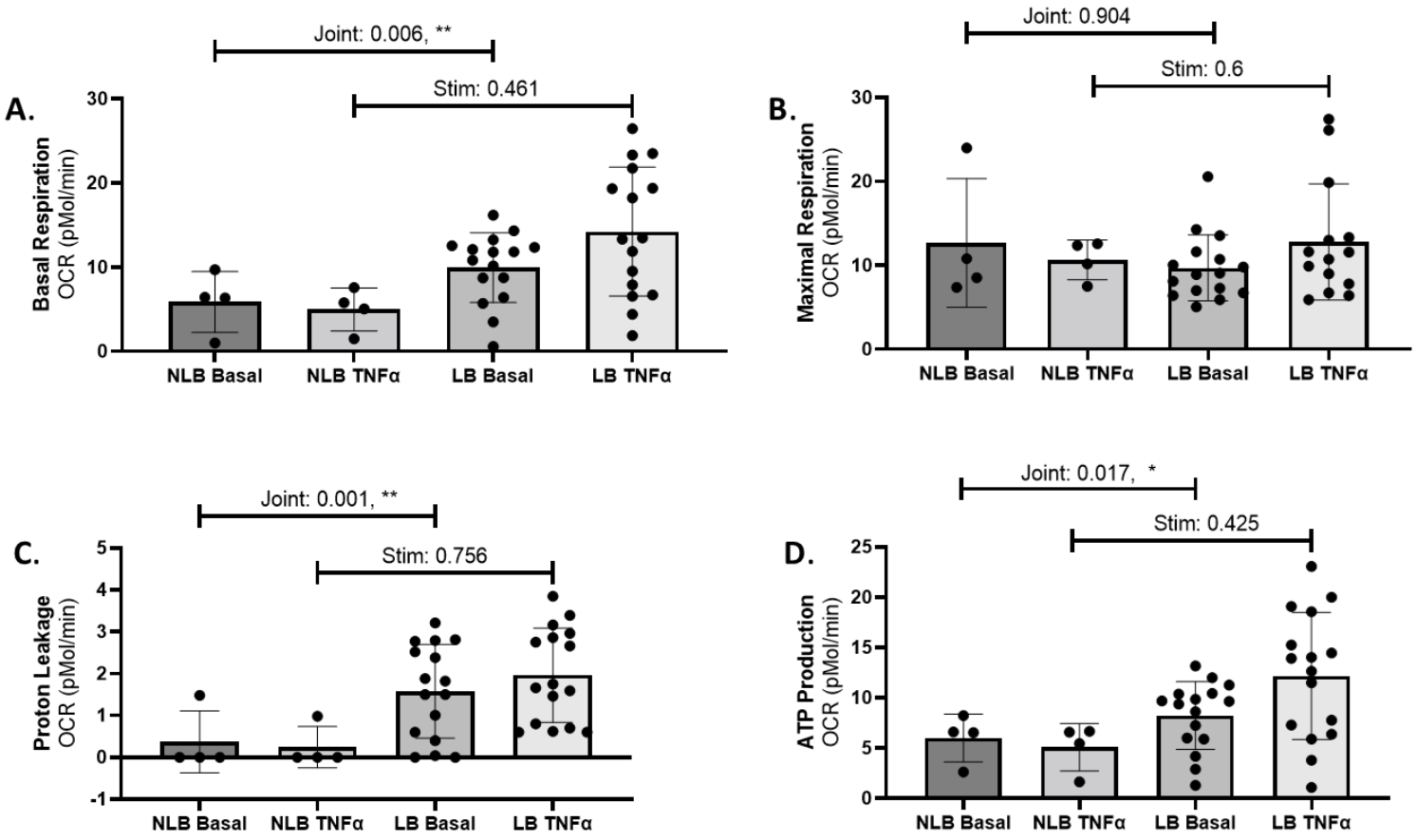

Figure 6.5: Mitochondrial stress test of OA synovial fibroblasts from loadbearing and non-loadbearing joints either basal or following TNFα stimulation.

Fibroblasts from n=16 loadbearing (LB) and n=4 non-loadbearing (NLB) joints were either unstimulated (basal) or stimulated for 24 h with TNFα (10 ng/ml). Mitochondrial stress test data is represented as **(A)** Basal Respiration, **(B)** Maximal respiration, **(C)** Proton leakage and **(D)** ATP production. Data was

In an attempt to discern the metabolic changes associated with loadbearing and obesity regardless of joint type, the next step was to investigate metabolic flux of OA synovial fibroblasts from different joints without grouping these samples. A clear difference observed in these OA synovial fibroblasts was an elevation in glycolysis in hip OA synovial fibroblasts compared to either knee or hand OA synovial fibroblasts (figure 6.6).

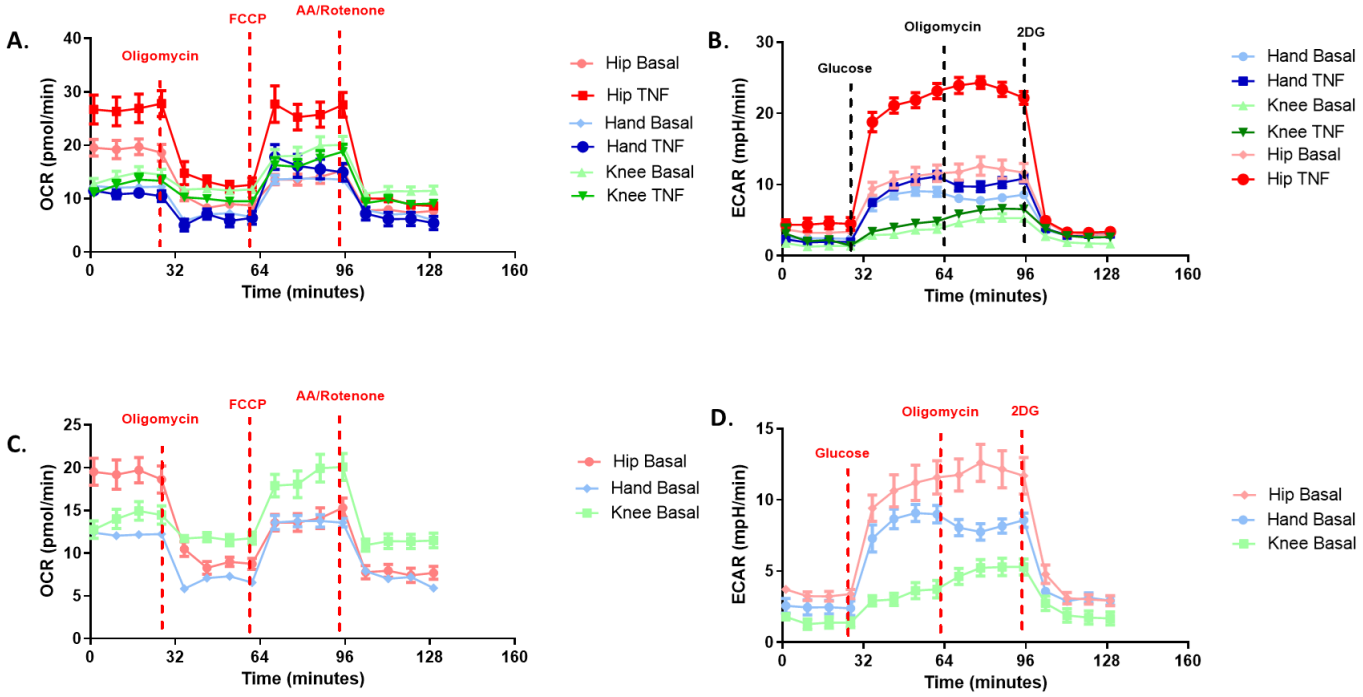

Figure 6.6: Metabolic rates of OA synovial fibroblasts from different joints either basal or following TNFα stimulation.

Representative data displayed with OCR as measure of oxidative phosphorylation in **(A)** and **(C)** and ECAR as a measure of glycolysis in **(B)** and **(D).** All data presented as mean ± SEM.

Metabolic flux analysis using Seahorse glycolysis stress test revealed a significant increase in glycolysis in hip OA synovial fibroblasts when stimulated with TNFα (figure 6.7). Glycolytic capacity increased in hip OA synovial fibroblasts but not significantly and did not increase for knee or hand OA synovial fibroblast (figure 6.7). Glycolytic reserve was higher in hip OA synovial fibroblasts compared to both knee and hand OA synovial fibroblast but did not increase with TNFα stimulation (figure 6.7). Mitochondrial stress test revealed a higher basal respiration, proton leakage and ATP production in hip OA synovial fibroblasts compared to both knee and hand OA synovial fibroblast (figure 6.8). There was also a significant increase in basal respiration and ATP production in hip OA synovial fibroblasts when stimulated with TNFα but this did not reach significance in maximal respiration (figure 6.8).

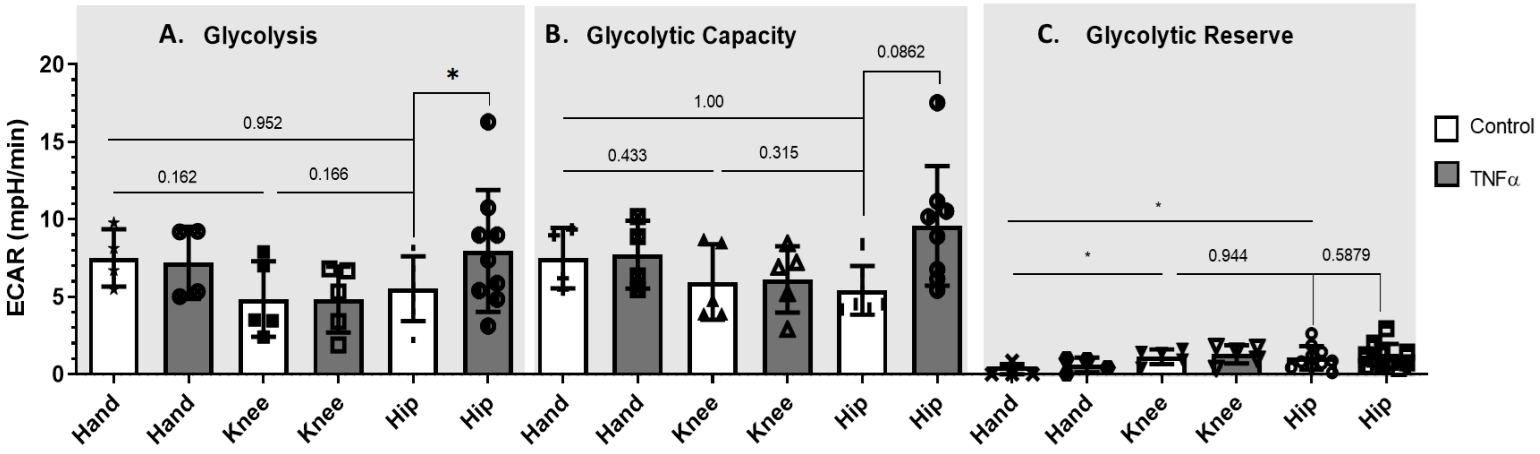

Figure 6.7: Glycolysis stress test of OA synovial fibroblasts from hip, knee, and hand joints either basal or following TNFα stimulation.

Fibroblasts from n=11 hip, n=5 knee and n = 4 hand joints were either unstimulated (basal) or stimulated for 24 h with TNFα (10 ng/ml). Glycolytic stress test data is represented as **(A)** Glycolysis, **(B)** Glycolytic capacity and **(C)** Glycolytic reserve. . Data was analysed by 2-way ANOVA and is presented as mean ± SD. * = $p < 0.05$, ** = $p \leq 0.01$

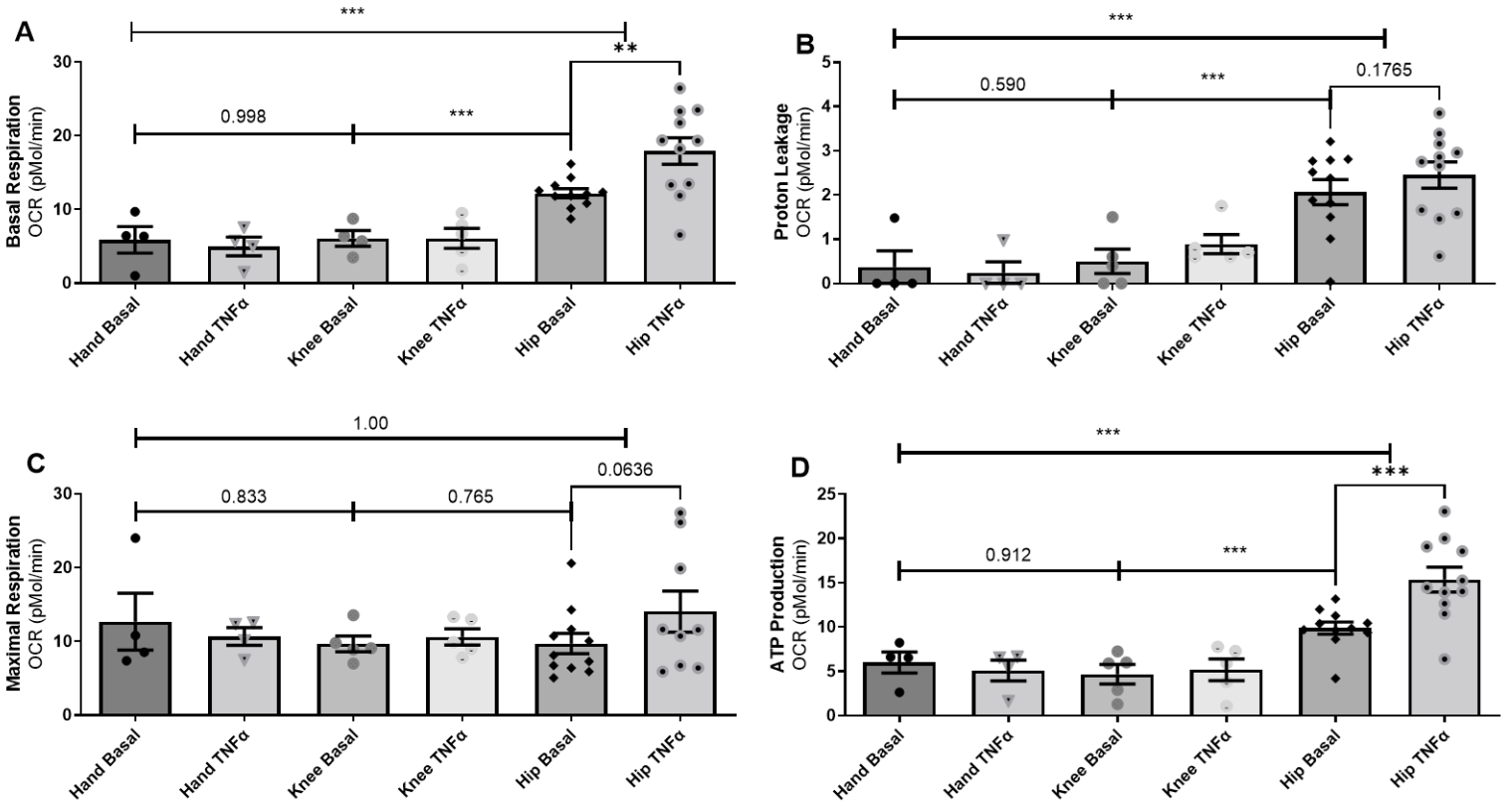

Figure 6.8: Mitochondrial stress test of OA synovial fibroblasts from hip, knee, and hand joints either basal or following TNFα stimulation.

Fibroblasts from n=11 hip, n=5 knee and n = 4 hand joints were either unstimulated (basal) or stimulated for 24 h with TNFα (10 ng/ml). Mitochondrial stress test data is represented as **(A)** Basal Respiration, **(B)** Proton leakage **(C)** Maximal respiration and **(D)** ATP production. Data was analysed by 2-way ANOVA and is presented as mean ± SD. * = $p < 0.05$, ** = $p \leq 0.01$, *** = $p \leq 0.001$.

6.4.4 Obese hip OA synovial fibroblasts show altered metabolic phenotype

Following data analysis of OA synovial fibroblasts from different joints, it was found that hip OA synovial fibroblasts were the most responsive to TNFα stimulation compared to knee and hand OA synovial fibroblast. Following this observation, hip OA synovial fibroblasts from normal weight and obese patients were treated with TNFα (10ng/ml) and IL-6 mRNA expression was measured using RT-qPCR (figure 6.9). IL6 expression increased in normal weight OA synovial fibroblasts after 4 and 24 hours however obese OA synovial fibroblast were not as responsive (figure 6.9). This was also mirrored in lactate secretion of these OA synovial fibroblasts, as TNFα stimulation (10ng/ml) increased lactate production in normal weight OA synovial fibroblasts but not in obese OA synovial fibroblasts which already had high basal level of lactate secretion within their conditioned media (figure 6.9).

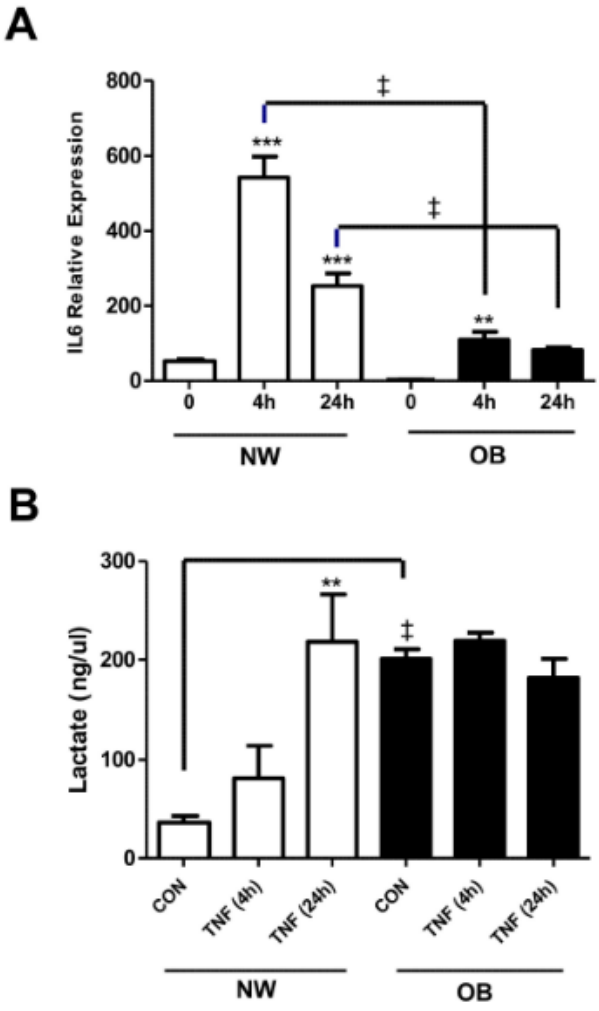

Figure 6.9: Lactate secretion is greater in obese OA synovial fibroblasts and is induced during the inflammatory response.

The effect of TNF (10 ng/mL) stimulation of synovial fibroblasts from normal-weight (NW) or obese OA patients (n = 3) on (A) the expression of IL-6 and (B) secretion of lactate after 4 h and 24 h stimulation. Data expressed as mean ± SEM. ** = $p < 0.01$, *** = $p < 0.001$, significantly different from time 0. ‡ = $p < 0.01$, significantly different between synovial fibroblasts from patients with different BMI. (Farah et al, 2022)

Following this observation, RT-qPCR was conducted to determine the expression of key lactate transporters (namely, MCT1, MCT2 and MCT4) within hip OA synovial fibroblasts in obese and normal weight patients following stimulation with TNFα stimulation (10ng/ml for 24 hrs) (figure 6.10). Both MCT2 and MCT4 lactate transporter expression increased following TNFα stimulation (10ng/ml for 24 hrs) in both normal weight and obese hip OA patients however MCT1 did not respond to TNFα stimulation for either group (figure 6.10). Therefore, protein expression of this lactate transporter was further investigated using immunoblotting of normal weight and obese hip OA synovial fibroblast lysates (figure 6.11). Although there was an increase in protein expression following TNFα stimulation (10ng/ml for 24 hrs), this did not reach statistical significance (figure 6.11).

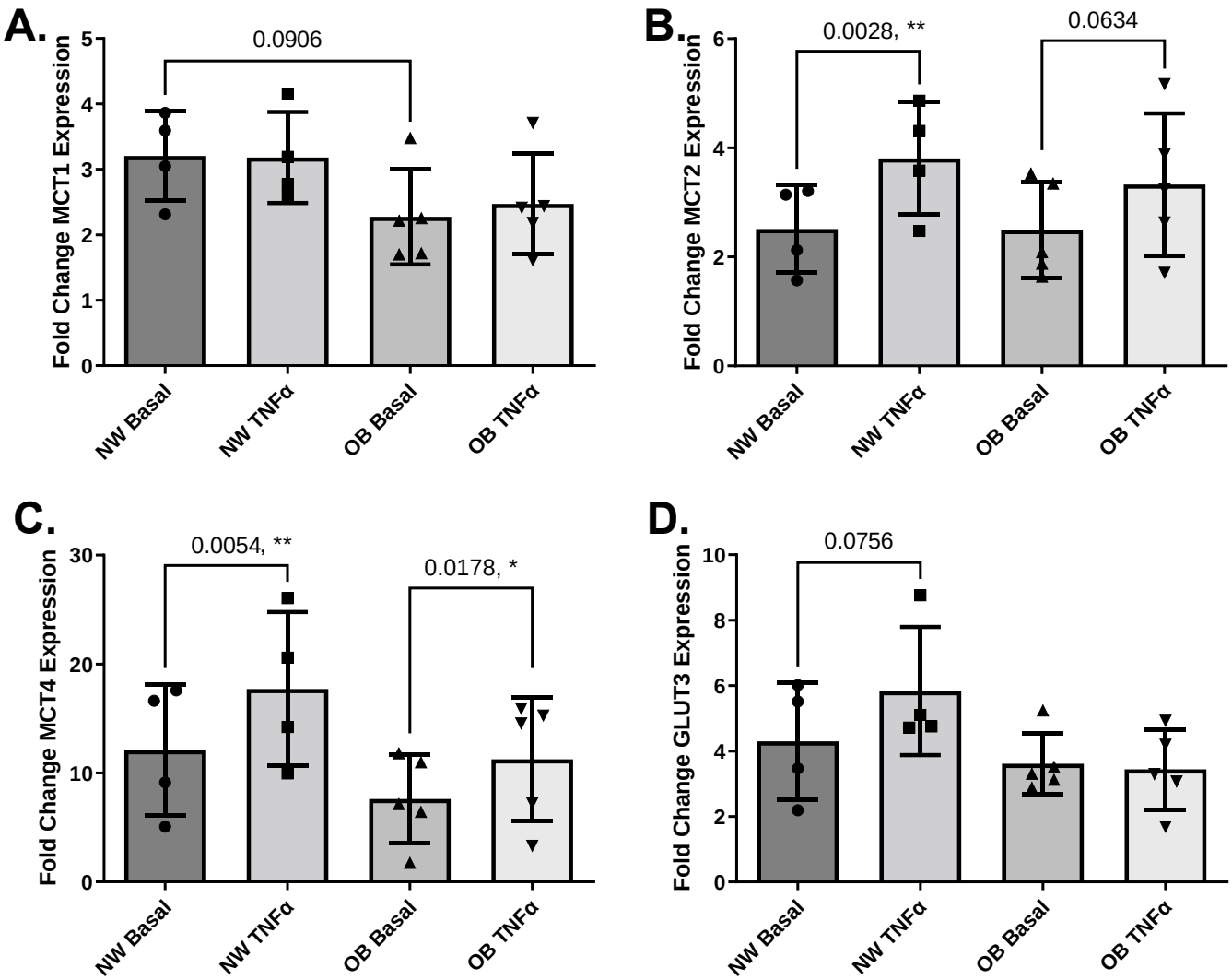

Figure 6.10: Gene expression of transporter proteins in hip OA synovial fibroblasts from normal weight and obese patients either basal or following TNFα stimulation.

Fibroblasts from n=4 normal weight (NW) hip and n = 5 obese (OB) hip were either unstimulated (basal) or stimulated for 24 h with TNFα (10 ng/ml). Gene expression was quantified using RT-qPCR for lactate transporters (A) MCT1, (B) MCT2, (C) MCT4 and glucose transporter (D) GLUT3. Statistical analysis was calculated using student t test. All data presented as mean ± SD. * = $p < 0.05$, ** = $p < 0.01$

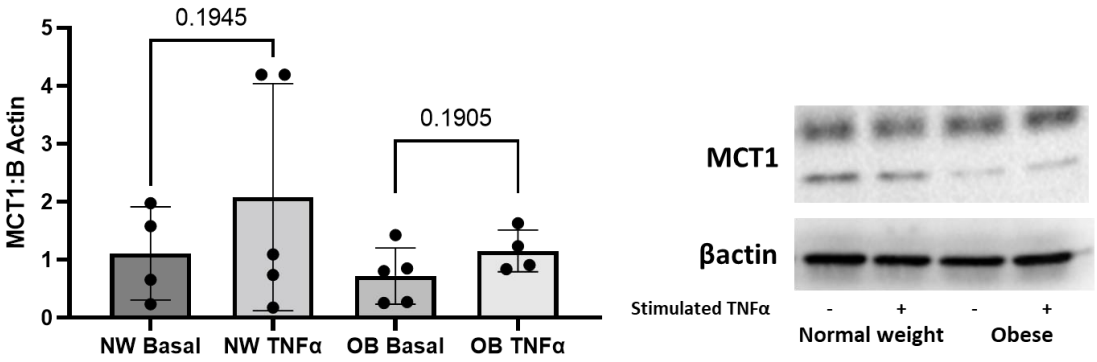

Figure 6.11: Protein expression of MCT1 lactate transporter in hip OA synovial fibroblast from normal weight and obese patients either basal or following TNFα stimulation.

Fibroblasts from n = 4 normal weight (NW) and n = 4 obese (OB) patients were either unstimulated (basal) or stimulated for 24 h with TNFα (10 ng/ml). Protein expression was quantified using Western blot. Statistical analysis was calculated using paired student t test. All data presented as mean ± SD.

Another area of interest within these hip OA synovial fibroblast was glucose uptake. mRNA expression of the GLUT3 transporter was increased following TNFα stimulation (10ng/ml for 24 hrs) in normal weight OA synovial fibroblasts however this did not reach statistical significance (figure 6.10). Notably, another highly expressed glucose transporter in OA synovial fibroblasts is GLUT1 which was significantly increased in obese hip OA synovial fibroblasts compared to normal weight OA synovial fibroblasts and therefore this does not rule out a changes in glucose transporter levels within these cells (table 6.4). Glucose uptake was increased in normal weight OA synovial fibroblasts following TNFα stimulation (10ng/ml for 24 hrs) however this again did not reach statistical significance (figure 6.12).

Table 6.4: Expression of glucose transporters from OA synovial fibroblasts in normal weight compared to obese OA patients (Nanus *et al.*, 2020)

Gene	Normal Weight (FPKM)	Obese (FPKM)	log2(fold change)	P value	Q value
GLUT1	17.3494	43.4279	1.32374	0.0001	0.00711927
GLUT2	0	0	0	1	1
GLUT3	7.63856	13.665	0.839111	0.002	0.0682198
GLUT4	0.0270409	0.0404998	0.582771	1	1
HIF1A	108.743	203.669	0.905296	0.00425	0.114713

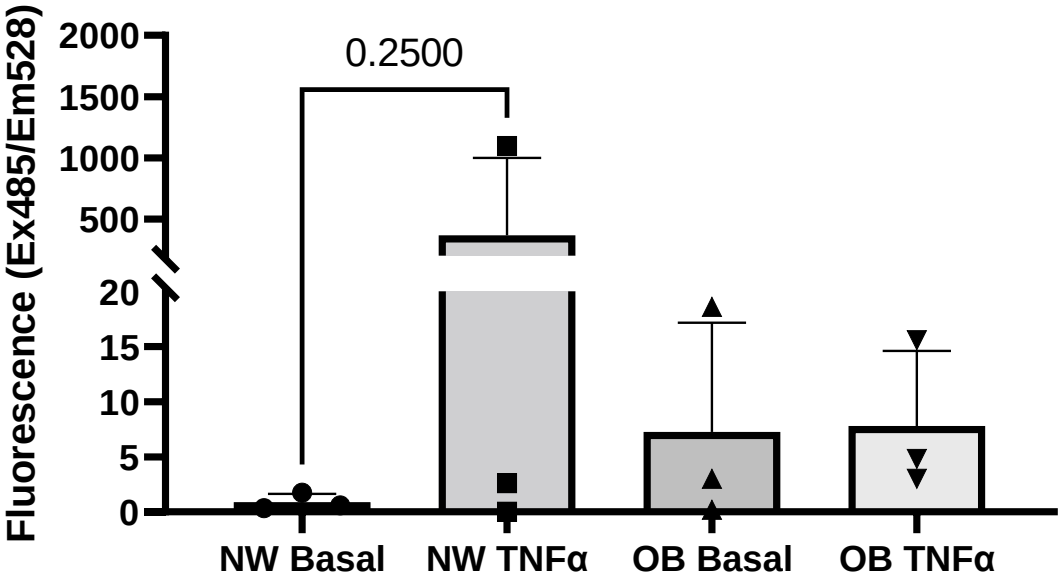

Figure 6.12: Glucose uptake of hip OA synovial fibroblasts from normal weight and obese patients either basal or following TNFα stimulation.

Fibroblasts from n=3 normal weight (NW) hip and n = 3 obese (OB) hip were either unstimulated (basal) or stimulated for 24 h with TNFα (10 ng/ml). Glucose uptake was measured using fluorescent uptake of glucose analog 6NBDG. Statistical analysis was calculated using student t test. All data presented as mean ± SD.

Following this examination into glucose and lactate metabolism, we next conducted seahorse glycolysis and mitochondrial stress tests in normal weight and obese hip OA synovial fibroblasts following TNFα stimulation (10ng/ml for 24 hrs) (figure 6.13 and 6.14). Glycolysis and glycolytic reserve were found to be higher in obese OA synovial fibroblasts, compared to normal weight OA synovial fibroblasts without stimulation (basally) (figure 6.13). There was also a significant increase in glycolytic capacity of normal weight OA synovial fibroblasts following TNFα stimulation (10ng/ml for 24 hrs) (figure 6.13).

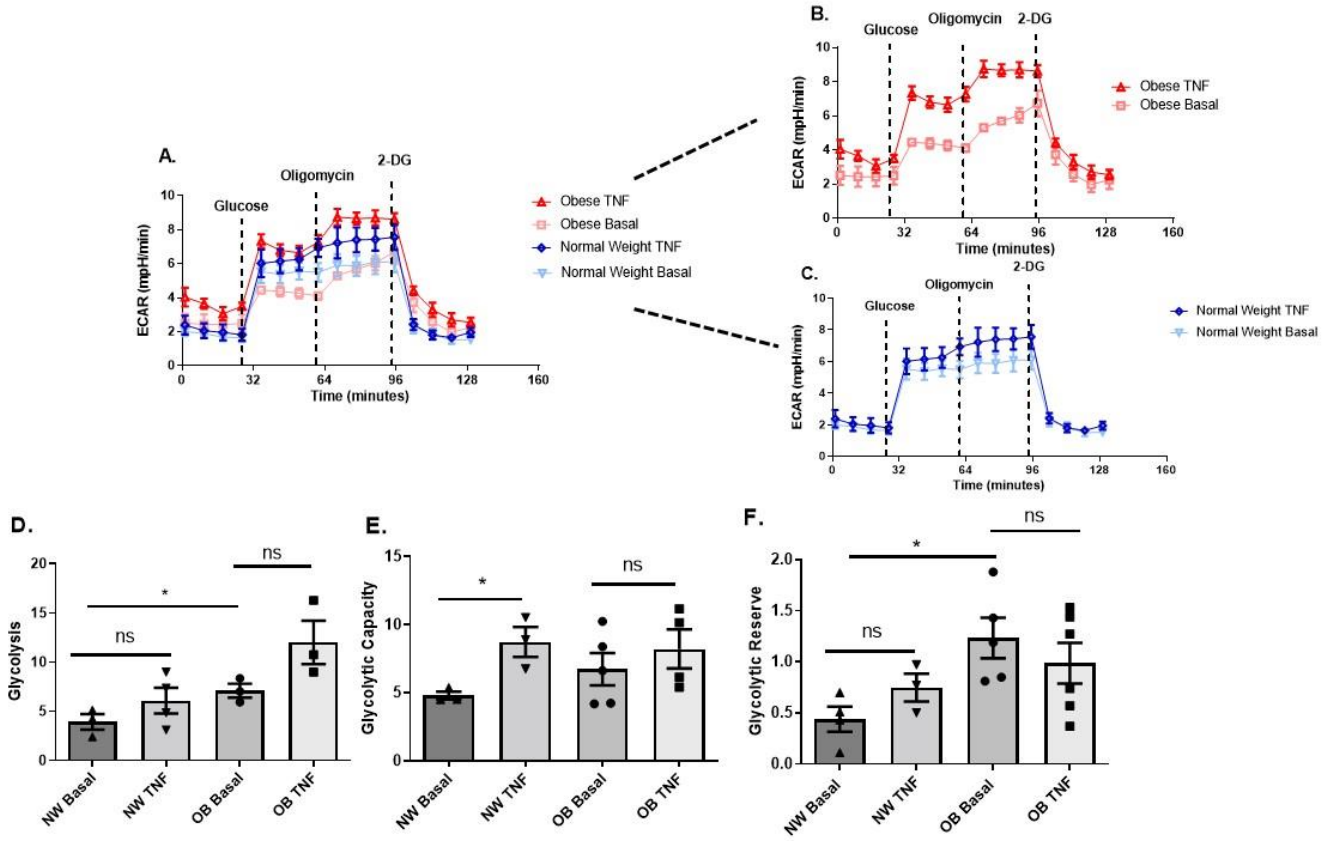

Figure 6.13. Obese and normal-weight OA synovial fibroblasts exhibit differential glycolytic metabolism.

(A–C) OA synovial fibroblasts from obese patients (n = 6 patients) stimulated with TNFα at 10 ng/mL for 24 h show elevated aerobic glycolysis, compared to stimulated and unstimulated OA synovial fibroblasts from normal weight (n = 6 patients, with 5 biological replicates per patient). (D) Glycolysis levels are significantly increased in obese OA synovial fibroblasts when stimulated with TNFα at 10 ng/mL for 24 h. (E) Glycolytic capacity of normal weight OA synovial fibroblasts is elevated when challenged with TNFα at 10 ng/mL for 24 h. (F) Glycolytic reserve is increased in unstimulated obese OA synovial fibroblasts, compared to unstimulated normal weight OA synovial fibroblasts. All data presented as mean ± SEM. * = $p < 0.05$. (Farah et al, 2022)

There was also an increase in basal, maximal respiration and ATP production in obese OA synovial fibroblasts following TNFα stimulation (10ng/ml for 24 hrs) but not in normal weight OA synovial fibroblasts (figure 6.14). Using Mito tracker green staining of obese OA synovial fibroblasts, mitochondrial mass was inferred, with an increase in mitochondria staining in obese OA synovial fibroblasts following TNFα stimulation (10ng/ml for 24 hrs) however normal weight OA synovial fibroblasts were not stained nor was data collected on mitochondrial size and number (figure 6.15).

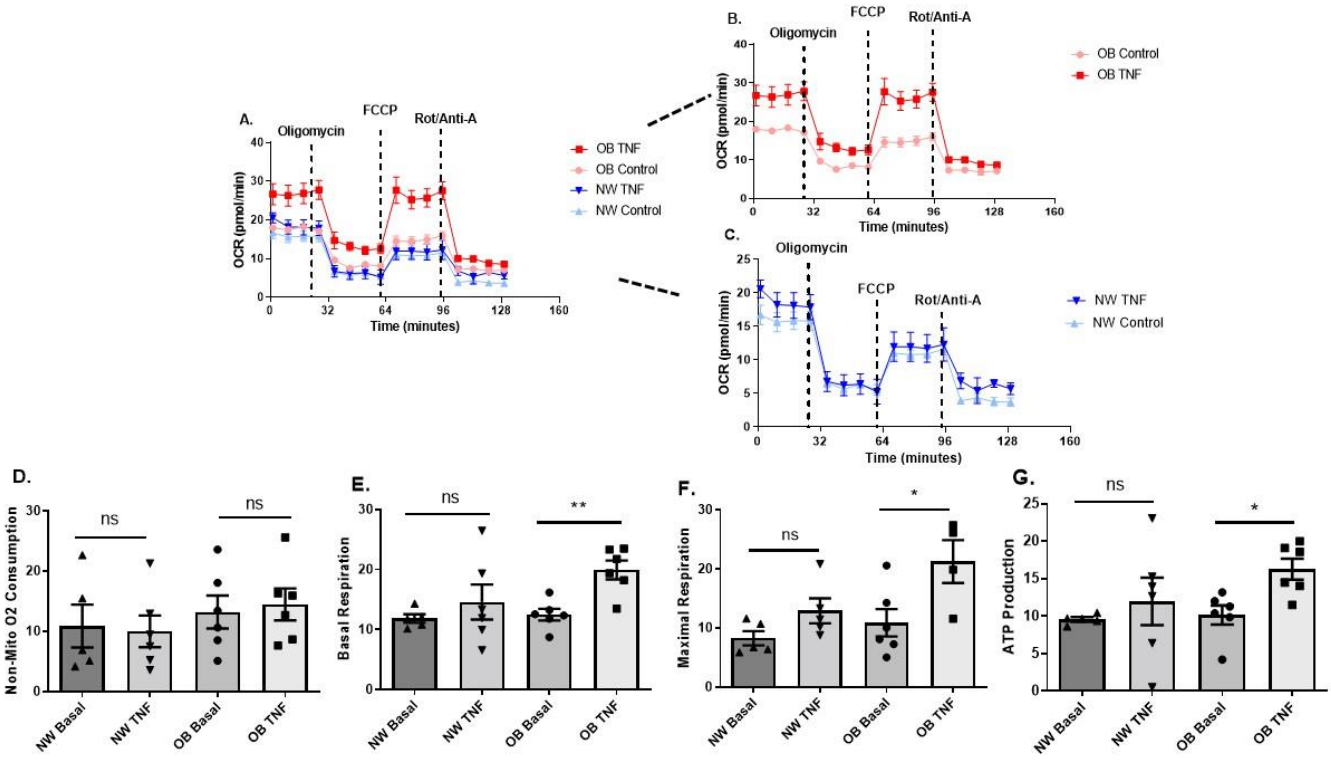

Figure 6.14. Obese and normal-weight OA synovial fibroblasts exhibit differential mitochondrial respiration.

(**A**–**C**) OA synovial fibroblasts from obese patients (n = 6 patients, with 5 biological replicates per patient) stimulated with TNFα at 10 ng/mL for 24 h show increased mitochondrial respiration, compared to fibroblasts from normal weight patients. (**D**) Non-mitochondrial oxygen consumption does not increase in OA synovial fibroblasts from obese or normal weight patients with TNFα stimulation. (**E**) basal respiration; (**F**) maximal respiration; and (**G**) ATP production from mitochondrial respiration significantly increase in obese OA synovial fibroblasts when stimulated with TNFα at 10 ng/mL for 24 h. All data presented as mean ± SEM. * = $p < 0.05$, ** = $p < 0.01$. (Farah et al, 2022)

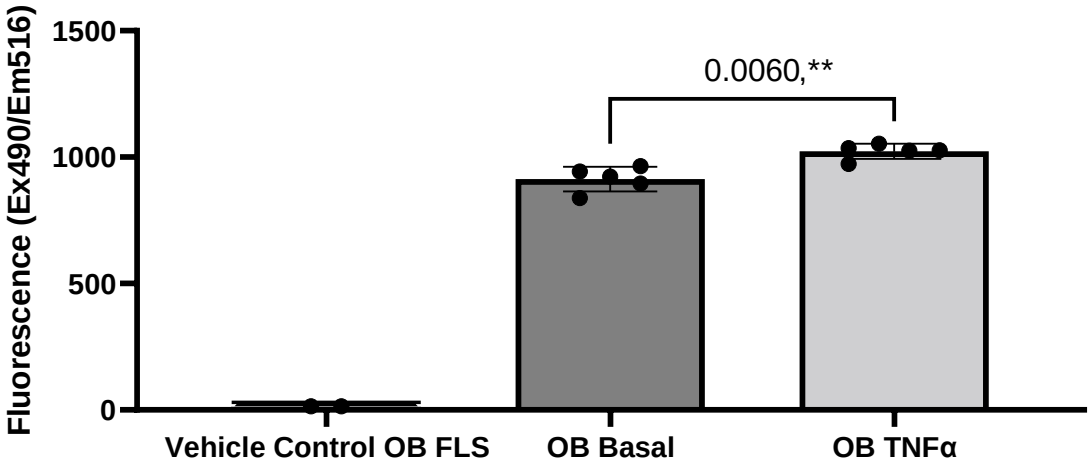

Figure 6.15: Mitochondrial mass of obese hip OA synovial fibroblasts either basal or following TNFα stimulation.

Fibroblasts from n=1 obese (OB) hip (n = 5 biological replicates) were either unstimulated (basal) or stimulated for 24 h with TNFα (10 ng/ml). Mitochondrial mass was measured using Mitotracker Green staining. Statistical analysis was calculated using student t test. All data presented as mean ± SD. * = $p < 0.05$, ** = $p \leq 0.01$

6.5 Discussion

In the previous chapter, metabolic pathway analysis was conducted using RNA sequencing of OA synovial fibroblasts from different joints and from this analysis, differences in metabolic pathways were identified in both loadbearing and obesity comparison. Following on from this, metabolic flux analysis of OA synovial fibroblasts from different joints was conducted to examine if there were any differences in glycolysis and oxidative phosphorylation.

Notably, despite no significant differences observed in glycolysis and oxidative phosphorylation when grouping based on BMI, there was a significant increase in glycolytic reserve, basal respiration, proton leakage and ATP production in loadbearing OA synovial fibroblasts compared to non-loadbearing OA synovial fibroblasts. This observation is most likely driven by the hip OA synovial fibroblast than the knee OA synovial fibroblasts. Since the hip OA synovial fibroblasts when analysed separately show a significant increase in these parameters (baring glycolytic reserve) indicative of being more metabolically active both basally and being more responsive to inflammatory stimulus.

Based on increased Mitotracker staining, one possible explanation to the greater metabolic activity of hip OA synovial fibroblasts could be their ability to increase mitochondria upon stimulation. However, confirmation of this hypothesis would require further investigation before establishing this as the means of increased oxidative phosphorylation within these cells. We have previously shown these obese hip OA synovial fibroblasts proliferate more than normal weight hip OA synovial fibroblasts (Nanus *et al.*, 2020). This increase in cell number does not however account for the differences observed in glycolysis or oxidative phosphorylation as

doubling the cell number to 60,000 cells/well did not result in an increase in either OCR or ECAR, possibly due to the limit of surface area per well and the numbers of cells which can adhere to the bottom of these wells (data not shown).

The data in this chapter shows changes in oxidative phosphorylation in obese hip OA synovial fibroblasts following TNFα stimulation and this could be partially explained by an increase in mitochondria based on mitotracker green staining however no data was collected on mitochondrial number or size which could be a good metric to determine whether mitotracker green staining is an accurate measure of mitochondrial number. Similarly, another issue which would require addressing is the functionality and quality of these mitochondria. There was an increase (although not statistically significant) in proton leakage within obese OA synovial fibroblasts following TNFα stimulation (data not shown) which suggests these mitochondria are not all entirely functional. One way to investigate this would be to conduct a mitochondrial function assay, looking into mitochondrial membrane potentials using commercially available fluorescent Mito probe which can be used to can be used to determine healthy versus depolarized mitochondria (based on changes in active mitochondria staining vs mitochondria with low membrane potential signal ratio) or electron microscopic imaging of these cells with a particular focus on the mitochondrial morphology to establish how many of these mitochondria are functional.

Likewise, stimulation using another pro-inflammatory cytokine (IL1β) did not elicit a similar response to TNFα (data not shown) suggesting this change in glycolysis and oxidative phosphorylation might be a specific TNFα dependant mechanism. Previous research has shown similar results in RA synovial fibroblasts when stimulated with TNFα, resulting in increased glycolysis and oxidative phosphorylation (Koedderitzsch

et al., 2021). In this study, TNFα stimulation did not result in an increase in total protein content but did result in an increased expression of HIF1α and GLUT1 as well as HIF1α target genes (Koedderitzsch *et al.*, 2021). This change in metabolic state was driven by NF-κB activation and blocking NF-κB through TAK1 inhibitor reduced this TNF-induced glycolysis, glycolytic capacity, and glycolytic reserve in synovial fibroblasts (Koedderitzsch *et al.*, 2021). Similarly, there was a reduction in GLUT1, HIF1α and its target genes as well as a reduction in pro-inflammatory chemokines and matrix metalloproteases, IL-6 and MMP-3, after TNF stimulation (Koedderitzsch *et al.*, 2021). This effect was similar to the positive control, an approved anti-TNF antibody, Adalimumab, suggesting the mechanism through which TNF induces increased glycolysis is through TNF/TAK1/HIF1A/glycolysis signalling axis (Koedderitzsch *et al.*, 2021). RNA sequencing analysis of obese hip OA synovial fibroblast showed a significant increase HIF1A expression compared to normal weight OA synovial fibroblasts (table 4) and although IPA canonical pathway analysis did not show a high z score or p value for HIF1A signalling (z score 1.1, log (p value) 1.24), RNA sequencing of TNFα stimulated hip OA synovial fibroblasts might provide a clear link, possibly similar to that observed in RA synovial fibroblasts.

Another area of particular interest is the role lactate plays in the inflammatory microenvironment of OA. It has recently been established that lactate accumulates in tissue environments of chronic inflammatory diseases, and is likely a key factor in driving immune-mediated inflammation through $CD4^+$ T cells and the adoption of their effector phenotype and retention within inflamed tissues (Certo *et al.*, 2020; Khatib-Massalha *et al.*, 2020; Farah *et al.*, 2022). Lactate levels in the synovial joint in inflammatory arthritis are particularly high, reaching 20mM in the rheumatoid joint, and even higher in the tumour microenvironment (Haas *et al.*, 2015). Lactate

secretion was increased in obese hip OA synovial fibroblasts compared to normal weight OA synovial fibroblast and OA synovial fibroblast increase expression of lactate transporters MCT2 and MCT4 upon TNFα stimulation. This increased export of lactate, particularly by obese OA synovial fibroblasts, could be utilised by immune cells in inflammatory joint to fuel their energy needs alongside polarising these infiltrating immune cells in order to adopt a more inflammatory phenotype. Although early data confirming the presence of infiltrating $CD3^+$ T lymphocytes at obese OA hip synovium has been collected, this theory would require further investigation in order to corroborate these findings, possibly through co-culture assays.

Notably, hip OA synovial fibroblasts from obese patients not only show increased basal lactate production but also exhibit greater mitochondrial respiration and glycolytic reserve. However, these obese OA synovial fibroblasts upon stimulation with TNFα could not secrete more lactate, unlike the more metabolically plastic normal weight OA synovial fibroblasts. This high constitutively active metabolic phenotype of obese OA synovial fibroblasts may be required to maintain the increased basal inflammatory phenotype of these cells, and therefore therapeutically targeting these metabolic pathways might reduce their metabolic capacity and ameliorate this deleterious phenotype and possibly reduce the synovitis within the OA joint.

6.5.1 Limitations

As with the majority of studies the design of the current study is subject to limitations. The first being the experiments conducted using fluorescence-based plate reader. Mitotracker green staining and glucose uptake assay was done using plate reader assay. It is well established that this method of detection is less sensitive than microscope or flow cytometers and therefore degrees of change in fluorescence may not be as accurate as using other technologies. Whilst visualisation of Mitotracker green staining using confocal microscope might yield some insights into mitochondrial number. Likewise, flow cytometry would also be an interesting method of detection, giving cell number as well as staining fibroblasts.

Another issue is the variability within the glucose uptake assay. This assay although useful would require further patient numbers to possibly see an effect and by only measuring the uptake after an hour, some of the information regarding glucose uptake maybe lost from earlier timepoint. Another future experiment which could be conducted would be to observe glucose uptake across a shorter time period, to see early effects.

The final limitation associated with this study would be the limited work conducted on lactate transporter protein expression. Data was shown only on the protein expression of one lactate transporter (MCT1). Whilst several attempts were made to purify and immunolabel these other lactate transporters, a consistent result could not be achieved. This may be due to lower protein expression or issues with the antibody utilised. Therefore, further optimisation of immunoblotting would be required to obtain accurate readings before establishing changes in protein transporter expression. Likewise, these transporters will also transport other short-chain monocarboxylates such as ketone bodies for MCT4 and pyruvate/ketone bodies for

MCT1 (Song *et al.*, 2020). This means although the relationship between transporter expression and lactate transport is inferred, it is not necessarily the only molecules being transported within these cells.

Along the same line, transporter expression was measured only after 24 hours of TNFα stimulation. Early research on quiescent fibroblasts, revealed increased transcription of GLUT1 after 15 minutes exposure to TNFα (Cornelius *et al.*, 1990). Similarly, prolonged exposure to TNFα (16hrs) resulted in two fold increase in glucose transporter content of both plasma and inner membrane compartments (Cornelius *et al.*, 1990). The amount of glucose being transported was also greater than the increased level of plasma membrane transporter expression, suggesting TNFα treatment alters the intrinsic activity of these glucose transporters (Cornelius *et al.*, 1990). This suggests stimulation of these fibroblasts with TNFα across different time points would possibly yield interesting insight into changes with transporter expression. Preliminary experiments were conducted on mRNA expression of these lactate transporters at earlier time points (4 hours) and with IL1β stimulation (1ng/ml), however due to low patient numbers and reduced effect size at earlier timepoints, the study then focused on 24 hours stimulation using TNFα, as a good model of chronic inflammation of synovitis.

6.5.2 Future Studies

Although this is the first study of its kind, looking into the effect of obesity and loadbearing in OA synovial fibroblast metabolism, much of the data within this study could be expanded upon. Some future areas of research could be to look into the directionality of lactate transport, as previously mentioned within the limitations section. This could be conducted using radiolabelled L-[C^{14}]lactate, which could be incubated with cells and measured at various time points and, following cell lysis,

radioactivity could be measured using scintillation counter as described in (Hahn, E, Halestrap, A. Gamelli, 2000). This could give insight into the activity of these transporters. This is particularly interesting as increased protein expression is not always directly correlated with increased activity of these transporters as mentioned in (Cornelius *et al.*, 1990).

Likewise, some preliminary assays were conducted looking into lactate stimulation however statistically significant changes were not observed in pro-inflammatory gene expression (IL6) and therefore these experiments were omitted. However, another area of interest in lactate metabolism would be to look into lactate dehydrogenase (LDH) expression and activity within these obese OA synovial fibroblasts compared to normal weight OA synovial fibroblasts. A number of genes previously mentioned, interact and regulate lactate dehydrogenase, including HIF1-1/2α which binds to LDHA under hypoxic conditions (Cui *et al.*, 2017).

Finally, although stimulation with TNFα did yield some promising insights into inflammatory and activated fibroblasts metabolism, another set of metabolic flux experiments of OA synovial fibroblasts cultured with adipose conditioned media from normal weight and obese patients might provide interesting information on fibroblast metabolism when in close contact with adipose tissue and would also provide a more representative model of inflammatory behaviour of fibroblasts due to obesity associated low grade inflammation.

CHAPTER 7. GENERAL DISCUSSION

7.1 Discussion of main findings

Obesity is a major risk factor for developing OA and is believed to contribute to disease progression through multiple factors, including increased biomechanical loading of the joint and chronic low-grade inflammation. As OA is now increasingly considered a disease of the whole joint, it is of principal importance to understand the pathophysiological changes that occur at the different tissues within the joint such as articular cartilage, muscle tissue, subchondral bone and adipose tissues. One tissue that has received much attention in inflammatory joint diseases is the synovial membrane (synovium). Within the synovium, cellular and molecular changes occur, including synovial fibroblast hyperplasia and the infiltration of immune cells, which promote the inflammatory microenvironment that contributes to the degeneration of cartilage tissue. Resident cells of this tissue, including the resident synovial fibroblasts, have therefore become the target of these studies to better understand the cellular and molecular mechanisms that mediate OA joint inflammation.

Recent research conducted within our group within the Institute of Inflammation and Ageing have discovered a number of changes in the OA synovial fibroblast phenotype which are particularly significant. For example, obesity has been shown to influence the phenotype of the synovial fibroblast in OA, with synovial fibroblasts from obese patients exhibiting increased secretion (IL6 and CXCL8) and expression of pro-inflammatory cytokines and chemokines (*IL6, CXCL8, CXCL5, IL1β* and *CCL2*), cell proliferation and altered transcriptomic profile which displayed a shift towards increased inflammatory gene pathways including cytokine-cytokine interactions and chemokine signalling pathways (Nanus *et al.*, 2020). Furthermore, interestingly there was also an increase in the levels of soluble IL-6 receptor (sIL-6R)

in the synovial fluid of obese OA patients compared to normal weight OA patients (Pearson *et al.*, 2017). This is particularly noteworthy as synovial fibroblasts do not express membrane bound IL6 receptor, however they depend on incorporation of sIL-6R bound to IL6 and its interaction to form a signalling complex with membrane bound gp130 (Hashizume, Hayakawa and Mihara, 2008). Likewise, IL6 is also involved in cellular cross-talk with cartilage resident chondrocytes *in vitro*. IL6 from chondrocytes conditioned media increases IL6 levels in synovial fibroblasts suggesting this cytokine is intricately involved in inflammation within OA joint (Pearson *et al.*, 2017). IL6 therefore plays a significant role in the pathology of the OA joint for obese patients.

However, understanding whether this difference was due to biomechanical loading of the joint or as a result of increased adipose-driven chronic low-grade inflammation, which results in metabolic imprinting of OA synovial fibroblast, was not established.

Therefore, a primary the aim of this thesis was to understand whether there were differences in the metabolic phenotype of obese OA synovial fibroblasts compared to the normal-weight OA synovial fibroblasts, and whether this potential metabolic imprinting was affecting or driving the inflammatory profile of obese OA synovial fibroblasts.

To that end, metabolomic profiling was conducted on synovial fluid and synovial fibroblast conditioned media, as well as transcriptomic profiling on synovial fibroblasts obtained from patients with OA who were either obese or normal weight (chapter 1 and 3). Metabolite set enrichment analysis found a significant enrichment of metabolic pathways involved in glycolysis, TCA cycle metabolites and glutamine and glutamate metabolism (Farah *et al.*, 2022). An independent analysis of changes

in metabolic pathways within transcriptomic profiling showed significant changes in NADH metabolism, cysteine/homocysteine metabolism and amino acyl tRNA biosynthesis. Furthermore, integration of both metabolic and transcriptomic datasets using joint pathway analysis revealed enrichment of metabolic pathways such as glycolysis and TCA cycle, which warranted further investigation *in vitro*.

Consequently, metabolic flux analysis was conducted to examine whether there were differences in the glycolytic activity or mitochondrial respiration activity of these obese OA synovial fibroblasts. Interestingly, hip OA synovial fibroblasts were considerably more metabolically active compared to fibroblasts from patients with either knee or hand OA, with significantly increased glycolytic reserve and basal respiration, proton leakage and ATP production. The reason for this is not known but could be related to the fact that the hip is anatomically closer to larger masses of adipose tissue, including abdominal adipose tissue, and therefore may be more metabolically primed than anatomically distant joints such as the knee and hand. Following on from this, particular focus was given to hip OA synovial fibroblasts and further investigation was conducted into whether there were any differences in metabolism in obese and normal weight samples and furthermore whether inflammatory stimulation would reveal any discrepancies in metabolic phenotype.

Metabolic flux analysis revealed an increased basal rate of glycolysis and glycolytic reserve in obese OA synovial fibroblasts, compared to normal weight OA synovial fibroblasts. Likewise, inflammatory stimulation of obese OA synovial fibroblasts, but not normal-weight fibroblasts, increased both basal and maximal respiration, as well as ATP production. This suggests that obese OA synovial fibroblasts have increased reliance on glycolysis basally, but that they can also adopt greater mitochondrial respiration to meet the greater energy demands of the inflammatory state.

Finally, having investigated changes in glycolysis and mitochondrial respiration another metabolic pathway that was investigated was glutamine-glutamate metabolism. This was a particularly interesting pathway as it was the most significantly enriched metabolic pathway in obese OA synovial fluid, compared to normal weight OA synovial fluid and was significantly enriched in normal weight and obese OA synovial fibroblast conditioned media upon inflammatory stimulation (TNFα). Furthermore, this particular pathway has received much attention in inflammatory pathologies and has even been identified as an altered metabolic pathway utilised by RA synovial fibroblasts (Farah *et al.*, 2020). Therefore, this warranted further investigation with the premise being to identify if there was a relationship between the activity of the glutamine-glutamate pathway and the inflammatory profile of OA synovial fibroblasts. To investigate this, the activity of glutamine-glutamate pathway was modulated in OA synovial fibroblasts by targeting the enzyme GLS1, which coverts glutamine to glutamate, either using a pharmacological small molecule inhibitor or using siRNA. Inhibition of GLS1 was found to reduce IL6 expression and IL-6 protein secretion but did not alter the rates of cellular proliferation or cellular apoptosis. One area of future research could be to examine whether this pathway is altered *in vivo* within murine models of obesity and OA, and whether targeting this pathway *in vivo* ameliorates obesity-driven OA and synovial inflammation.

Taken together, the findings of this thesis provide support for the notion that the metabolic differences underpin the inflammatory phenotype of the OA synovial fibroblast and further suggest that not only is the metabolic phenotype of obese OA synovial fibroblasts different from normal weight OA synovial fibroblasts, but that these differences will be exacerbated in states of inflammatory challenge. These

findings therefore support the rationale for the therapeutic targeting of metabolic pathways to reduce the pathological effects of joint inflammation of obese patients with OA.

7.2 Future directions

7.2.1 Rationale for the therapeutic targeting of metabolism in stromal synovial fibroblast pathotypes in inflammatory joint disease

Immunometabolism is an emerging field which investigates the links between intracellular metabolic pathways and the effects these changes have on cellular function (Mobasheri *et al.*, 2017) Metabolic reprogramming of immune cells accompanies the pathological and progressive changes in chronic inflammatory diseases making this area of research critical to understanding how disease development occurs and how immune cells acquire and sometimes support these pathological changes. Likewise, due to the intricate relationship between these metabolic pathways and immune cell function, targeting and modulating these pathways alters cellular responses and can sometimes reverse cell states to a pre-disease state (Schruf *et al.*, 2019; O'Leary *et al.*, 2020).

Although much effort has been expended on investigating these associations in immune cells there has not been the same amount of effort put into understanding the role of metabolism in stromal cells.

In the field of cancer biology, a paradigm shift has occurred in switching from a sole focus on understanding how genetic changes and mutations drive and support cancerous phenotype in cancer cells to now looking at the wider picture of the tumour microenvironment, particularly at the cells that are resident at these sites, which phenotypically change to support the cancer cells during their development.

These cells are known as cancer associated fibroblasts (CAFs). CAFs have received much attention as of late due to their ability to support these cancer cells, through moulding and shaping the tumour environment. In carcinoma, the expansion of CAFs precedes conversion to malignancy and circumscribe pre-malignant lesions and interact with immune cells that seek to locate and destroy these aberrant cells (Sahai *et al.*, 2020). The expansion of these CAFs has been termed stromagenesis and it proceeds alongside and is associated with tumorigenesis (Sahai *et al.*, 2020).

However, beyond their role of moulding and shaping the tumour environment is the metabolic support they provide which is vital for cancer cell survival. Cancer cells in their need to expand rapidly are widely known to undergo metabolic changes, often referred to as the Warburg effect, which is the switch from oxidative phosphorylation as the primary source of energy to aerobic glycolysis due to the rapid energy requirements and eventually as a result of their expansion, the reduced oxygen supply. Cancer cells will then utilise other metabolites to generate energy, including lactate, which can be converted into pyruvate. CAFs increase the rate of aerobic glycolysis to generate more lactate, which is secreted and then taken up by cancer cells, a phenomenon termed the ”Reverse Warburg Effect” (Sanford-Crane, Abrego and Sherman, 2019). Furthermore, cancer cells also use up a key amino acid, glutamine which cannot be further synthesised and so CAF’s utilise the carbons and nitrogen from aspartate, asparagine, and lactate in order to synthesise glutamine which can be exported and taken up by cancer cells (Sanford-Crane, Abrego and Sherman, 2019). This is one of many examples of the major role fibroblasts and mesenchymal stromal cells in general play in disease pathology, often altering their metabolic state to support their own pathological changes or tailoring their metabolism to support dysfunctional cells.

A similar change in perspective is required for other disease states, particularly conditions like arthritis. In these disease states, cells will undergo pathological changes such as increased inflammatory profile, which is supported and underpinned by their metabolic state. Without the changes in metabolic pathways which provide energy and the biosynthetic materials to support their “activated” status, these cells remain in their quiescent and non-activated phenotype.

7.2.2 Metabolism and Inflammation are Intricately Connected in Synovial Fibroblasts and Present Potential Targetable Pathways to Modulate Inflammation

In inflammatory joint diseases, synovial fibroblasts undergo pathological changes, which result in a switch from quiescent state to inflammatory and invasive state. In RA, synovial fibroblasts will increase the rates of proliferation and become hyperplastic, resulting in the formation of pannus-like structures upon loss of contact inhibition (Farah *et al.*, 2020). In OA, synovial fibroblasts have been shown to increase secretion of pro-inflammatory cytokines and chemokines, such as IL6 and CXCL8 (Nanus *et al.*, 2020).

These alterations in synovial fibroblast phenotype are accompanied by concomitant changes in their metabolic status often to support the adopted inflammatory phenotype.

Targeting the metabolic state of these cells is a means to modulate and possibly return these cells to their original, quiescent state. In RA, synovial fibroblasts upregulate glycolysis and glucose starvation and hexokinase inhibition (using 2DG) reduces proliferation and migration of these cells alongside reduced secretion of IL6 and degradative enzyme MMP3 (Garcia-Carbonell *et al.*, 2016). Inhibition of

glycolytic enzymes, such as PFKFB3 and PGK1, reduces the secretion of pro-inflammatory cytokines TNFα, IL-1β and IFN-γ (M Biniecka *et al.*, 2016; Zhao *et al.*, 2016). Likewise, silencing of TNFα with RNAi treatment reduced the expression of GLUT1 and glyceraldehyde 3 phosphate (G3P), providing further evidence of the link between aerobic glycolysis and inflammation in synovial fibroblasts (Farah *et al.*, 2020).

Furthermore, amino acid metabolism is also altered with synovial fibroblasts, with RA synovial fibroblasts showing increased dependency on glutamine metabolism and increased expression of GLS1 (Takahashi *et al.*, 2017). Pharmacological inhibition of GLS1 in a SKG mouse model ameliorated autoimmune arthritis and reduced the number of synoviocytes (Takahashi *et al.*, 2017).

PRINCIPLE	EXPLANATION	EXAMPLE
SPECIFICITY	Due to the universal nature of metabolic pathway utilisation by different cell types, treatments involving inhibition of pathways shared by multiple cell types would need to be specific to targeted cell.	Antibody-conjugated anti-sense oligonucleotide therapy
PREDICTION	Cells use multiple isoforms of enzymes and different protein transporters to transport metabolites into and out of cell. Understanding therapeutics effect on different isoforms critical for efficacy.	Cell specific isoform screening prior to treatment
PLASTICITY	Metabolic pathways flux depending on nutrient availability and therefore depletion of nutrient of choice for cell results in a shift in metabolic programme which in turn effects cell function (to the desired response)	Computational model of metabolic pathways altered by treatment (based on omics integration)
REDUCTIVISM	Unlike other pathways such as kinase inhibition of signalling cascades, metabolic pathways are tightly regulated and therefore sensitive to modulation. Reduced inhibition results in large scale effects	Reduced dosage of therapeutic
TIME MANAGMENT	A major principle of therapeutic treatment of metabolic pathways would be adverse effects and therefore short-term treatment to favour certain cell responses would be ideal	Acute and Episodic treatment

Table 7.1: Considerations prior to development of potential metabolic therapeutic treatments (adapted from Rhoads, Major and Rathmell, 2017)

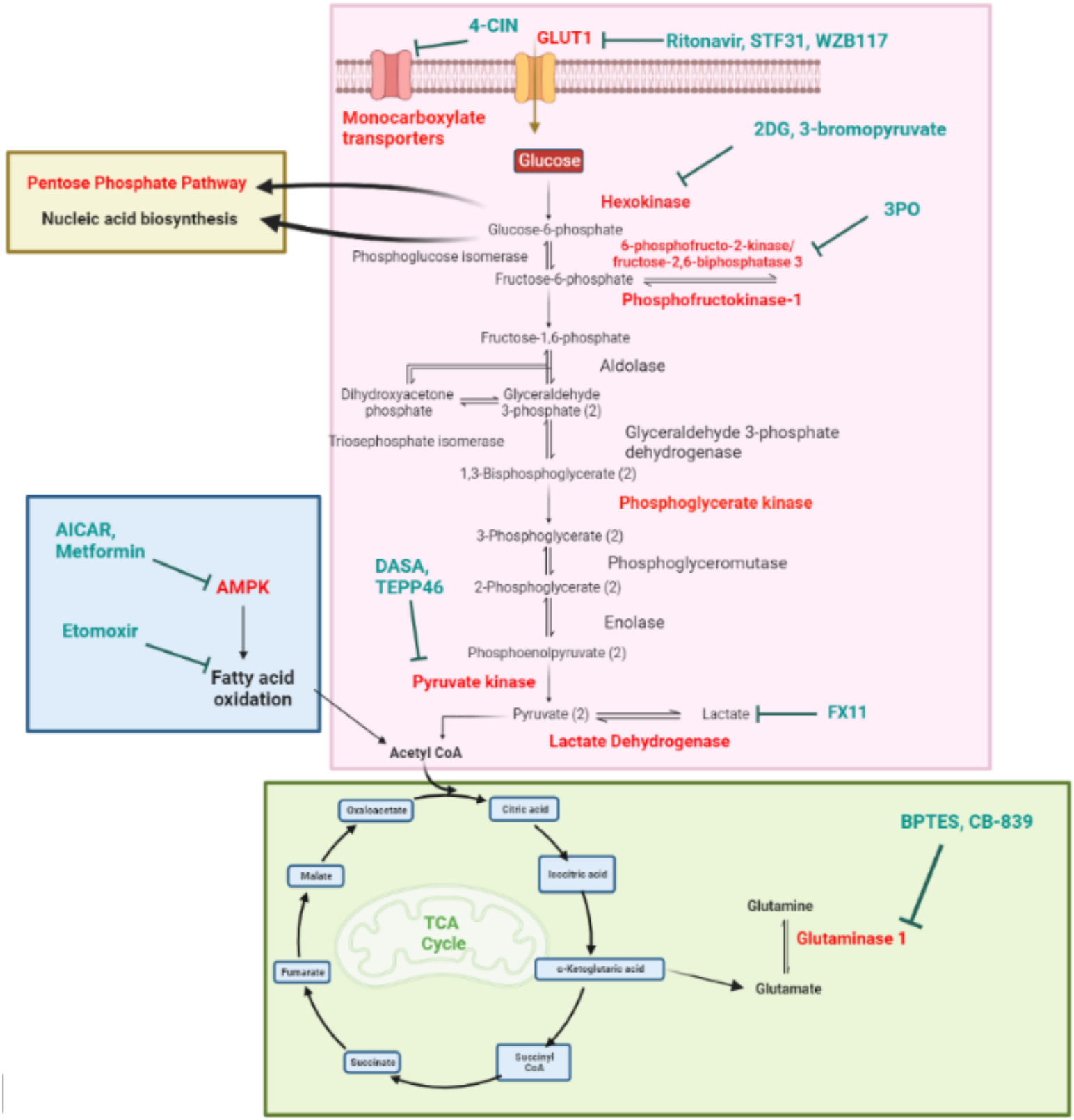

Figure 7.1: Altered metabolic pathways in synovial fibroblast can be targeted through multiple therapeutics to ameliorate inflammatory phenotype (adapted from Farah *et al.*, 2020)

These metabolic pathways can be activated or inhibited using small molecule inhibitors which often target rate-limiting enzymes that have already been shown to be upregulated in synovial fibroblasts. In glycolysis, there are a few small molecule inhibitors that can target rate limiting enzymes such as dipyridinyl-propenone (3PO) which selectively inhibits PFKFB3 (figure 7.1). Likewise, it's also possible to use selective hexokinase inhibitors 2DG and 3-bromopyruvate (figure 7.1). Lactate dehydrogenase is another enzyme increased in RA synovial fibroblasts and can be selectively inhibited using 3-dihydroxy-6-methyl-7-(phenylmethyl)-4-propylnaphthalene-1-carboxylic acid (FX11) (figure 7.1).

Furthermore, other metabolic pathways which are upregulated in synovial fibroblasts including glutamine-glutamate metabolism can be targeted using the previously mentioned pharmacological inhibitor of GLS1, BPTES and CB-839 (figure 7.1).

In this thesis, glutamine and glutamate metabolism was increased in obese OA synovial fluid compared to normal weight synovial fluid. Therefore, to reduce the inflammatory profile of these fibroblasts, a key enzyme in this pathway was targeted, namely glutaminase 1, which converts glutamine to glutamate. This was done using small molecule inhibitor BPTES and through siRNA knockdown. Inhibition of GLS1 resulted in reduced IL6 expression and protein secretion, showing synovial fibroblast require glutamine-glutamate metabolism to support their inflammatory status. This study provides proof of principle in targeting altered metabolic pathways in synovial fibroblasts may yield potential therapeutic effects in ameliorating the inflammation observed in OA.

7.2.3 Pre-clinical animal models

The next step following the data collected within this thesis would be to modulate these metabolic pathways *in vivo*. In order to model obesity associated OA in an animal model, the ideal comparison would be an obese animal model induced by high fat diet, alongside a classic inflammatory arthritis model like CIA model. In this comparison there would be ideally 4 groups, chow diet sham surgery (vehicle control), high fat diet sham surgery, chow diet CIA treatment and high fat diet CIA treatment. In this experiment the high fat diet CIA model would be the closest comparison to obesity associated OA. However, this would require statistical modelling to separate the effects of inflammation due to CIA treatment and the low-grade inflammation observed in obesity. In this experiment *in vivo*, treatment with the metabolic inhibitors for glycolysis or glutamine-glutamate metabolism (mentioned in figure 7.1) would be used to observe whether inhibition of these pathways resulted in changes in disease course (i.e., reduced synovitis, articular cartilage degradation etc). Likewise, looking into secondary endpoints such as behavioural outcomes of these animal models (i.e., gait changes, weight-bearing on joints, burrowing behaviour and activity status) might also provide important information on other areas of interest in personalised medicine, the equivalent aspects being lifestyle and quality of life (figure 7.2).

7.2.4 Precision and Personalised Medicine: Treating Obese Osteoarthritis Patients

Personalised medicine (PM) is a method of treatment which is premised on the patient individual characteristics influencing their susceptibility and development of disease and their response to treatment.

Personalised medicine is not a new approach to treatment and was mentioned by Hippocrates, were he stated “different drugs to different patients, for the sweet ones do not benefit everyone, nor do the astringent ones, nor are all the patients able to drink the same things” (Sykiotis, Kalliolias and Papavassiliou, 2005; Strianese *et al.*, 2020).

Personalised and precision medicine subvert the trial-and-error approach in conventional medicine which is based on providing treatment using the most effective treatment available based on general population data and does not consider the inherent differences in populations and thereby can result in non-effective treatments in certain patient groups. This approach leads to poorer outcomes for patients and patient dissatisfaction alongside misdiagnosis and wrong treatment which also results in increasing healthcare costs (Mathur and Sutton, 2017).

By integrating different aspects of patient characteristics including clinical data, environmental factors and molecular characterisation, personalised medicine can provide a more targeted approach to successfully treat patients based on the primary drivers of their disease (figure 7.2)

An example of this approach is in breast cancer treatment where patients who have high expression of HER2 receptor are given monoclonal antibody based therapeutic

Herceptin, whereas some patients who have mutations in the HER2 gene are inherently resistant to Herceptin treatment and so therefore would not benefit from this treatment (Mathur and Sutton, 2017).

Likewise, immunotherapy in prostate cancer treatment is based on highly PM centric approach. Sipuleucel (Provenge) treatment which uses patient derived dendritic cells that are incubated in the presence of prostatic acid phosphatase (which is expressed in 95% of prostate cancer cells) are re-introduced into the patient's immune system thereby training the immune system to target and destroy prostate cancer cells (Mathur and Sutton, 2017).

In osteoarthritis, diagnosis is often late in the disease course with pain and loss of function being the primary clinical features which are used to diagnose the disease (Bijlsma, Berenbaum and Lafeber, 2011). This results in late treatment within disease course and therefore reduces the opportunity for disease modifying therapeutics to provide effective treatment for patients and so a new approach is required to improve patient outcomes.

Personalised medicine might provide a unique opportunity for treating patients with osteoarthritis by developing and collating data on markers of disease (such as biochemical markers or MRI and radiological imaging) and by using computational tools and statistical analysis. Importantly there is a significant potential to understand disease processes and provide methods of stratifying patients into subtypes based on these parameters.

Randomised control trials of disease modifying drugs in OA patients have largely failed to show significant changes in pain relief and structural outcomes due to issues such as heterogeneity of disease, study cohort selection (inclusion and

exclusion criteria) and duration of studies (Siaton, Hogans and Hochberg, 2020). When trying to design clinical trials in OA the main issue that often arises is the complexity in accurately defining which particular patient population will demonstrate the strongest outcomes to treatment (Siaton, Hogans and Hochberg, 2020).

By using personalised medicine, patient groups can be stratified into those which display strongest shift towards certain molecular endotypes. These molecular endotypes are a means of delineating different phenotypes of osteoarthritis and are based on clinical features and molecular characterisation of OA patients (as previously mentioned in figure 1.1).

In this thesis high throughput technologies like, metabolomics and transcriptomics alongside inflammatory profiling have been used to differentiate between patient groups with different BMI's in obesity-driven OA.

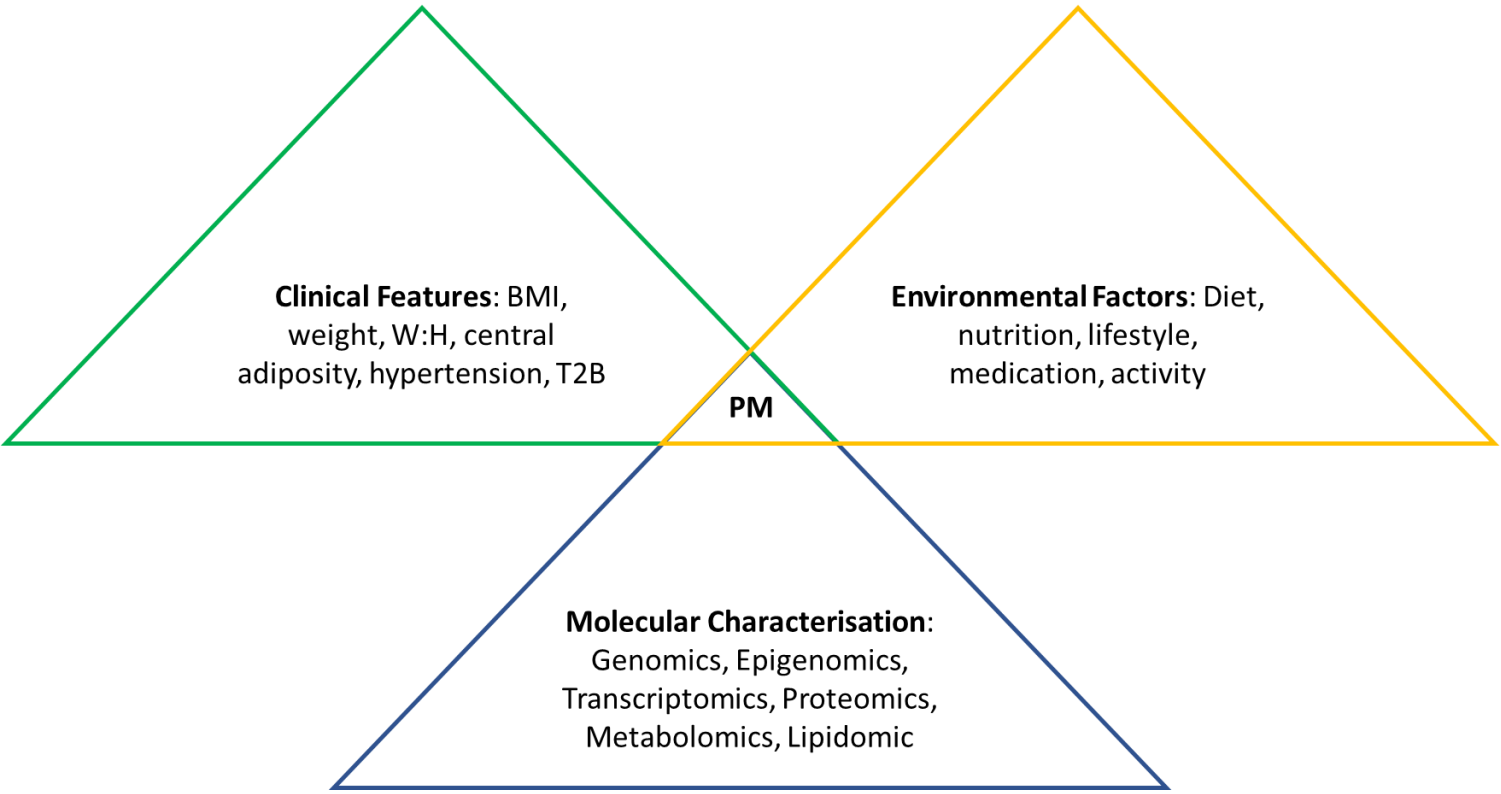

Figure 7.2: Personalised medicine (PM) can be derived from the amalgamation of three patient characteristics which include clinical features, environmental factors, and molecular characterisation

Key features that have been established from these obese OA patients compared to non-obese OA patients are differences in metabolic and inflammatory profile of OA synovial fibroblasts. By therapeutically targeting these metabolic changes in synovial fibroblasts in obese OA patients using criteria established in table 7.1, obese OA patients could benefit from the reduced inflammation and potentially partially reduced pain at the synovial joint.

Personalised medicine however is not only about developing new therapeutics but repurposing therapeutics currently available and approved for use by governmental medical authorities like the FDA or EMA. An example of potential therapeutics which

could be repurposed to target the obesity driven inflammatory changes observed in obese OA synovial fibroblast is Methotrexate.

Low-dose methotrexate therapy is currently the gold standard in RA treatment. Methotrexate works by multiple modes of action including inhibition of aminoimidazole-4-carboxamide ribonucleotide (AICAR) transformylase (ATIC) (which results in increased adenosine release and binding of its cell-surface receptors reducing immune responses and inflammation) and inhibition dihydrofolate reductase resulting in reduced dihydrobiopterin to tetrahydrobiopterin and nitric oxide synthase uncoupling and a shift towards T cell apoptosis (Cronstein and Aune, 2020).

Another key mode of action is its inhibition of one-carbon metabolism which could have important implications in obese OA synovial fibroblasts which show enrichment of one carbon metabolic pathways such as glycine, serine, and threonine metabolism and altered salvage pathways of deoxyribonucleotide synthesis.

Methotrexate has already undergone phase III clinical trials in knee OA patients and has been shown to successfully reduce knee OA pain at 6 months and WOMAC stiffness and function (Kingsbury et al., 2015, 2019). However, while methotrexate treatment for erosive hand OA significantly reduced progression of joint damage compared to placebo, it did not demonstrate superior efficacy over placebo on pain and function evolution at 3 and 12 months (Ferrero et al., 2021). This lends more weight to the previous principle of stratifying patients further and using different treatment strategies for patients with primary OA of different joints.

CHAPTER 8. REFERENCES

Aderemi, A. V. *et al.* (2021) ‘Metabolomics: A Scoping Review of Its Role as a Tool for Disease Biomarker Discovery in Selected Non-Communicable Diseases’, *Metabolites*, 11(7). doi: 10.3390/METABO11070418.

Ahn, J. *et al.* (2016) ‘AIMP1 downregulation restores chondrogenic characteristics of dedifferentiated/degenerated chondrocytes by enhancing TGF-β signal’, *Cell Death & Disease 2016 7:2*, 7(2), pp. e2099–e2099. doi: 10.1038/cddis.2016.17.

Alonzi, T. *et al.* (1998) ‘Interleukin 6 Is Required for the Development of Collagen-induced Arthritis’, *The Journal of Experimental Medicine*, 187(4), p. 461. doi: 10.1084/JEM.187.4.461.

Altman, B. J., Stine, Z. E. and Dang, C. V. (2016) ‘From Krebs to clinic: glutamine metabolism to cancer therapy’, *Nature Reviews Cancer 2016 16:10*, 16(10), pp. 619–634. doi: 10.1038/nrc.2016.71.

Avagliano, A. *et al.* (2018) ‘Metabolic Reprogramming of Cancer Associated Fibroblasts: The Slavery of Stromal Fibroblasts’, *BioMed Research International*, 2018, pp. 6075403–6075412. doi: 10.1155/2018/6075403.

Ayral, X. *et al.* (2005) ‘Synovitis: a potential predictive factor of structural progression of medial tibiofemoral knee osteoarthritis – results of a 1 year longitudinal arthroscopic study in 422 patients’, *Osteoarthritis and Cartilage*, 13(5), pp. 361–367. doi: 10.1016/J.JOCA.2005.01.005.

Bagheri, M. *et al.* (2018) ‘Obesity-Related Metabolomic Profiles and Discrimination of Metabolically Unhealthy Obesity’, *Journal of Proteome Research*, 17(4), pp. 1452–1462. doi: 10.1021/ACS.JPROTEOME.7B00802/SUPPL_FILE/PR7B00802_SI_001.PDF.

Balaskas, P. *et al.* (2020) 'Small Non-Coding RNAome of Ageing Chondrocytes', *International Journal of Molecular Sciences 2020, Vol. 21, Page 5675*, 21(16), p. 5675. doi: 10.3390/IJMS21165675.

Balla, T. (2013) 'Phosphoinositides: Tiny Lipids With Giant Impact on Cell Regulation', *Physiological Reviews*, 93(3), p. 1019. doi: 10.1152/PHYSREV.00028.2012.

Bassit, R. A. *et al.* (2000) 'The effect of BCAA supplementation upon the immune response of triathletes', *Medicine and science in sports and exercise*, 32(7), pp. 1214–1219. doi: 10.1097/00005768-200007000-00005.

Bateman, A. *et al.* (2021) 'UniProt: the universal protein knowledgebase in 2021', *Nucleic Acids Research*, 49(D1), pp. D480–D489. doi: 10.1093/NAR/GKAA1100.

Benito, M. J. *et al.* (2005) 'Synovial tissue inflammation in early and late osteoarthritis', *Annals of the Rheumatic Diseases*, 64(9), p. 1263. doi: 10.1136/ARD.2004.025270.

Berg, A. H. and Scherer, P. E. (2005) 'Adipose tissue, inflammation, and cardiovascular disease', *Circulation Research*, 96(9), pp. 939–949. doi: 10.1161/01.RES.0000163635.62927.34.

Beswick, A. D. *et al.* (2012) 'What proportion of patients report long-term pain after total hip or knee replacement for osteoarthritis? A systematic review of prospective studies in unselected patients', *BMJ Open*, 2(1), p. e000435. doi: 10.1136/BMJOPEN-2011-000435.

Bijlsma, J. W. J., Berenbaum, F. and Lafeber, F. P. J. G. (2011) 'Osteoarthritis: an update with relevance for clinical practice', *The Lancet*, 377(9783), pp. 2115–2126.

doi: 10.1016/S0140-6736(11)60243-2.

Biniecka, M. *et al.* (2016) 'Dysregulated bioenergetics: a key regulator of joint inflammation', *Annals of the Rheumatic Diseases*, 75(12), pp. 2192–2200. doi: 10.1136/ANNRHEUMDIS-2015-208476.

Blagojevic, M. *et al.* (2010) 'Risk factors for onset of osteoarthritis of the knee in older adults: a systematic review and meta-analysis', *Osteoarthritis and cartilage*, 18(1), pp. 24–33. doi: 10.1016/J.JOCA.2009.08.010.

Bliddal, H., Leeds, A. R. and Christensen, R. (2014) 'Osteoarthritis, obesity and weight loss: evidence, hypotheses and horizons – a scoping review', *Obesity Reviews*, 15(7), pp. 578–586. doi: 10.1111/obr.12173.

Bogdanov, M. *et al.* (2008) 'Metabolomic profiling to develop blood biomarkers for Parkinson's disease', *Brain*, 131(2), pp. 389–396. doi: 10.1093/BRAIN/AWM304.

Bustamante, M. F. *et al.* (2017) 'Fibroblast-like synoviocyte metabolism in the pathogenesis of rheumatoid arthritis', *Arthritis Research & Therapy*, 19(1). doi: 10.1186/S13075-017-1303-3.

Cai, L. *et al.* (2011) 'Acetyl-CoA Induces Cell Growth and Proliferation by Promoting the Acetylation of Histones at Growth Genes', *Molecular cell*, 42(4), p. 426. doi: 10.1016/J.MOLCEL.2011.05.004.

Capuron, L. *et al.* (2011) 'Chronic Low-Grade Inflammation in Elderly Persons Is Associated with Altered Tryptophan and Tyrosine Metabolism: Role in Neuropsychiatric Symptoms', *Biological Psychiatry*, 70(2), pp. 175–182. doi: 10.1016/J.BIOPSYCH.2010.12.006.

Carlson, A. K. *et al.* (2018) 'Application of Global Metabolomic Profiling of Synovial

Fluid for Osteoarthritis Biomarkers', *Biochemical and biophysical research communications*, 499(2), p. 182. doi: 10.1016/J.BBRC.2018.03.117.

Carr, E. L. *et al.* (2010) 'Glutamine Uptake and Metabolism Are Coordinately Regulated by ERK/MAPK during T Lymphocyte Activation', *The Journal of Immunology*, 185(2), pp. 1037–1044. doi: 10.4049/JIMMUNOL.0903586.

Certo, M. *et al.* (2020) 'Lactate: Fueling the fire starter', *Wiley Interdisciplinary Reviews. Systems Biology and Medicine*, 12(3). doi: 10.1002/WSBM.1474.

Chang, H. Y. *et al.* (2002) 'Diversity, topographic differentiation, and positional memory in human fibroblasts', *Proceedings of the National Academy of Sciences of the United States of America*, 99(20), pp. 12877–12882. doi: 10.1073/PNAS.162488599.

Chen, D. *et al.* (2017) 'Osteoarthritis: toward a comprehensive understanding of pathological mechanism', *Bone Research 2017 5:1*, 5(1), pp. 1–13. doi: 10.1038/boneres.2016.44.

Chen, H. H. *et al.* (2015) 'The metabolome profiling and pathway analysis in metabolic healthy and abnormal obesity', *International Journal of Obesity 2015 39:8*, 39(8), pp. 1241–1248. doi: 10.1038/ijo.2015.65.

Chen, L. and Cui, H. (2015) 'Targeting Glutamine Induces Apoptosis: A Cancer Therapy Approach', *International Journal of Molecular Sciences 2015, Vol. 16, Pages 22830-22855*, 16(9), pp. 22830–22855. doi: 10.3390/IJMS160922830.

Clarke, C. J. *et al.* (2016) 'The Initiator Methionine tRNA Drives Secretion of Type II Collagen from Stromal Fibroblasts to Promote Tumor Growth and Angiogenesis', *Current Biology*, 26(6), pp. 755–765. doi: 10.1016/j.cub.2016.01.045.

Clements, K. M. *et al.* (2003) 'Gene Deletion of Either Interleukin-1β, Interleukin-1β -Converting Enzyme, Inducible Nitric Oxide Synthase, or Stromelysin 1 Accelerates the Development of Knee Osteoarthritis in Mice after Surgical Transection of the Medial Collateral Ligament and Partia', *Arthritis and Rheumatism*, 48(12), pp. 3452–3463. doi: 10.1002/ART.11355.

Coggon, D. *et al.* (2001) 'Knee osteoarthritis and obesity', *International Journal of Obesity and Related Metabolic Disorders: Journal of the International Association for the Study of Obesity*, 25(5), pp. 622–627. doi: 10.1038/sj.ijo.0801585.

Connor, S. C. *et al.* (2010) 'Integration of metabolomics and transcriptomics data to aid biomarker discovery in type 2 diabetes', *Molecular bioSystems*, 6(5), pp. 909–921. doi: 10.1039/B914182K.

Cornelius, P. *et al.* (1990) 'The growth factor-like effects of tumor necrosis factor-alpha. Stimulation of glucose transport activity and induction of glucose transporter and immediate early gene expression in 3T3-L1 preadipocytes', *Journal of Biological Chemistry*, 265(33), pp. 20506–20516. doi: 10.1016/S0021-9258(17)30532-X.

Coryell, P. R., Diekman, B. O. and Loeser, R. F. (2020) 'Mechanisms and therapeutic implications of cellular senescence in osteoarthritis', *Nature Reviews Rheumatology 2020 17:1*, 17(1), pp. 47–57. doi: 10.1038/s41584-020-00533-7.

Covarrubias, A. J. *et al.* (2021) 'NAD+ metabolism and its roles in cellular processes during ageing', *Nature reviews. Molecular cell biology*, 22(2), p. 119. doi: 10.1038/S41580-020-00313-X.

Creamer, P. (2000) 'Osteoarthritis pain and its treatment', *Current opinion in rheumatology*, 12(5), pp. 450–455. doi: 10.1097/00002281-200009000-00019.

Croft, Adam P *et al.* (2019) 'Distinct fibroblast subsets drive inflammation and damage in arthritis', *Nature (London)*, 570(7760), pp. 246–251. doi: 10.1038/s41586-019-1263-7.

Cui, H. *et al.* (2019) 'Inhibition of glutaminase 1 attenuates experimental pulmonary fibrosis', *American Journal of Respiratory Cell and Molecular Biology*, 61(4), pp. 492–500. doi: 10.1165/RCMB.2019-0051OC/SUPPL_FILE/DISCLOSURES.PDF.

Cui, X. G. *et al.* (2017) 'HIF1/2α mediates hypoxia-induced LDHA expression in human pancreatic cancer cells', *Oncotarget*, 8(15), p. 24840. doi: 10.18632/ONCOTARGET.15266.

Curthoys, N. P. and Watford, M. (1995) 'Regulation of glutaminase activity and glutamine metabolism', *Annual review of nutrition*, 15, pp. 133–159. doi: 10.1146/ANNUREV.NU.15.070195.001025.

Damyanovich, A. Z. *et al.* (1999) 'Comparative study of normal and osteoarthritic canine synovial fluid using 500 MHz 1H magnetic resonance spectroscopy', *Journal of Orthopaedic Research*, 17(2), pp. 223–231. doi: 10.1002/JOR.1100170211.

Davidson, E. N. B. *et al.* (2009) 'Increase in ALK1/ALK5 Ratio as a Cause for Elevated MMP-13 Expression in Osteoarthritis in Humans and Mice', *The Journal of Immunology*, 182(12), pp. 7937–7945. doi: 10.4049/JIMMUNOL.0803991.

Diekman, B. O. *et al.* (2018) 'Expression of p16INK4a is a biomarker of chondrocyte aging but does not cause osteoarthritis', *Aging Cell*, 17(4). doi: 10.1111/ACEL.12771.

Douni, E. *et al.* (1995) 'Transgenic and knockout analyses of the role of TNF in immune regulation and disease pathogenesis.', *Journal of inflammation*, 47(1–2), pp.

27–38.

Ducker, G. S. *et al.* (2016) ‘Reversal of cytosolic one-carbon flux compensates for loss of mitochondrial folate pathway’, *Cell metabolism*, 23(6), p. 1140. doi: 10.1016/J.CMET.2016.04.016.

Dudka, I. *et al.* (2021) ‘Metabolomic profiling reveals plasma GlycA and GlycB as a potential biomarkers for treatment efficiency in rheumatoid arthritis’, *Journal of pharmaceutical and biomedical analysis*, 197. doi: 10.1016/J.JPBA.2021.113971.

Eagle, H. *et al.* (1956) ‘THE GROWTH RESPONSE OF MAMMALIAN CELLS IN TISSUE CULTURE TO l-GLUTAMINE AND l-GLUTAMIC ACID’, *Journal of Biological Chemistry*, 218(2), pp. 607–616. doi: 10.1016/S0021-9258(18)65826-0.

Elgogary, A. *et al.* (2016) ‘Combination therapy with BPTES nanoparticles and metformin targets the metabolic heterogeneity of pancreatic cancer’, *Proceedings of the National Academy of Sciences of the United States of America*, 113(36), pp. E5328–E5336. doi: 10.1073/PNAS.1611406113/SUPPL_FILE/PNAS.201611406SI.PDF.

Elsas Ii, L. J. and Lai, K. (1998) ‘The molecular biology of galactosemia’. doi: 10.1097/00125817-199811000-00009.

Emwas, A. H. M. (2015) ‘The Strengths and Weaknesses of NMR Spectroscopy and Mass Spectrometry with Particular Focus on Metabolomics Research’, *Methods in Molecular Biology*, 1277, pp. 161–193. doi: 10.1007/978-1-4939-2377-9_13.

Erdogan, B. *et al.* (2017) ‘Cancer-associated fibroblasts promote directional cancer cell migration by aligning fibronectin’, *The Journal of cell biology*, 216(11), pp. 3799–3816. doi: 10.1083/jcb.201704053.

Eriksson, L., Trygg, J. and Wold, S. (2008) 'CV-ANOVA for significance testing of PLS and OPLS® models', *Journal of Chemometrics*, 22(11–12), pp. 594–600. doi: 10.1002/CEM.1187.

Everts, A. G. *et al.* (2013) 'Quantitative dynamics of the link between cellular metabolism and histone acetylation', *The Journal of biological chemistry*, 288(17), pp. 12142–12151. doi: 10.1074/JBC.M112.428318.

Farah, H. *et al.* (2020) 'Metabolic dysfunction and inflammatory disease: the role of stromal fibroblasts', *The FEBS journal*. doi: 10.1111/febs.15644.

Farah, H. *et al.* (2022) 'Differential Metabotypes in Synovial Fibroblasts and Synovial Fluid in Hip Osteoarthritis Patients Support Inflammatory Responses', *International Journal of Molecular Sciences 2022, Vol. 23, Page 3266*, 23(6), p. 3266. doi: 10.3390/IJMS23063266.

Farr, J. N. *et al.* (2016) 'Identification of Senescent Cells in the Bone Microenvironment', *Journal of bone and mineral research : the official journal of the American Society for Bone and Mineral Research*, 31(11), p. 1920. doi: 10.1002/JBMR.2892.

Felson, D. T. (2006) 'Osteoarthritis of the Knee', *https://doi.org/10.1056/NEJMcp051726*, 354(8), pp. 841–8. doi: 10.1056/NEJMCP051726.

Ferreira, A. P. S. *et al.* (2013) 'Active Glutaminase C Self-assembles into a Supratetrameric Oligomer That Can Be Disrupted by an Allosteric Inhibitor', *The Journal of Biological Chemistry*, 288(39), p. 28009. doi: 10.1074/JBC.M113.501346.

Flora, G. D. and Nayak, M. K. (2019) 'A Brief Review of Cardiovascular Diseases,

Associated Risk Factors and Current Treatment Regimes', *Current Pharmaceutical Design*, 25(38), pp. 4063–4084. doi: 10.2174/1381612825666190925163827.

Foote, A. G. *et al.* (2019) 'Tissue specific human fibroblast differential expression based on RNAsequencing analysis', *BMC Genomics*, 20(1). doi: 10.1186/S12864-019-5682-5.

Frank-Bertoncelj, M. *et al.* (2017) 'Epigenetically-driven anatomical diversity of synovial fibroblasts guides joint-specific fibroblast functions', *Nature Communications 2017 8:1*, 8(1), pp. 1–14. doi: 10.1038/ncomms14852.

Fujigaki, Y. *et al.* (2005) 'Transient myofibroblast differentiation of interstitial fibroblastic cells relevant to tubular dilatation in uranyl acetate-induced acute renal failure in rats', *Virchows Archiv*, 446(2), pp. 164–176. doi: 10.1007/S00428-004-1155-5/FIGURES/11.

Garcia-Carbonell, R. *et al.* (2016) 'Critical Role of Glucose Metabolism in Rheumatoid Arthritis Fibroblast-like Synoviocytes', *Arthritis and Rheumatology*, 68(7), pp. 1614–1626. doi: 10.1002/ART.39608/ABSTRACT.

Gardner, L. C. and Cox, T. M. (1988) 'THE JOURNAL OF BIOLOGICAL CHEMISTRY Biosynthesis of Heme in Immature Erythroid Cells THE REGULATORY STEP FOR HEME FORMATION IN THE HUMAN ERYTHRON*', 263(14). doi: 10.1016/S0021-9258(18)68695-8.

Ge, J. *et al.* (2018) 'Glutaminolysis Promotes Collagen Translation and Stability via α-Ketoglutarate-mediated mTOR Activation and Proline Hydroxylation', *American journal of respiratory cell and molecular biology*, 58(3), pp. 378–390. doi: 10.1165/rcmb.2017-0238OC.

Giesbertz, P. *et al.* (2015) 'Metabolite profiling in plasma and tissues of ob/ob and db/db mice identifies novel markers of obesity and type 2 diabetes', *Diabetologia*, 58(9), pp. 2133–2143. doi: 10.1007/S00125-015-3656-Y.

Glyn-Jones, S. *et al.* (2015) 'Osteoarthritis', *Lancet (London, England)*, 386(9991), pp. 376–387. doi: 10.1016/S0140-6736(14)60802-3.

Gonzalez-Franquesa, A. *et al.* (2016) 'What have metabolomics approaches taught us about Type 2 Diabetes?', *Current diabetes reports*, 16(8), p. 74. doi: 10.1007/S11892-016-0763-1.

Green, J. A. *et al.* (2020) 'tRNA-derived fragments (tRFs) regulate post-transcriptional gene expression via AGO-dependent mechanism in IL-1β stimulated chondrocytes', *Osteoarthritis and Cartilage*, 28(8), pp. 1102–1110. doi: 10.1016/J.JOCA.2020.04.014.

Grimstein, C. *et al.* (2011) 'Alpha-1 antitrypsin protein and gene therapies decrease autoimmunity and delay arthritis development in mouse model', *Journal of translational medicine*, 9. doi: 10.1186/1479-5876-9-21.

Gwangwa, M. V., Joubert, A. M. and Visagie, M. H. (2019) 'Effects of glutamine deprivation on oxidative stress and cell survival in breast cell lines', *Biological research*, 52(1), p. 15. doi: 10.1186/S40659-019-0224-9/FIGURES/10.

Haas, R. *et al.* (2015) 'Lactate Regulates Metabolic and Pro-inflammatory Circuits in Control of T Cell Migration and Effector Functions', *PLoS Biology*, 13(7), p. 1002202. doi: 10.1371/JOURNAL.PBIO.1002202.

Hahn, E, Halestrap, A. Gamelli, R. (2000) 'Expression of the lactate transporter MCT1 in macrophages', *Shock*, 13(4), pp. 253–260.

Hashizume, M., Hayakawa, N. and Mihara, M. (2008) 'IL-6 trans-signalling directly induces RANKL on fibroblast-like synovial cells and is involved in RANKL induction by TNF-α and IL-17', *Rheumatology*, 47(11), pp. 1635–1640. doi: 10.1093/RHEUMATOLOGY/KEN363.

Haynes, M. K., Hume, E. L. and Smith, J. B. (2002) 'Phenotypic Characterization of Inflammatory Cells from Osteoarthritic Synovium and Synovial Fluids', *Clinical Immunology*, 105(3), pp. 315–325. doi: 10.1006/CLIM.2002.5283.

Heath, E. L. *et al.* (2021) 'Patient-reported outcomes after hip and knee arthroplasty: results from a large national registry', *Bone & Joint Open*, 2(6), p. 422. doi: 10.1302/2633-1462.26.BJO-2021-0053.R1.

Heberle, H. *et al.* (2015) 'InteractiVenn: A web-based tool for the analysis of sets through Venn diagrams', *BMC Bioinformatics*, 16(1), pp. 1–7. doi: 10.1186/S12859-015-0611-3/FIGURES/4.

Vander Heiden, M. G. *et al.* (2010) 'Evidence for an alternative glycolytic pathway in rapidly proliferating cells', *Science (New York, N.Y.)*, 329(5998), pp. 1492–1499. doi: 10.1126/SCIENCE.1188015.

Henderson, B. and Pettipher, E. R. (1989) 'Arthritogenic actions of recombinant IL-1 and tumour necrosis factor alpha in the rabbit: evidence for synergistic interactions between cytokines in vivo.', *Clinical and Experimental Immunology*, 75(2), p. 306. Available at: /pmc/articles/PMC1542106/?report=abstract (Accessed: 20 July 2022).

Hildebrandt, V. H. *et al.* (2010) 'Dutch Musculoskeletal Questionnaire: description and basic qualities', *https://doi.org/10.1080/00140130110087437*, 44(12), pp. 1038–1055. doi: 10.1080/00140130110087437.

Hirasawa, N. (2019) ‘Expression of Histidine Decarboxylase and Its Roles in Inflammation’, *International Journal of Molecular Sciences 2019, Vol. 20, Page 376*, 20(2), p. 376. doi: 10.3390/IJMS20020376.

Den Hollander, W. *et al.* (2014) ‘Knee and hip articular cartilage have distinct epigenomic landscapes: implications for future cartilage regeneration approaches’, *Annals of the rheumatic diseases*, 73(12), pp. 2208–2212. doi: 10.1136/ANNRHEUMDIS-2014-205980.

Horrigan, L. A., Kelly, J. P. and Connor, T. J. (2004) ‘Caffeine suppresses TNF-α production via activation of the cyclic AMP/protein kinase A pathway’, *International Immunopharmacology*, 4(10–11), pp. 1409–1417. doi: 10.1016/J.INTIMP.2004.06.005.

Horrigan, L. A., Kelly, J. P. and Connor, T. J. (2006) ‘Immunomodulatory effects of caffeine: Friend or foe?’, *Pharmacology & Therapeutics*, 111(3), pp. 877–892. doi: 10.1016/J.PHARMTHERA.2006.02.002.

Howden, A. J. M. *et al.* (2019) ‘Quantitative analysis of T cell proteomes and environmental sensors during T cell differentiation’, *Nature immunology*, 20(11), pp. 1542–1554. doi: 10.1038/S41590-019-0495-X.

Hsueh, M. F. *et al.* (2021) ‘Synergistic roles of macrophages and neutrophils in osteoarthritis progression’, *Arthritis & rheumatology (Hoboken, N.J.)*, 73(1), p. 89. doi: 10.1002/ART.41486.

Hu, F. B., Satija, A. and Manson, J. A. E. (2015) ‘Curbing the Diabetes Pandemic: The Need for Global Policy Solutions’, *JAMA*, 313(23), pp. 2319–2320. doi: 10.1001/JAMA.2015.5287.

Huang, Z. *et al.* (2020) 'Insight into osteoarthritis through integrative analysis of metabolomics and transcriptomics', *Clinica Chimica Acta*, 510, pp. 323–329. doi: 10.1016/J.CCA.2020.07.010.

Hussein, M. R. *et al.* (2008) 'Alterations of the CD4+, CD8+ T Cell Subsets, Interleukins-1β, IL-10, IL-17, Tumor Necrosis Factor-α and Soluble Intercellular Adhesion Molecule-1 in Rheumatoid Arthritis and Osteoarthritis: Preliminary Observations'. doi: 10.1007/s12253-008-9016-1.

Institute for Health Metrics and (IHME), E. (2019) *Global Burden of Disease Collaborative Network (2020)*. Seattle. Available at: https://ghdx.healthdata.org/gbd-2019.

Ishii, H. *et al.* (2002) 'Characterization of infiltrating T cells and Th1/Th2-type cytokines in the synovium of patients with osteoarthritis', *Osteoarthritis and Cartilage*, 10, pp. 277–281. doi: 10.1053/joca.2001.0509.

Jeon, O. H. *et al.* (2017) 'Local clearance of senescent cells attenuates the development of post-traumatic osteoarthritis and creates a pro-regenerative environment', *Nature Medicine*, 23(6), pp. 775–781. doi: 10.1038/nm.4324.

Jerosch, J. (2011) 'Effects of Glucosamine and Chondroitin Sulfate on Cartilage Metabolism in OA: Outlook on Other Nutrient Partners Especially Omega-3 Fatty Acids', *International journal of rheumatology*, 2011. doi: 10.1155/2011/969012.

Ji, Q. *et al.* (2019) 'Translational science: Single-cell RNA-seq analysis reveals the progression of human osteoarthritis', *Annals of the Rheumatic Diseases*, 78(1), p. 100. doi: 10.1136/ANNRHEUMDIS-2017-212863.

Jiang, L. *et al.* (2011) 'The relationship between body mass index and hip

osteoarthritis: a systematic review and meta-analysis', *Joint Bone Spine*, 78(2), pp. 150–155. doi: 10.1016/j.jbspin.2010.04.011.

Jiang, L. *et al.* (2012) 'Body mass index and susceptibility to knee osteoarthritis: a systematic review and meta-analysis', *Joint Bone Spine*, 79(3), pp. 291–297. doi: 10.1016/j.jbspin.2011.05.015.

Johmura, Y. *et al.* (2021) 'Senolysis by glutaminolysis inhibition ameliorates various age-associated disorders', *Science*, 371(6526), pp. 265–270. doi: 10.1126/SCIENCE.ABB5916/SUPPL_FILE/ABB5916_MDAR_REPRODUCIBILITY_CHECKLIST.PDF.

Joseph, J. S., Ayeleso, A. O. and Mukwevho, E. (2017) 'Role of exercise-induced calmodulin protein kinase (CaMK)II activation in the regulation of omega-6 fatty acids and lipid metabolism genes in rat skeletal muscle', *Physiological research*, 66(6), pp. 969–977. doi: 10.33549/PHYSIOLRES.933509.

Julià, A. *et al.* (2016) 'Urine metabolome profiling of immune-mediated inflammatory diseases', *BMC Medicine*, 14(1), pp. 1–12. doi: 10.1186/S12916-016-0681-8/FIGURES/4.

Kaneva, M. K. *et al.* (2021) 'Alpha-1-antitrypsin reduces inflammation and exerts chondroprotection in arthritis', *The FASEB Journal*, 35(5), p. e21472. doi: 10.1096/FJ.202001801R.

Kapoor, M. *et al.* (2011) 'Role of proinflammatory cytokines in the pathophysiology of osteoarthritis', *Nature reviews. Rheumatology*, 7(1), pp. 33–42. doi: 10.1038/NRRHEUM.2010.196.

Kawano, M. M. *et al.* (2015) 'Assessment of quality of life in patients with knee

osteoarthritis', *Acta Ortopedica Brasileira*, 23(6), p. 307. doi: 10.1590/1413-785220152306150596.

KELLGREN, J. H. and LAWRENCE, J. S. (1957) 'Radiological Assessment of Osteo-Arthrosis', *Annals of the Rheumatic Diseases*, 16(4), pp. 494–502. doi: 10.1136/ARD.16.4.494.

Khatib-Massalha, E. *et al.* (2020) 'Lactate released by inflammatory bone marrow neutrophils induces their mobilization via endothelial GPR81 signaling', *Nature Communications 2020 11:1*, 11(1), pp. 1–18. doi: 10.1038/s41467-020-17402-2.

Kim, D. S. *et al.* (2015) 'Anti-inflammatory effects of glutamine on LPS-stimulated human dental pulp cells correlate with activation of MKP-1 and attenuation of the MAPK and NF-κB pathways', *International endodontic journal*, 48(3), pp. 220–228. doi: 10.1111/IEJ.12303.

Kim, Jong Hyun *et al.* (2017) 'Control of leucine-dependent mTORC1 pathway through chemical intervention of leucyl-tRNA synthetase and RagD interaction', *Nature communications*, 8(1). doi: 10.1038/S41467-017-00785-0.

King, L. K., March, L. and Anandacoomarasamy, A. (2013) 'Obesity & osteoarthritis', *The Indian Journal of Medical Research*, 138(2), pp. 185–193. Available at: https://www.ncbi.nlm.nih.gov/pmc/articles/PMC3788203/.

Koedderitzsch, K. *et al.* (2021) 'TNF induces glycolytic shift in fibroblast like synoviocytes via GLUT1 and HIF1A', *Scientific Reports 2021 11:1*, 11(1), pp. 1–11. doi: 10.1038/s41598-021-98651-z.

Kowalski, G. M. *et al.* (2015) 'Application of dynamic metabolomics to examine in vivo skeletal muscle glucose metabolism in the chronically high-fat fed mouse',

Biochemical and biophysical research communications, 462(1), pp. 27–32. doi: 10.1016/J.BBRC.2015.04.096.

Krebs, H. A. (1935) 'Metabolism of amino-acids: The synthesis of glutamine from glutamic acid and ammonia, and the enzymic hydrolysis of glutamine in animal tissues', *The Biochemical journal*, 29(8), pp. 1951–1969. doi: 10.1042/BJ0291951.

Lacey, J. M. and Wilmore, D. W. (1990) 'Is Glutamine a Conditionally Essential Amino Acid?', *Nutrition Reviews*, 48(8), pp. 297–309. doi: 10.1111/J.1753-4887.1990.TB02967.X.

de Lange-Brokaar, B. J. E. *et al.* (2012) 'Synovial inflammation, immune cells and their cytokines in osteoarthritis: a review', *Osteoarthritis and cartilage*, 20(12), pp. 1484–1499. doi: 10.1016/J.JOCA.2012.08.027.

Laura J Pallett, Sarah Dimeloe, Linda V Sinclair, Adam J Byrne, A. S. (2021) 'A glutamine "tug-of-war": targets to manipulate glutamine metabolism for cancer immunotherapy', *Immunotherapy Advances*, 1(1). doi: https://doi.org/10.1093/immadv/ltab010.

LeBleu, V. S. and Neilson, E. G. (2020) 'Origin and functional heterogeneity of fibroblasts', *FASEB Journal*, 34(3), pp. 3519–3536. doi: 10.1096/FJ.201903188R.

Leheita, O. *et al.* (2005) 'Lymphocytes subsets in osteoarthritis versus rheumatoid arthritis.', *The Egyptian journal of immunology*, 12(2), pp. 113–124.

Lelo, A. *et al.* (1986) 'Quantitative assessment of caffeine partial clearances in man.', *British Journal of Clinical Pharmacology*, 22(2), p. 183. doi: 10.1111/J.1365-2125.1986.TB05247.X.

Li, X. S. *et al.* (2018) 'Untargeted metabolomics identifies trimethyllysine, a TMAO-

producing nutrient precursor, as a predictor of incident cardiovascular disease risk', *JCI insight*, 3(6). doi: 10.1172/JCI.INSIGHT.99096.

Li, Y. *et al.* (2018) 'Succinate induces synovial angiogenesis in rheumatoid arthritis through metabolic remodeling and HIF-1α/VEGF axis', *Free radical biology & medicine*, 126, pp. 1–14. doi: 10.1016/J.FREERADBIOMED.2018.07.009.

Lin, M. T. *et al.* (2005) 'Glutamine-supplemented total parenteral nutrition attenuates plasma interleukin-6 in surgical patients with lower disease severity', *World Journal of Gastroenterology : WJG*, 11(39), p. 6197. doi: 10.3748/WJG.V11.I39.6197.

Lindblad, S. and Hedfors, E. (1987) 'Arthroscopic and immunohistologic characterization of knee joint synovitis in osteoarthritis', *Arthritis & Rheumatism*, 30(10), pp. 1081–1088. doi: 10.1002/ART.1780301001.

Van de Loo, F. A. J. *et al.* (1997) 'Interleukin-6 reduces cartilage destruction during experimental arthritis. A study in interleukin-6-deficient mice.', *The American Journal of Pathology*, 151(1), p. 177. Available at: /pmc/articles/PMC1857913/?report=abstract (Accessed: 20 July 2022).

Love, M. I., Huber, W. and Anders, S. (2014) 'Moderated estimation of fold change and dispersion for RNA-seq data with DESeq2', *Genome Biology*, 15(12), pp. 1–21. doi: 10.1186/S13059-014-0550-8.

Lu, C. and Thompson, C. B. (2012) 'Metabolic regulation of epigenetics', *Cell Metabolism*, 16(1), p. 9. doi: 10.1016/J.CMET.2012.06.001.

Ludwig, C. and Günther, U. L. (2011) 'MetaboLab - advanced NMR data processing and analysis for metabolomics', *BMC Bioinformatics*, 12(1), pp. 1–6. doi: 10.1186/1471-2105-12-366/FIGURES/2.

Lystad, A. H. and Simonsen, A. (2016) ‘Phosphoinositide-binding proteins in autophagy’, *FEBS Letters*, 590(15), pp. 2454–2468. doi: 10.1002/1873-3468.12286.

Mammoto, A., Mammoto, T. and Ingber, D. E. (2012) ‘Mechanosensitive mechanisms in transcriptional regulation’, *Journal of cell science*, 125(Pt 13), pp. 3061–3073. doi: 10.1242/JCS.093005.

Marat, A. L. and Haucke, V. (2016) ‘Phosphatidylinositol 3-phosphates—at the interface between cell signalling and membrane traffic’, *The EMBO Journal*, 35(6), p. 561. doi: 10.15252/EMBJ.201593564.

Mathiessen, A. and Conaghan, P. G. (2017) ‘Synovitis in osteoarthritis: Current understanding with therapeutic implications’, *Arthritis Research and Therapy*, 19(1), pp. 1–9. doi: 10.1186/S13075-017-1229-9/FIGURES/2.

Mathur, S. and Sutton, J. (2017) ‘Personalized medicine could transform healthcare’, *Biomedical Reports*, 7(1), p. 3. doi: 10.3892/BR.2017.922.

Mcdonnell, J. *et al.* (1993) ‘Comparison of the proteoglycanolytic activities of human leukocyte elastase and human cathepsin G in vitro and in vivo’, *Connective tissue research*, 30(1), pp. 1–9. doi: 10.3109/03008209309032926.

McNearney, T. *et al.* (2000) ‘Excitatory Amino Acid Profiles of Synovial Fluid from Patients withArthritis’, *The Journal of rheumatology*, 27(3), p. 739. Available at: /pmc/articles/PMC7894989/ (Accessed: 27 February 2022).

Menni, C. *et al.* (2013) ‘Biomarkers for type 2 diabetes and impaired fasting glucose using a nontargeted metabolomics approach’, *Diabetes*, 62(12), pp. 4270–4276. doi: 10.2337/DB13-0570.

Mi, H. *et al.* (2021) ‘PANTHER version 16: a revised family classification, tree-based

classification tool, enhancer regions and extensive API', *Nucleic Acids Research*, 49(D1), pp. D394–D403. doi: 10.1093/NAR/GKAA1106.

Mickiewicz, B., Kelly, J. J., *et al.* (2015) 'Metabolic analysis of knee synovial fluid as a potential diagnostic approach for osteoarthritis', *Journal of Orthopaedic Research*®, 33(11), pp. 1631–1638. doi: 10.1002/JOR.22949.

Mickiewicz, B., Heard, B. J., *et al.* (2015) 'Metabolic profiling of synovial fluid in a unilateral ovine model of anterior cruciate ligament reconstruction of the knee suggests biomarkers for early osteoarthritis', *Journal of orthopaedic research*, 33(1), pp. 71–77. doi: 10.1002/jor.22743.

Mickiewicz, B. *et al.* (2016) 'Serum metabolite profiles are altered by erlotinib treatment and the integrin α1-null genotype, but not by post traumatic osteoarthritis', *Journal of proteome research*, 15(3), p. 815. doi: 10.1021/ACS.JPROTEOME.5B00719.

Mobasheri, A. *et al.* (2017) 'The role of metabolism in the pathogenesis of osteoarthritis', *Nature reviews. Rheumatology*, 13(5), pp. 302–311. doi: 10.1038/NRRHEUM.2017.50.

Mobasheri, A. *et al.* (2019) 'Recent advances in understanding the phenotypes of osteoarthritis', *F1000Research 2019 8:2091*, 8, p. 2091. doi: 10.12688/f1000research.20575.1.

Molepo, M. *et al.* (2018) 'A Study on Neonatal Intake of Oleanolic Acid and Metformin in Rats (Rattus norvegicus) with Metabolic Dysfunction: Implications on Lipid Metabolism and Glucose Transport', *Molecules : A Journal of Synthetic Chemistry and Natural Product Chemistry*, 23(10). doi: 10.3390/MOLECULES23102528.

Mosana, M. *et al.* (2020) 'Potential Protective Effects of Neonatal Supplementation with Oleanolic Acid on Peroxisome Proliferator-Activated Receptor Gamma (PPARγ)-Ligand Dependent Regulation of Glucose Homeostasis in High Fructose-Fed Rats':, *https://doi.org/10.1177/1934578X20913747*, 15(3), pp. 1–7. doi: 10.1177/1934578X20913747.

Moschen, A. R. *et al.* (2007) 'Visfatin, an adipocytokine with proinflammatory and immunomodulating properties', *Journal of immunology (Baltimore, Md. : 1950)*, 178(3), pp. 1748–1758. doi: 10.4049/JIMMUNOL.178.3.1748.

Myers, S. L. *et al.* (1990) 'Synovial inflammation in patients with early osteoarthritis of the knee', *Journal of rheumatology*, 17(12), pp. 1662–1669. Available at: https://www.ncbi.nlm.nih.gov/pubmed/2084242.

Nanus, Dominika E. *et al.* (2020) 'Regulation of the Inflammatory Synovial Fibroblast Phenotype by Metastasis-Associated Lung Adenocarcinoma Transcript 1 Long Noncoding RNA in Obese Patients With Osteoarthritis', *Arthritis and Rheumatology*, 72(4), pp. 609–619. doi: 10.1002/ART.41158/ABSTRACT).

Nazet, U. *et al.* (2021) 'Differential gene expression response of synovial fibroblasts from temporomandibular joints and knee joints to dynamic tensile stress', *Journal of Orofacial Orthopedics*, pp. 1–15. doi: 10.1007/S00056-021-00309-Y/FIGURES/6.

Nelson 1942-, D. L. (David L. (2005) *Lehninger principles of biochemistry*. Fourth edition. New York : W.H. Freeman, 2005. Available at: https://search.library.wisc.edu/catalog/999964334502121.

Neumann, E. *et al.* (2010) 'Cell culture and passaging alters gene expression pattern and proliferation rate in rheumatoid arthritis synovial fibroblasts', *Arthritis Research and Therapy*, 12(3), pp. 1–10. doi: 10.1186/AR3010/FIGURES/5.

NHS Digital (2019) *Health Survey for England 2018: Longstanding Conditions. Health and Social Care Information Centre*. Available at: http://healthsurvey.hscic.gov.uk/%0Asupport-guidance/public-health/health-survey-for-england-2018/longstandingconditions.aspx.

NICE (2020) *Recommendations | Osteoarthritis: care and management | Guidance | NICE*. Available at: https://www.nice.org.uk/guidance/cg177/chapter/Recommendations#pharmacological-management (Accessed: 20 July 2022).

Nicklin, P. *et al.* (2009) 'Bidirectional transport of amino acids regulates mTOR and autophagy', *Cell*, 136(3), pp. 521–534. doi: 10.1016/J.CELL.2008.11.044.

Nigdelioglu, R. *et al.* (2016) 'Transforming Growth Factor (TGF)-β Promotes de Novo Serine Synthesis for Collagen Production', *The Journal of biological chemistry*, 291(53), pp. 27239–27251. doi: 10.1074/jbc.M116.756247.

Nowbar, A. N. *et al.* (2019) 'Mortality from ischemic heart disease: Analysis of data from the world health organization and coronary artery disease risk factors from NCD risk factor collaboration', *Circulation: Cardiovascular Quality and Outcomes*, 12(6). doi: 10.1161/CIRCOUTCOMES.118.005375.

O'Leary, E. M. *et al.* (2020) 'TGF-b promotes metabolic reprogramming in lung fibroblasts via mTORC1-dependent ATF4 activation', *American Journal of Respiratory Cell and Molecular Biology*, 63(5), pp. 601–612. doi: 10.1165/RCMB.2020-0143OC.

Ogura, S. I. *et al.* (2011) 'The effect of 5-aminolevulinic acid on cytochrome c oxidase activity in mouse liver', *BMC Research Notes*, 4(1), pp. 1–4. doi: 10.1186/1756-0500-4-66/FIGURES/3.

de Oliveira, P. G. *et al.* (2019) 'Fibroblast-Like Synoviocytes Glucose Metabolism as a Therapeutic Target in Rheumatoid Arthritis', *Frontiers in immunology*, 10, p. 1743. doi: 10.3389/FIMMU.2019.01743/BIBTEX.

Oliveria, S. *et al.* (1999) 'Body Weight, Body Mass Index, and Incident Symptomatic Osteoarthritis of the Hand, Hip, and Knee', *Epidemiology (Cambridge, Mass.)*, 10(2), pp. 161–166. doi: 10.1097/00001648-199903000-00013.

Ostalowska, A. *et al.* (2006) 'Lipid peroxidation and antioxidant enzymes in synovial fluid of patients with primary and secondary osteoarthritis of the knee joint', *Osteoarthritis and Cartilage*, 14(2), pp. 139–145. doi: 10.1016/J.JOCA.2005.08.009.

Paige, L. A. *et al.* (2007) 'A preliminary metabolomic analysis of older adults with and without depression', *International Journal of Geriatric Psychiatry*, 22(5), pp. 418–423. doi: 10.1002/GPS.1690.

Paneni, F. *et al.* (2013) 'Diabetes and vascular disease: pathophysiology, clinical consequences, and medical therapy: part I', *European heart journal*, 34(31), pp. 2436–2446. doi: 10.1093/EURHEARTJ/EHT149.

Pang, Y. L. J., Poruri, K. and Martinis, S. A. (2014) 'tRNA synthetase: tRNA aminoacylation and beyond', *Wiley Interdisciplinary Reviews: RNA*, 5(4), pp. 461–480. doi: 10.1002/WRNA.1224.

Pang, Z. *et al.* (2021) 'MetaboAnalyst 5.0: narrowing the gap between raw spectra and functional insights', *Nucleic Acids Research*, 49(W1), pp. W388–W396. doi: 10.1093/NAR/GKAB382.

Park, H. *et al.* (2002) 'Monocyte cell adhesion induced by a human aminoacyl-tRNA synthetase-associated factor, p43: identification of the related adhesion molecules

and signal pathways', *Journal of Leukocyte Biology*, 71(2), pp. 223–230. doi: 10.1189/JLB.71.2.223.

Parry-Billings, M. *et al.* (1992) 'Effects of Major and Minor Surgery on Plasma Glutamine and Cytokine Levels', *Archives of Surgery*, 127(10), pp. 1237–1240. doi: 10.1001/ARCHSURG.1992.01420100099017.

Payab, M. *et al.* (2021) 'Metabolomics prospect of obesity and metabolic syndrome; a systematic review', *Journal of Diabetes and Metabolic Disorders*, pp. 1–29. doi: 10.1007/S40200-021-00917-W/FIGURES/3.

Pearson, Mark J. *et al.* (2017) 'IL-6 secretion in osteoarthritis patients is mediated by chondrocyte-synovial fibroblast cross-talk and is enhanced by obesity', *Scientific Reports*, 7(1). doi: 10.1038/S41598-017-03759-W.

Pereira, R. C. *et al.* (2016) 'Human Articular Chondrocytes Regulate Immune Response by Affecting Directly T Cell Proliferation and Indirectly Inhibiting Monocyte Differentiation to Professional Antigen-Presenting Cells', *Frontiers in immunology*, 7(OCT). doi: 10.3389/FIMMU.2016.00415.

Petrus, P. *et al.* (2020) 'Glutamine Links Obesity to Inflammation in Human White Adipose Tissue', *Cell Metabolism*, 31(2), pp. 375-390.e11. doi: 10.1016/J.CMET.2019.11.019/ATTACHMENT/7ED98A82-6684-4238-B8A2-4124620D2E52/MMC5.XLSX.

Pham, C. T. N. (2006) 'Neutrophil serine proteases: specific regulators of inflammation', *Nature Reviews Immunology 2006 6:7*, 6(7), pp. 541–550. doi: 10.1038/nri1841.

Philp, A. M. *et al.* (2021) 'eNAMPT Is Localised to Areas of Cartilage Damage in

Patients with Hip Osteoarthritis and Promotes Cartilage Catabolism and Inflammation', *International Journal of Molecular Sciences*, 22(13). doi: 10.3390/IJMS22136719.

Pietzke, M., Meiser, J. and Vazquez, A. (2020) 'Formate metabolism in health and disease', *Molecular Metabolism*, 33, pp. 23–37. doi: 10.1016/J.MOLMET.2019.05.012.

Pisarsky, L. *et al.* (2016) 'Targeting Metabolic Symbiosis to Overcome Resistance to Anti-angiogenic Therapy', *Cell Reports*, 15(6), pp. 1161–1174. doi: 10.1016/j.celrep.2016.04.028.

Ponchel, F. *et al.* (2015) 'Changes in peripheral blood immune cell composition in osteoarthritis', *Osteoarthritis and Cartilage*, 23(11), p. 1870. doi: 10.1016/J.JOCA.2015.06.018.

Porter, L. *et al.* (2020) 'Metabolomic Biomarkers of Multiple Sclerosis: A Systematic Review', *Frontiers in Molecular Biosciences*, 7, p. 356. doi: 10.3389/FMOLB.2020.574133/BIBTEX.

Prieto-Potin, I. *et al.* (2015) 'Characterization of multinucleated giant cells in synovium and subchondral bone in knee osteoarthritis and rheumatoid arthritis', *BMC musculoskeletal disorders*, 16(1), p. 226. doi: 10.1186/s12891-015-0664-5.

Probert, L. *et al.* (1995) 'The type I interleukin-1 receptor acts in series with tumor necrosis factor (TNF) to induce arthritis in TNF-transgenic mice', *European Journal of Immunology*, 25(6), pp. 1794–1797. doi: 10.1002/EJI.1830250647.

Quinones, M. P. and Kaddurah-Daouk, R. (2009) 'Metabolomics tools for identifying biomarkers for neuropsychiatric diseases', *Neurobiology of Disease*, 35(2), pp. 165–

176. doi: 10.1016/J.NBD.2009.02.019.

Rahman, I., Athar, M. T. and Islam, M. (2021) ‘Type 2 Diabetes, Obesity, and Cancer Share Some Common and Critical Pathways’, *Frontiers in Oncology*, 10, p. 2995. doi: 10.3389/FONC.2020.600824/BIBTEX.

Ramachandran, S. *et al.* (2016) ‘Structural basis for exploring the allosteric inhibition of human kidney type glutaminase’, *Oncotarget*, 7(36), p. 57943. doi: 10.18632/ONCOTARGET.10791.

Rehman, T. *et al.* (2020) ‘Cysteine and homocysteine as biomarker of various diseases’, *Food Science and Nutrition*, 8(9), pp. 4696–4707. doi: 10.1002/FSN3.1818.

Revell, P. A. *et al.* (1988) ‘The synovial membrane in osteoarthritis: a histological study including the characterisation of the cellular infiltrate present in inflammatory osteoarthritis using monoclonal antibodies.’, *Annals of the Rheumatic Diseases*, 47(4), p. 300. doi: 10.1136/ARD.47.4.300.

Del Rey, Manuel J *et al.* (2019) ‘Senescent synovial fibroblasts accumulate prematurely in rheumatoid arthritis tissues and display an enhanced inflammatory phenotype’, *Immunity & Ageing*, 16(1), p. 29. doi: 10.1186/s12979-019-0169-4.

Del Rey, Manuel J. *et al.* (2019) ‘Senescent synovial fibroblasts accumulate prematurely in rheumatoid arthritis tissues and display an enhanced inflammatory phenotype’, *Immunity & Ageing : I & A*, 16(1). doi: 10.1186/S12979-019-0169-4.

Rhoads, J. P., Major, A. S. and Rathmell, J. C. (2017) ‘Fine tuning of immunometabolism for the treatment of rheumatic diseases’, *Nature reviews. Rheumatology*, 13(5), p. 313. doi: 10.1038/NRRHEUM.2017.54.

Rieger, A. M. *et al.* (2011) 'Modified Annexin V/Propidium Iodide Apoptosis Assay For Accurate Assessment of Cell Death', *Journal of Visualized Experiments : JoVE*, (50), p. 2597. doi: 10.3791/2597.

Rinn, J. L. *et al.* (2006) 'Anatomic demarcation by positional variation in fibroblast gene expression programs', *PLoS genetics*, 2(7), pp. 1084–1096. doi: 10.1371/JOURNAL.PGEN.0020119.

Rockel, J. S. *et al.* (2022) 'Identification of a differential metabolite-based signature in patients with late-stage knee osteoarthritis', *Osteoarthritis and Cartilage Open*, p. 100258. doi: 10.1016/J.OCARTO.2022.100258.

Rodas, P. C. *et al.* (2012) 'Glutamine and glutathione at ICU admission in relation to outcome', *Clinical Science (London, England : 1979)*, 122(Pt 12), p. 591. doi: 10.1042/CS20110520.

Romano, M. *et al.* (1997) 'Role of IL-6 and its soluble receptor in induction of chemokines and leukocyte recruitment', *Immunity*, 6(3), pp. 315–325. doi: 10.1016/S1074-7613(00)80334-9.

Roos, E. M. (2005) 'Joint injury causes knee osteoarthritis in young adults', *Current opinion in rheumatology*, 17(2), pp. 195–200. doi: 10.1097/01.BOR.0000151406.64393.00.

Rumping, L. *et al.* (2019) 'GLS hyperactivity causes glutamate excess, infantile cataract and profound developmental delay', *Human molecular genetics*, 28(1), pp. 96–104. doi: 10.1093/HMG/DDY330.

Saalbach, A. and Anderegg, U. (2019) 'Thy-1: more than a marker for mesenchymal stromal cells', *FASEB Journal*, 33(6), pp. 6689–6696. doi: 10.1096/FJ.201802224R.

Sabatine, M. S. *et al.* (2005) ‘Metabolomic identification of novel biomarkers of myocardial ischemia’, *Circulation*, 112(25), pp. 3868–3875. doi: 10.1161/CIRCULATIONAHA.105.569137.

Sacitharan, P. K. and Vincent, T. L. (2016) ‘Cellular ageing mechanisms in osteoarthritis’, *Mammalian genome : official journal of the International Mammalian Genome Society*, 27(7–8), pp. 421–429. doi: 10.1007/S00335-016-9641-Z.

Sahai, E. *et al.* (2020) ‘A framework for advancing our understanding of cancer-associated fibroblasts’, *Nature Reviews Cancer 2020 20:3*, 20(3), pp. 174–186. doi: 10.1038/s41568-019-0238-1.

Salameh, Y., Bejaoui, Y. and El Hajj, N. (2020) ‘DNA Methylation Biomarkers in Aging and Age-Related Diseases’, *Frontiers in Genetics*, 11, p. 171. doi: 10.3389/FGENE.2020.00171/BIBTEX.

Sanford-Crane, H., Abrego, J. and Sherman, M. H. (2019) ‘Fibroblasts as Modulators of Local and Systemic Cancer Metabolism’, *Cancers*, 11(5). doi: 10.3390/CANCERS11050619.

Sang, G. P. *et al.* (2005) ‘Human lysyl-tRNA synthetase is secreted to trigger proinflammatory response’, *Proceedings of the National Academy of Sciences of the United States of America*, 102(18), pp. 6356–6361. doi: 10.1073/PNAS.0500226102/SUPPL_FILE/0226FIG9.GIF.

Saraiva, A. L. *et al.* (2018) ‘Succinate receptor deficiency attenuates arthritis by reducing dendritic cell traffic and expansion of T h 17 cells in the lymph nodes’, *FASEB journal : official publication of the Federation of American Societies for Experimental Biology*, 32(12), pp. 6550–6558. doi: 10.1096/FJ.201800285.

Schruf, E. *et al.* (2019) ‘Human lung fibroblast-to-myofibroblast transformation is not driven by an LDH5-dependent metabolic shift towards aerobic glycolysis’, *Respiratory research*, 20(1), p. 87. doi: 10.1186/s12931-019-1058-2.

Sebastian, A. *et al.* (2018) ‘Comparative Transcriptomics Identifies Novel Genes and Pathways Involved in Post-Traumatic Osteoarthritis Development and Progression’, *International Journal of Molecular Sciences*, 19(9). doi: 10.3390/IJMS19092657.

Sebastian, A. *et al.* (2021) ‘Single-cell RNA-seq reveals transcriptomic heterogeneity and post-traumatic osteoarthritis-associated early molecular changes in mouse articular chondrocytes’, *Cells*, 10(6). doi: 10.3390/CELLS10061462/S1.

Selvarajah, B. *et al.* (2019) ‘mTORC1 amplifies the ATF4-dependent de novo serine-glycine pathway to supply glycine during TGF-β1–induced collagen biosynthesis’, *Science signaling*, 12(582), p. eaav3048. doi: 10.1126/scisignal.aav3048.

Shah, S. H. and Newgard, C. B. (2015) ‘Integrated Metabolomics and Genomics: Systems Approaches to Biomarkers and Mechanisms of Cardiovascular Disease’, *Circulation. Cardiovascular genetics*, 8(2), p. 410. doi: 10.1161/CIRCGENETICS.114.000223.

Shan, B. *et al.* (2010) ‘Thy-1 Attenuates TNF-α-Activated Gene Expression in Mouse Embryonic Fibroblasts via Src Family Kinase’, *PLoS ONE*, 5(7). doi: 10.1371/JOURNAL.PONE.0011662.

Shang, H., Zheng, J. and Tong, J. (2020) ‘Integrated analysis of transcriptomic and metabolomic data demonstrates the significant role of pyruvate carboxylase in the progression of ovarian cancer’, *Aging*, 12(21), pp. 21874–21889. doi: 10.18632/AGING.104004.

Shet, K. *et al.* (2012) ‘High resolution magic angle spinning (HR-MAS) NMR spectroscopy of human osteoarthritic cartilage’, *Nmr in Biomedicine*, 25(4), p. 538. doi: 10.1002/NBM.1769.

Siaton, B. C., Hogans, B. H. and Hochberg, M. C. (2020) ‘Precision medicine in osteoarthritis: not yet ready for prime time’, *https://doi.org/10.1080/23808993.2020.1842731*, 6(1), pp. 5–8. doi: 10.1080/23808993.2020.1842731.

SIMCA (2020) *SIMCA® 15 User Guide*. Available at: https://www.sartorius.com/download/544940/simca-15-user-guide-en-b-00076-sartorius-data.pdf (Accessed: 24 July 2022).

Sjöstedt, E. *et al.* (2020) ‘An atlas of the protein-coding genes in the human, pig, and mouse brain’, *Science*, 367(6482). doi: 10.1126/SCIENCE.AAY4106.

Soares Severo, J. *et al.* (2021) ‘Effects of glutamine supplementation on inflammatory bowel disease: A systematic review of clinical trials’. doi: 10.1016/j.clnesp.2020.12.023.

Sohn, D. H. *et al.* (2012) ‘Plasma proteins present in osteoarthritic synovial fluid can stimulate cytokine production via Toll-like receptor 4’, *Arthritis Research & Therapy*, 14(1), p. R7. doi: 10.1186/AR3555.

Sokolove, J. and Lepus, C. M. (2013) ‘Role of inflammation in the pathogenesis of osteoarthritis: latest findings and interpretations’, *Therapeutic advances in musculoskeletal disease*, 5(2), pp. 77–94. doi: 10.1177/1759720X12467868.

Song, W. *et al.* (2020) ‘Solute carrier transporters: the metabolic gatekeepers of immune cells’, *Acta Pharmaceutica Sinica. B*, 10(1), p. 61. doi:

10.1016/J.APSB.2019.12.006.

Sorokin, L. (2010) ‘The impact of the extracellular matrix on inflammation’, *Nature Reviews Immunology 2010 10:10*, 10(10), pp. 712–723. doi: 10.1038/nri2852.

Spégel, P. *et al.* (2011) ‘Metabolomic analyses reveal profound differences in glycolytic and tricarboxylic acid cycle metabolism in glucose-responsive and -unresponsive clonal β-cell lines’, *The Biochemical journal*, 435(1), pp. 277–284. doi: 10.1042/BJ20100655.

Sports England (2020) *Active Lives Adult Survey November 2020-21 Report*. London. Available at: https://sportengland-production-files.s3.eu-west-2.amazonaws.com/s3fs-public/2022-04/Active Lives Adult Survey November 20-21 Report.pdf?VersionId=nPU_v3jFjwG8o_xnv62FcKOdEiVmRWCb.

Steinberg, J. *et al.* (2017) ‘Integrative epigenomics, transcriptomics and proteomics of patient chondrocytes reveal genes and pathways involved in osteoarthritis’, *Scientific Reports*, 7(1). doi: 10.1038/S41598-017-09335-6.

Sthle, L. and Wold, S. (1990) ‘Multivariate analysis of variance (MANOVA)’, *Chemometrics and Intelligent Laboratory Systems*, 9(2), pp. 127–141. doi: 10.1016/0169-7439(90)80094-M.

Strianese, O. *et al.* (2020) ‘Precision and Personalized Medicine: How Genomic Approach Improves the Management of Cardiovascular and Neurodegenerative Disease’, *Genes*, 11(7), pp. 1–24. doi: 10.3390/GENES11070747.

Sutbeyaz, S. T. *et al.* (2007) ‘Influence of knee osteoarthritis on exercise capacity and quality of life in obese adults’, *Obesity (Silver Spring, Md.)*, 15(8), pp. 2071–2076. doi: 10.1038/OBY.2007.246.

Sykiotis, G. P., Kalliolias, G. D. and Papavassiliou, A. G. (2005) 'Pharmacogenetic Principles in the Hippocratic Writings', *The Journal of Clinical Pharmacology*, 45(11), pp. 1218–1220. doi: 10.1177/0091270005281091.

Symons, J. A. *et al.* (1991) 'Soluble CD4 in patients with rheumatoid arthritis and osteoarthritis.', *Clinical immunology and immunopathology*, 60(1), pp. 72–82. doi: 10.1016/0090-1229(91)90113-o.

Takahara, T. *et al.* (2020) 'Amino acid-dependent control of mTORC1 signaling: A variety of regulatory modes', *Journal of Biomedical Science*, 27(1), pp. 1–16. doi: 10.1186/S12929-020-00679-2/FIGURES/4.

Takahashi, S. *et al.* (2017) 'Glutaminase 1 plays a key role in the cell growth of fibroblast-like synoviocytes in rheumatoid arthritis', *Arthritis Research and Therapy*, 19(1), pp. 1–10. doi: 10.1186/S13075-017-1283-3/FIGURES/6.

Tannahill, G. M. *et al.* (2013) 'Succinate is an inflammatory signal that induces IL-1β through HIF-1α', *Nature*, 496(7444), pp. 238–242. doi: 10.1038/NATURE11986.

Tastan, B. *et al.* (2021) 'Dimethyl Fumarate Alleviates NLRP3 Inflammasome Activation in Microglia and Sickness Behavior in LPS-Challenged Mice', *Frontiers in Immunology*, 12, p. 4736. doi: 10.3389/FIMMU.2021.737065/BIBTEX.

Taylor, S. E. B. *et al.* (2015) 'Genome-wide mapping of DNA hydroxymethylation in osteoarthritic chondrocytes', *Arthritis & rheumatology (Hoboken, N.J.)*, 67(8), pp. 2129–2140. doi: 10.1002/ART.39179.

Titze, I. R. *et al.* (2004) 'Design and validation of a bioreactor for engineering vocal fold tissues under combined tensile and vibrational stresses', *Journal of biomechanics*, 37(10), pp. 1521–1529. doi: 10.1016/J.JBIOMECH.2004.01.007.

Tonge, D. P., Pearson, M. J. and Jones, S. W. (2014) 'The hallmarks of osteoarthritis and the potential to develop personalised disease-modifying pharmacological therapeutics', *Osteoarthritis and cartilage*, 22(5), pp. 609–621. doi: 10.1016/J.JOCA.2014.03.004.

Tufts, L. *et al.* (2015) 'Correlating HRMAS NMR Spectroscopy and Gene Analysis in OA Cartilage', *NMR in biomedicine*, 28(5), p. 523. doi: 10.1002/NBM.3285.

Underwood, B. R. *et al.* (2006) 'Huntington disease patients and transgenic mice have similar pro-catabolic serum metabolite profiles', *Brain*, 129(4), pp. 877–886. doi: 10.1093/BRAIN/AWL027.

Unneberg, K. *et al.* (1997) 'Both growth hormone and exogenous glutamine increase gastrointestinal glutamine uptake in trauma', *Annals of surgery*, 225(1), pp. 97–102. doi: 10.1097/00000658-199701000-00011.

Ussher, J. R. *et al.* (2016) 'The Emerging Role of Metabolomics in the Diagnosis and Prognosis of Cardiovascular Disease', *Journal of the American College of Cardiology*, 68(25), pp. 2850–2870. doi: 10.1016/J.JACC.2016.09.972.

Varghese, S. *et al.* (2007) 'Glucosamine modulates chondrocyte proliferation, matrix synthesis, and gene expression', *Osteoarthritis and Cartilage*, 15(1), pp. 59–68. doi: 10.1016/J.JOCA.2006.06.008.

Viester, L. *et al.* (2013) 'The relation between body mass index and musculoskeletal symptoms in the working population', *BMC Musculoskeletal Disorders*, 14, p. 238. doi: 10.1186/1471-2474-14-238.

Wang, G. *et al.* (2021) 'Neutrophil Elastase Induces Chondrocyte Apoptosis and Facilitates the Occurrence of Osteoarthritis via Caspase Signaling Pathway',

Frontiers in Pharmacology, 12. doi: 10.3389/FPHAR.2021.666162.

Wang, T. J. *et al.* (2011) 'Metabolite profiles and the risk of developing diabetes', *Nature medicine*, 17(4), pp. 448–453. doi: 10.1038/NM.2307.

Whitaker-Menezes, D. *et al.* (2011) 'Evidence for a stromal-epithelial "lactate shuttle" in human tumors: MCT4 is a marker of oxidative stress in cancer-associated fibroblasts', *Cell cycle (Georgetown, Tex.)*, 10(11), pp. 1772–1783. doi: 10.4161/CC.10.11.15659.

Wilkinson, D. J. *et al.* (2022) 'Matrix metalloproteinase-13 is fully activated by neutrophil elastase and inactivates its serpin inhibitor, alpha-1 antitrypsin: Implications for osteoarthritis', *The FEBS Journal*, 289(1), pp. 121–139. doi: 10.1111/FEBS.16127.

Wong, C. C., Qian, Y. and Yu, J. (2017) 'Interplay between epigenetics and metabolism in oncogenesis: mechanisms and therapeutic approaches', *Oncogene 2017 36:24*, 36(24), pp. 3359–3374. doi: 10.1038/onc.2016.485.

World Health Organisation (2016) *Obesity and overweight*. Available at: https://www.who.int/news-room/fact-sheets/detail/obesity-and-overweight (Accessed: 20 July 2022).

Wurtz, P. *et al.* (2013) 'Branched-chain and aromatic amino acids are predictors of insulin resistance in young adults', *Diabetes care*, 36(3), pp. 648–655. doi: 10.2337/DC12-0895.

Xiao Z *et al.* (2021) 'Metabolic profiling of serum for osteoarthritis biomarkars', *Bio*. Available at: https://www.biorxiv.org/content/biorxiv/early/2021/12/06/2021.12.04.471213.full.pdf

(Accessed: 9 March 2022).

Xie, N. *et al.* (2015) 'Glycolytic reprogramming in myofibroblast differentiation and lung fibrosis', *American Journal of Respiratory and Critical Care Medicine*, 192(12), pp. 1462–1474. doi: 10.1164/RCCM.201504-0780OC/SUPPL_FILE/DISCLOSURES.PDF.

Xing, Z. *et al.* (1998) 'IL-6 is an antiinflammatory cytokine required for controlling local or systemic acute inflammatory responses.', *Journal of Clinical Investigation*, 101(2), p. 311. doi: 10.1172/JCI1368.

Xu, B. *et al.* (2019) 'Excessive mechanical stress induces chondrocyte apoptosis through TRPV4 in an anterior cruciate ligament-transected rat osteoarthritis model', *Life Sciences*, 228, pp. 158–166. doi: 10.1016/J.LFS.2019.05.003.

Xu, D. *et al.* (2019) 'PKM2: A Potential Regulator of Rheumatoid Arthritis via Glycolytic and Non-Glycolytic Pathways', *Frontiers in Immunology*, 10, p. 2919. doi: 10.3389/FIMMU.2019.02919.

Xu, M. *et al.* (2016) 'Structural insights into the regulatory mechanism of the Pseudomonas aeruginosa YfiBNR system', *Protein and Cell*, 7(6), pp. 403–416. doi: 10.1007/S13238-016-0264-7.

Yamakado, M. *et al.* (2012) 'Plasma amino acid profile is associated with visceral fat accumulation in obese Japanese subjects', *Clinical obesity*, 2(1–2), pp. 29–40. doi: 10.1111/J.1758-8111.2012.00039.X.

Yang, J. *et al.* (2018) 'Association of one-carbon metabolism-related vitamins (Folate, B6, B12), homocysteine and methionine with the risk of lung cancer: Systematic review and meta-analysis', *Frontiers in Oncology*, 8(OCT), p. 493. doi:

10.3389/FONC.2018.00493/BIBTEX.

Yang, R. Y. *et al.* (2015) 'Association of branched-chain amino acids with coronary artery disease: A matched-pair case-control study', *Nutrition, metabolism, and cardiovascular diseases : NMCD*, 25(10), pp. 937–942. doi: 10.1016/J.NUMECD.2015.06.003.

Yilmaz, A. *et al.* (2017) 'Diagnostic Biomarkers of Alzheimer's Disease as Identified in Saliva using 1H NMR-Based Metabolomics', *Journal of Alzheimer's disease : JAD*, 58(2), pp. 355–359. doi: 10.3233/JAD-161226.

Yoon, I. *et al.* (2020) 'Glucose-dependent control of leucine metabolism by leucyl-tRNA synthetase 1', *Science (New York, N.Y.)*, 367(6474), pp. 205–210. doi: 10.1126/SCIENCE.AAU2753.

York Health Economics (2017) *The Cost of Arthritis: Calculation conducted on behalf of Arthritis Research UK*. York.

Yu, Y. C., Han, J. M. and Kim, S. (2021) 'Aminoacyl-tRNA synthetases and amino acid signaling', *Biochimica et biophysica acta. Molecular cell research*, 1868(1). doi: 10.1016/J.BBAMCR.2020.118889.

Yuan, C. *et al.* (2020) 'Classification of four distinct osteoarthritis subtypes with a knee joint tissue transcriptome atlas', *Bone Research*, 8(1). doi: 10.1038/S41413-020-00109-X.

Zacharjasz, J. *et al.* (2021) 'Small noncoding rnas in knee osteoarthritis: The role of micrornas and trna-derived fragments', *International Journal of Molecular Sciences*, 22(11). doi: 10.3390/IJMS22115711.

Zezina, E. *et al.* (2020) 'Glucose transporter 1 in rheumatoid arthritis and

autoimmunity', *Wiley Interdisciplinary Reviews: Systems Biology and Medicine*, 12(4), p. e1483. doi: 10.1002/WSBM.1483.

Zhai, G. *et al.* (2010) 'Serum branched-chain amino acid to histidine ratio: a novel metabolomic biomarker of knee osteoarthritis', *Annals of the Rheumatic Diseases*, 69(6), pp. 1227–1231. doi: 10.1136/ARD.2009.120857.

Zhang, D. *et al.* (2015) 'Metabolic Reprogramming of Cancer-Associated Fibroblasts by IDH3α Downregulation', *Cell Reports*, 10(8), pp. 1335–1348. doi: 10.1016/j.celrep.2015.02.006.

Zhang, J. *et al.* (2022) 'Whole Transcriptome Mapping Identifies an Immune- and Metabolism-Related Non-coding RNA Landscape Remodeled by Mechanical Stress in IL-1β-Induced Rat OA-like Chondrocytes', *Frontiers in Genetics*, 13, p. 821508. doi: 10.3389/FGENE.2022.821508/FULL.

Zhang, W. *et al.* (2016) 'Metabolomic analysis of human plasma reveals that arginine is depleted in knee osteoarthritis patients', *Osteoarthritis and Cartilage*, 24(5), pp. 827–834. doi: 10.1016/J.JOCA.2015.12.004/ATTACHMENT/41D27E8D-C9D6-4E49-AD2F-7C521E00F4B6/MMC3.DOCX.

Zhao, X. *et al.* (2019) 'Metabolic regulation of dermal fibroblasts contributes to skin extracellular matrix homeostasis and fibrosis', *Nature Metabolism 2019 1:1*, 1(1), pp. 147–157. doi: 10.1038/s42255-018-0008-5.

Zhao, Y. *et al.* (2016) 'PGK1, a glucose metabolism enzyme, may play an important role in rheumatoid arthritis', *Inflammation research*, 65(10), pp. 815–825. doi: 10.1007/s00011-016-0965-7.

Zhawar, V. K., Kandpal, R. P. and Athwal, R. S. (2020) 'Senescence of Normal

Human Fibroblasts Relates to the Expression of Ionotropic Glutamate Receptor GluR6/Grik2', *Cancer Genomics & Proteomics*, 17(6), pp. 707–714. doi: 10.21873/CGP.20225.

Zheng, K. *et al.* (2017) 'Global and targeted metabolomics of synovial fluid discovers special osteoarthritis metabolites', *Journal of Orthopaedic Research*, 35(9), pp. 1973–1981. doi: 10.1002/JOR.23482.

Zou, Y. *et al.* (2017) 'Inhibition of 6-phosphofructo-2-kinase suppresses fibroblast-like synoviocytes-mediated synovial inflammation and joint destruction in rheumatoid arthritis', *British Journal of Pharmacology*, 174(9), p. 893. doi: 10.1111/BPH.13762.